Defining novel molecular mechanisms in hindbrain development

Miguel Tillo

Thesis submitted in fulfilment of the degree of Doctor of Philosophy

University College London

UCL Institute of Ophthalmology

Supervisor: Prof Christiana Ruhrberg

DECLARATION

I, Miguel Tillo, confirm that the work presented in this thesis is my own. Where information has been derived from other sources, I confirm that this has been indicated in my thesis.

ABSTRACT

During development, neurons migrate to their correct position and extend axons to their appropriate targets to form functional neuronal networks. Both these processes require the combination of many molecular signals. The hindbrain is a powerful model to uncover specific roles of these signals in axon guidance and neuronal migration. I have used the hindbrain model to investigate roles for specific isoforms of the vascular endothelial growth factor (VEGF-A) and enzymes that modify heparan sulfate proteoglycans (HSPGs) in motor neuron migration and cranial nerve development.

VEGF-A is a potent angiogenic signal that has been described to also have functions during nervous system development. *VEGFA* is an alternatively spliced gene and its three main isoforms are termed $VEGF_{121}$, $VEGF_{165}$ and $VEGF_{189}$. $VEGF_{165}$ can bind the transmembrane receptor neuropilin 1 (NRP1) to regulate axon guidance, neuronal migration and neuronal survival, whilst $VEGF_{121}$ is unable to signal through NRP1. Using *in situ* ligand-binding assays, I show that $VEGF_{189}$ can also bind NRP1 *in vivo*, similar to $VEGF_{165}$ and unlike $VEGF_{121}$. Furthermore, I show that $VEGF_{189}$ can promote NRP1-dependent migration of facial branchiomotor (FBM) neurons similar to $VEGF_{165}$, and also has similar functions in retinal ganglion cell guidance at the optic chiasm and neuronal survival in the nose.

HSPGs are extracellular matrix proteins that interact with various signalling proteins, including VEGF-A, but also fibroblast growth factors (FGFs) and their receptors. I found that the HSPG modifying enzymes HS6ST1 and HS6ST2 cooperate during cranial axon guidance, while HS2ST is required for normal FBM neuron migration. Furthermore, I demonstrated that HS2ST is dispensable for VEGF/NRP1-dependent FBM neuron migration, but promotes a novel pathway involving FGF-induced migration of these neurons.

Finally, I investigated the suitability of genetic tools to study FBM neuron migration and cranial axon guidance.

AKNOWLEDGEMENTS

I would like to thank all the members of the Ruhrberg lab for creating an excellent working environment and always being willing to help. In particular, I would like to thank the research technicians, Andy, Laura, Kathryn and Valentina, without whom I could not have obtained even half of my results. I would like to specially thank Christiana for all her time, support and mentoring during this long process!

I would like to thank my mother and my family for all their unconditional support and patience along the way. I also want to thank all my friends who have kept me going.

TABLE OF CONTENTS

LIST OF FIGURES

LIST OF TABLES

ABBREVIATIONS

aa	Amino acid
AP	Alkaline phosphatase
BCIP	5-bromo-4-chloro-3-indolyl phosphate
Bp	Base pair
CNS	Central nervous system
DAB	Diaminobenzidine
DiI	fluorescent lipophilic cationic indocarbocyanine dye
DIG	Digoxigening
DMSO	Dimethylsulfoxide
dNTP	Deoxyribonucleotide triphosphate
DTA	Dipheteria toxin fragment A
cDNA	Complementary deoxyribonucleic acid
E	Embryonic day
EDTA	Ethylenediaminetetraacetic acid, disodium salt
EXT	Exostosin
FBM	Facial branchiomotor neurons
FGF	Fibroblast growth factor
FGFR	Fibroblast growth factor receptor
fl	Floxed (LoxP-flanked)
FLK1	Fetal liver kinase 1 (VEGFR2)

FLT1	Fms-like tyrosine kinase 1 (VEGFR1)
GAG	Glycosaminoglycan
GnRH	Gonadotrophin-releasing hormone
HRP	Horseradish peroxidase
HS2ST	Heparan sulphate 2-*O*-sulfotransferase
HS6ST	Heparan sulphate 6-*O*-sulfotransferase
Hypo	Hypomorphic
IB4	Lectin from *Bandeiraea simplicifolia*
ISH	*In situ* hybridisation
ISL1	Islet 1
LacZ	β-galactosidase (lac operon)
mRNA	Messenger RNA
NBT	4-Nitro-blue-tetrazoliumchloride
Nes	Nestin
NGS	Normal goat serum
NRP	Neuropilin
OST	*O*-sulfotransferase
PBS	Phosphate buffered saline
PCR	Polymerase chain reaction
PFA	Paraformaldehyde
PNS	Peripheral nervous system

r	Rhombomere
RNase	Ribonuclease
Rpm	Revolutions per minute
SDS	Sodium dodecyl sulphate
SEMA3	Class 3 semaphorin
SS	Sheep serum (lamb)
SSC	Salt sodium citrate
SVP	Subventricular plexus
TAE	Tris acetate EDTA buffer
TBE	Tris borate EDTA buffer
TBS	Tris buffered saline
TE	Tris EDTA buffer
TUJ1	β-tubulin iii
VEGF	Vascular endothelial growth factor
VEGFR	Vascular endothelial growth factor receptor
VIIn	Facial nuclei
Vn	Trigeminal nuclei
Wt	Wild type
(w/v)	Weight:volume ratio
X-gal	5-bromo-4-chloro-3-beta-D-galactopyranoside
YFP	Yellow fluorescent protein

Chapter 1 INTRODUCTION

1.1 DEVELOPMENT OF THE HINDBRAIN

1.1.1 Hindbrain patterning and development

1.1.1.1 Development of the hindbrain

During early embryonic development the process of gastrulation initiates early morphogenetic movements that result in the specification of the endoderm, mesoderm and ectoderm (Holtfreter, 1943; Holtfreter, 1944). During gastrulation cells must migrate collectively in a process known as convergent-extension, where cells first converge and then slide over each other creating a narrow axis that leads to the elongation of the embryo (Keller et al., 1992; Wallingford et al., 2002). Following gastrulation the process of neurogenesis is initiated, through which new neurons can be generated to populate the different areas of the brain (reviewed in (Gotz and Huttner, 2005; Paridaen and Huttner, 2014). The hindbrain is one of these areas, and also described as the oldest area of the brain (Jimenez-Guri and Pujades, 2011).

During early development, several swellings arise in the anterior part of the neural tube, which will generate the forebrain, midbrain and hindbrain. In vertebrates, all cranial motor neurons are located in the brainstem, where they form distinct motor nuclei, whilst their axons extend out to control the muscles in the head and neck (reviewed by (Cordes, 2001; Guthrie, 2007). Depending on their positional arrangement in the hindbrain and synaptic target, cranial motor neurons are arranged in three groups, somatic motor (SM), visceral motor (VM), and branchiomotor (BM) neurons.

1.1.1.2 Segmentation of the hindbrain

The hindbrain is divided into 8 compartments known as rhombomeres (r), which provide positional information and specific signals that promote the

differentiation of neurons (Lumsden and Keynes, 1989). Rhombomere segmentation of the hindbrain is mostly conserved across different vertebrate species (Gilland and Baker, 1993). Rhombomere identity of the hindbrain is established by the segmental expression of transcription factors and secreted signals as well as inter-rhombomere interactions, which together fine-tune the final two-segment periodicity. One key signal in hindbrain structural specificity is *Krox20*, a zinc finger transcription factor that is expressed in early development in r3 and r5 and is important for the development of odd numbered rhombomeres (Wilkinson et al., 1989). In *Krox20*-null mice, the hindbrain lacks r3 and r5, thus it has a reduced length and lacks motor neurons that would originate in those rhombomeres (Schneider-Maunoury et al., 1993; Swiatek and Gridley, 1993). The leucine zipper transcription factor *Kreisler* is expressed early in r5 and r6 (Cordes and Barsh, 1994). Mice lacking *Kreisler* develop an aberrant r5 and lack motor neurons that are generated at that level (McKay et al., 1994; McKay et al., 1997). These transcription factors are key in hindbrain development and act upstream of *Hox* genes, which are also expressed in a segmented fashion across rhombomeres.

Vertebrate Hox genes are related to the *Drosophila* HOM genes and their discovery was key in discovering common patterning mechanisms across species (Carrasco et al., 1984; McGinnis et al., 1984). There are 39 *Hox* genes in the mouse, divided into four clusters (*Hoxa*, *Hoxb*, *Hoxc* and *Hoxd*). Correct segmentation and rhombomere identity results from the combined level and timed expression of different *Hox* gene clusters (Cordes, 2001; Guthrie, 2007). The midbrain-hindbrain boundary (isthmus) is controlled by fibroblast growth factor 8 (FGF8), which determines the start of *Hox* gene expression as well as the boundary between r1 and r2 (Reifers et al., 1998; Irving and Mason, 1999). Moreover, r4 expresses *Hoxb1* at higher levels than other *Hox* gene clusters, thus *Hoxb1*-null mice have correct segmentation but lose r4 identity, which initially results in abnormal facial branchiomotor (FBM) neuron migration from r4 to r5 and later the facial nucleus is lost (Goddard et al., 1996; Studer et al., 1996). *Hoxa1* is also expressed on r4 before *Hoxb1* expression, and *Hoxa1;Hoxb1* double mutants completely lack migrating FBM neurons, indicating that these *Hox* genes act together to specify r4 identity (Gavalas et al., 1998).

1.1.1.3 Neuronal specificity in the hindbrain and spinal cord

The patterning of the hindbrain requires the rhombomere anterior-posterior code and integration with dorsoventral signals. Sonic hedgehog (SHH) is a signal derived from the floorplate and notochord that forms a ventral (high) to dorsal (low) gradient to specify neuronal progenitor classes in the spinal cord (Figure 1.1) (reviewed in (Jessell, 2000; Price and Briscoe, 2004). SHH is defined as a morphogen, for its ability to induce different effects depending on its concentration, a term that defines other signals with similar properties (Turing, 1952; Wolpert, 1969). Several groups have shown that transplanting the notochord and/or expressing SHH ectopically leads to the differentiation of floorplate, ventral interneurons and motor neurons in a concentration dependent manner (Watterson et al., 1954; Marti et al., 1995; Roelink et al., 1995; Ericson et al., 1996). SHH gradient promotes neuronal differentiation in a dose dependent manner by controlling expression of essential homoedomain proteins at specific dorsoventral levels (Ericson et al., 1997a; Briscoe et al., 2000). These homoedomain proteins are divided into class I and class II proteins, which mutually repress each other and respond to SHH concentrations differently. The expression of class I proteins are repressed at specific SHH concentrations, whilst the class II proteins need SHH signalling and are also induces by specific SHH concentrations (Briscoe et al., 2000). Targeting transcription factors downstream of SHH increases the specificity of different population of neurons in the spinal cord and hindbrain.

In the hindbrain, VM and BM neurons originate from neural progenitors expressing the homeobox genes *Nkx2.2* and *Nkx2.9* (Figure 1.2) (Ericson et al., 1997b; Briscoe et al., 1999). Furthermore, *Nkx6.1* and *Nkx6.2* are expressed in BM and VM neuron precursors, but are not required for neuronal differentiation. However, *Nkx6.1* single and *Nkx6.1;Nkx6.2* double mutants have abnormal neuronal migration and axon guidance, whilst *Nkx6.2*-null mice are viable and have no motor neuron defects (Muller et al., 2003; Pattyn et al., 2003a; Chandrasekhar, 2004).

All postmitotic motor neurons express *Isl1*, whilst VM and BM neurons also express *Tbx20* as well as the homeobox genes *Phox2a* and *Phox2b* (Ericson et al.,

1992; Pattyn et al., 1997; Kraus et al., 2001). Interestingly, *Phox2b* expression is observed before *Phox2a* in BM neurons, whilst *Phox2a* is expressed before *Phox2b* in some SM neurons (oculomotor and trochlear) (Figure 1.2). *Phox2a*-null mice fail to form oculomotor and trochlear motor neurons, while in *Phox2b* mutants BM progenitors do not differentiate into motor neurons (Pattyn et al., 1997; Pattyn et al., 2000). Moreover, *Nkx* genes and *Hoxb1* together regulate the expression of *Phox2b* in the hindbrain, which determines the differentiation of *Nkx2.2*-positive precursors into BM or serotonergic neurons (Pattyn et al., 2003b). Furthermore, one study generated two knock-in mice replacing the *Phox2b* and *Phox2a* coding sequence with one another and showed there was only a partial rescue of single mutant phenotypes, which indicates these two genes are not functionally analogous (Coppola et al., 2005).

1.1.1.4 Organisation of motor neurons in the hindbrain

BM and VM neurons are found only in the hindbrain, while SM neurons are present in the hindbrain and midbrain. Motor nuclei in the hindbrain can be composed of more than one type of neuron. In mice, the vagus (X) and cranial accessory (XI) motor nuclei occupy r7 and r8, whilst the abducens (VI) nerve extends from somata in r5. The trochlear (IV) nucleus lies in r1; the trigeminal (V) nucleus spans r1-r3; the facial (VII) nucleus contains both BM and VM neurons along r4 and r5 level; the glossopharyngeal (IX) nucleus occupies r6; and the oculomotor (III) nucleus is contained in the midbrain.

Cranial motor axons converge and exit the brainstem through the cranial nerves (reviewed by (Cordes, 2001; Guthrie, 2007). All BM and VM axons exit the hindbrain dorsally, while all SM neurons, except the trochlear axons, exit from the basal plate of the neural tube (Lumsden and Keynes, 1989). SM neurons give rise to the hypoglossal (XII) nerve, which innervates the tongue muscles. SM neurons also form the trochlear (IV), abducens (VI) and oculomotor (III) nerves that project to the muscles of the eye. VM neurons control the salivary and lacrimal glands through branches of the facial (VII) nerve that innervate parasympathetic ganglia. VM neurons also project to visceral organs and smooth muscle. BM neuron axons merge

to form the glossopharyngeal (IX), vagus (X), trigeminal (V), and facial (VII) cranial nerves that innervate muscles in the face, jaw, larynx that derive from the brachial arches.

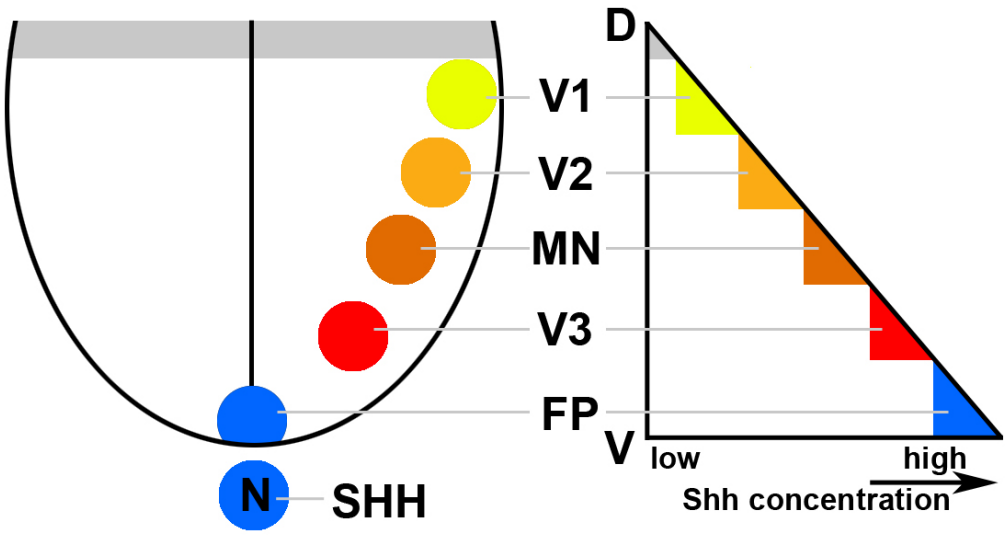

Figure 1.1 Ventral neural tube patterning by SHH

A graded concentration of SHH induces the specification of neuronal progenitors in the spinal cord. The notochord and floorplate express SHH which diffused from the ventral spinal cord to more dorsal areas that will be presented with low concentrations of SHH. V3-1 indicates the different classes of interneurons. MN, motor neurons; N, notochord; FP, floorplate. Adapted from (Jessell, 2000; Price and Briscoe, 2004).

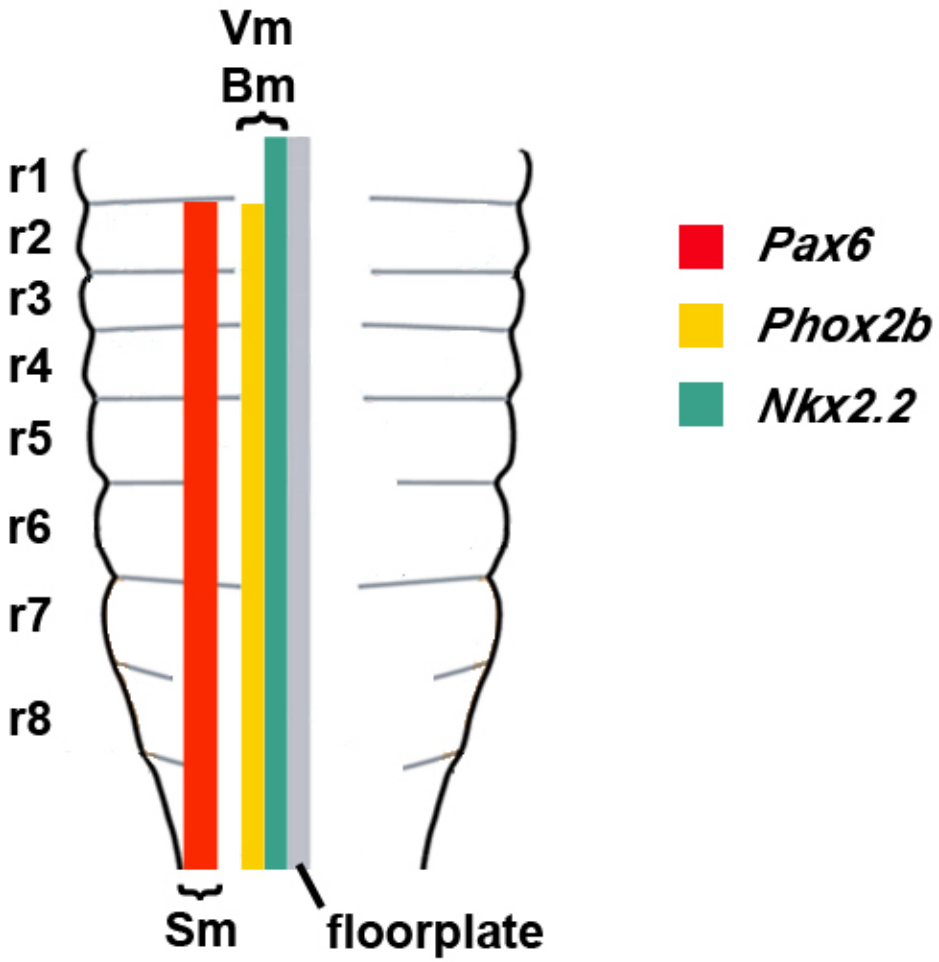

Figure 1.2 Specification of motor neuron type in the hindbrain.

The expression of key transcriptional factors for the determination of motor neuron types in the mouse E10.5 hindbrain. Pax6 is expressed in the domain where somatic motor (sm) neurons are born. *Phox2b* is expressed in the domains where visceral motor (vm) and branchiomotor (bm) neurons are born. Expression of these genes is essential for the specification and development of the different motor neuron types. *Nkx2.2* is expressed in the same domain as *Phox2b*. Adapted from (Cordes, 2001).

1.1.2 Facial branchiomotor (FBM) neurons

1.1.2.1 Neuronal migration

In the early nineteenth century Santiago Ramon y Cajal and Wilhelm His used histology on embryonic brains to describe the migration of neurons in along glial guide cells (reviewed in (Sidman and Rakic, 1973; Bentivoglio and Mazzarello, 1999). Neuronal migration can occur in two axes in the CNS, radial and migration. Radial migration takes place in an apical-basal direction and many neurons use radial glial as guide cells. The correct development and layering of the cerebral cortex is dependent on radial migration (Hatten, 1999). Tangential migration occurs along the dorsa-ventral axes. One example of tangential migration involves the migration of interneurons migrated form the cerebral cortex to the olfactory bulb, and from the ganglionic eminences into the cortex (Marin et al., 2010).

1.1.2.2 FBM neuron development

The FBM neurons are a powerful model to study neuronal migration and axon guidance in the hindbrain. FBM neurons are born on the ventricular side of the hindbrain at the r4 level and their axons form the facial nerve. The cell bodies of FBM neurons migrate caudally and laterally, away from the floor plate, to form one facial nucleus on each side of the midline at r6 level in mice, and r6/7 level in zebrafish (reviewed by (Chandrasekhar, 2004; Wanner et al., 2013). In chicks, the migration of FBM neurons is negligible (Jacob and Guthrie, 2000), although when a chick r4 is transplanted into the mouse, the chick r4-derived FBM neurons migrate into mouse r5/6 (Studer, 2001). FBM axons exit the hindbrain through r4 and as cell bodies continue to migrate the motor axons are positioned along the migratory stream. During their caudal migration, mouse FBM neurons first move along the ventricular surface (Figure 1.3), while in zebrafish initial caudal migration is influenced by the laminin rich r4/5 boundary, which briefly changes the orientation of migration towards the pial surface (Grant and Moens, 2010). After caudal migration is completed, FBM neurons in mice also migrate radially from the

ventricular to the pial side of the hindbrain where they reach their final location (Figure 1.3).

1.1.2.3 Molecular control of FBM neuron migration in mice

FBM neuron migration is regulated by several growth factors with chemoattractive effects (summarised in Table 1.1). For example, vascular endothelial growth factor (VEGF-A) signalling through neuropilin 1 (NRP1) guides FBM neurons from r4 to r6 in the mouse hindbrain. FBM neurons normally migrate in an organised stream and form paired nuclei on each side of the midline on the pial side of the hindbrain, but in *Nrp1*-null mice they migrate in disorganised streams and form misplaced, dumbbell shaped nuclei (Schwarz et al., 2004). Consistent with a role in chemoattraction, *Vegfa* is expressed in r6 where the facial nuclei form, and $VEGF_{164}$-soaked beads attract migrating FBM neurons in a hindbrain explant assay (Schwarz et al., 2004). VEGF expression at the final destination may also promote motor neuron survival, but this has not yet been demonstrated formally. The finding that the class 3 semaphorin *Sema3a*$^{-/-}$ mice show normal FBM migration, whilst *Vegfa*$^{120/120}$ mice lacking $VEGF_{164}$ phenocopy the FBM defects seen in *Nrp1*-null mice suggests that VEGF is the NRP1 ligand that controls FBM migration (Schwarz et al., 2004). In contrast, the same study shows that SEMA3A, but not $VEGF_{164}$ signalling through NRP1 is required for correct facial nerve guidance. The extracellular matrix protein reelin, which is known to control radial migration (reviewed by (Zhao and Frotscher, 2010) resulting in inverted neuronal layers (Caviness and Sidman, 1973; D'Arcangelo et al., 1995) and is also expressed at the final target of migrating FBM neurons. Mice null for *reelin* or its receptor *Dab1* also have FBM neuron migration defects and form abnormal facial nuclei (Rossel et al., 2005).

WNTs also have an important chemoattractive function during FBM neuron migration, and several components of the planar cell polarity (PCP) have been implicated in FBM neuron migration. The PCP pathway is responsible for the inducing an orientation/polarity in cells that is perpendicular to the apical-basal axis, and consequently very important for cell movement/migration and tissue

morphogenesis (reviewed in (Axelrod and McNeill, 2002). *Wnt5a* is expressed in the hindbrain during FBM neuron migration in a rostral-caudal gradient-like pattern where expression increases from r4 to r6 (Vivancos et al., 2009). Moreover, beads soaked in WNT5A or WNT7A attract migrating FBM neurons in a hindbrain explant assay. Interestingly, mice null for *Wnt5a* or its receptor *Frizzled 3* (*Fz3*) have defective FBM neuron migration, while FBM neurons migrate normally in *Wnt7a* mutants (Vivancos et al., 2009). Furthermore, the same study showed that the cytoplasmic protein SCRB1 and the membrane protein VANGL2, two components of the WNT/PCP pathway, are also required during FBM neuron migration (Vivancos et al., 2009). In *Scrib1* mutants FBM neurons fail to migrate out of r4, and in two different *Vangl2* mouse mutants FBM neurons were unable to migrate caudally (Vivancos et al., 2009; Glasco et al., 2012).

The atypical cadherins CELSR1-3, part of the PCP signalling pathway, are also important for FBM neuron migration. CELSR1 is expressed in neuronal precursors but not migrating FBM neurons, while CELSR2 and CELSR3 are expressed more broadly in the hindbrain. FBM neurons in *Celsr1* mutant mice fail to migrate caudally and remain in r4 or sometimes migrate into r3/2 (Qu et al., 2010). Moreover, *Celsr2* single and *Celsr2*;*Celsr3* double mutants show early and excessive lateral migration of FBM neuron around r5/6 (Qu et al., 2010). These defects are very similar to those observed in *Fz3*-null mice, another integral part of the PCP pathway.

Several signalling molecules have been associated with FBM migration, and yet the downstream signal transducers controlling the cytoskeleton changes required for migration have not been fully characterised. Mice carrying a mutation in non-muscle myosin heavy chain (NMHCIIB) have abnormal FBM neuron migration as a consequence of defective actomyosin contractility (Ma et al., 2004). In these mutants, the facial nuclei form as protrusions in the 4th ventricle. Furthermore, some downstream effectors of the PCP pathway, important for cytoskeletal control, have also been shown to play a part in FBM neuron migration. Inhibitors of ROCK, JNK and Myosin II induce abnormal migration of FBM neurons in a hindbrain explant assay (Vivancos et al., 2009).

1.1.2.4 Molecular control of FBM neuron migration in zebrafish

FBM neuron migration in zebrafish differs to mice but several PCP pathway components have also been shown to be important during zebrafish FBM neuron migration (summarised in Table 1.1) (Wanner et al., 2013). Similar to mice, *Celsr2* and *Fz3a* are also required for distinct functions during FBM migration. Both genes are expressed in the neuroepithelium, which maintains FBM neurons migrating along the pial surface of the hindbrain. Mutations these genes result in abnormal caudal and radial FBM migration (Wada et al., 2006). Knockdown of *Prikle1b* leads to defective FBM neuron polarisation, which results in abnormal cell protrusions and an aberrant axis of cell elongation both necessary during directed migration (Mapp et al., 2010). Zebrafish *Vangl2* mutants (*trilobite*) are also unable to maintain stable cell protrusions, which results in abnormal FBM neuronal caudal migration (Jessen et al., 2002). *Nshl1b* is expressed in FBM neuron membrane protrusions and interacts with *Prickle1b*. Mutations in *Nshl1b* leads to defective caudal migration through a cell autonomous function interacting with other components of the PCP pathway (Walsh et al., 2011).

Moreover, additional signalling pathways, including SDF1/CXCR4/CXCR7 and MET/HGF1/HGF2, are important during FBM migration in zebrafish, but have not yet been described to have a role in mouse (Sapede et al., 2005; Cubedo et al., 2009; Elsen et al., 2009). Knockdown of *Sdf1a*, *Cxcr4* or *Cxcr7* leads to varying levels of defective FBM neuron caudal migration (Sapede et al., 2005; Cubedo et al., 2009). *Hgf1* or *Hgf2* single knockdown also results in abnormal caudal migration, whilst simultaneous knockdown of both genes (*Hgf1*/*Hgf2*) leads to almost complete failure of FBM neurons to migrate caudally (Elsen et al., 2009).

Zebrafish FBM neuron migration requires 'pioneer' neurons and their trailing axons to lead the bulk of migrating FBM neurons (Wanner and Prince, 2013). Using laser ablation techniques, researchers showed that without this FBM neuron 'pioneer' population, other FBM neurons are unable to migrate out of r4 into r5. The later stage of FBM neuron migration from r5 to r6 depends on a physical interaction between migrating neurons and the medial longitudinal fasciculus (MLF), a bundle of axons that extends alongside FBM neurons (Wanner and Prince, 2013). The adhesion molecule CDH2 (N-cadherin) is essential for the cell-cell interactions

between FBM neurons and both the ‘pioneer’ neurons and the MLF (Wanner and Prince, 2013). Unfortunately, the type of live imaging experiments performed in the zebrafish to demonstrate the role of the pioneer population are difficult to perform in the mouse. Therefore, the pioneer model has not yet been tested in the mouse.

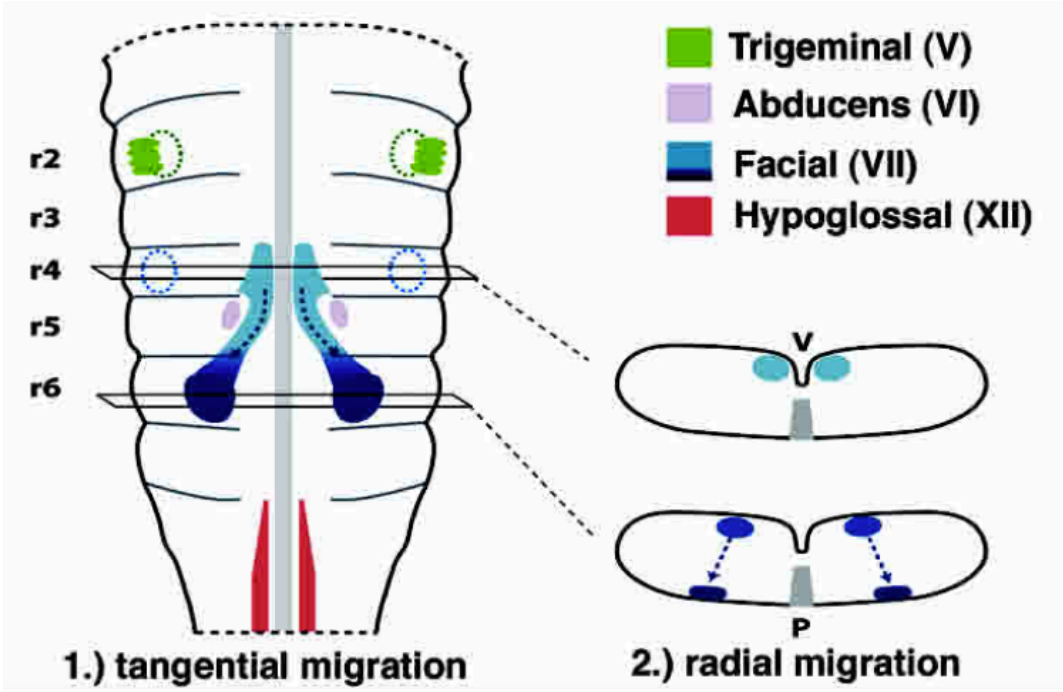

Figure 1.3 Migration of FBM neurons in the hindbrain.

Schematic representation of a E12.5 hindbrain showing the position of the trigeminal (V), abducens (VI), hypoglossal (XII) and facial (VII) motor nuclei. The schematic shows the two stages of FBM migration, tangential and radial migration. During tangential migration, FBM neurons move from r4 to r6 along the ventricular side (v); when they reach r6, they migrate radially from the ventricular to the pial (p) side of the hindbrain. The diagram on the right is a transverse section through the hindbrain. Dotted lines show exit point for trigeminal and facial axons. Adapted from (Schwarz et al., 2004).

Gene/molecule	Animal/Experiment	Phenotype (reference)
Nrp1/*Vegfa*	Mouse KO and hindbrain explants	Defective FBM neuron radial migration leading to dumbbell shaped facial nucleus. $VEGF_{164}$ or $VEGF_{188}$ soaked beads attract migrating FBM neurons in hindbrain explants (Schwarz et al., 2004; Tillo et al., 2015).
Dab/*reelin*	Mouse KO	Disorganise and scattered facial nucleus (Rossel et al., 2005).
Wnt5a Wnt7a Fz3	Mouse KO and hindbrain explants	*Wnt5a* and *Fz3* knockout mice have defective FBM neuron migration. Wnt5a or Wnt7a soaked beads attract migrating FBM neurons in hindbrain explants (Vivancos et al., 2009).
Vangl2	Mouse KO	FBM neurons fail to migrate from r4 (Vivancos et al., 2009; Glasco et al., 2012).
Scrib1	Mouse KO; Zebrafish mutants	Defective FBM neuron caudal migration (Wada et al., 2005; Vivancos et al., 2009).
Celsr1-3	Mouse KO	$Celsr1^{-/-}$ mice fail to migrate from r4. $Celsr2^{-/-}$ and $Celsr2^{-/-};Celsr3^{-/-}$ show uncontrolled lateral migration around r5/6 (Qu et al., 2010).
NMHCIIB	Mouse KO	Reduced size of facial nucleus and nucleus forms as a protrusion in the 4th ventricle (Ma et al., 2004).
Hgf1/2	Zebrafish Morpholino	Defective caudal migration, most neurons

	knockdown	fail to migrate in *Hgf1/2* double knockdown. Milder phenotype in single knockdown (Elsen et al., 2009).
Cdh2	Zebrafish Morpholino knockdown and mutants	FBM neurons fail to migrate out of r4. Occasionally there is fusion of FBMs at the midline (Stockinger et al., 2011).
Cxcr4 Cxcr7 Sdf1a	Zebrafish Morpholino knockdown	*Sdf1a* knockdown leads to defective caudal migration. *Cxcr4* knockdown also leads to defective caudal migration with neurons spread over r4-6. *Cxcr7* knockdown neurons cluster in r5. *Cxcr7/Cxcr4* double knockdown leads also to clustering around r4-5. (Sapede et al., 2005; Cubedo et al., 2009).
Dcsh1/Fat4	Mouse KO	Defective polarity and tangential migration of FBM neurons. (Zakaria et al., 2014).
Lamininα1	Zebrafish mutants	Defective caudal migration. Some neurons exit the neuroepithelium through the basement membrane (Paulus and Halloran, 2006).

Table 1.1 Mutations affecting facial branchiomotor neuron development

1.2 MOLECULAR CONTROL OF CNS PATTERNING

1.2.1 Vascular endothelial growth factor (VEGF)

1.2.1.1 VEGF family

The vascular endothelial growth factor (VEGF) family of secreted glycoproteins includes cysteine knot proteins that are termed VEGF-A, VEGF-B, VEGF-C, VEGF-D and PGF (PlGF) (Ferrara et al., 2003). The VEGFs are best known as growth and patterning factors for blood vessels and lymphatic vessels. In addition, they are important for neuronal development. For example, VEGF-C regulates murine neurogenesis as well as axon guidance, and it can also act as a neurotrophic factor (Calvo et al., 2011; Piltonen et al., 2011; Kwon et al., 2013). VEGF-A, the most widely studied family member, is essential for blood vascular development, but also regulates neuronal migration, birth, survival and axon guidance (e.g. (Jin et al., 2002; Zhu et al., 2003; Schwarz et al., 2004; Cariboni et al., 2011; Erskine et al., 2011; Mackenzie and Ruhrberg, 2012)**.**

1.2.1.2 VEGF-A isoforms

VEGF-A exists in several different isoforms that arise through alternative splicing of the *VEGFA* gene, which comprises 8 exons (Tischer et al., 1991). This splicing results in the inclusion or exclusion of exons 6 and/or 7, which encode domains that enhance binding to heparin *in vitro* and heparan sulfate proteoglycans *in vivo* (Figure 3.1; (Houck et al., 1991; Park et al., 1993). The major and most studied human isoforms are $VEGF_{189}$, $VEGF_{165}$ and $VEGF_{121}$, whilst their murine homologues, encoded by the *Vegfa* gene, are one aa shorter and termed $VEGF_{188}$, $VEGF_{164}$ and $VEGF_{120}$ (Figure 1.4). Due to their varying ability to bind heparin in the extracellular matrix (ECM), the VEGF isoforms are differentially distributed in the environment. The longest isoforms $VEGF_{189}$ is found bound to the ECM and therefore poorly diffusible, whilst $VEGF_{121}$ is very diffusible and $VEGF_{165}$ has intermediate characteristics, and this property allows them to form growth factor gradients (Park et al., 1993; Ruhrberg et al., 2002).

Furthermore, in cooperation with the exon 8-encoded domain, the exon 6/7-encoded domains are also essential for binding to the non-tyrosine kinase receptors of the neuropilin family, NRP1 and NRP2 (Soker et al., 1998; Gluzman-Poltorak et al., 2000). The sequence for $VEGF_{165}$ contains both exons 7 and 6, which enables high affinity binding to NRP1 (Gluzman-Poltorak et al., 2000; Parker et al., 2012). $VEGF_{189}$ is also predicted to bind NRP1, given that it contains the exon 7 and 8 domains (Vintonenko et al., 2011), but prior to my PhD research, this not yet been demonstrated *in vivo*. Even though $VEGF_{121}$ does not contain exons 6 or 7, it still maintains the exon 8 domain, but it can only weakly interact with NRP1, resulting in a low affinity of NRP1 for $VEGF_{121}$ *in vitro* (Jia et al., 2006; Parker et al., 2012). Accordingly, $VEGF_{121}$ is not believed to bind NRP1 with high specificity, although this idea has been contested in one *in vitro* study using cultured endothelial cells (Pan et al., 2007). As part of my aims, I have investigated further the NRP1 binding properties of the major VEGF isoforms, and my results are discussed in detail in Chapter 3.

1.2.1.3 Receptor kinase receptors for VEGF-A

VEGF-A binds to two transmembrane tyrosine kinase receptors termed VEGFR1 (FLT1) and VEGFR2 (KDR, FLK1). VEGFR1 and VEGFR2 are transmembrane glycoproteins of 180 and 200 kDa, respectively. The role of these receptors has been mainly described in the context of vascular development, and mice lacking either VEGFR1 or VEGFR2 are embryonic lethal around E8.5 (Fong et al., 1995; Shalaby et al., 1995). VEGFR2 can also be recruited into plexin/neuropilin receptor complexes to modulate signalling response induced by semaphorins in neurons (Bellon et al., 2010).

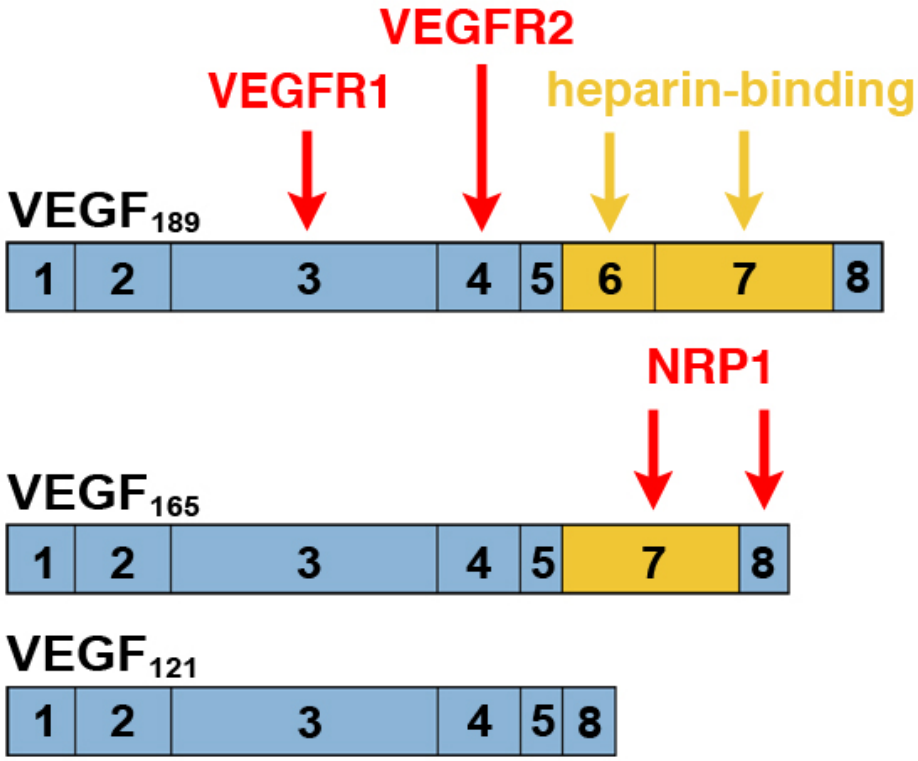

Figure 1.4 Major human VEGF-A isoforms and receptors.

The *Vegfa* gene encodes can be alternatively spliced and encodes for 3 major isoforms termed $VEGF_{189}$, $VEGF_{165}$ and $VEGF_{121}$ in humans. This diagram indicated the number of exons in each isoform. The yellow section indicates the VEGF exons that can promote binding to heparin *in vitro* and heparin sulfate proteoglycans (HSPGs) *in vivo*. Red arrows indicate specific sites for receptor binding. The VEGF specific tyrosine kinase receptors VEGFR1 and VEGFR2 can bind to all isoforms through exons 3 and 4 respectively. The non-tyrosine kinase receptor Neuropilin 1 (NRP1) is known to bind $VEGF_{165}$ through its heparin binding domains and exon 8, whilst it is still not known if it can also bind $VEGF_{189}$.

1.2.2 Semaphorins and neuropilins

1.2.2.1 Semaphorins

The semaphorins (SEMA) belong to a large family of glycoproteins that includes both secreted and membrane-bound forms; they are categorised into 8 classes, with invertebrates using classes 1, 2 and 5 and vertebrates using classes 3-7 (Zhou et al., 2008) To convey their signals, semaphorins bind transmembrane receptors of the plexin (PLXN) family or composite receptors consisting of a plexin as a signal transducing and a neuropilin as a ligand-binding co-receptor. Although initially discovered due to their function as chemorepellents in axon guidance (He and Tessier-Lavigne, 1997; Kolodkin et al., 1997), members of the semaphorin classes 1, 3, 4 and 5 have also been implicated in dendrite patterning (Polleux et al., 2000), vascular growth and function (Arese et al., 2011) and synapse development (Tran et al., 2009; Tillo et al., 2012).

1.2.2.2 Neuropilins

The interaction of VEGF-A with the single transmembrane protein NRP1 was initially identified in human umbilical vein derived endothelial cells (HUVEC) (Gitay-Goren et al., 1996) and later in tumour cell lines (Soker et al., 1998). Interestingly, at this time, NRP1 had already been identified in the nervous system as an adhesion protein (Takagi et al., 1987) and as receptor for the class 3 semaphorin family (He and Tessier-Lavigne, 1997; Kolodkin et al., 1997). A second member of the neuropilin family was identified later and termed NRP2 (Chen et al., 1997). NRP2 shares 44% homology at the aa level with NRP1 and has a similar domain structure comprised of a large N-terminal extracellular domain (835 aa for NRP1, 844 for NRP2), a short membrane-spanning domain (23 aa for NRP1, 25 for NRP2) and a small cytoplasmic domain (44 aa for NRP1, 42 for NRP2).

The neuropilin extracellular part contains two coagulation factor V/VIII homology domains, termed b1 and b2, and they mediate binding to different members of the VEGF family (Figure 1.5). Both neuropilins can bind VEGF-A, but NRP1 has a much higher affinity than NRP2 for VEGF-A. Whilst NRP1 is a receptor

for SEMA3A, NRP2 preferentially binds SEMA3F (Chen et al., 1997; He and Tessier-Lavigne, 1997; Kolodkin et al., 1997; Gluzman-Poltorak et al., 2000).

The neuropilin extracellular part contains two complement-binding homology domains, termed a1 and a2, which are essential for binding to the SEMA domain present in all members of the semaphorin family. The cytoplasmic neuropilin tail contains a PDZ-domain binding motif; in the case of NRP1, this motif binds synectin (GIPC1), which bridges NRP1 and a myosin 6-driven cell transport machinery for endocytic trafficking (Figure 1.5) (Lanahan et al., 2010; Schwarz and Ruhrberg, 2010; Lanahan et al., 2013; Raimondi and Ruhrberg, 2013).

Due to the variety of structural domains present on both sides of the cell membrane that allow neuropilins to interact with several ligands, they are able to modulate a number of different signalling pathways to control neuronal and vascular cell behaviour.

Different hypotheses exist for how NRP1 acts in endothelial cells: it was originally proposed to enhance VEGFR2 affinity for $VEGF_{165}$ (Whitaker et al., 2001) and promote VEGFR2 clustering (Soker et al., 2002), but current research is focused on its role in VEGFR2 trafficking by endocytosis (Salikhova et al., 2008; Lanahan et al., 2013). All models agree that $VEGF_{165}$ binding to NRP1 promotes complex formation between NRP1 and VEGFR2 via a $VEGF_{165}$ bridge. This pathway appears to be particular important for arteriogenesis (Lanahan et al., 2013). Mice lacking the NRP1 cytoplasmic domain ($Nrp1^{cyto/cyto}$) do not have general defects in assembling blood vessel networks, with the exception of a subtle arteriovenous patterning defect in the developing retina (Fantin et al., 2011) and impaired VEGFR2-dependent arteriogenesis due to abnormal VEGFR2 trafficking (Lanahan et al., 2013). Whether the cytoplasmic tail of NRP1 might signal in neural development has so far only been explored in gonadotropin hormone releasing hormone (GnRH) neurons; in these cells, $VEGF_{164}$ signalling through NRP1 enhances survival independently of VEGFR2 through an unknown co-receptor, and the NRP1 cytoplasmic tail does not appear to play a role in this process (Cariboni et al., 2011). NRP1 also promotes angiogenesis through unknown adhesion ligands in a VEGF-independent pathway, but the role of this pathway in neuronal development remains to be defined (Shimizu et al., 2000; Raimondi et al., 2014).

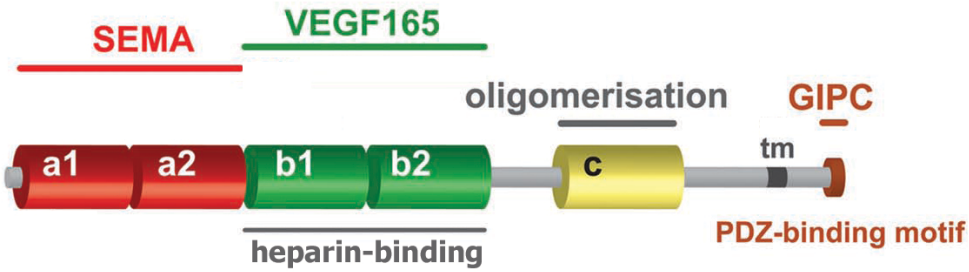

Figure 1.5 Neuropilin 1 structure and ligand binding.

SEMA3A can bind NRP1 through a1/a2 domains whilst $VEGF_{165}$ can bind through b1/b2 domains. The b1/b2 domain is also available for heparin binding. The cytoplasmic domain of NRP1 contains a sequence of 3 amino acids that allows the binding of the protein GIPC/Synectin through its PDZ-binding motif. Adapted from (Schwarz and Ruhrberg, 2010).

1.2.3 Neuropilin and VEGF-A signalling in the vascular system

1.2.3.1 Vascular development

During development the cardiovascular system is the first organ system to assemble in vertebrates. A cardiovascular system is essential to provide other organs with blood and nutrients during development (Risau and Flamme, 1995). Initially vessels are assembled from single cell precursors in a process termed vasculogenesis. These single blood vessels then begin to sprout through filopodia processes and lead to the formation of a complex vascular plexus network in a process termed angiogenesis (Ruhrberg, 2003; Carmeliet, 2005). Vessel sprouts are made up of endothelial stalk cells, which proliferate and form the lumen of blood vessels, and endothelial tip cells, which guide the growing sprouts (Gerhardt et al., 2003).

VEGF signals through NRP1 and VEGR2 complexes to control different aspects of vascular development. VEGF requires VEGFR2 for a wide variety of functions during vascular development such as promoting survival, proliferation and migration of endothelial cells (Clauss et al., 1990; Praloran et al., 1991; Guerrin et al., 1995). VEGR2 mutants are embryonic lethal as they are unable to form blood vessels through vasculogenesis early in development (Shalaby et al., 1995). Following vasculogenesis, VEGR2 is important during angiogenesis to sense a concentration of diffusing VEGF and promote the extension of tip cell filopodia (Figure 1.6) (Ruhrberg et al., 2002; Gerhardt et al., 2003).

During angiogenesis NRP1 is expressed in endothelial cells as well as in other cell types including tissue macrophages and neural progenitors that secrete VEGF in the brain (Figure 1.6) (Haigh et al., 2003; Fantin et al., 2010; Fantin et al., 2013). NRP1 mutant mice have reduced vessel growth and are embryonic lethal, whilst overexpressing NRP1 results in increased vessel growth, leakiness of vessels and also embryonic lethality (Kitsukawa et al., 1995; Kawasaki et al., 1999). Defective vessel sprouting and vessel patterning has also been observed in zebrafish knockdown of NRP1 homologues (*Nrp1a*; *Nrp1b*) (Lee et al., 2002; Martyn and Schulte-Merker, 2004). NRP1 and VEGFR2 form complexes in cultured endothelial cells for the binding of $VEGF_{165}$ (Whitaker et al., 2001; Soker et al., 2002). However, genetic experiments demonstrate that NRP1 is essential during sprouting

angiogenesis to control tip cell filopodia whilst it does not play a role in cell proliferation (Figure 1.6) (Fantin et al., 2013).

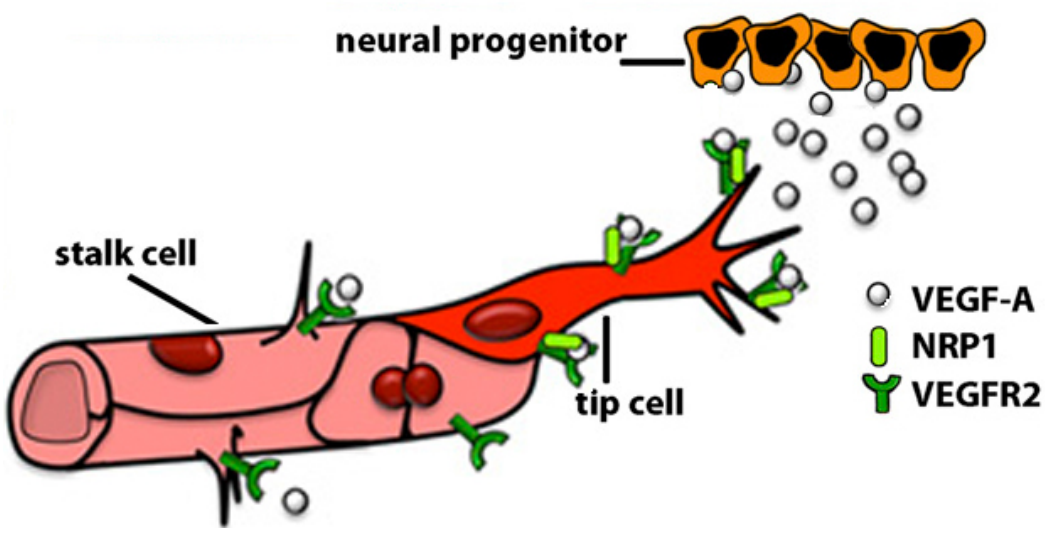

Figure 1.6 NRP1 and VEGR2 distribution and function in the brain during angiogenesis

VEGFR2 is expressed in stalk and tip cells whilst NRP1 is only expressed in tip cells. Neural progenitors secrete VEGF-A, which is required for both tip cell extension (signalling via NRP1+VEGR2 complex) and stalk cell proliferation (signalling via VEGR2). Adapted from (Fantin et al., 2013).

1.2.4 Neuropilin and semaphorin signalling in the nervous system

1.2.4.1 Axon guidance

One of the crucial mechanisms available to modulate a wide variety of neuronal responses is the idea that a small number of ligands act through a large combination of receptors and co-receptors. For example, individual semaphorins have differential affinities for NRP1 and/or NRP2, and both receptors have preferential interactions with members of the signal-transducing plexin family. Thus, several different semaphorin-plexin-neuropilin ternary signalling complex combinations act in axonal growth cones to modulate attraction and repulsion during axon path finding (Zhou et al., 2008).

A variety of neuron subtypes in the developing CNS have been used to study the function of these combinations. SEMA3C can bind both neuropilins in axons projecting from neurons in the dorsal root ganglia (Takahashi et al., 1998). However, other class 3 semaphorins bind preferentially to either NRP1 or NRP2. Thus, SEMA3A predominantly binds to NRP1, whilst axons expressing NRP2 more typically respond to SEMA3F (Kitsukawa et al., 1997; Taniguchi et al., 1997; Chen et al., 2000; Giger et al., 2000; Sahay et al., 2003). Interestingly, in the case of spinal motor neurons, the SEMA3A/NRP1 and SEMA3F/NRP2 pathways cooperate to control axon pathfinding. In this case, the fasciculation of lateral motor column (LMC) nerve axons and their timing of limb invasion are regulated by SEMA3A/NRP1 signalling, whereas SEMA3F/NRP2 signalling guides a medial subset of LMC axons into the ventral compartment of the limb (Huber et al., 2005).

Neuropilins also preferentially recruit certain plexin co-receptors. Most commonly, PLXNA4 is co-receptor for NRP1 for axon sensing of SEMA3A, whilst PLXNA3 interacts mainly with NRP2 to mediate SEMA3F signalling (Cheng et al., 2001; Suto et al., 2005; Yaron et al., 2005). For example, axons from the visceromotor branch of the facial nerve (FVM) are organised by SEMA3A signalling through the NRP1/PLXNA4 complex (Chauvet et al., 2007; Schwarz et al., 2008), whereas, axon pruning in the infrapyramidal tract is regulated by SEMA3F signalling through NRP2/PLXNA3 (Giger et al., 2000; Cheng et al., 2001; Bagri et al., 2003; Sahay et al., 2003). Both mechanisms may synergistically pattern other neuronal subtypes, as disruption of either the SEMA3A/NRP1/PLXNA4 or the

SEMA3F/NRP2/PLXNA3 complex causes fasciculation and guidance defects of cranial nerves (Chauvet et al., 2007; Schwarz et al., 2008). Moreover, the combined loss of both plexins causes a significantly more severe phenotype, suggesting that SEMA3A and SEMA3F cooperate to regulate cranial nerve development (Chauvet et al., 2007; Schwarz et al., 2008).

In addition to the typical preference of NRP1 for PLXNA4 and NRP2 for PLXNA3 (Giger et al., 2000; Sahay et al., 2003), other combinations also occur, as demonstrated by the analysis of trochlear axon patterning (Yaron et al., 2005). In this system, axons are guided by SEMA3F/NRP2 signalling, but PLXNA4 can compensate for the loss of PLXNA3, and only the combined loss of both plexins recapitulates the guidance defects observed in *Sema3f*-null mice (Yaron et al., 2005).

SEMA3E is the only class 3 semaphorin known to bind directly to a plexin, PLXND1, without requiring a neuropilin as a ligand-binding subunit (Gu et al., 2005). Thus, the axons of striatonigral and corticofugal neurons are repelled by SEMA3E via PLXND1 signalling (Chauvet et al., 2007). However, NRP1 can still bind to the receptor complex, which can alter the axon response to SEMA3E. The extracellular domains of NRP1 and PLXND1 are able to associate, and this interaction is required for NRP1 to convert SEMA3E/PLXND1-mediated repulsion into attraction (Chauvet et al., 2007). Specifically, SEMA3E attracts subiculo-mammilary axons expressing both PLXND1 and NRP1, which project from the hippocampus to the hypothalamus (Chauvet et al., 2007).

Even though SEMA3 signalling through neuropilins is best known for roles in axon repulsion, some SEMA3 proteins elicit chemoattractive responses. The ability to stimulate either axon repulsion or attraction was initially demonstrated for different compartments of the same neuron; thus, SEMA3A functions as a chemorepellent for their axons but have chemoattractive functions for the apical dendrites of cortical pyramidal neurons (Polleux et al., 2000). Furthermore, SEMA3F can also act as a chemoattractant for cerebellar granule sprouting axons (Ding et al., 2007). In both situations, increased intracellular cyclic GMP levels are believed to convert repulsive into attractive responses (Polleux et al., 2000).

1.2.4.2 Neuronal migration

Semaphorin signalling through neuropilins can also guide migrating neuronal subtypes both during tangential or radial migration (MarÌn and Rubenstein, 2003; Tamamaki et al., 2003; Chen et al., 2008; Ito et al., 2008).

The progenitors of GABAergic cortical interneurons migrate tangentially from the ganglionic eminence, where they are generated, around the striatum and into the cortex (Tamamaki et al., 2003). Both SEMA3A and SEMA3F are expressed in the developing striatum, and this region contains excess neurons in *Nrp2*-null embryos, suggesting a role for semaphorin signalling in their migration. Due to early embryonic lethality of *Nrp1*-null mutants, a dominant negative form of NRP1 was used to show impairment in the migration of cortical interneurons in a similar manner to NRP2 loss (Tamamaki et al., 2003). In addition, both neuropilins are involved in positioning cortical interneurons within the correct layer of the embryonic cortex (Tamamaki et al., 2003). SEMA3F signals through NRP2-expressing interneurons to guide them dorsally into the intermediate zone, whilst SEMA3A guides NRP1-expressing interneurons into the more medial layers of the subplate and cortical plate (Tamamaki et al., 2003).

NRP1 also plays a key role in the organisation of the mammalian cortex, which relies on radial migration of cortical neurons. In contrast to its repulsive role for other types of migrating neurons, SEMA3A is a chemoattractant for migrating cortical neurons (Chen et al., 2008). Knockdown of NRP1 impairs the migration of cortical neurons to the outer layers of the cortex, in a process that requires PLXNA2 and PLXNA4 to act as co-receptors (Chen et al., 2008). Cortical neurons also fail to extend neurites correctly in the *Nrp1*-null brain, raising the possibility that migration and projection rely on similar downstream signalling transduction pathways (Polleux et al., 2000; Chen et al., 2008).

Semaphorin signalling through neuropilins also guides the tangential migration of lateral olfactory tract neurons across the telencephalon. Thus, lateral olfactory tract neurons migrate towards the ganglionic eminence and then change direction and spread laterally along the interface between the cortex and ganglionic eminence to guide lateral olfactory tract axons (Ito et al., 2008). The mantle layer of the ganglionic eminence expresses SEMA3F, and in *Sema3f*$^{-/-}$ mice many lateral

olfactory tract neurons continue to migrate ectopically towards the ganglionic eminence and do not adopt the lateral migratory path (Ito et al., 2008).

1.2.5 Neuropilin and VEGF-A signalling in the nervous system

1.2.5.1 Axon guidance

NRP1 was also found to regulate axon guidance in the CNS, where it promotes the growth of retinal ganglion cell (RGC) axons across the diencephalic commissure known as the optic chiasm (Erskine et al., 2011). In this system, semaphorins do not play any role in axon guidance. Instead, VEGF-A promotes the growth of RGC axons to project contralaterally across the optic chiasm (Erskine et al., 2011). For this guidance event to proceed correctly, VEGF-A is expressed at the chiasm midline, and RGCs destined to project contralaterally express NRP1 (Erskine et al., 2011). Thus, *Nrp1*-null and $Vegfa^{120/120}$ mice that express only the non-NRP1 binding $VEGF_{120}$ at the expense of other isoforms have excessive ipsilateral projections in the optic chiasm. Furthermore, the NRP1-binding isoform $VEGF_{165}$ stimulates extension and turning of cultured RGC axons (Erskine et al., 2011). VEGF signalling in the optic chiasm cooperates with other guidance systems. Thus, a small population of ipsilaterally projecting axons expresses the EphB1 receptor and is repelled by the ephrin B2 ligand at the optic chiasm (Nakagawa et al., 2000; Williams et al., 2003). Furthermore, SLITs are expressed around the diencephalon and act as axon chemorepellents through ROBO2 to define the boundaries through which RGC axons should travel to form the optic chiasm (Plump et al., 2002).

During spinal cord development, neurons in the dorsal spinal cord project their axons across the floor plate, which expresses attractive molecules such as Netrin and sonic hedgehog (SHH), and floor plate bone morphogenic proteins (BMPs) that are essential for axons to form a correct commissure (Kennedy et al., 1994; Augsburger et al., 1999; Charron et al., 2003). The floor plate also expresses VEGF, which signals as a chemoattractant to FLK1-expressing commissural axons (Ruiz de Almodovar et al., 2011). Thus, the floorplate-specific knockdown of *Vegfa* or the knockdown of *Flk1* in the spinal cord region where the commissural neurons originate caused defasciculation of the axons and they failed to cross the floorplate (Ruiz de Almodovar et al., 2011). Moreover, VEGF-induced axon attraction is blocked by FLK, but not NRP1 inhibition *in vitro* (Ruiz de Almodovar et al., 2011). The spinal cord commissural axons also require repulsive signals from SLITs to extend past the floor plate after crossing the midline (Long et al., 2004).

1.2.5.2 Neuronal migration

Even though facial axons require SEMA3A/NRP1 to extend correctly, $VEGF_{164}$ signals through NRP1 to control FBM neuron migration (section 1.1.2.3; (Taniguchi et al., 1997; Schwarz et al., 2004). VEGF also promotes the tangential migration of cerebellar granule cells from the external granule cells layer to the Purkinje cell layer (Ruiz de Almodovar et al., 2010). Thus, mice with hypomorphic levels of VEGF expression display delayed cerebellar granule cell migration, whilst ectopic expression of VEGF also disturbs migration, suggesting that VEGF gradients are important to guide these cells (Ruiz de Almodovar et al., 2010). The granule cells do not express either neuropilin, but FLK1; accordingly, mice with a granule cell specific knockout of *Flk1* have similar migration defects to those caused by disrupting VEGF levels, and anti-FLK1 treatment perturbs the guidance of their axons *in vitro* (Ruiz de Almodovar et al., 2010).

1.3 THE ROLE OF HSPG IN NERVOUS SYSTEM PATTERNING

1.3.1 Heparan sulfate proteoglycan structure

1.3.1.1 Heparan sulfate structure and core proteins

Heparan sulfate proteoglycans (HSPGs) are membrane-bound glycoproteins related to heparin. HSPGs are present in virtually all cells, whilst heparin is only released from connective tissue-type mast cells. Heparin is release at the site of vascular injury and made up of a Serglycin core protein. On the other hand, HSGPs consist of one core protein and at least one covalently linked HS chain and can have one of 17 different core proteoglycans that have been described to date (reviewed by (Kreuger and Kjellen, 2012; Xu and Esko, 2014). They are grouped into three main families of transmembrane-associated (syndecan 1-4, betaglycan, CD44v3), Glycosylphosphatidylinositol (GPI)-linked (glypican 1-6), and secreted (perlecan, agrin, collagen XVIII) HSPGs. The tissue-dependent expression of each core protein correlates with its physiological role. The structure of each HS chain is dependent on a wide number of specific modifying enzymes that are expressed in a cell specific manner. Altogether, these account for the huge diversity of potential HSPG isoforms (reviewed by (Lindahl and Hook, 1978; Hook et al., 1984; Iozzo, 1998; Esko and Lindahl, 2001; Esko and Selleck, 2002).

1.3.2 Heparan sulfate biosynthesis

1.3.2.1 Heparan sulfate chain initiation

Proteoglycans are an assorted class of glycoproteins composed of unbranched, long glycosaminoglycan (GAG) chains covalently bonded to a core protein serine residue. All GAGs share an initiating tetrasaccharide core, xylose-galactose-galactose-gluconic acid (Xyl-Gal-Gal-GlcA), which is common to chondroitin sulfate, heparan sulfate (HS), dermatan sulfate and heparin. Subsequently, disaccharides are added to this core to elongate the chain in patterns that are unique to each class of proteoglycans (Prydz and Dalen, 2000). HS is composed of repeating disaccharide units made up of uronic acid (GlcA, or *L*-iduronic acid (IdoA) and a glucosamine derivative (N-sulfated glucosamine (GlcNS), or N-acetylglucosamine (GlcNAc)).

1.3.2.2 Heparan sulfate chain polymerisation

A GlcNAc residue is first attached to one end of the initial tetrasaccharide structure by the exostosin-like (EXTL) family of glycosyltransferases, whereby three members of the EXTL family have the capacity to initiate HS polymerisation (Kim et al., 2001), although some studies using *Drosophila* and zebrafish have shown that EXTL3 is the primary enzyme required for this process *in vivo* (Han et al., 2004; Holmborn et al., 2012). Following the initial steps, the essential enzymes EXT1 and EXT2 polymerise the rest of the HS chain. Individually, the two exostosins have very low activity, thus require translocation from the endoplasmic reticulum to the Golgi apparatus where they function optimally as a heterodimer (McCormick et al., 2000; Senay et al., 2000). The EXT1/2 complex sequentially transfers GlcNAc and GlcA residues to elongate the HS chain (Lidholt and Lindahl, 1992).

1.3.2.3 Heparan sulfate chain modification

During polymerisation, the HS chain undergoes a number of modifications in the Golgi apparatus by epimerase and sulfotransferases. HS modifications must

occur in a particular sequence, evidence shows that the product of one reaction is a necessary substrate for the next modifying enzyme (Hook et al., 1975; Jacobsson and Lindahl, 1980; Riesenfeld et al., 1982a). The first and prerequisite modification to the HS chain is the removal of N-acetyl groups from selected GlcNAc residues and their replacement with sulfate. N-sulfation can only take place in N-deacetylated GAGs, hence N-deacetylation is key to maintain normal sulfation in HS (Riesenfeld et al., 1982a; Riesenfeld et al., 1982b). The four members of the family of N-deacetylase/N-sulfotransferase (NDST) modifiers carry out both reactions (Orellana et al., 1994; Aikawa and Esko, 1999; Aikawa et al., 2001). NDST1 has a lower ratio of N-deacetylase/N-sulfotransferase activity than NDST2 (Forsberg et al., 1999; Humphries et al., 1999), but both family members are ubiquitously expressed in tissues that have been implicated in HS formation (Kusche-Gullberg et al., 1998; Toma et al., 1998). In contrast, NDST3 is a more active N-acetylase, and NDST4 acts mostly as an N-sulfotransferase, and their expression pattern is restricted to specific tissues (Aikawa et al., 2001). The relative expression of each enzyme in a tissue-specific manner results in varying degrees of N-sulfation of the HS chain (Pikas et al., 2000).

Epimerases are responsible for an isomerisation reaction that leads to the change in position of two groups at a chiral carbon. A single C5-epimerase isomerises multiple *D*-GlcA residues that are attached to a GlcNS unit and turns them into the 5' epimer *L*-IdoA (Li et al., 1997). Epimerisation can lead to various IdoA conformations, which add another element of complexity to the HS structure and leads to varying ligand specificity. Epimerases do not modify *O*-sulfated GlcA, or any GlcA adjacent to *O*-sulfated GlcNS, suggesting these are active after NDST modifications, but before any *O*-sulfation (Hagner-McWhirter et al., 2000).

The ability of HSPGs to interact with other protein ligands is determined by the number of *O*-sulfate groups available (Kreuger and Kjellen, 2012). All of the *O*-sulfotransferases are expressed and function in a cell specific manner. The 2-*O*-sulfotransferase, encoded by a single gene (*Hs2st*), transfers a sulfate group to a C-2 in hexuronic acid residues. The enzyme prefers to sulfate IdoA, but can also transfer a sulfate group to GlcA. Most HS chains contain some amount of IdoA C-2-sulfated

residues, and the variable number of IdoA residues adds complexity to HSPG structure (Safaiyan et al., 2000; Wilson et al., 2002).

The next enzymes to modify HSPGs are the three members of the 6-*O*-sulfotransferase family (HS6ST). All three HS6STs have been shown to sulfate both GlcNAc and GlcNS (Smeds et al., 2003), although they have selective preferences for different uronic acid isomers attached to the target GlcNS (Habuchi et al., 2000; Jemth et al., 2003). Finally the seven members of the 3-O-sulftotransferase (HS3ST) family modify the structure of HSPGs (Kreuger and Kjellen, 2012). HS3STs modify HS motifs important for the interaction with other proteins, such as those in glycoprotein gD of the herpes simplex virus (Petitou et al., 2003), antithrombin (Petitou et al., 2003) and the chemokine cyclophilin B (Vanpouille et al., 2007).

Another family of HSPG modifiers are the heparan sulfate 6-*O*-endo-sulfatases (SULF). Sulfatases are extracellular enzymes that hydrolyse sulfates from the C-6 position of glucosamine, but before their discovery it was thought that HS structure was not changed after it localised to the cell surface (Nagamine et al., 2012). There are two members of this enzyme family, SULF1, which was first described in quail (QSULF1), and SULF2 (Dhoot et al., 2001; Morimoto-Tomita et al., 2002). Interestingly, they seem to have a similar role, but are expressed differently across cell types and generate organ-specific sulfation patterns in the mouse (Nagamine et al., 2012).

Altogether these modifications allow for huge heterogeneity in HSPG structure, and, accordingly, their expression is both spatially and temporally regulated depending on their role in specific physiological responses (Lindahl et al., 1998; Esko and Lindahl, 2001).

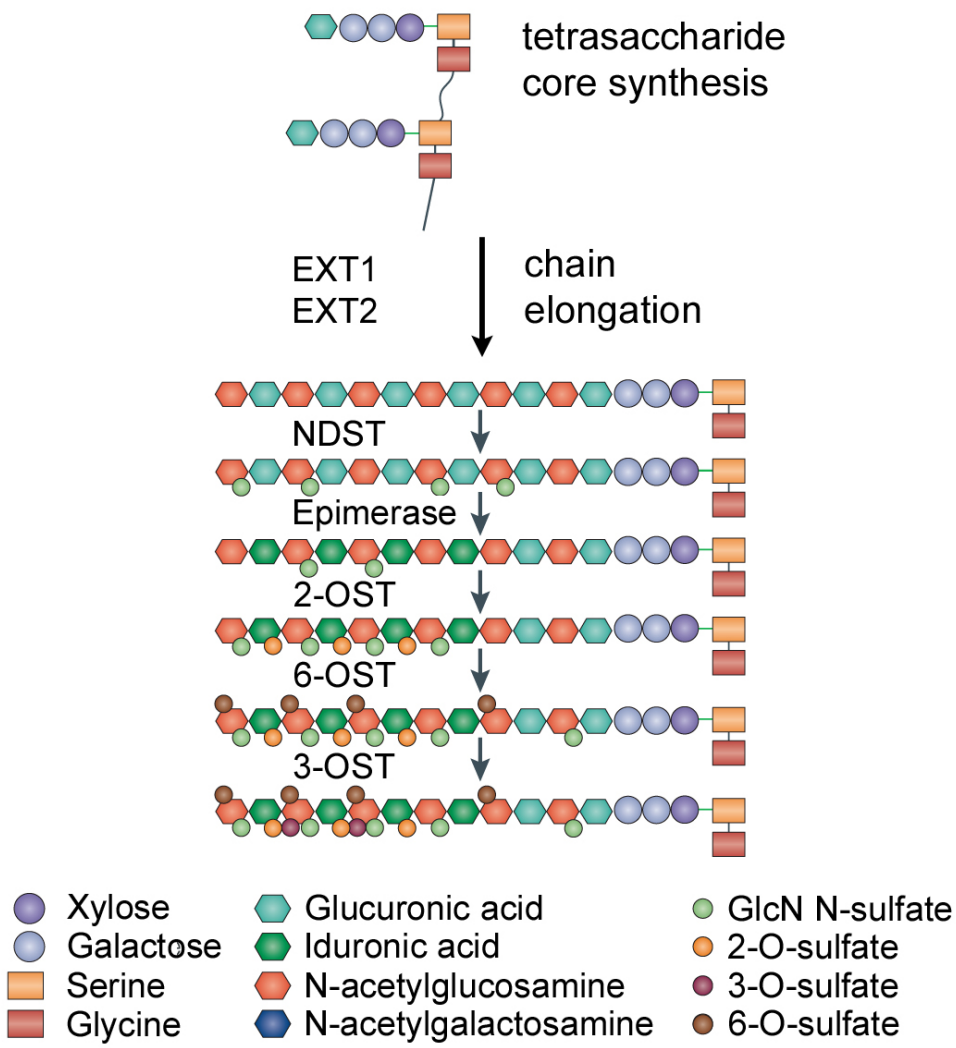

Figure 1.7 Heparan sulfate biosynthesis

In the first stage of heparan sulfate synthesis a tetrasaccharide linker (xylose-galactose-galactose-gluconic acid (Xyl-Gal-Gal-GlcA) is attached to a serine and a glycine residue. A functional EXT1-EXT2 dimer then elongates the sugar chain by adding GlcNAc and GlcA disaccharide elements. These chains are then modified by a number of processes including epimerisation and sulfations to synthesise a wide variety of HS. The order of modifications is not always sequential; some modifications are dependent on previous steps whilst others occur independently. Adapted from (Hacker et al., 2005).

1.3.3 HSPG gene targeting

1.3.3.1 Mutants targeting heparan sulfate core proteins

Various mouse models are available to study the role of HSPGs during development (summarised in Table 1.2). I will discuss below the phenotypes caused by null mutations. All *syndecan 1-4* (*Sdc*) knockout mice are viable after birth, but have various developmental defects (Alexander et al., 2000; Echtermeyer et al., 2001; Reizes et al., 2001; Li et al., 2002) (Professor Michael Simons, personal communication). Syndecans 1, 2 and 4 are expressed and required in endothelial cells, while syndecan 3 is expressed in the endothelial cells but *Sdc3*-null mice are do not have any endothelial phenotypes (Echtermeyer et al., 2001; Gotte et al., 2002; Li et al., 2002; Patterson et al., 2005; Noguer et al., 2009). *Sdc3*-null mice show enhanced long-term potentiation in the hippocampus (Kaksonen et al., 2002) and develop abnormal cortical laminar organisation due to impaired neuronal migration (Hienola et al., 2006).

So far mutants for *glypicans* (*Gpc*) 1,3 and 4 have been published, and none are embryonic lethal (Cano-Gauci et al., 1999; Tang et al., 2010). Mice carrying the *Gpc1*-null allele have reduced brain size due to impaired neurogenesis (Jen et al., 2009), whilst *Gpc3*-null mice have a multitude of developmental defects including cardiac and vascular defects (Ng et al., 2009), and *Gpc4*-null mice have a defective excitatory synapse formation in the hippocampus (Allen et al., 2012).

Targeting the extracellular matrix perlecan (*Hspg2*) or agrin (*Agn*) alleles leads to embryonic lethal mutations in mice. Deletion of *Hspg2* results in a multitude of defects, including neuromuscular junctions lacking acetylcholinesterase, cephalic abnormalities and cardiac outflow tract malformations (Arikawa-Hirasawa et al., 1999; Arikawa-Hirasawa et al., 2002; Costell et al., 2002). Agrin is essential for neuronal development and $Agn^{-/-}$ mice have smaller brains, reduced size, density and number of acetylcholine receptors in muscles, as well as abnormal synapse number and assembly in the CNS (Gautam et al., 1996; Serpinskaya et al., 1999; Gingras et al., 2007; Ksiazek et al., 2007).

1.3.3.2 Mutants targeting heparan sulfate biosynthesis

Most of the enzymes required for HSPG synthesis have also been targeted to generate knockout mouse models. Unsurprisingly, targeting essential steps in HS biosynthesis results leads to more severe defects than targeting individual HS core proteins. For example, mice null for *Ext1* or *Ext2*, which cannot polymerise HS chains, will die during gestation around E6-7.5 (Lin et al., 2000; Stickens et al., 2005). A floxed allele of *Ext1* is also available, which when targeted with CRE recombinase will delete *Ext1* and will consequently not form any functional EXT1/2 heterodimers. *Nestin-Cre* targeting of floxed *Ext1* results in complete penetrance brain structure malformations as well as midline axon guidance defects (Inatani et al., 2003).

The *Ndst1*-null mutation causes perinatal lethality and mice have abnormal forebrain and craniofacial development as well as lung hypoplasia (Fan et al., 2000; Ringvall et al., 2000; Grobe et al., 2005). In contrast, both *Ndst2*$^{-/-}$ and *Ndst3*$^{-/-}$ mutant mice are viable and display mild defects (Forsberg et al., 1999; Humphries et al., 1999; Pallerla et al., 2008). An *Ndst4*-null mouse has not been reported.

Several mutant mice have also been generated to target different *O*-sulfotransferases, which I have analysed further during nervous system development in Chapter 4. The *Hs2st*-null mouse was generated using a gene trap approach; this mutation is perinatal lethal with kidney agenesis, skeletal and ocular defects as well as reduced cell proliferation in the cortex (Bullock et al., 1998; Merry et al., 2001; McLaughlin et al., 2003). Interestingly, the loss of 2-*O*-sulfotransferase, both in mice and *Drosophila*, increases levels of 6-*O* and N-sulfation (Merry et al., 2001; Dejima et al., 2013). *Hs6st1*-null mice are embryonic lethal due to abnormal placenta microvessels and also develop commissural axon defects (Pratt et al., 2006; Habuchi et al., 2007; Conway et al., 2011). On the other hand, *Hs6st2* does not seem to be as essential for development, as *Hs6st2*-mice are viable and develop only metabolic defects (Sedita et al., 2004). *Hs6st3* mutant mice have not been reported.

1.3.4 HSPG signalling interactions

1.3.4.1 HSPGs and VEGF-A signalling

HSPGs can interact with a variety of signalling pathways including FGFs, VEGF, glial cell-line derived neurotrophic factor (GDNF), hedgehog and SLITs by either forming functional signalling complexes or by affecting their tissue distribution (Hacker et al., 2005; Bishop et al., 2007). Studies *in vitro* have shown that heparin promotes $VEGF_{165}$-binding to FLK1, FLT1 and NRP1 (Gitay-Goren et al., 1992; Tessler et al., 1994; Soker et al., 1998). Furthermore, VEGF-A also binds to heparin with high affinity through domains encoded in exons 6 and 7, which affects its distribution *in vivo* (section 1.2.1.2; (Park et al., 1993; Ruhrberg et al., 2002; Gerhardt et al., 2003). Thus, mice expressing only the $VEGF_{120}$ isoform, which lacks the heparin-binding domains and is consequently very diffusible, have impaired tip cell filopodia extension and reduced branch points in the brain vasculature (Ruhrberg et al., 2002). Vice versa, mice that only expressed the heparin binding isoform $VEGF_{188}$ show excessive and ectopic vascular branching (Ruhrberg et al., 2002). This evidence shows that VEGF requires HSPGs to localise different isoforms in the ECM and thereby forms gradients in a tissue specific manner.

One study has shown that VEGF can use HSPGs in a *trans* complex to signal correctly. Embryonic stem cells expressing FLK1 can form vessels upon VEGF induction, whilst in *Ndst1/2*$^{-/-}$ embryoid bodies there is a reduced response to VEGF (Jakobsson et al., 2006). However, mosaic embryoid bodies, containing *Flk*$^{-/-}$ and *Ndst1/2*$^{-/-}$ cells, can respond to VEGF and form vessels. The resulting vessels contained pericytes with normal HSPG content (derived from *Flk*$^{-/-}$ cells) and FLK1 expressing endothelial cells (derived from *Ndst1/2*$^{-/-}$ cells). This suggests that in some situations VEGF requires HSPGs to signal through FLK1.

Some HSPG modifications have been described as important for the interaction with VEGF. Interestingly, *Ndst1*$^{-/-}$ mice have reduced VEGF induced vascular hyperpermeability *in vivo* (Xu et al., 2011). Several studies have shown that VEGF requires the presence of 6-*O*-sulfated proteins to correctly signal in endothelial cells *in vitro* (Ashikari-Hada et al., 2005; Robinson et al., 2006). *In vivo*,

its been shown that *Hs6st2* and *Vegfa* interact for correct caudal vein development in zebrafish (Chen et al., 2005).

1.3.4.2 HSPGs and FGF signalling

The interaction between FGFs and HSPGs has been thoroughly characterised (reviewed by (Mohammadi et al., 2005; Matsuo and Kimura-Yoshida, 2013). Early experiments showed that HS chains enable the formation of a ternary complex that is required for FGF2 to bind FGFR1 in cultured cells (Rapraeger et al., 1991; Yayon et al., 1991). Crystal structure analysis has shown that a unit consisting of a 1:1:1 FGF:FGFR:HS dimer is required for correct FGF signalling, in this context HSPGs act as co-receptors (Schlessinger et al., 2000). In this dimer complex, each FGF binds both receptors, and the two receptors are also in direct contact. Furthermore, HSPGs have other functions during FGF signalling, as they can also determine the rate of FGF diffusion, act as a storage reservoir and also stabilise FGFs by lowering their degradation (Hacker et al., 2005; Sarrazin et al., 2011; Venero Galanternik et al., 2015).

Several *in vitro* studies have demonstrated that FGF signalling is mostly dependent on 2- and 6-*O*-sulfated groups as well as N-sulfation in HSPGs (Turnbull et al., 1992; Guimond et al., 1993; Maccarana et al., 1993). Interestingly, one study has shown that HS without 6-*O*-sulfation will bind FGF, but prevents it from forming a complex with FGFR (Lundin et al., 2000). Similarly to VEGF, evidence shows that FGFs require HSPGs with specific characteristics to signal appropriately in a tissue specific manner.

The neuronal tissue-specific knockout of *Ext1* in mice results in midbrain/hindbrain patterning defects caused by altered FGF8 distribution (Inatani et al., 2003). In *Drosophila*, both 2- and 6-*O*-sulfotransferases cooperate to control FGF signalling during tracheal development (Kamimura et al., 2006). In this case, deleting only one *O*-sulfotransferase does not cause tracheal defects, possibly because of compensation mechanisms. During lacrimal gland development, mice also require both HS2ST and HS6ST1 as well as NDST1/2 in a tissue specific manner for correct *Fgf10-Fgfr2b*.

Using a *Cre* targeting approach, it was shown that *Hs2st1* and *Hs6st1* are required in lacrimal gland epithelia, but dispensable in mesenchyme, whilst NDST1/2 are essential in both epithelia and mesenchyme (Pan et al., 2008; Qu et al., 2011a; Qu et al., 2012). Furthermore, *Hs6st1*-null mice have increase FGF8 levels in the corpus callosum, and *Ndst1*$^{-/-}$ mice have defective lens development because of disrupted FGF signalling (Pan et al., 2006; Clegg et al., 2014).

Gene/Mutation	Proteoglycan	Phenotype (reference)
Sdc3$^{-/-}$	Syndecan 3	Enhanced long-term potentiation in the hippocampus (Kaksonen et al., 2002). Impaired neuronal migration leading to abnormal cortical laminar organisation (Hienola et al., 2006).
Gpc1$^{-/-}$	Glypican 1	Impaired neurogenesis and reduced brain size (Jen et al., 2009).
Gpc3$^{-/-}$	Glypican 3	Cardiac and vascular defects (Ng et al., 2009).
Gpc4$^{-/-}$	Glypican 4	Defects in the formation of excitatory synapses in the hippocampus (Allen et al., 2012).
Hspg2$^{-/-}$	Perlecan	Neuromuscular junctions lacking acetylcholinesterase (Arikawa-Hirasawa et al., 2002). Cardiac flow tract defects (Costell et al., 2002). Defects in cephalic development (Arikawa-Hirasawa et al., 1999).
Agn$^{-/-}$	Agrin	Defective number and formation of synapses in the CNS (Serpinskaya et al., 1999; Gingras et al., 2007). Small brain (Ksiazek et al., 2007). Reduction in the number, density and size of acetylcholine receptors in muscles (Gautam et al., 1996).
Nsdt1$^{-/-}$	N-deacetylase/N-sulfotransferase 1	Abnormal craniofacial and forebrain development (Grobe et al., 2005). Lung hypoplasia (Fan et al., 2000).

Hs2st$^{-/-}$	2-*O*-sulfotranferase	Kidney agenesis (Bullock et al., 1998). Reduced proliferation during cortical development (McLaughlin et al., 2003).
Hs6st1$^{-/-}$	6-*O*-sulfotranferase 1	Commissural axon guidance defects (Pratt et al., 2006; Habuchi et al., 2007; Conway et al., 2011).
Hs6st2$^{-/-}$	6-*O*-sulfotranferase 2	Metabolic defects (Sedita et al., 2004).
Ext$^{fl/fl}$ *Nestin-Cre*	Exotosin 1	Midline axon guidance defects and brain structure malformations (Inatani et al., 2003).

Table 1.2 Mutation in HSPGs affecting neuronal development in the mouse.

1.4 AIMS OF THIS STUDY

For the correct development of the nervous system neurons must find their appropriate location in the brain and make synaptic connections with their targets. A combinatorial use of several different signalling molecules is required during cranial axon guidance and vertebrate neuronal migration. However, the way in which these different signalling pathways collaborate or differ is not well understood. I used mouse genetic models to analyse the individual and combinatorial signal of different signalling molecules required during FBM neuron migration and cranial axon guidance.

- The NRP1 binding properties of the $VEGF_{165}$ and $VEGF_{121}$ isoforms have been extensively studied, while the longer isoform $VEGF_{189}$ has been neglected. In Chapter 3 I aim to investigate $VEGF_{189}$ binding and signalling through NRP1 in the developing nervous system.
- In Chapter 4 I aim to investigate the role of HSPG modifying enzymes 2- and 6-*O*-sulfotransferases in FBM neuron migration and cranial axon guidance. I also aim to analyse the interaction between HSPG modifiers and other signalling pathways.
- In Chapter 5 I aim to characterise different *Cre* lines under the control of neuronal promoters by targeting new and known pathways important during FBM neuron development.

Chapter 2 MATERIALS AND METHODS

2.1 MATERIALS

2.1.1 General laboratory materials

All reagents were obtained form Sigma Aldrich, besides where indicated. Glassware was obtained from VWR international. Plasticware was obtained from Corning or Nunc.

2.1.2 General laboratory solutions

Water was purified using a MilliRo 15 Water Purification System (Millipore). Where necessary water was further purified using a Milli-Q reagent Grade Water Ultrafiltration system (Millipore). DNAse- and RNAse-free water was obtained from Sigma Aldrich. Absolute ethanol, methanol and isopropanol were obtained from Fischer Scientific.

1X PBS	137mM NaCl, 3mM KCl, 10mM Na_2HPO_4, 1.8mM KH_2PO_4, pH 7.2
1X PBT	1X PBS + 0.1% Triton X100 (for immunolabelling)
1X PBT	1X PBS + 0.1% Tween 20 (for *in situ* hybridisation)
1X TAE	40mM Tris-acetate, 1mM EDTA, pH 8.0
1X TBS	10mM Tris-HCl pH 8.0, 150mM NaCl (for immunolabelling)
1X TBS	25mM Tris pH 7.5, 150mM NaCl, 3mM KCl (for *in situ* hybridisation)
1X TBST	1X TBS + 1% Tween 20
1X TE	10mM Tris-HCl, 1mM EDTA, pH 8.0
4% PFA	4% formaldehyde, made freshly from paraformaldehyde, in PBS

2.2 ANIMAL METHODS

All animal research was conducted under the ethical approval of the United Kingdom Home Office.

2.2.1 Animal maintenance and husbandry

Mice were mated in the evening and checked for vaginal plugs the following morning. The morning of vaginal plug formation was counted as 0.5 days post coitum. Females were culled by cervical dislocation and embryos were harvested in ice cold PBS. All mice were on CD1 or C57Bl/6 genetic backgrounds.

2.2.2 Genetic mouse strains

See Table 2.1 for details of mouse strains used.

Gene/Mutation	Provider	Reference
Nrp1 Knockout	Dr Hajime Fujisawa	(Kitsukawa et al., 1997)
Nrp1 floxed	Dr David Ginty	(Gu et al., 2003)
Nrp2 floxed	Dr Alex Kolodkin	(Walz et al., 2002)
Vegfa$^{120/120}$ Knockin	Dr David Shima	(Carmeliet, 1999)
Vegfa$^{188/188}$ Knockin	Dr Peter Carmeliet	(Stalmans et al., 2002)
Hs6st1 LacZ Knockin	Dr Tom Pratt	(Leighton et al., 2001; Mitchell et al., 2001)
Hs6st2 LacZ Knockin	Lexicon Pharmaceuticals	(Sugaya et al., 2008)
Hs2st LacZ Knockin	Dr Valerie Wilson	(Bullock et al., 1998)
Ext1 floxed	Dr Yu Yamaguchi	(Inatani et al., 2003)
Sdc1 Knockout	Dr Michael Simons	(Alexander et al., 2000)
Sdc2 Knockout	Dr Michael Simons	(Skarnes et al., 2011)
Sdc4 Knockout	Dr Michael Simons	(Li et al., 2002)
Vegfa floxed	Dr Napoleone Ferrara	(Gerber et al., 1999)
Vegfa^{Hypo} LacZ Knockin	Dr Jody Haigh	(Damert et al., 2002)
Rosa26^{Yfp} floxed	Dr J. P. Barbera	(Srinivas et al., 2001)
Rosa26^{Dta} floxed	Dr J. P. Barbera	(Ivanova et al., 2005)
Nestin-Cre	Dr Jody Haigh	(Tronche et al., 1999)
NesCre8	Dr Weimin Zhong	(Petersen et al., 2002)
Phox2b-Cre	Dr Jean-Francois Brunet	(D'Autreaux et al., 2011)

Table 2.1 Mouse genetic strains, with source and reference.

2.2.3 Compound Hs6st1;Hs6st2 mutant mice

To obtain compound *Hs6st1;Hs6st2* mutants, mice heterozygous for the *Hs6st1* null mutation were crossed with mice heterozygous for the *Hs6st2* null mutation, and compound heterozygous mice were crossed to each other. This crossing resulted in mixtures of *Hs6st1* and *Hs6st2* heterozygous and homozygous mutations as well as wild types, and the Mendelian probability of obtaining a wild type or a compound homozygous *Hs6st1;Hs6st2* mutant in these matings was 1/16.

2.2.4 Vegfa isoform specific mice

Mice expression only a single *Vegfa* specific isoform were used in this thesis termed $Vegfa^{120/120}$, which expresses only the $VEGF_{120}$ isoform and $Vegfa^{188/188}$, which expressed only the $VEGF_{188}$ isoform. $Vegfa^{120/120}$ mice were generated using a *Cre-LoxP* system to remove *Vegfa* exons 6 and 7 in embryonic stem cells (Carmeliet et al., 1999). $Vegfa^{188/188}$ mice were generated by replacing the *Vegfa* genomic sequence with $Vegfa^{188}$ cDNA containing exons 4 to 8 (Stalmans et al., 2002).

2.2.5 Tissue specific genetic targeting

The *Cre-LoxP* recombination system was used for tissue specific gene targeting (reviewed by (Nagy, 2000). This system uses the P1 phage CRE recombinase, a 38kDa enzyme that specifically recognises a 34bp sequence called *LoxP*. Inserting *LoxP* sites in flanking positions of a DNA target sequence allows CRE recombinase binding when present and leads to the excision or inversion of this sequence, depending on the orientation of the *LoxP* sites. For specific tissue targeting CRE recombinase can be inserted under the control of a selected tissue specific promoter. Depending on the choice of promoter to drive CRE expression, genetic deletions can occur somatic cells and consequently their entire progeny.

To evaluate the tissue targeting of different *Cre* lines, I used *Rosa26* reporter mice that have a *LoxP*-flanked (floxed) stop cassette upstream of an enhance *eYfp* gene coding for enhanced yellow fluorescent protein ($Rosa26^{Yfp}$) (Srinivas et al.,

2001). I also used a *Rosa26*^{Dta} line that is constructed in the same way as *Rosa26*^{Yfp} but expresses the diphtheria toxin A (*Dta*) gene instead (Ivanova et al., 2005). This means that *Cre* targeting will excise the floxed stop cassette flanked by *LoxP* sites, which results in the expression of *eYfp* or *Dta* in the Cre expressing cells (*Rosa26*^{Yfp}; *Rosa26*^{DTA}). I analysed three *Cre* lines using this method, *Phox2b-Cre* (D'Autreaux et al., 2011); *Nestin-Cre* (Tronche et al., 1999); and *NesCre8* (Petersen et al., 2002), to determine the level of targeting in migrating FBM neurons in the embryonic hindbrain.

Phox2b-Cre; *Nestin-Cre*; and *NesCre8* were used to target floxed *Nrp1* (Gu et al., 2003) and *Ext1* (Inatani et al., 2003) genes. The floxed *Nrp1* and *Ext1* mice were in some cases bred on a heterozygous null background to yield *Nrp1*$^{fl/-}$ and *Ext1*$^{fl/-}$ mice, respectively. I also targeted floxed *Vegfa* in neuronal progenitors; because crossing *Vegfa*$^{fl/fl}$ (Gerber et al., 1999) mice to *Nestin-Cre* line results in offspring that is lethal during early embryonic development, I crossed a *Vegfa* hypomorphic strain (*Vegfa*$^{Hypo/+}$) (Damert et al., 2002) and the floxed *Vegfa* line to create mice with one hypomorphic and one floxed *Vegfa* allele (*Vegfa*$^{Hypo/fl}$). This approach was previously used successfully to substantially knock down *Vegfa* in the neural lineage without causing early embryonic lethality (Haigh et al., 2003).

2.2.6 Genotyping

Tissue biopsies were taken from mice, either ear punches from pre-weaning age mice or tail snips or yolk sacs from embryos. The biopsy tissue was incubated overnight at 55°C in 500 µl of lysis buffer (100 mM Tris-HCl pH 8.5, 5 mM EDTA, 0.2% SDS, 200 mM NaCl add 100 µg/ml proteinase K) for protein digestion. DNA was precipitated by adding 1 ml of ethanol and collect by centrifugation at 13000 rpm for 5 minutes. The remaining pellet was washed with 70% ethanol, centrifuged as previously, and air-dried for 30 minutes before being resuspended in 100 µl of 0.2X TE buffer. All genotyping was carried out by Kathryn Davidson, Laura Denti, Valentina Senatore and Andy Joyce in the Ruhrberg lab. Polymerase chain reaction (PCR) amplification was performed using extracted genomic DNA on a MJ Research PTC-200 Peltier Thermal Cycler. A single reaction used 1 µl of genomic DNA with

10 µl Megamix Blue reaction mix (Microzone, contains Taq polymerase, dNTS, buffer loading dye) and 1 µg/µl of each oligonucleotide primer specific for the gene being targeted (synthesized by Sigma, see Table 2.2) using the relevant cycle and temperature program (Table 2.3).

Gene	Primer	Primer sequence
Nrp1 *Nrp1*^{fl}	NPneo	5'-CGTGATATTGCTGAAGAGCTTGGC-3'
	NP-F	5'-CAATGACACTGACCAGGCTTATCATC-3'
	NP-R	5'-GATTTTTATGGTCCCGCCACATTTGTC-3'
Nrp2^{fl}	Wt1	AGCTTTTGCCTCAGGACCCA
	Wt1	CAGGTGACTGGGGATAGGGTA
	loxP	CCTGACTACTCCCAGTCATAG
Hs6st1	6OST-F	5'-ATGGTGACTGTGACCCACAA-3'
	6OST-R	5'-GGGATATAGGGGACCTTGGA-3'
	hPLAP-F	5'-ACAGCTGCCAGGATCCTAAA-3'
	hPLAP-R	5'-CAAGCCAATGGTCTGGAAGT-3'
Hs6st2	HS6ST2-34	5'- GTTCGGCCAGGTTTGTACC-3'
	HS6ST2-35	5'- CAGCTGGTGAGCTCGGTC-3'
	HS6ST2-neo	5'- GCAGCGCATCGCCTTCTATC-3'
	HS6ST2-7	5'- CTAAGATAGGCTCTAGTGTCTAC-3'
Hs2st	Hs2st1	5'-ATCAATGAATAATTGCCTAGGTC-3'
	Hs2st2	5'-GGGAAGAAATTCACCCCAACA-3'
	Hs2stV	5'-TACTCAGTGCAGTGCAGTCA-3'
Vegfa^{120}	120F2	5'-CAGTCTATTGCCTCCTGACCTTCAGGGTC-3'
	120R2	5'-CTTGCGTCCACACCGTCACATTAAGTCAC-3'

	120E2	5’- TTCAGAGCGGAGAAAGCATTTGTTTGTCCA-3’
Vegfa$^{188/164}$	F	5’-CAAAGCCAGCACATAGGAGAGA-3’
	E	5’-GTGGGTAGAGAAAGGAGGAGAA-3’
	R	5’-TGGCTTGTCACATCTGCAAGTA-3’
Ext^{fl}	Ext-11	5’- AAGGATTCTCGCTGTGACAG-3’
	Ext-35	5’- CCAAAACTTGGATACGAGCC-3’
Vegfa^{fl}	F	5’- CCTGGCCCTCAAGTACACCTT-3’
	R	5’- TCCGTACGACGCATTTCTAG-3’
Rosa26$^{Yfp/Dta}$	WT-F1	5’-AAAGTCGCTCTGAGTTGTTAT-3’
	WT-R1	5’-GGAGCGGGAGAAATGGATATG-3’
	KO-F1	5’-GCGAAGAGTTTGTCCTCAACC-3’
Vegfa^{Hypo}	Stop	5’-GAGCATTTATTCCCATGTCTG-3’
	Fusion	5’-CAGGCTTTCTGGATTAAGGAC-3’
	Lac	5’-CATTACCAGTGGGTCTGGTG-3’
NesCre8	Nes8-F1	5’-GAATACCCTCGCTTCAGCTC-3’
	Creb	5’-GCATTTTCCAGGTATGCTCAG-3’
Nestin-Cre *Phox2b-Cre*	Cre1	5’-GCCTGCATTACCGGTCGATGCAACGA-3’
	Cre2	5’-GTGGCAGATGGCGCGGCAACACCATT-3’

Table 2.2 Specific oligonucleotide primers used in genotyping.

Gene	Start	Denaturing	Annealing	Extension	Cycles	End
Nrp1	94°C 3 min	94°C, 40 s	66°C, 1 min	72°C, 1.5 min	35 x	72°C, 5 min
Nrp1^{fl}	95°C 3 min	95°C, 30 s	69°C, 30 s	72°C, 1 min	34 x	72°C, 5 min
Nrp2^{fl}	95°C 2 min	94°C, 40 s	60°C, 1 min	72°C, 1 min	34 x	72°C, 5 min
Hs6st1	94°C 4 min	94°C, 20 s	58°C, 30 s	72°C, 30 s	29 x	72°C, 1 min
Hs6st2	94°C 4 min	94°C, 30 s	65°C, 1 min	72°C, 1 min	32 x	72°C, 10 min
Hs2st	94°C 3 min	94°C, 40 s	60°C, 45 s	72°C, 2 min	36 x	72°C, 5 min
Vegfa^{120}	94°C 3 min	94°C, 40 s	52°C, 1 min	72°C, 1.5 min	5 x	
		94°C, 40 s	60°C, 1 min	72°C, 1.5 min	28 x	72°C, 5 min
Vegfa$^{188/164}$	94°C 4 min	94°C, 40 s	55°C, 1 min	72°C, 1.5 min	34 x	72°C, 5 min
Ext^{fl}	94°C 2 min	94°C, 45 s	56°C, 45 s	72°C, 2 min	32 x	72°C, 5 min

Vegfa^{fl}	94°C 3 min	94°C, 40 s	52°C, 1 min	72°C, 1.5 min	5 x	
		94°C, 40 s	60°C, 1 min	72°C, 1.5 min	28 x	72°C, 5 min
Rosa26$^{Yfp/Dta}$	94°C 4 min	94°C, 30 s	59°C, 45 s	72°C, 1 min	34 x	72°C, 3 min
Vegfa^{Hypo}	94°C 4 min	94°C, 40 s	55°C, 1 min	72°C, 1.5 min	34 x	72°C, 5 min
NesCre8	94°C 3 min	94°C 1 min	67°C, 1 min	72°C, 1 min	32 x	72°C, 3 min
Cre	94°C 3 min	94°C, 1 min	67°C, 1 min	72°C, 1 min	40 x	72°C, 3 min

Table 2.3 Details of PCR cycling parameters used in genotyping.

2.3 TISSUE PROCESSING

2.3.1 Tissue fixation

Pregnant mice at the appropriate day of gestation were culled in accordance with the Home Office Schedule 1 regulations. Embryos were removed from the pregnant uterus and the umbilical cord severed in ice-cold 1X PBS and fixed in 4% formaldehyde solution at 4°C for 2 hours (immunolabelling) or overnight (*in situ* hybridisation). For hindbrain experiments, the head was severed from the trunk above the limbs and fixed separately. Embryos required for wholemount TUJ1 immunolabelling were fixed and maintained in Dents fixative (4:1 methanol:DMSO) at -20°C.

2.3.2 Cryosectioning

Fixed samples washed twice in PBS, and incubated in 30% sucrose in PBS at 4°C until the tissue was equilibrated, i.e. sank to the bottom of the tray holding the sucrose. Tissue for *in situ* hybridisation was fixed as described above, then washed twice in PBS and incubated in methanol overnight at -20°C. Tissue was then embedded in OCT (Sakura Tissue-Tek), frozen on dry ice and stored at -80°C. Frozen samples were cut at various thicknesses ranging from 10-40 μm using a histology cryostat (Leica CM 1850) and collected on Superfrost Plus slides (VWR International). Slides with cryosections were stored at -20°C.

2.4 IMMUNOLABELLING

2.4.1 Immunolabelling of cryosections

Slides containing cryosections were allowed to air dry at room temperature for 1 hour. Cryosections were rehydrated and excess OCT was washed off with 2 PBS washes. Cryosections were incubated for 10 minutes in PBT to permeabilise the tissue. Slides were incubated in blocking solution (10% normal goat serum in PBT; or 100% Dako serum free) for 30 minutes at room temperature. Slides were then incubated in a wet chamber overnight at 4°C with primary antibody and appropriate blocking solution (see Table 2.4 for antibody dilutions and blocking solutions). The next day slides were washed 3 times for 5 minutes each at room temperature in PBT. Cryosections were then incubated at room temperature with secondary antibody in blocking solution in the dark. The slides were then washed 3 times for 5 minutes each at room temperature in PBS and post-fixed for 5 minutes with 4% formaldehyde solution. Sections were mounted in Mowiol 4-88 (Calbiochem). For all experiments a minimum of three embryos were analysed for each genotype. All mutants analysed were compared to control littermates.

2.4.2 Wholemount Immunolabelling

Samples were incubated at room temperature for 30 minutes in PBT to permeabilise the tissue. Wholemount samples were then incubated for 1 hour at room temperature in blocking solution (10% normal goat serum in PBT; or 100% protein block, serum free; Dako), then incubated overnight (anti-ISL1 antibody is incubated for 4 days) at 4°C with primary antibody and appropriate blocking solution (Table 2.4). Samples were then washed at least 4 times in PBT for 30 minutes each and then incubated for 1-2 hours at room temperature with secondary antibody. Samples were then washed as described above and post-fixed for 15 minutes with 4% formaldehyde solution.

Fluorescently labelled wholemount hindbrains were mounted using SlowFade (Life Technologies).

Wholemount immunolabelling of samples for TUJ1 staining was bleached using hydrogen peroxidase (10% H_2O_2 in Dents fixative) overnight hours at room temperature. Embryos were washed 3 times with TBS for 60 minutes each at room temperature, then incubated overnight in TUJ1 antibody dilute in blocking serum (normal goat serum with 20% DMSO and 0.12% thimerosal) at room temperature. The following day embryos were washed 5 times with TBS for 1 hour each at room temperature then incubated overnight in secondary antibody (peroxidase conjugated) dilute in blocking serum. Stained embryos were then incubated in DAB and hydrogen peroxide (SigmaFast, Sigma) until colour developed. To stop the reaction embryos were washed several times in TBS and postfixed in 4% formaldehyde solution.

Wholemount HRP stained embryos were cleared before imaging using BAAB (1:2 benzyl alcohol:benzyl benzoate). Embryos were dehydrated in 100% methanol for 30 minutes, followed by 50% methanol 50% BAAB for 30 minutes, and finally 100% BAAB solution. For all experiments a minimum of three embryos were analysed for each genotype. All mutants analysed were compared to control littermates.

Primary antibody **(dilution, supplier)**	**Secondary antibody** **(dilution)**	**Blocking solution**
Goat anti-NRP1 (1:100, R&D Systems)	Alexa594-conjugated donkey anti-goat Fab fragment (1:200)	Dako serum free protein block
Rabbit anti-GnRH (1:1000, Immunostar)	HRP-conjugated goat anti-rabbit IgG (1:200)	10% NGS/PBT
Rabbit anti-TUJ1 (1:250, Millipore)	Alexa488-conjugated donkey anti-rabbit Fab fragment (1:200) HRP-conjugated goat anti-rabbit IgG (1:200)	10% NGS/PBT or NGS and 20% DMSO
Rabbit anti-GFP (1:500, Medical and Biological Laboratories)	Alexa488-conjugated donkey anti-rabbit Fab fragment (1:200)	10% NGS/PBT
Bandeiraea simplicifolia Isolectin B4 (1:200, Sigma)	Streptavidin-Alexa633	10% NGS/PBT
Mouse anti-ISL1 (1:100, Developmental Studies Hybridoma Bank)	Alexa488-conjugated donkey anti-mouse Fab fragment (1:200)	10% NGS/PBT

Table 2.4 List of antibodies and lectin used for immunolabelling.

2.5 *IN SITU* HYBRIDISATION (ISH)

2.5.1 Bacterial culture of plasmid containing in situ probe

Chemical transformation competent bacteria were prepared by culturing a single colony of DH5α overnight at 37°C without shaking in 10 ml 2YT medium (16 g/l bacto tryptone, 10 g/l bacto yeast extract, 5 g/l NaCl, pH 7.2). The culture was then used to inoculate 100 ml of P-media (50 ml 10X P-buffer (6.92 g K_2HPO_4, 2.15 g KH_2PO_4, 4.96 g NH_4SO_4 in 250 ml distilled water), 50 ml 10% (w/v) casamino acids, 5 ml 1 M $MgSO_4$, 0.5 ml 1.8 mM $FeSO_4$, 6.25 ml 20% glucose (w/v) in 500 ml distilled water) and grown at 37°C with shaking until the O.D600 reached 0.4. The bacteria was centrifuged at 6000 rpm for 10 minutes at 4°C, the pellet was washed once in ice cold 10mM NaCl, suspended in 100 ml ice cold 50 mM CaCl2 and incubated on ice for 15 minutes. The bacteria was centrifuged again at 6000 rpm for 10 minutes at 4°C, resuspended in 10 ml ice cold 50 mM CaCl containing 16% glycerol (w/v), aliquoted and stored at -80°C.

Chemically competent cells were used to transform plasmids containing cDNA. Competent cells were thawed on ice and 1 ng of plasmid DNA was incubated on ice with 100 µl of competent cells. The bacteria were heat-shocked for 90 seconds at 42°C and then placed on ice for 10 seconds. 600 µl of L-broth medium (10g/l bacto tryptone, 5 g/l yeast extract, 5 g/l NaCl) were added and the bacterial suspension was allowed to grow for 30 minutes at 37°C. The bacterial culture was then spread on L-agar plates containing the appropriate antibiotic (L-broth, 100 µg/ml ampicillin, 15 g/l agar) and incubated overnight at 37°C. A single colony was picked and grown in L-broth with the appropriate antibiotic (100 µg/ml ampicillin) overnight with shaking at 37°C.

2.5.2 RNA probe synthesis

Plasmids were isolated with the QIAprep Spin Miniprep kit (Qiagen), according to manufacturer's instructions. The isolated plasmid was linearized using the appropriate restriction enzyme (New England Biolabs) (see Table 2.5 for individual probe details) for 2 hours at 37°C in a reaction mixture according to

manufacturer's instruction: 5 µl plasmid DNA, 2 µl 10X buffer, 1 µl enzyme, 12 µl water. Phenol/chloroform was used to extract linearized plasmid DNA. RNA for *in situ* hybridisation was synthesized by reverse transcription using the appropriate polymerase (Roche) (Table 2.5) for 2 hours at 37°C in a reaction mixture according to manufacturer's instruction: 14.5 µl DNA, 2 µl 10X buffer, 2 µl 10X DIG labelling mixture (Roche), 1 µl polymerase and 0.5 µl RNAse inhibitor (Roche). RNA was precipitated by adding 80 µl of water, 8 µl 5 M lithium chloride, 1 µl GlycoBlue (Life Technologies) and 300 µl ethanol. The mixture was incubated overnight at -80°C followed by centrifugation for 15 minutes at 13000 rpm and 4°C, the pellet was washed in 70% ethanol and allowed to air dry for 5 minutes before suspension in 40 µl of water.

2.5.3 Wholemount in situ hybridisation

As described previously tissue was fixed overnight at 4°C in 4% formaldehyde solution and stored at -20°C in methanol. Wholemount samples were then bleached with 6% hydrogen peroxide in methanol for 1 hour at room temperature. Samples were then rehydrated in serial dilutions of methanol and PBT. Rehydrated samples were permeabilised with 10 µg/ml Proteinase K in PBT at room temperature, 10 minutes for E10.5-12.5 hindbrains and 1 hour for E15.5 hindbrains. Samples were incubated in hybridisation solution (50% formamide (Roche), 5X SSC pH 4.5 (Sigma; sodium citrate, sodium chloride, citric acid), 50 µg/ml tRNA (Sigma), 50 µg/ml heparin (Sigma), 1% sodium dodecyl sulphate (Sigma) for 30 minutes at 70°C and then incubated with RNA probe solution (3.5 µl in 1 ml hybridisation solution) overnight at 65°C. The next day samples were washed 3 times in solution 1 (50% formamide, 5X SSC pH 4.5, 1% SDS) and 3 times in solution 3 (50% formamide, 2X SSC pH 4.5) at 65°C for 30 minutes each. I then washed the samples briefly twice with TBST (1X TBS, 1% Tween 20) at room temperature and blocked the tissue using 10% sheep serum in TBST for 30 minutes are room temperature, then incubated overnight at 4°C with anti-digoxigenin alkaline phosphatase antibody (Roche) at 1:5000 in 1% sheep serum in TBST. The following day, the samples were washed with TBST at least 5 times for 1 hour each at room temperature and left washing overnight at 4°C. Samples were washed 3 times for 10

minutes at room temperature in NTMT buffer (100 mM NaCl, 100 mM Tris-HCl pH 9.5, 1% Tween20, 50 mM $MgCl_2$), then incubated in developing solution containing (3.5 µl BCIP and 4.5 µl NBT (Roche) per ml of NTMT) at room temperature until alkaline phosphatase develops. The reaction was stopped by washing in TBST and the tissue stored in 4% formaldehyde solution at 4°C. For all experiments a minimum of three embryos were analysed for each genotype. All mutants analysed were compared to control littermates.

Probe	Anti-sense restriction enzyme	Polymerase	Source	Reference
Isl1	NcoI	Sp6	Dr Tom Jessel	(Ericson et al., 1992)
Nrp1	NotI	T7	Dr Marcus Fruttiger	(He and Tessier-Lavigne, 1997)
Nrp2	XhoI	T3	Dr Marc Tessier-Lavigne	(Chen et al., 1997)
Hs6st1	EcoRI	T3	Dr Xin Zhang	(Sedita et al., 2004)
Hs6st2	EcoRI	T3	Dr Xin Zhang	(Sedita et al., 2004)
Hoxb1	EcoRI	T3	Dr Linda Ariza-McNaughton	(Gavalas et al., 2003)
Fgfr1	HindIII	T3	Dr Siew-Lan Ang	(Trokovic et al., 2003)
Fgfr2	NdeI	T7	Dr Quenten Schwarz	
Fgfr3	XhoI	T3	Dr Siew-Lan Ang	(Pringle et al., 2003)
Fgfr4	ApaI	Sp6	Dr Quenten Schwarz	
Erm	Sal1	T7	Dr Siew-Lan Ang	(Trokovic et al., 2005)

Table 2.5 Restriction enzyme and polymerase specific to anti-sense *in situ* hybridisation probes.

2.6 LABELLING TECHNIQUES

2.6.1 X-gal assay

β-galactosidase activity was visualised in samples containing a *lacZ* inserted in the locus of a specific gene. Embryos were dissected and fixed with 4% formaldehyde solution for 30 minutes at 4°C and then processed for wholemount staining or frozen for cryosections. Tissue was then washed in 0.02% NP-40 in PBS three times for 15 minutes at room temperature. Samples were incubated at 37°C in X-gal (stock: 40 mg/ml in dimethylformamide) diluted 1:40 in staining solution (5mM $K_3Fe(CN)_6$, 5mM $K_4Fe(CN)_6.3H_2O$, 2mM $MgCl_2$, 0.01% sodium deoxycholate) until sufficient blue colour developed. The reaction was stopped by washing with PBS, and tissue was stored in 4% formaldehyde solution at 4°C.

2.6.2 Alkaline phosphatase (AP)-binding assay

To generate $VEGF_{121}$, $VEGF_{165}$ and $VEGF_{189}$ isoform-specific AP probes, the open reading frames for each VEGF isoform was amplified from pBluescript plasmid containing the relevant cDNA sequences by PCR with the oligonucleotides 5'-AATAATGGATCCGCACCCATGGCAGAAGGAG-3' and 5'-TATATGCTCGAGCTCACCGCCTCGGCTTGTC-3'. The PCR products were cloned into pAG3-AP containing an upstream in-frame AP cassette, which was kindly donated by Dr Jonathan Raper, University of Pennsylvania. For this, the pAG3-AP plasmid was cut using the restriction enzymes BglII and XhoI (New England Biolabs) and ligated using T4 ligase (New England Biolabs) to the PCR product digested with BamHI and XhoI. The ligation products were transformed using chemically competent bacteria and the plasmid was isolated with a HiSpeed Plasmid Maxi kit (Qiagen) according to the manufacturer's instructions.

AP expression vectors were transfected into HEK-293T or Cos cells using Lipofectamine 2000 (Life Technologies). Briefly, cells were transfected using 1 ml of Opti-MEM (Life Technologies) containing 31 µl of Lipofectamine 2000 and 13 µg of plasmid DNA which was mixed with cells cultured in DMEM and incubated at 37°C in 5% $CO_2$for 4-6 hours. The medium was then replaced with DMEM

supplemented with 10% FBS and PenStrep. Cells were incubated at 37°C in 5% CO_2 for 48 hours and the conditioned media containing AP-fusion protein was collected and stored in aliquots at -80°C. AP activity was checked by spotting conditioned media on nitrocellulose filters and incubating in NTMT buffer (100 mM NaCl, 100 mM Tris-HCl pH 9.5, 1% Tween20, 50 mM $MgCl_2$) with BCIP and NBT.

For wholemount AP assays, freshly dissected E12.5 hindbrains were incubated in PBS containing 10% FBS for 30 minutes at room temperature, then incubated overnight with conditioned media containing AP-fusion protein at 4°C. The following day, tissue was washed with PBS 3 times for 10 minutes at room temperature, then fixed with 4% formaldehyde solution for 1 hour at room temperature, and washed with PBT 3 times for 10 minutes also at room temperature. The samples were incubated for 3 hours at 65°C in order to heat-inactivate endogenous AP. After that the samples were washed 2 times in PBS for 10 minutes and incubated in NTMT buffer containing BCIP and NBT at room temperature until colour developed. To stop the developing reaction samples were washed in PBS and kept at 4°C in formaldehyde solution.

2.6.3 DiI labelling

DiI labelling was performed with fixed tissues as described (Erskine et al., 2011). A DiI crystal (Life Technologies) was placed over the optic disc of one eye for anterograde labelling. After 3 days at 37˚C, dissected brains were imaged ventral side up. ImageJ was used to determine the pixel intensity in defined areas of the ipsilateral and contralateral optic tracts, and the ipsilateral index calculated as the ratio of fluorescent intensity in the ipsilateral relative to the ipsilateral plus contralateral tracts. For retrograde labelling, the cortex was removed unilaterally and DiI crystals placed in a row over the dorsal thalamus for 15 weeks at room temperature; we imaged flatmounted retinas as above and determined the percentage of labelled ipsilateral RGCs relative to the ipsilateral plus contralateral RGCs. A minimum of three embryos were analysed for each genotype. Tissue was collected and fixed by Miguel Tillo and DiI labelling was performed by Professor Lynda Erskine, University of Aberdeen.

2.7 HINDBRAIN EXPLANTS

Culture inserts with 8-micrometer pore size (Corning) were washed in sterile PBS and incubated in Neurobasal (Life Technologies) supplemented with 20 μg/ml laminin (Life Technologies) for at least 1 hour at 37°C in 5% CO_2. Hindbrains were dissected from E11.25 embryos in ice cold L15 (Life Technologies), meninges were removed and hindbrains left in an open-book preparation. After dissection, 1-3 Affi-Gel heparin beads (Biorad), soaked overnight in 100 μg/ml VEGF (Peprotech) or 10 μg/ml FGF2 (Sigma), were implanted on one side of the hindbrain at the level of rhombomere 6. Each hindbrain was placed ventral side up in one previously coated culture insert and dried using a paper towel. The embryos were cultured in Neurobasal medium supplemented with 20 μl/ml 50X B-27 (Life Technologies) and 6 ng/ml glucose and incubated for 30 hours at 37°C in 5% CO2. FBM neuron migration was measured with ImageJ (NIH) as the distance travelled from r5 to the leading group of cells in r6 in each hindbrain and normalised to the control side of each hindbrain. This protocol has been published in (Tillo et al., 2014) (a copy of the publication is appended to this thesis).

2.8 GnRH NEURON (GN11) CULTURE AND SURVIVAL ASSAY

GN11 cells were grown in standard conditions (Dulbecco's MEM containing 1 mM sodium pyruvate, 100 mg/ml streptomycin, 100 U/ml penicillin and 10% FBS; Life Technologies). The cells were then seeded in 24-well plates at a density of 5000 cells/well and grown for 24 hours in same standard conditions. For survival assays, cells were serum starved for 72 h and treated for 12 h with media containing 10% FBS, 10 ng/ml $VEGF_{120}$, $VEGF_{164}$ or $VEGF_{188}$. Cells were labelled with propidium iodide (PI) (Life Technologies) and Hoechst fluorochrome (Life Technologies). The number of non-viable cells was determined as the relative number of PI-labelled cells compared to the total number of Hoechst fluorochrome-positive cells.

2.9 GnRH NEURON QUANTIFICATION IN VIVO

E14.5 heads were fixed in 4% PFA for 4-8 hours at room temperature. The tissue was cryoprotected in 30% sucrose in PBS and embedded in Tissue-Tek OCT. Using a cryostat the heads were sectioned sagitally in 20 μm sections. The sections were then incubated in 3% H_2O_2 for 1 hour at room temperature before immunolabelling with anti-GnRH antibody as previously described in Section 2.4. A minimum of three embryos were analysed for each genotype. The total number of GnRH-positive cells was counted across every section in each head.

2.10 IMAGING

Fluorescently labelled samples were imaged using a laser scanning confocal microscope (LSM510, LSM700, LSM710, Zeiss). HRP labelled tissue and *in situ* hybridisation were photographed using an Olympus SZX16 equipped with a camera (QImaging Micropublisher 3.3 RTV) and the imaging software OpenLab 5.5.2 (Improvision Ltd.). Images were processed using Adobe Photoshop CS4 (Adobe Systems, Inc.).

2.11 RT-PCR

Tissue was homogenised using a 23G needle syringe and RNA was extracted with 1 ml of Tri-Reagent (Sigma) according to manufacturers instructions. 250 µl of chloroform were added to each sample, shaken vigorously, and centrifuged at 12000 rpm for 15 minutes at 4°C. Samples separated into 3 phases and the upper aqueous phase was transferred to a new tube and 500 µl of isopropanol were added. The mixture was incubated for 10 minutes at room temperature and then centrifuged at 12000 rpm for 10 minutes at 4°C. The remaining pellet was washed with 70% ethanol, air dried and resuspended in 20 µl of water. The concentration of RNA was quantified and quality was assessed using a NanoDrop Spectrophotometer ND-1000 (Thermo Scientific).

cDNA was synthesised using Superscript Reverse Transcriptase III kit (Life Technologies). The mixture contained 1 µg of RNA, 3 µg of random primers and 1 µl of dNTPs made up with water to a total volume of 12 µl, and was heated to 65°C for 5 minutes then rapidly chilled on ice. Following this, 4 µl of 5X First Strand Buffer, 2 µl of 0.1 M dithiothreitol (DTT) and 1 µl of RNAse OUT (40 units/µl), 1 µl of Superscript Reverse Transcriptase III was added and the mixture was incubated at 25°C for 10 minutes, 50°C for 1 hour and lastly at 70°C for 15 minutes to stop the reaction. All cDNA was stored at -20°C.

RT-PCR was carried out using Megamix Blue reaction mix (Microzone) and oligonucleotides (see Table 2.6 for sequences) (Sigma).

Gene	Primer	Sequence
Fgfr1	Forward	5'-AACCTCTAACCGCAGAAC-3'
	Reverse	5'-GAGACTCCACTTCCACAG-3'
Fgfr2	Forward	5'-AATCTCCCAACCAGAAGCGTA-3'
	Reverse	5'-CTCCCCAATAAGCACTGTCCT-3'
Fgfr3	Forward	5'-GGAGGACGTGGCTGAAGAC-3'
	Reverse	5'-GGAGCTTGATGCCCCCAAT-3'
Fgfr4	Forward	5'-ATGACCGTCGTACACAATCTTAC-3'
	Reverse	5'-TGTCCAGTAGGGTGCTTGC-3'
Vegfa 120	Forward	5'-GTAACGATGAAGCCCTGGAG-3'
	Reverse	5'-CCTTGGCTTGTCACATTTTTC-3'
Vegfa 164	Forward	5'-AGCCAGAAAATCACTGTGAGC-3'
	Reverse	R 5'-GCCTTGGCTTGTCACATCT-3'
Vegfa 188	Forward	5'-AGTTCGAGGAAAGGGAAAGG-3'
	Reverse	5'-GCCTTGGCTTGTCACATCT-3'

Table 2.6 Oligonucleotide sequences for RT-PCR.

Chapter 3 $VEGF_{189}$ BINDS TO NRP1 IN THE DEVELOPING NERVOUS SYSTEM

3.1 INTRODUCTION

VEGF-A is a potent inducer of blood vessel growth, but also has essential roles in neurodevelopment (Mackenzie and Ruhrberg, 2012). In humans, VEGF is encoded by a single gene (*VEGFA)* of eight exons that is alternatively spliced into isoforms, the major ones containing 121, 165 and 189 amino acid residues in humans and therefore termed $VEGF_{121}$, $VEGF_{165}$ and $VEGF_{189}$, respectively (Figure 3.1 **A**; (Koch et al., 2011). The alternatively spliced exons 6 and 7 encode domains enable ECM binding, with $VEGF_{121}$ being the most diffusible and $VEGF_{189}$ the least soluble, whilst $VEGF_{165}$ has intermediate properties. Furthermore, these exons additionally mediate differential binding to VEGF receptors. All VEGF isoforms bind the receptor tyrosine kinases VEGFR1 and VEGFR2, whereas the non-catalytic receptors NRP1 and NRP2 are VEGF isoform-specific receptors that preferentially bind $VEGF_{165}$ over $VEGF_{121}$ (Figure 3.1 **A**; (Soker et al., 1998; Gluzman-Poltorak et al., 2000). Unexpectedly, recent studies from our lab and others showed that VEGF binding to NRP1 is largely dispensable for embryonic angiogenesis (Fantin et al., 2014; Gelfand et al., 2014). In contrast, VEGF signalling through NRP1 has multiple roles in neurodevelopment, including guiding FBM neurons in the hindbrain (Schwarz et al., 2004), promoting the survival of migrating gonadotropin-releasing hormone (GnRH) neurons (Cariboni et al., 2011) and enhancing the contralateral projection of RGC axons across the optic chiasm (Erskine et al., 2011).

To demonstrate roles for VEGF binding to NRP1 in neurons, prior studies used $Vegfa^{120/120}$ mice, which express $VEGF_{120}$, the murine equivalent of $VEGF_{121}$, but lack $VEGF_{164}$ and $VEGF_{188}$, corresponding to human $VEGF_{165}$ and $VEGF_{189}$, respectively (Carmeliet et al., 1999). $Vegfa^{120/120}$ mice phenocopy the defects of NRP1 knockouts in FBM neuron migration, GnRH neuron survival and RGC axon guidance (Schwarz et al., 2004; Cariboni et al., 2011; Erskine et al., 2011). In all three systems, VEGF signalling was attributed to the activity of $VEGF_{164}$, because it evokes appropriate neuronal responses in *in vitro* models including neuronal migration in hindbrain explants; axon outgrowth in RGC explants; survival in GnRH

neuron cultures (Schwarz et al., 2004; Cariboni et al., 2011; Erskine et al., 2011), and because NRP1's ability to bind $VEGF_{165}$ is well established (Soker et al., 1998; Parker et al., 2012) However, *Vegfa*$^{120/120}$ mutants lack $VEGF_{188}$ in addition to $VEGF_{164}$. Yet, it has never previously been examined if $VEGF_{189}$ can also function as a NRP1 ligand *in vivo*. Moreover, it is not known if $VEGF_{121}$ can bind NRP1 in a physiologically relevant context, even though it has been suggested that the exon 8 domain, present in all major VEGF isoforms including $VEGF_{121,}$ can mediate NRP1 binding *in vitro* (Jia et al., 2006; Pan et al., 2007; Parker et al., 2012).

I have generated alkaline phosphatase (AP)-conjugated VEGF isoforms for *in situ* ligand binding assays (Fantin et al., 2014) to examine if $VEGF_{121}$ or $VEGF_{189}$ can bind NRP1 *in vivo*, as previously reported for $VEGF_{165}$. In this chapter, I demonstrate that $VEGF_{189}$ binds NRP1-expressing axon tracts in intact hindbrain tissue, but that $VEGF_{121}$ is unable to do so. I further show that $VEGF_{188}$ is co-expressed with the other isoforms during VEGF/NRP1-dependent FBM neuron migration, GnRH neuron survival and RGC axon guidance. In collaboration with Dr Anna Cariboni and Dr Lynda Erskine, I further show that $VEGF_{188}$ is sufficient to control FBM migration, GnRH neuron survival and RGC axon guidance, whilst $VEGF_{120}$ is not. I conclude that $VEGF_{188}$ effectively binds NRP1 and has the capacity to evoke NRP1-dependent signalling events, similar to $VEGF_{164}$. This work has been published in (Tillo et al., 2015) (a copy of the publication is appended to this thesis). Considering that $VEGF_{189}$ has the highest affinity for ECM and therefore tissue retention amongst the VEGF isoforms, future research may therefore wish to consider the mechanistic contribution and therapeutic potential of this understudied VEGF isoform.

3.2 RESULTS

3.2.1 $VEGF_{188}$ is co-expressed with $VEGF_{120}$ and $VEGF_{164}$ in developing hindbrain, nose and diencephalon

Because prior studies implicated VEGF signalling through NRP1 in FBM neuron migration in the hindbrain, GnRH neuron survival in the nose and RGC axon guidance in the diencephalon (Schwarz et al., 2004; Cariboni et al., 2011; Erskine et al., 2011), I asked which *Vegfa* isoforms were expressed in these developmental contexts. For this experiment, I collaborated with Dr Alessandro Fantin, who designed isoform specific primers that can distinguish the most *Vegfa120*, *Vegfa164* and *Vegfa188* mRNA species by reverse transcription (RT)-PCR (Figure 3.1 **A, B**). The isoform specific primers were sometimes required to span across two exons and target exons 3 to 5/8 to amplify *Vegfa120* (size 179 bp), exons 5/7 to 7/8 to amplify *Vegfa164* (size 159 bp), and exons 6 to 7/8 to amplify *Vegfa188* (size 215 bp) (red arrows in Figure 3.1 **A**). I validated the specificity of each isoform specific primer in collaboration with Dr Fantin and Ms Laura Denti using a pBlueScript vectors containing mouse *Vegfa120*, *Vegfa164* and *Vegfa188* cDNA. Results showed that each isoform specific primer was specific and only amplified its corresponding *Vegfa* isoform vector (Figure 3.1 **B**). I also prepared cDNA from the isoform-specific mouse strains $Vegfa^{120/120}$ and $Vegfa^{164/164}$ for further validation of the specificity of the designed isoform specific primers (Figure 3.1 **C**). Using these primers for RT-PCR of cDNA derived from mouse embryo nose, hindbrain and diencephalon tissue, I then demonstrated that all 3 isoforms were co-expressed at relevant periods of VEGF/NRP1-dependent neurodevelopment (Figure 3.1 **D**).

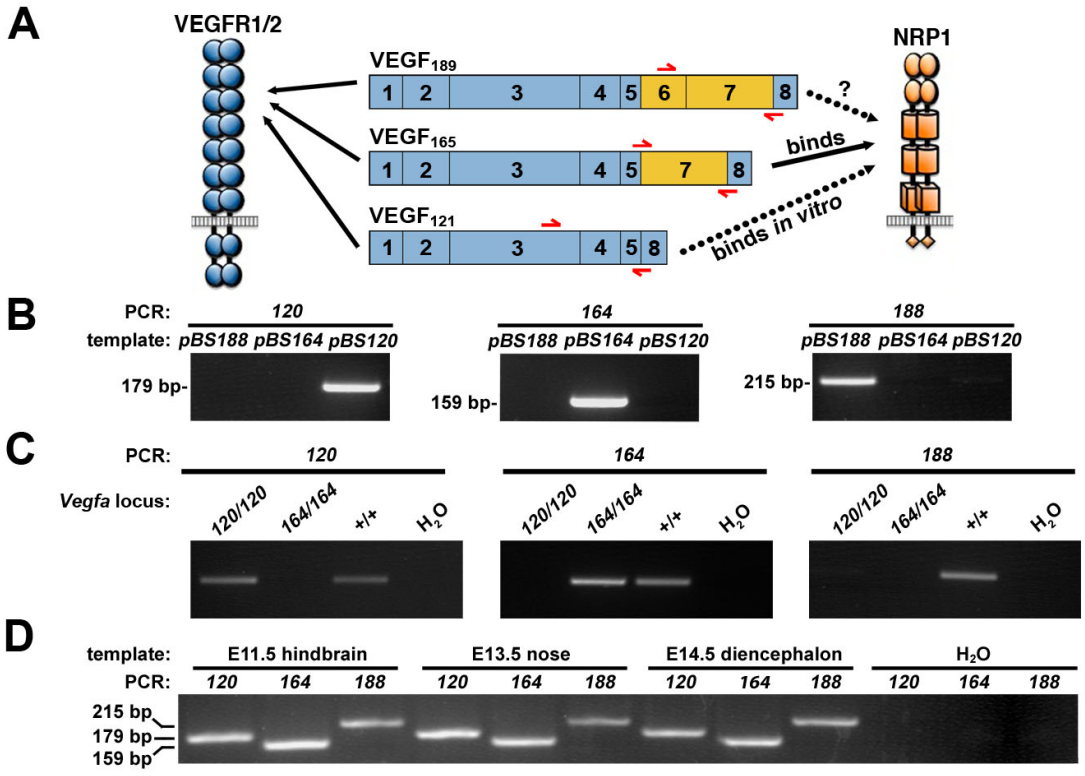

Figure 3.1 VEGF$_{189}$ is expressed in developing mouse tissues.

(A) Current knowledge of VEGF isoform binding to their receptors. All isoforms bind VEGFR1/2, whilst only VEGF$_{165}$ is known to bind NRP1. VEGF$_{121}$ can bind NRP1 with low affinity *in vitro*, but whether this association occurs *in vivo* has not been shown. Moreover, it is not known whether VEGF$_{189}$ binds NRP1 *in vivo*. Red arrows indicate the position of oligonucleotide primers used for RT-PCR in (**B**).

(B) *Vegfa* isoform-specific oligonucleotide primers for RT-PCR were validated with pBlueScript vectors (pBS) containing mouse *Vegfa120*, *Vegfa164* or *Vegfa188* cDNA, respectively. Unspecific amplification was not observed using any of the isoform specific primers.

(**C**) The specificity of oligonucleotide primers for *Vegfa* isoform expression analysis was validated by RT-PCR using cDNA derived from *Vegfa*$^{120/120}$, *Vegfa*$^{164/164}$ or wild type E12.5 mouse embryo trunks, respectively. Note that a molecular weight standard confirmed the predicted sizes of each isoform as 179, 159 and 215 bp, respectively.

(**D**) RT-PCR analysis of the indicated tissues shows that *Vegfa120* (179 bp), *Vegfa164* (159 bp) and *Vegfa188* (215 bp) are co-expressed in E11.5 hindbrain, E13.5 nose and E14.5 diencephalon mouse tissue.

3.2.2 $VEGF_{189}$ binds axons in a NRP1-dependent fashion

Because prior studies of VEGF binding to NRP1 have not examined if $VEGF_{189}$ or $VEGF_{121}$ can bind NRP1 *in vivo*, I used the mouse hindbrain as a physiologically relevant model to compare the ability of the three major VEGF isoforms to bind NRP1 in a tissue context. I first performed immunostaining on wholemount E12.5 hindbrains with a validated antibody for NRP1 (Fantin et al., 2010) to confirm that NRP1 localises to blood vessels in wild type, but not NRP1 knockout hindbrains (Figure 3.2 **A**; note unspecific staining of blood in the dilated vessels of mutants). Immunolabelling also confirmed NRP1 is expressed in TUJ1-positive dorsolateral axons on the pial side of wild type, but not mutant hindbrains (Figure 3.2 **A**). *Nrp1*$^{-/-}$ hindbrains showed some defasciculation of these dorsolateral axons, but they were still clearly present in the mutant, as shown by TUJ1 staining. Overall, these observations suggest that the hindbrain dorsolateral axons are a suitable model to examine VEGF-A isoform binding to NRP1.

To compare the binding properties of $VEGF_{121,}$ $VEGF_{165}$ and $VEGF_{189}$, I fused the cDNA for each isoform to an expression cassette encoding alkaline phosphatase (AP). I then transfected these expression plasmids into Cos cells and used the cell supernatants containing the fusion proteins to perform *in situ* ligand binding assays on E12.5 hindbrains. By visualising alkaline phosphate activity, this technique allowed me to analyse *in vivo*, which VEGF isoforms can bind to tissues expressing the different VEGF receptors. As expected from previous work, all 3 isoforms bound vessels (Figure 3.3 **A**), correlating with their expression of the pan-VEGF isoform receptor VEGFR2 (Lanahan et al., 2013). I next examined binding to the dorsolateral axons, because they express NRP1, but lack VEGFR2 or VEGFR1 (Lanahan et al., 2013), which makes them an ideal model to study VEGF/NRP1 binding. Both $VEGF_{165}$ and $VEGF_{189}$ bound these axons, whilst $VEGF_{121}$ did not (Figure 3.3 **A**). These observations indicate that all VEGF isoforms are capable of binding VEGFR2/NRP1-positive vessels. In contrast, only $VEGF_{165}$ and $VEGF_{189}$, but not $VEGF_{121}$, bound NRP1-expressing axons lacking VEGFR2.

I next confirmed that axonal $VEGF_{189}$ binding is NRP1-dependent, similar to $VEGF_{165}$ binding. For this experiment, I performed *in situ* ligand binding assays on *Nrp1*$^{-/-}$ hindbrains that have no NRP1 expression in any tissue. This assay showed

that $VEGF_{189}$ bound vessels (Figure 3.3 **B**) in *Nrp1*-null mutant hindbrains with their characteristic vascular tufts (Fantin et al., 2013). This correlates with the retention of VEGFR2 in *Nrp1*-null mutants. In contrast, AP-$VEGF_{189}$ failed to bind axons in *Nrp1*-null hindbrains, similar to AP-$VEGF_{165}$, because these axons do not express NRP1 or any other VEGF receptor type (Figure 3.3 **B**). This shows that $VEGF_{189}$ can bind axons in a NRP1-dependent fashion. To further confirm that AP-$VEGF_{189}$ binding was specific to NRP1, I also performed binding assays in *Nrp2*-null mutant hindbrains. NRP2 is expressed in a subpopulation of dorsolateral axons, but loss of NRP2 (Giger et al., 2000) did not abolish $VEGF_{189}$ binding (Figure 3.3 **B**). Taken together, the ligand binding assays of intact hindbrain tissue show that NRP1 serves as a neuronal receptor for $VEGF_{165}$ and $VEGF_{189,}$ but not $VEGF_{121}$.

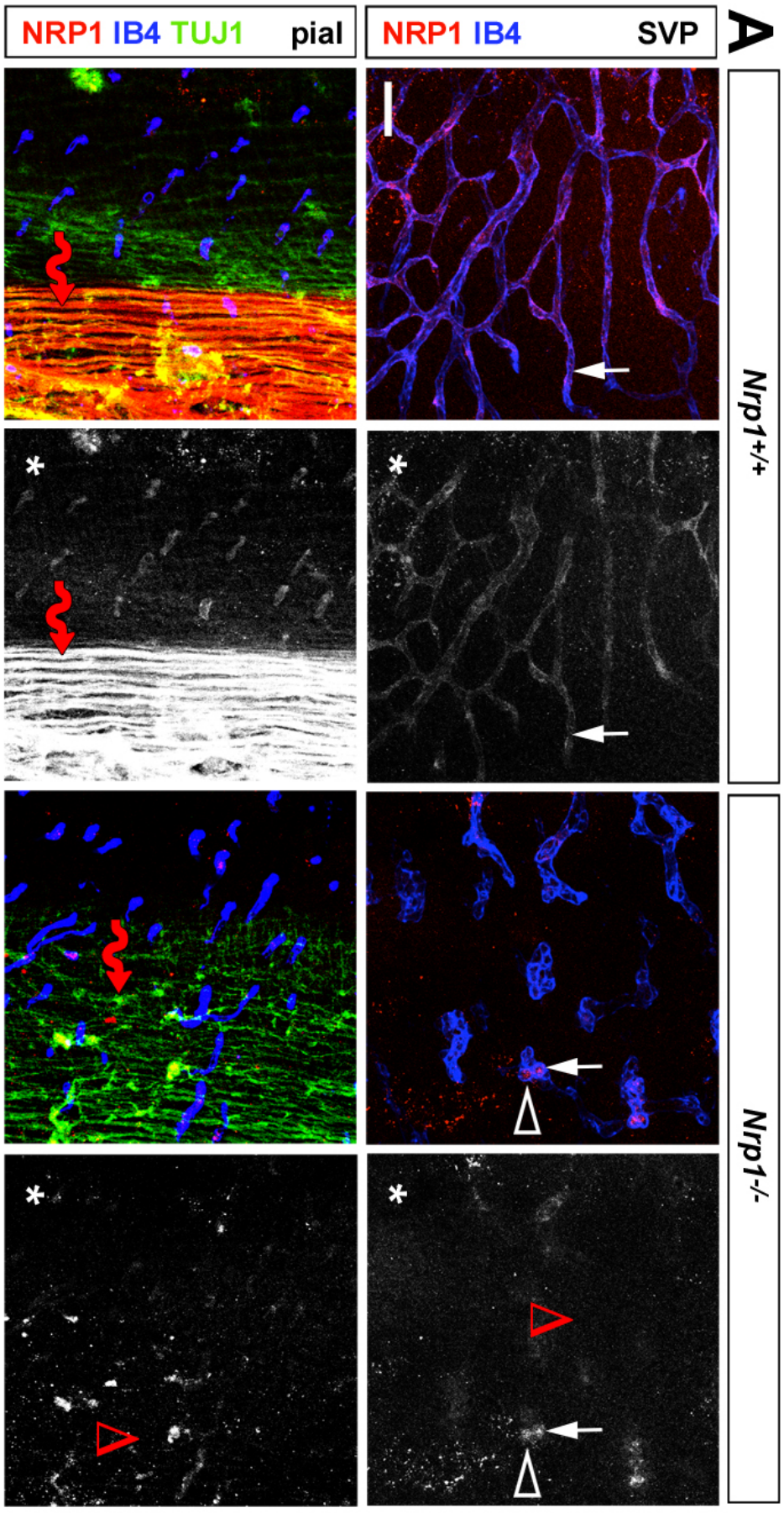
A
NRP1 IB4 TUJ1 pial
NRP1 IB4 SVP
Nrp1+/+
Nrp1-/-

Figure 3.2 NRP1 is expressed in the developing hindbrain.

(**A**) Wholemount staining of E12.5 wild type hindbrains for NRP1 and TUJ1 together with IB4; single NRP1 channels are shown in grey scale adjacent to each panel. The white arrow indicates IB4-positive vessels, the arrowhead unspecific NRP1 staining of blood cells inside mutant vessels and the red wavy arrow TUJ1-positive axons; open triangles indicate absent NRP1 staining in subventricular plexus (SVP) vessels and pial axons. Asterisks indicate most medial section of the hindbrain, towards the midline. Scale bar: 200 μm.

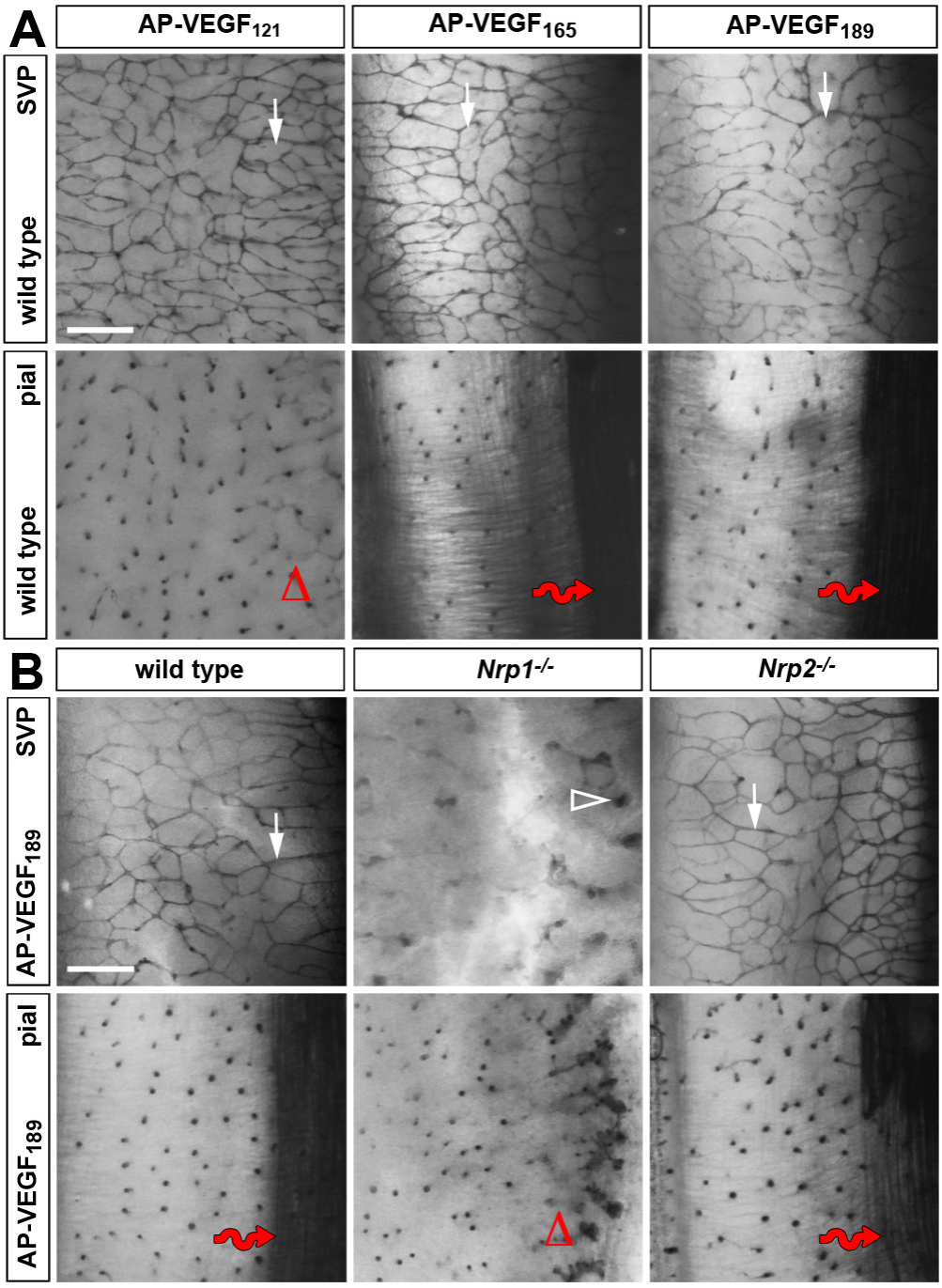

Figure 3.3 VEGF$_{189}$ binds NRP1 in the developing hindbrain.

(**A, B**) AP-VEGF$_{121}$, AP-VEGF$_{165}$ and AP-VEGF$_{189}$ binding to E12.5 wild type hindbrains (**A**) and AP-VEGF$_{189}$ binding assay on E12.5 *Nrp1*$^{-/-}$ and *Nrp2*$^{-/-}$ hindbrains (**B**). The white arrows indicate VEGF binding to vessels, the red wavy arrows binding to axons; the open triangles indicate absence of VEGF$_{121}$ binding to wild type axons in (**A**) and absence of VEGF$_{189}$ binding to axons in *Nrp1*$^{-/-}$ hindbrains in (**B**). The arrowhead indicates vascular tufts. Scale bar: 25 µm.

3.2.3 $VEGF_{188}$ is sufficient for the NRP1-dependent migration of FBM neurons

Vegfa is a haploinsufficient gene, as deletion of just one allele causes early embryonic lethality due to a complete failure of blood vessel formation (Carmeliet et al., 1996; Ferrara et al., 1996). However, retention of any one of the major VEGF isoforms rescues this severe phenotype and instead gives rise to more subtle vascular and neuronal phenotypes (Ruhrberg et al., 2002; Stalmans et al., 2002). I first examined if $VEGF_{188}$ can substitute for $VEGF_{164}$ in NRP1-dependent FBM neuron guidance with an established hindbrain explant assay. In this assay, implanted beads provide exogenous VEGF and FBM neuron migration is visualised by immunolabelling with the motor neuron marker ISL1 (Schwarz et al., 2004; Tillo et al., 2014). As had been previously observed, FBM neurons were attracted to $VEGF_{164}$, but not to control beads soaked in PBS only (Figure 3.4 **A**). I then used $VEGF_{188}$ soaked beads and observed that these also attracted FBM neurons in similar manner to $VEGF_{164}$ (Figure 3.4 **A**). Quantification of the distance travelled by FBM neurons confirmed that migration was significantly enhanced on the hindbrain side containing a $VEGF_{164}$- or $VEGF_{188}$-soaked bead relative to the control side of the same hindbrain (Figure 3.4 **B**). $VEGF_{188}$ can therefore promote NRP1-dependent neuronal migration similar to $VEGF_{164}$.

I next examined FBM neuron migration *in vivo* by wholemount *Isl1* ISH. As previously shown (Schwarz et al., 2004), $Vegfa^{120/120}$ hindbrains demonstrated abnormal split stream of FBM neurons on the ventricular side and dumbbell-shaped nuclei on the pial side (Figure 3.4 **C**). This is similar but less severe to the phenotype observed in $Nrp1^{-/-}$ mice (Schwarz et al., 2004). In contrast, $Vegfa^{188/188}$ mice, which express only $VEGF_{188}$ at the expense of other isoforms, showed normal FBM neuron migration similar to what was previously described in $Vegfa^{164/164}$ mice (Schwarz et al., 2004) (Figure 3.4 **C**). Heterozygous $Vegfa^{120/+}$ mice display normal FBM neuron migration and replacing one $Vegfa^{120}$ allele in $Vegfa^{120/120}$ mutants with the $Vegfa^{188}$ allele ($Vegfa^{120/188}$) was also sufficient to prevent FBM neuron migration defects (Figure 3.4 **C**). Altogether these results show that unlike $VEGF_{120}$, $VEGF_{188}$ is therefore sufficient to direct NRP1-dependent neuronal migration.

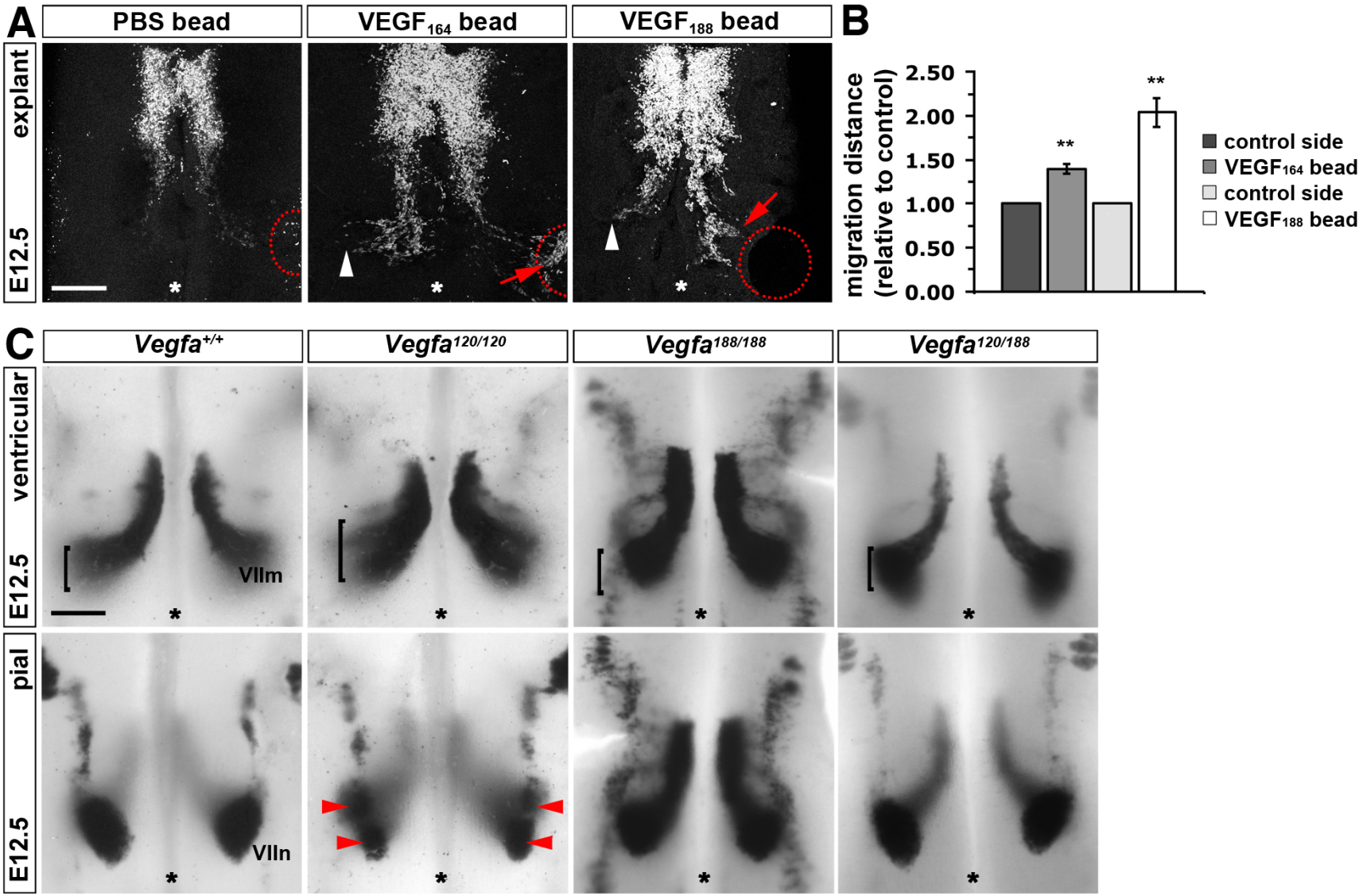
A
PBS bead
VEGF164 bead
VEGF188 bead
explant
E12.5
B
migration distance (relative to control)
2.50
2.00
1.50
1.00
0.50
0.00
**
**
control side
VEGF164 bead
control side
VEGF188 bead
C
Vegfa+/+
Vegfa120/120
Vegfa188/188
Vegfa120/188
ventricular
pial
E12.5
VIIm
VIIn

Figure 3.4 $VEGF_{188}$ is sufficient for FBM neuron migration.

(**A**) ISL1 staining of E12.5 hindbrain explants containing implanted heparin beads soaked in PBS (n=10) or PBS containing $VEGF_{164}$ (n=10) or $VEGF_{188}$ (n=6). Red dotted circles indicate the position of heparin beads; white arrowheads indicate normal migration; red arrows indicate migration towards heparin beads; asterisks indicate the midline. Scale bar 200 μm.

(**B**) Distance migrated by FBM neurons. Migration distance was quantified as migration away from r5 territory on the hindbrain side with a bead relative to the control half of the same hindbrain; mean ± s.e.m. control 1 ± 0.09 vs. $VEGF_{164}$ bead 1.39 ± 0.05 and control 1 ± 0.11 vs. $VEGF_{188}$ bead 2.04 ± 0.17; asterisks indicate **$p<0.01$ VEGF compared to control (t-test).

(**C**) Wholemount *Isl1* ISH of E12.5 hindbrains of the indicated genotypes detects migrating FBM neurons (VIIm) (control n=10, $Vegfa^{120/120}$ n=6, $Vegfa^{188/188}$ n=4, $Vegfa^{120/188}$ n=5) Brackets indicate the width of the neuronal stream on the ventricular side; red arrowheads indicate dumbbell-shaped nuclei on the pial side; asterisks indicate the midline. Scale bar 25 μm.

3.2.4 $VEGF_{188}$ is sufficient to guide NRP1-dependent axons at the optic chiasm

Professor Lynda Erskine and I (herein referred to as "we") next investigated if $VEGF_{188}$ can evoke neuronal responses similar to $VEGF_{164}$ in the developing visual system. To establish binocular vision, RGC axons project through the optic chiasm to both the ipsilateral and contralateral brain hemispheres (Erskine and Herrera, 2007). $VEGF_{164}$, but not $VEGF_{120}$, promotes RGC axon guidance in a NRP1-dependent fashion *in vitro* (Erskine et al., 2011). Furthermore *Nrp1*-null mice have an abnormal chiasm with too many ipsilateral projecting axons, and a similar defect is seen in $Vegfa^{120/120}$ mice (Erskine et al., 2011). To examine if $VEGF_{188}$ can also promote RGC axon guidance, we performed DiI labelling in VEGF isoform mutants in a similar way to the experiments to study FBM neuron migration.

Anterograde DiI labelling of RGC axons from one $Vegfa^{188/188}$ eye at E14.5 demonstrated that $VEGF_{188}$ was sufficient for NRP1-mediated chiasm patterning (Figure 3.5 **A**). Thus, $Vegfa^{120/120}$ mice had a significantly increased ipsilateral projection index as well as defasciculation of the ipsilateral and contralateral optic tracts (Erskine et al., 2011), but the ipsilateral index and shape of the optic chiasm appeared unaffected in $Vegfa^{188/188}$ mice (Figure 3.5 **B, C**). Moreover, replacing one $Vegfa^{120}$ with the $Vegfa^{188}$ allele was sufficient to prevent chiasm defects observed in $Vegfa^{120/120}$ mutants (Figure 3.5 **B, C**).

We next performed retrograde DiI labelling of RGC axons from the dorsal thalamus in VEGF isoform mice and compared the number of labelled RGCs in flatmounted ipsilateral and contralateral retina (Figure 3.6 **A**). Quantitation showed that the proportion of DiI-labelled ipsilateral RGCs was significantly increased in $Vegfa^{120/120}$ compared to control mice, but was normal in $Vegfa^{188/188}$ and $Vegfa^{120/188}$ mice (Figure 3.6 **B**). Flatmount images also revealed the preferential origin of ipsilaterally projecting neurons from the ventrotemporal retina in wild types (Figure 3.6 **C**). Their distribution is affected in $Vegfa^{120/120}$ mice, which contain ipsilaterally projecting RGCs throughout the nasal retina (Erskine et al., 2011), but this defect was rescued by the introduction of a single $Vegfa^{188}$ allele (Figure 3.6 **C**). Therefore $VEGF_{188}$ is sufficient to promote NRP1-dependent aspects of optic chiasm development. All mouse tissue was collected and processed by me and subsequently DiI labelled and quantified by Professor Lynda Erskine.

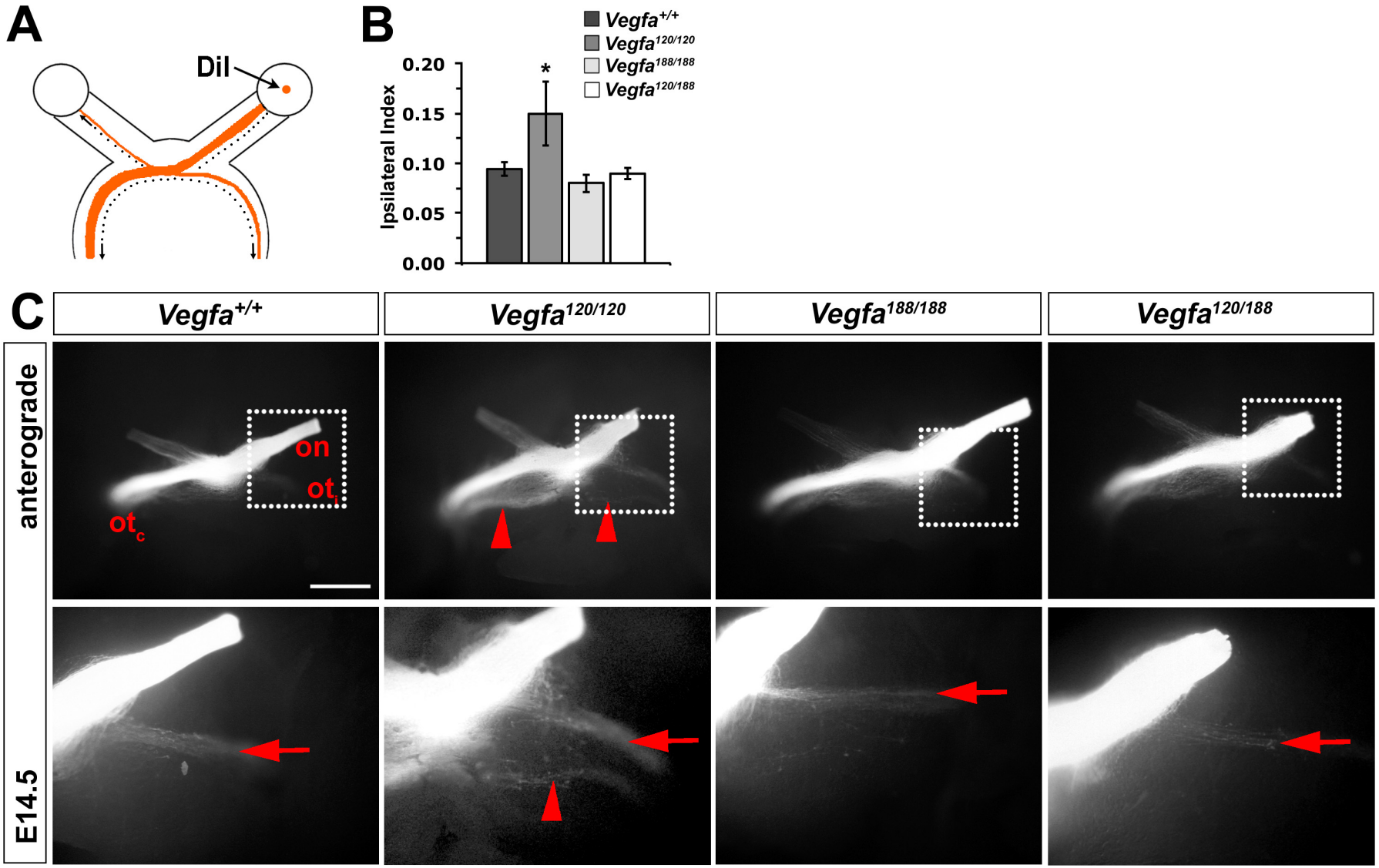
A
DiI
B
Vegfa+/+
Vegfa120/120
Vegfa188/188
Vegfa120/188
Ipsilateral Index
0.20
0.15
0.10
0.05
0.00
*
C
Vegfa+/+
Vegfa120/120
Vegfa188/188
Vegfa120/188
anterograde
E14.5
on
otl
otc

Figure 3.5 $VEGF_{188}$ is sufficient to guide anterogradely labelled commissural axons across the optic chiasm.

(**A**) Schematic illustration of the method used to anterogradely label RGC projections. DiI crystals were placed onto the retina in one eye to label axons extending through the optic chiasm into the ipsilateral and contralateral optic tracts.

(**B**) Ipsilateral index in the indicated genotypes (mean ± s.e.m.): control 0.095 ± 0.01, n=11; $Vegfa^{120/120}$ 0.15 ± 0.03, n=5; $Vegfa^{188/188}$ 0.083 ± 0.01, n=3; $Vegfa^{120/188}$ 0.09 ± 0.01, n=3; t-test, *p<0.05 compared to control.

(**C**) Representative wholemount views of RGC axons at the optic chiasm from embryos of the indicated genotypes, labelled anterogradely with DiI at E14.5; ventral view, anterior up; optic nerve (on), contralateral optic tract (ot_c) and ipsilateral optic tract (ot_i). Red arrows indicate the normal position of the ipsilateral projection, red arrowheads the secondary tract and axon defasciculation in $Vegfa^{120/120}$ mutants. Scale bar: 500 μm. High magnifications of each boxed areas are shown beneath the respective panels.

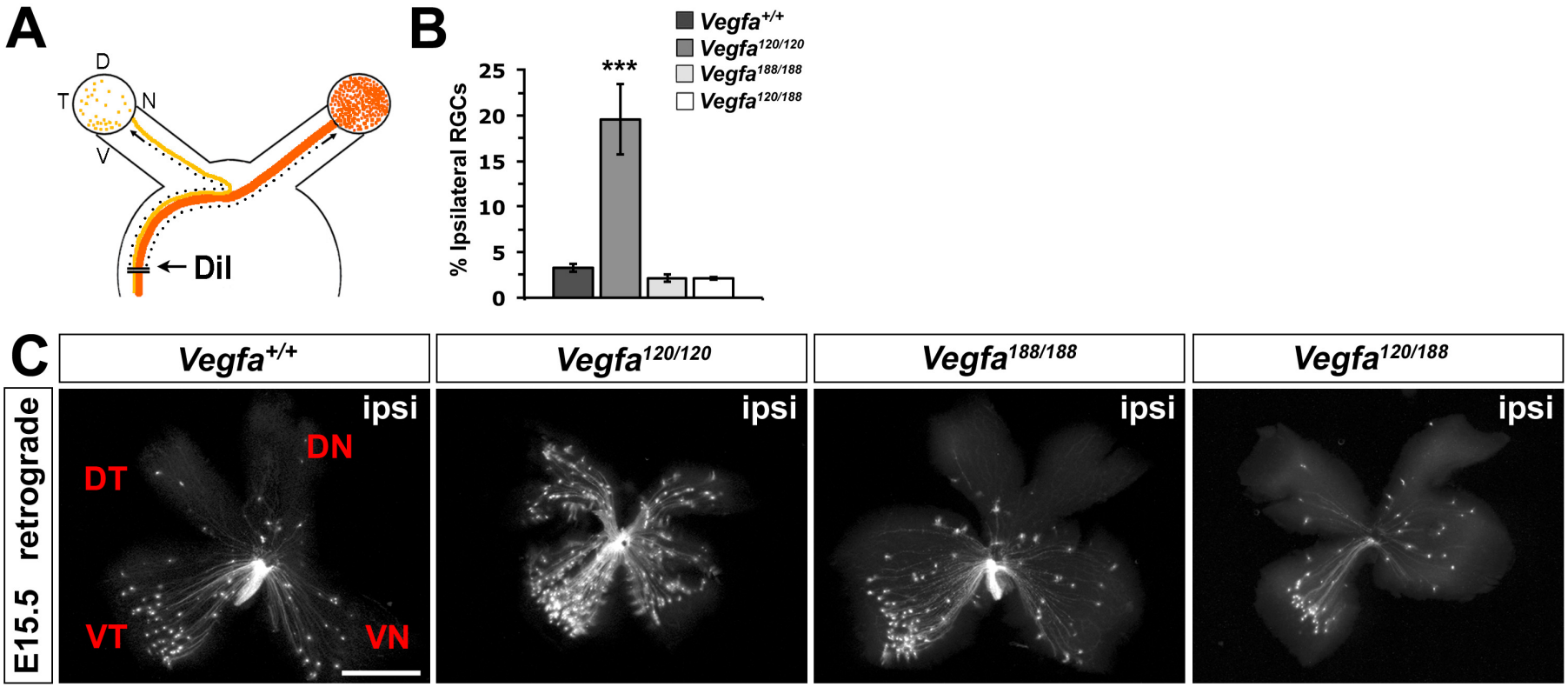
A
D
T
N
V
DiI
B
Vegfa+/+
Vegfa120/120
Vegfa188/188
Vegfa120/188
% Ipsilateral RGCs
25
20
15
10
5
0
***
C
Vegfa+/+
Vegfa120/120
Vegfa188/188
Vegfa120/188
E15.5 retrograde
ipsi
ipsi
ipsi
ipsi
DT
DN
VT
VN

Figure 3.6 $VEGF_{188}$ is sufficient to guide retrogradely labelled commissural axons across the optic chiasm.

(**A**) Schematic illustration of the method used to retrogradely label RGC projections. DiI crystals were placed unilaterally into the optic tract in the dorsal thalamus.

(**B**) Proportion of ipsilaterally projecting RGCs relative to total number of RGCs in both eyes of the indicated genotypes at E15.5 (mean ± s.e.m): control 3.28 ± 0.44%, n=8; *Vegfa*$^{120/120}$ 19.64 ± 3.89%, n=4; *Vegfa*$^{188/188}$ 2.16 ± 0.42%, n=4; *Vegfa*$^{120/188}$ 2.12 ± 0.14%, n=2; t-test, ***=p<0.001 compared to control.

(**C**) Representative examples of flatmounted ipsilateral retinas from E15.5 embryos of the indicated genotypes after retrograde labelling from the optic tract in the right thalamus. DT, dorsotemporal; VN, ventronasal; DN, dorsonasal; VT, ventrotemporal. Scale bar: 500 μm.

3.2.5 $VEGF_{188}$ is sufficient to ensure normal GnRH neuron survival

As a third model to study $VEGF_{188}$ in neurodevelopment, Dr Anna Cariboni and I (herein referred to as "we") investigated GnRH neuron survival. GnRH neurons are born in the nasal placode and travel along olfactory and vomeronasal axons to reach the forebrain (Figure 3.7 **A**; (Cariboni et al., 2007). The Ruhrberg lab has previously shown that $VEGF_{164}$ signals through NRP1 to promote the survival of migrating GnRH neurons by demonstrating that $Nrp1^{-/-}$ and $Vegfa^{120/120}$ mice have significantly fewer GnRH neurons in the embryonic nose (Cariboni et al., 2011). This study further used GN11 cells as an *in vitro* model that recapitulates many features of migratory GnRH neurons to show that $VEGF_{164}$ signals through NRP1 to promote GnRH neurons survival (Cariboni et al., 2011).

We first examined if $VEGF_{188}$ promotes GN11 survival, similar to $VEGF_{164}$. Whilst 72h of serum withdrawal caused the death of over half of the GN11 cells, the inclusion of serum, $VEGF_{164}$ or $VEGF_{188}$ for the last 12h of culture significantly reduced cell death, and $VEGF_{188}$ was as effective as $VEGF_{164}$ in preventing cell death; in contrast, and as expected, $VEGF_{120}$ did not promote survival (Figure 3.7 **B**; percentage of propidium iodide positive cells, mean ± s.e.m: control 44 ± 3%; serum 2 ± 1%; $VEGF_{120}$ 37 ± 3%; $VEGF_{164}$ 11 ± 2%, $VEGF_{188}$ 11 ± 2%). These observations suggest that $VEGF_{188}$, similar to $VEGF_{164}$, can promote GnRH neuron survival.

In agreement with the *in vitro* findings, the GnRH neuron number was normal in $Vegfa^{188/188}$ mice that express $VEGF_{188}$, but lack $VEGF_{164}$ (Figure 3.7 **C, D**). Moreover, replacing one $Vegfa^{120}$ allele in $Vegfa^{120/120}$ mutants with the $Vegfa^{188}$ allele ($Vegfa^{120/188}$) was sufficient to prevent the GnRH survival defect seen in $Vegfa^{120/120}$ mice (Figure 3.7 **C, D**; number of GnRH positive cells, mean ± s.e.m: control 1246 ± 46; $Vegfa^{120/120}$ 854 ± 21; $Vegfa^{188/188}$ 1335 ± 63; $Vegfa^{120/188}$ 1314 ± 58). Together, these data show that $VEGF_{188}$ is sufficient to promote NRP1-dependent GnRH neuron survival.

All tissue was collected, processed and immunostained by Miguel Tillo; cell counting and GN11 cell culture experiments were performed by Dr Anna Cariboni.

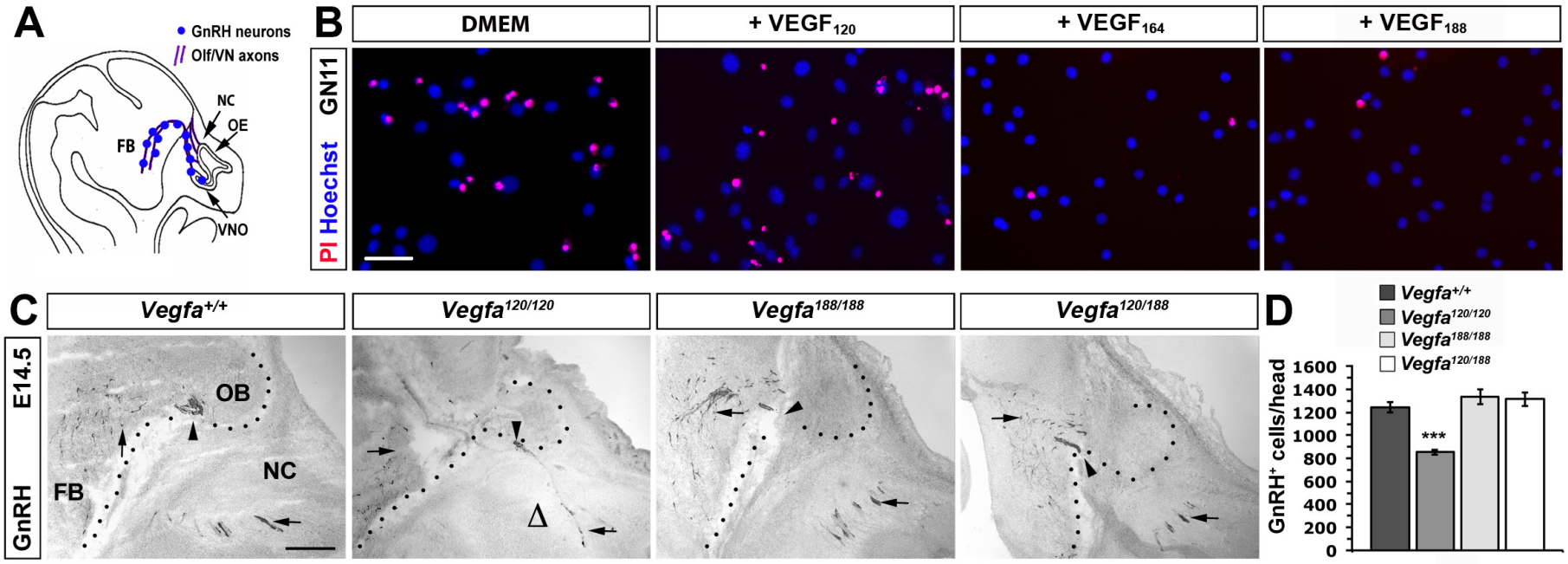
A
GnRH neurons
Olf/VN axons
NC
OE
FB
VNO
B
DMEM
+ VEGF120
+ VEGF164
+ VEGF188
GN11
PI Hoechst
C
Vegfa+/+
Vegfa120/120
Vegfa188/188
Vegfa120/188
E14.5
GnRH
OB
NC
FB
Δ
D
Vegfa+/+
Vegfa120/120
Vegfa188/188
Vegfa120/188
GnRH+ cells/head
1600
1400
1200
1000
800
600
400
200
0
***

Figure 3.7 $VEGF_{188}$ is sufficient to promote GnRH neuron survival.

(**A**) Schematic illustration of GnRH neuron migration (blue dots) in a mouse embryo head. The neurons are born in the nasal placodes that give rise to the olfactory and vomeronasal epithelia (OE, VNO) and migrate along olfactory and vomeronasal axons (purple, Olf/VN) through the nasal compartment (NC) to reach the forebrain (FB).

(**B**) Serum-starved GN11 cells were treated with DMEM or DMEM containing 10% FBS, $VEGF_{120}$, $VEGF_{164}$ or $VEGF_{188}$; cell death was visualised by propidium iodide staining (red); counterstaining with Hoechst (blue) was used to determine the proportion of PI+ cells in the total number of cells. Scale bar 25 μm.

(**C**) Sagittal sections of E14.5 mouse heads of the indicated genotypes, immunolabelled for GnRH. Arrows indicate migrating neurons, arrowheads blood vessels, open triangles absence of migrating neurons, dotted lines indicate the FB boundary; OB, olfactory bulb. Scale bar 100 μm.

(**D**) GnRH neuron number in E14.5 heads of the indicated genotypes (mean ± s.e.m.): control 1246 ± 46, n=6; $Vegfa^{120/120}$ 854 ± 21, n=5; $Vegfa^{188/188}$ 1335 ± 63, n=3; $Vegfa^{120/188}$ 1314 ± 58, n=3; t-test, *=$p<0.05$ compared to control.

3.3 DISCUSSION

Understanding the precise binding affinities of the VEGF-A isoforms for their various receptors has become a priority in the field. It was originally proposed that the VEGF domain encoded by exon 7 is responsible for VEGF binding to NRP1 (Soker et al., 1997), and that it binds the NRP1 b1 domain (Mamluk et al., 2002). However, it was subsequently shown that the exon 8-encoded C-terminus present in all VEGF isoforms also contributes to NRP1 binding (Jia et al., 2006). Thus, the most recent model of VEGF binding to NRP1 predicts that a C-terminal arginine residue encoded by exon 8 mediates high affinity binding of the b1 domain, whilst exon 7-encoded residues engage NRP1 for enhanced and selective receptor binding (Parker et al., 2012). In agreement with this model, $VEGF_{121}$ lacking exon 7 residues binds NRP1 *in vitro*, but with almost 10-fold lower affinity than $VEGF_{165}$ (Pan et al., 2007; Parker et al., 2012). The low affinity of $VEGF_{121}$ for NRP1 may explain why some experiments using plasmon resonance with immobilised NRP1 confirmed binding to NRP1 (Pan et al., 2007), whilst others did not observe it (Herve et al., 2008). However, none of these previous studies had examined the binding affinity of $VEGF_{121}$ for NRP1 in a tissue context.

Here, I have combined AP-ligand binding assays with intact hindbrains, neuronal tissue culture assays and the analysis of genetically modified mice to compare the ability of the three major VEGF isoforms to bind NRP1 and regulate NRP1-dependent-neurodevelopmental processes. Ligand binding assays showed that $VEGF_{121}$, lacking the exon 7 domain, does not bind endogenous neuronal NRP1 *in situ* at detectable levels. This is consistent with the previously reported 10-fold lower affinity of $VEGF_{121}$ for NRP1 *in vitro* (Parker et al., 2012). The finding that $VEGF_{121}$ does not bind endogenous neuronal NRP1 at detectable levels also agrees with prior genetic studies, which showed that $VEGF_{120}$ is unable to compensate for $VEGF_{164}$ in FBM neuron migration, RGC axon guidance and GnRH neuron survival (Schwarz et al., 2004; Cariboni et al., 2011; Erskine et al., 2011). Thus, low affinity binding of $VEGF_{121}$ to NRP1 shown *in vitro* is unlikely to be relevant *in vivo*, at least in a neuronal context.

In contrast, $VEGF_{189}$, which carries the exon 7 domain, was able to bind endogenous NRP1-expressing axons in the hindbrain AP-ligand binding assay.

Moreover, these experiments demonstrated that binding relied on NRP1, not NRP2. Similar studies had not previously been carried out with either blood vessels or neurons. Importantly, our findings agree with prior *in vitro* studies performed with $VEGF_{165}$, which demonstrated that exon 7-encoded residues interact well with NRP1, but not NRP2 (Parker et al., 2012).

Consistent with human $VEGF_{189}$ binding NRP1 in neurons, I observed that mouse $VEGF_{188}$ expressed from the endogenous *Vegfa* locus was able to evoke NRP1-dependent neuronal responses *in vitro* and *in vivo*, similar to $VEGF_{164}$. Extending prior knowledge that $VEGF_{188}$ contains the NRP1 binding domains encoded by exons 6-8, I have therefore demonstrated for the first time that $VEGF_{188}$ binds NRP1 in a tissue context.

Future work on the role of VEGF signalling in neurons, especially studies utilising $Vegfa^{120/120}$ or tissue-specific *Vegfa* null alleles, should therefore address which endogenous VEGF isoform is the predominant regulator for each neuronal process under investigation. This may be done through isoform expression profiling at relevant developmental stages. Some studies have suggested that $VEGF_{164}$ is most abundant in neuronal tissues, whilst $VEGF_{188}$ is relatively more abundant in highly vascular tissues such as the lung (Ng et al., 2001; Ruiz de Almodovar et al., 2010). By extension, studies on the role of VEGF in bone development or vascular physiology have previously largely focused on $VEGF_{164}$, but if the pathways under investigation involve NRP1, should consider that $VEGF_{188}$ has similar signalling capacity.

Our finding that the relatively understudied $VEGF_{189}$ is capable of evoking VEGF isoform-specific signalling events may also have broad implications for the therapeutic use of VEGF. Thus, VEGF application has been considered in many studies as a tool for pro-angiogenic, pro-neurogenic and neuroprotective therapies e.g. amyotrophic lateral sclerosis treatment (reviewed by (Storkebaum et al., 2011). Most prior studies used $VEGF_{165}$ to ensure comprehensive receptor targeting; however, the retention of $VEGF_{165}$ in tissues is inferior to that of $VEGF_{189}$ due to the presences of only one versus two heparin/matrix-binding domains. Our work demonstrating that $VEGF_{189}$ is fully capable of engaging NRP1, in the context of its known ability to bind the alternative VEGF receptors VEGFR1 and VEGFR2,

therefore suggests that $VEGF_{189}$ may be better suited than $VEGF_{165}$ to induce localised tissue effects.

3.4 SUMMARY

VEGF-A regulates both vascular and neuronal patterning. Alternative splicing of the *Vegfa* gene gives rise to three major isoforms termed $VEGF_{121}$, $VEGF_{165}$ and $VEGF_{189}$ in reference to their amino acid length. $VEGF_{165}$, the most widely studied isoform, binds NRP1 to promote the migration, survival and axon guidance of subsets of neurons, whereas $VEGF_{121}$ cannot activate NRP1-dependent neuronal responses. In contrast, the role of $VEGF_{189}$ in NRP1-mediated signalling pathways has not yet been examined. Here, I combined expression studies and *in situ* ligand binding assays to demonstrate that $VEGF_{189}$ can bind NRP1. Furthermore, we analysed genetically altered mice containing single VEGF isoforms and *in vitro* models to demonstrate that $VEGF_{189}$, similarly to $VEGF_{165}$, is sufficient to control NRP1-dependent neuronal responses in neuronal migration, survival and axon guidance.

Chapter 4 2- AND 6-*O*-SULFATED PROTEOGLYCANS HAVE DISTINCT AND COMPLEMEMTARY ROLES IN CRANIAL AXON GUIDANCE MOTONEURON MIGRATION

4.1 INTRODUCTION

HSPGs are polymerised by exotosin enzymes and further modified by sulfation, epimerisation or deacetylation through modifying enzymes to generate vast structural and functional heterogeneity (Bishop et al., 2007; Sarrazin et al., 2011). These HSPG modifying enzymes are expressed and utilised throughout development in a tissue dependent manner. Two modifying enzymes have previously been implicated in brain development, the 2- and 6-*O*-sulfotransferases, which regulate axon guidance in the *Xenopus* and mouse brain (Irie et al., 2002; Pratt et al., 2006; Conway et al., 2011; Clegg et al., 2014). Both enzymes also control neuronal migration in *C. elegans* (Kinnunen et al., 2005). However, it is not known whether these enzymes regulate neuronal migration in the vertebrate brain.

The proper positioning of neurons along the dorsoventral and anterior-posterior axes in the developing brain and spinal cord and the correct extension of their neurites to suitable targets are fundamental processes for the appropriate wiring and therefore function of the nervous system. The VIIth and Vth cranial nerves are useful models to define molecular mechanisms that regulate axon guidance (Kitsukawa et al., 1997). Whilst the trigeminal motor neurons arise in two paired columns adjacent to the midline in the ventricular zone of hindbrain r2, the FBM neurons arise in r4, and both types of neurons extend their axons dorsally into the branchial arches by following stereotypical trajectories relative to the cranial ganglia and branchial arches (reviewed by (Chandrasekhar, 2004; Wanner et al., 2013).

Many molecular signals that control axon guidance and neuronal migration have been identified and shown to depend on an overlapping set of guidance cues (Dickson, 2002; Cooper, 2013). For example, the secreted extracellular matrix protein reelin and members of the WNT/PCP pathway promote correct FBM neuron migration (Rossel et al., 2005; Vivancos et al., 2009; Qu et al., 2010; Glasco et al., 2012). VEGF-A also guides FBM neuron migration by acting via its receptor NRP1;

interestingly, NRP1 also serves as a receptor for repulsive SEMA3A signals during FBM axon guidance (Taniguchi et al., 1997; Schwarz et al., 2004).

HSPGs can interact with a variety of other signalling molecules by either binding directly through singling complexes, presenting other molecules so these can bind to receptors, or sequestering and reducing the diffusion of other cues (Bishop et al., 2007; Aman and Piotrowski, 2008; Sarrazin et al., 2011; Venero Galanternik et al., 2015). *O*-sulfotransferases have previously been implicated in VEGF, FGF and WNT signalling (Ai et al., 2003; Kamimura et al., 2006; Mitsi et al., 2006). For example, the 6-*O*-sulfotransferases HS6ST1 and HS6ST2 promote the formation of VEGF/VEGFR and FGF/FGFR signalling complexes in vascular endothelial cells (Ferreras et al., 2012). HS6ST2 was also reported to be required for VEGF signalling during zebrafish vascular development (Chen et al., 2005). Moreover, FGFs interact with both 2- and 6-*O*-sulfated HSPGs for correct lacrimal gland and tracheal development (Kamimura et al., 2006; Qu et al., 2011b). WNT signalling is also regulated by HS2ST during zebrafish epiboly and by HS6STs for muscle development (Bink et al., 2003; Cadwalader et al., 2012).

Here, I show that mice lacking HS6ST1 and HS6ST2 have defective axon extension of specific branches of the Vth and VIIth cranial nerves, but normal FBM neuron migration. Inversely, I found that mice lacking HS2ST showed normal patterning of cranial nerve axons, but defective FBM neuron migration. I identified FBM neuron migration defects in HS2ST-deficient mice that were similar to those previously observed in mice lacking VEGF-A signalling through NRP1. However, HS2ST was not required for VEGF-A signalling in these neurons. Instead, HS2ST enabled FGF-mediated FBM neuron migration in an explant model, consistent with the expression of FGF receptors in migrating FBM neurons. Moreover, the expression of *Erm*, a genetic readout of FGF signalling (Firnberg and Neubuser, 2002), was altered in these mutants. Thus, our study has revealed a hitherto unrecognised role for HSPG-mediated FGF signalling in neuronal migration and demonstrated distinct and complementary roles for 2- and 6-*O*-sulfotransferases during cranial nerve development.

4.2 RESULTS

4.2.1 HSPGs are require for FBM neuron migration

To examine if HSPGs regulate FBM neuron migration, I used an *ex vivo* hindbrain culture assay (Figure 4.1 **A**). In this model, FBM neurons migrate rostrally from their site of origin in r4 to the site of nucleus formation in r6, similar to the migration they undergo *in vivo* (Schwarz et al., 2004; Tillo et al., 2014). The inclusion of heparitinase in the culture medium to remove heparan sulfate side chains from HSPGs (Linhardt et al., 1990) prevented FBM neuron migration beyond r5 (Figure 4.1 **B**). This observation suggested that HSPGs are important for FBM neuron migration.

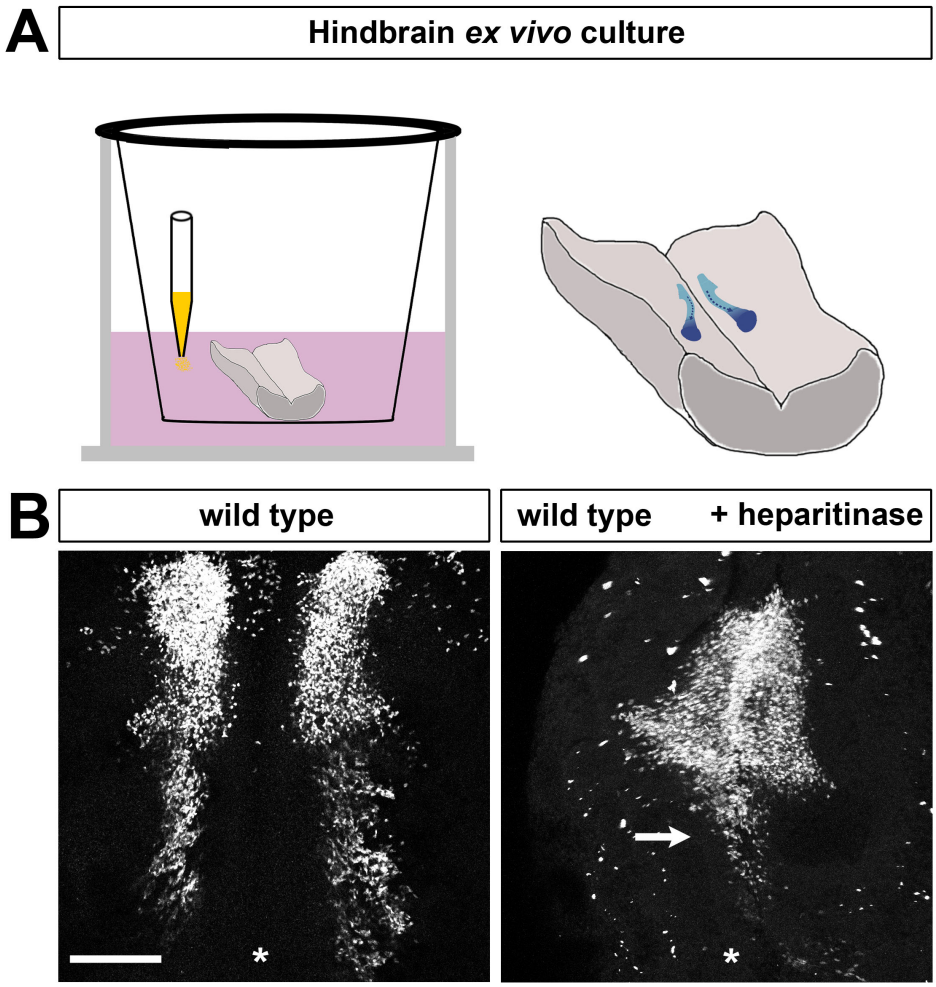

Figure 4.1 Heparitinase treatment induces FBM neuron migration defects.

(A) Schematic representation of hindbrain *ex vivo* culture. E11.5 hindbrains were cultured in the absence of presence of inhibitors in the culture medium (indicated with a pipette). In some experiments, I implanted agarose beads soaked in growth factors.

(B) Heparitinase treatment impairs FBM migration. Wild type hindbrains were cultured *ex vivo* and treated with PBS or heparitinase. White arrow indicates arrested FBM neuron migration at the level of r5; asterisks indicate the midline. Scale bar 200 μm.

4.2.2 Hs6st1 and Hs6st2 cooperate in cranial axon guidance, but are dispensable for FBM neuron migration

With the knowledge that HSPGs are required for FBM neuron migration, I therefore asked if 6-*O*-sulfotransferases played a role in this process. I first used ISH to establish the expression pattern of *Hs6st1* and *Hs6st2* in the mouse hindbrain at E12.5, when both the trigeminal and facial nuclei have formed. Both *Hs6st1* and *Hs6st2* were expressed in r5- and r6-derived hindbrain territories, where *Isl1*-expressing FBM neurons migrate (Figure 4.2 **A**). However, *Hs6st1*$^{-/-}$ and *Hst6s2*$^{-/-}$ single mutants showed normal FBM neuron migration, and 2/5 double mutant *Hs6st1*$^{-/-}$*;Hs6st2*$^{-/-}$ hindbrains only showed minor displacement of a small proportion of FBM neurons (Figure 4.2 **B**).

Because 6-*O*-sulfotransferases have previously been implicated in axon guidance (Irie et al., 2002; Pratt et al., 2006; Conway et al., 2011; Clegg et al., 2014) I next examined cranial nerve axon guidance in *Hs6st1* and *Hs6st2* mutants by TUJ1 wholemount immunostaining at E11.5. I observed that *Hs6st1*$^{-/-}$ and *Hst6s2*$^{-/-}$ mutant heads both showed normal guidance of facial nerve axons, including those in the facial branchiomotor nerve (VII_{bm}), the chorda tympani (VII_{ct}) and the greater superficial petrosal nerve (VII_{gspn}) (Figure 4.2 **C**). These mutants also had normal guidance of trigeminal axons, including the mandibular nerve (V_{md}), the maxillary nerve (V_{mx}) and the ophthalmic nerve (V_{op}). Interestingly, however, *Hs6st1*$^{-/-}$*;Hs6st2*$^{-/-}$ double mutants had severe defects in both cranial nerves. Thus, the VII_{bm}, VII_{ct} and VII_{gspn} and the V_{mx} nerve failed to extend normally (symbols, Figure 3.1 **C**), and both the V_{md} and V_{op} nerves were absent (symbols, Figure 4.2 **C**). Taken together, these results demonstrate that 6-*O*-sulfotransferases are dispensable for FBM neuron migration, but essential for cranial nerve axon guidance.

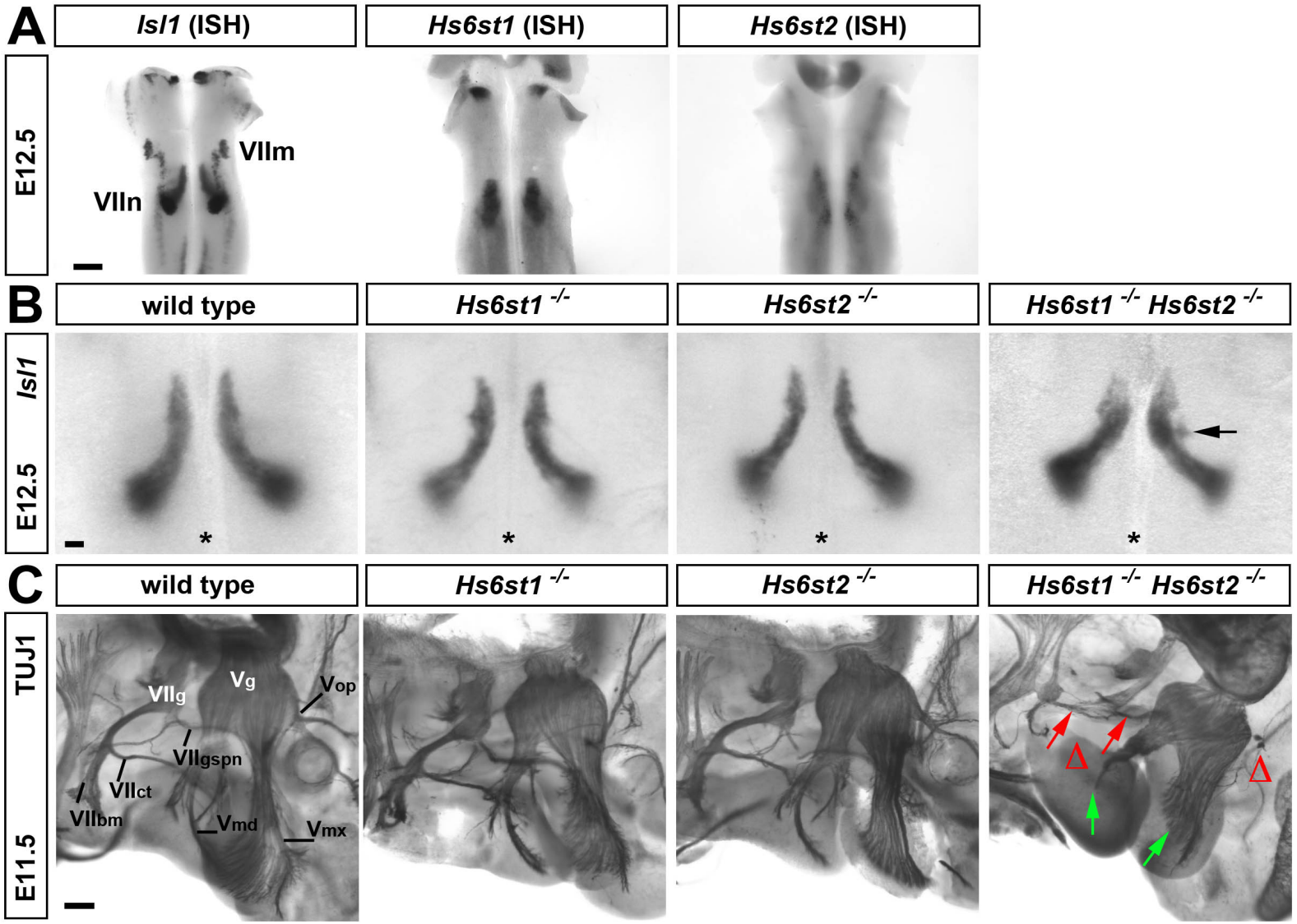
A
Isl1 (ISH)
Hs6st1 (ISH)
Hs6st2 (ISH)
E12.5
VIIn
VIIm
B
wild type
Hs6st1 -/-
Hs6st2 -/-
Hs6st1 -/- Hs6st2 -/-
E12.5 Isl1
*
C
wild type
Hs6st1 -/-
Hs6st2 -/-
Hs6st1 -/- Hs6st2 -/-
E11.5 TUJ1
VIIg
Vg
Vop
VIIgspn
VIIct
VIIbm
Vmd
Vmx

Figure 4.2 *Hs6st1* and *Hs6st2* are essential for cranial axon guidance, but not required for FBM neuron migration.

(A) *Hs6st1* and *Hs6st2* expression during FBM neuron migration. ISH of E12.5 hindbrains shows the expression pattern of *Hs6st1* and *Hs6st2* relative to motor neurons identified by *Isl1*. VIIm indicates the migrating FBM neurons, VIIn the facial motor nuclei. Scale bar 100 μm.

(B) FBM neuron migration in *Hs6st1* and *Hs6st2* mutants. *Isl1* ISH of *Hs6st1*$^{-/-}$ (n=3) and *Hs6st2*$^{-/-}$ (n=10) hindbrains at E12.5 relative to controls; a minor defect in FBM neuron migration in a *Hs6st1*$^{-/-}$;*Hs6st2*$^{-/-}$ hindbrain (arrow). Scale bar 100 μm.

(C) Cranial axon patterning in *Hs6st1* and *Hs6st2* mutants. Lateral view of E11.5 *Hs6st1*$^{-/-}$, *Hs6st2*$^{-/-}$ and *Hs6st1*$^{-/-}$;*Hs6st2*$^{-/-}$ mutant (n=3 each) relative to control heads, immunolabelled with TUJ1. Double mutants have misplaced facial nerve branches (red arrow), delayed extension of the mandibular (V_{md}) and maxillary (V_{mx}) nerves (green arrow), lack the ophthalmic nerve (V_{op}), the chorda tympani (VII_{ct}) and the facial branchiomotor nerve (VII_{bm}) (open triangles). VII_g, geniculate ganglion; V_g, trigeminal ganglion, VII_{gspn}, greater superficial petrosal nerve. Scale bar 200 μm.

4.2.3 Hs2st is expressed in rhombomere 4 at the onset of FBM neuron migration

Because 6-*O*-sulfotransferases have been shown to cooperate with 2-*O*-sulfotransferase during *Drosophila* tracheal and mouse lacrimal gland development (Kamimura et al., 2006; Qu et al., 2011b), I next asked if HS2ST also regulates cranial nerve guidance, or if it instead controlled neuronal migration. To determine the expression pattern and function of HS2ST during hindbrain development, I used mice carrying an $Hs2st^{Lacz}$ knock-in allele that faithfully recapitulates the expression of the endogenous *Hs2st* gene when visualised as β-galactosidase X-gal staining (Bullock et al., 1998). $Hs2st^{Lacz/+}$ hindbrains showed prominent X-gal staining in r4 at E10.5, close to the domain in which the *Isl1*-positive FBM neurons differentiate (Figure 4.3 **A**). X-gal staining of cryosections through $Hs2st^{Lacz/+}$ hindbrains, followed by immunolabelling for ISL1, showed that this expression domain was adjacent to, but did not overlap with the FBM neurons (Figure 4.3 **B**). At later stages of FBM neuron development, *Hs2st* expression appeared to be restricted to an area adjacent to the midline (Figure 4.3 **C**). This expression pattern suggested that HS2ST is involved in modifying proteoglycans that act in trans to regulate FBM neuron development.

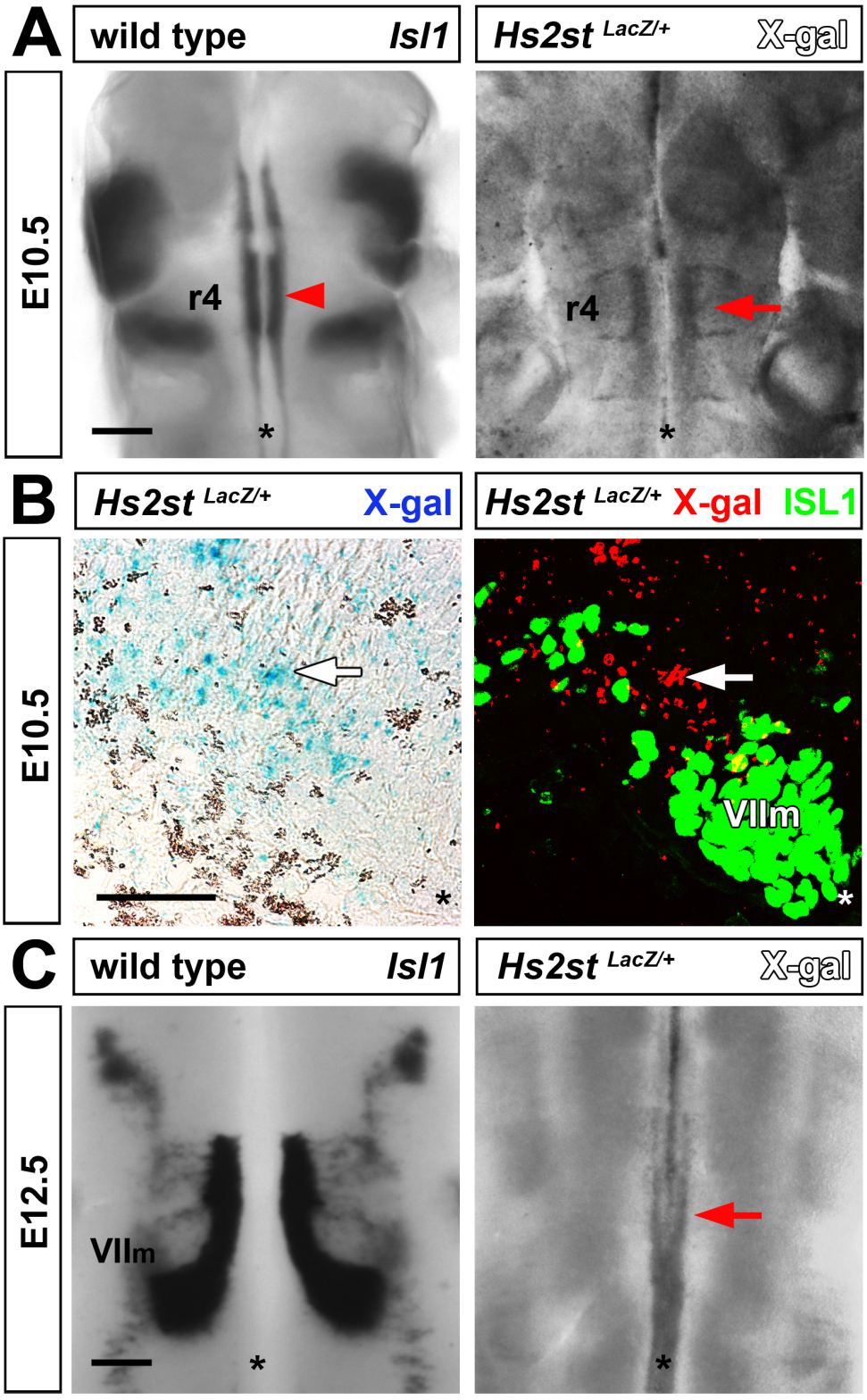

Figure 4.3 ***Hs2st* is transiently expressed near migrating FBM neurons.**

(A-C) *Hs2st* expression was visualised as X-gal staining in *Hs2st*$^{Lacz/+}$ hindbrains. In wholemount hindbrains at E10.5 (**A**), expression was prominent in rhombomere 4

(r4) near the *Isl1*-positive motor columns (compare the position of the red arrowhead and red arrow). Asterisks indicate the midline. Scale bar 200 μm. In sections through r4 at E10.5 (**B**), X-gal staining (arrow) was present just outside the motor column, which was visualised by ISL1 immunolabelling. X-gal staining was pseudocoloured red in the right hand panel. VIIm indicates migrating FBM neurons. Scale bar 50 μm. In wholemount hindbrains at E12.5 (**C**), during FBM neuron migration, X-gal staining (red arrow) is observed in the midline in an area between the migrating *Isl1*-positive FBM streams. Scale bar 200 μm.

4.2.4 Hs2st is essential for FBM neuron migration, but dispensable for cranial axon guidance

To determine whether HS2ST is required for FBM neuron migration, I examined E12.5 hindbrains from *Hs2st*-null mutants (*Hs2st*$^{Lacz/Lacz}$) using *Isl1* ISH. I observed splitting of the migratory stream in all mutants examined (Figure 4.4 **A**). In contrast, wholemount TUJ1 immunolabelling at E11.5 showed that *Hs2st* mutants had normal axon extension of all branches of the facial (VII) and trigeminal (V) nerves (Figure 4.4 **B**). Together, these results imply that 2-*O*-sulfotransferase is important for FBM neuron migration, whilst 6-*O*-sulfotransferases are essential for cranial axon guidance.

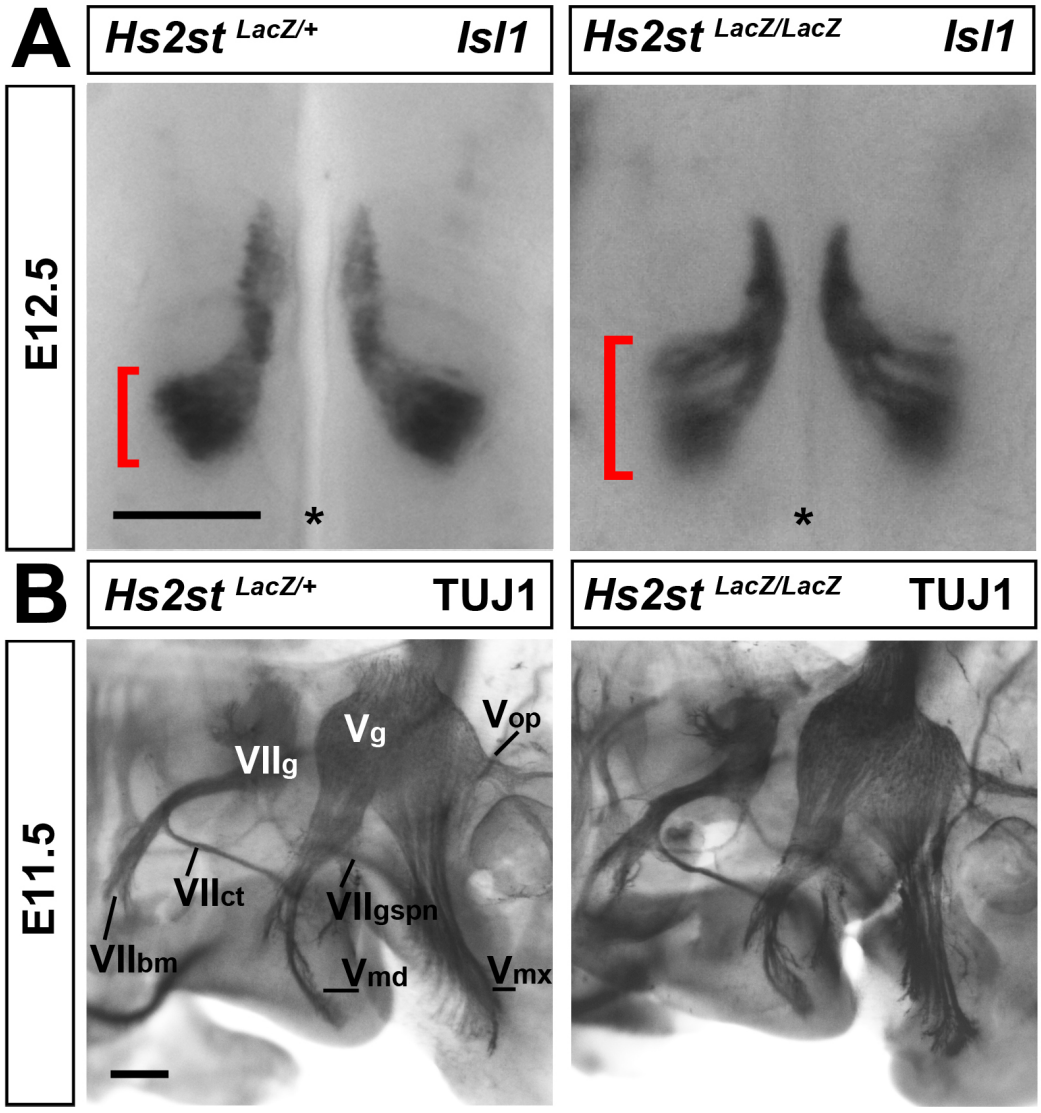

Figure 4.4 ***Hs2st*** **is essential for FBM neuron migration, but dispensable for cranial axon guidance.**

(A) *Isl1* wholemount ISH at E12.5 shows abnormal FBM neuron migration in *Hs2st*$^{Lacz/Lacz}$ (n=6) homozygous compared to *Hs2st*$^{Lacz/+}$ heterozygous hindbrains. Brackets indicate the width of the neuronal stream. Scale bar 200 µm.

(B) Normal cranial axon patterning in *Hs2st* mutants. Lateral views of E11.5 *Hs2st*$^{Lacz/Lacz}$ (n=3) wholemount heads and *Hs2st*$^{Lacz/+}$ controls, immunolabelled with TUJ1. Note normal cranial nerve extension of the mandibular (V_{md}), maxillary (V_{mx}) and ophthalmic (V_{op}) nerves, the chorda tympani (VII_{ct}), facial branchiomotor nerve (VII_{bm}) and the greater superficial petrosal nerve (VII_{gspn}). VII_g, facial ganglion; V_g, trigeminal ganglion. Scale bar: 200 µm.

4.2.5 Hs2st is dispensable for VEGF-mediated FBM neuron migration

HSPGs have been shown to interact with VEGF and its receptor NRP1 (Sarrazin et al., 2011), which have previously been implicated in FBM neuron migration (Schwarz et al., 2004). I therefore asked if loss of 2-*O*-sulfated HSPGs caused an FBM neuron defect that was similar to that of mice lacking *Nrp1* (Kitsukawa et al., 1997) or the NRP1-binding VEGF isoforms (*Vegfa*$^{120/120}$) (Carmeliet et al., 1999). ISL1 immunostaining of cryosections from E12.5 hindbrains showed that migrating FBM neurons split into two main streams in *Hs2st*-null mice, as observed in *Nrp1*$^{-/-}$ mice or *Vegfa*$^{120/120}$ mice lacking NRP1-binding VEGF isoforms (Figure 4.5 **A**).

To examine if HS2ST-modified HSPGs were required for VEGF-induced FBM neuron migration, I again used the hindbrain explant model. Thus, I unilaterally implanted $VEGF_{165}$-coated heparin beads into explanted *Hs2st*-null and littermate control hindbrains. As expected, FBM neurons migrated towards the beads in controls (Figure 4.5 **B**), as previously shown (Schwarz et al., 2004). Unexpectedly, these neurons also still migrated towards the $VEGF_{165}$-coated beads in the *Hs2st*-null hindbrains (Figure 4.5 **D**). Quantitation confirmed that $VEGF_{165}$-coated heparin beads promoted FBM neuron migration in both genotypes (Figure 4.5 **C**, **E**). These results suggest that the similar *in vivo* phenotypes of mutants lacking HS2ST or NRP1-binding VEGF isoforms cannot be explained by a requirement for HS2ST-modified HSPGs in VEGF-induced FBM neuron migration.

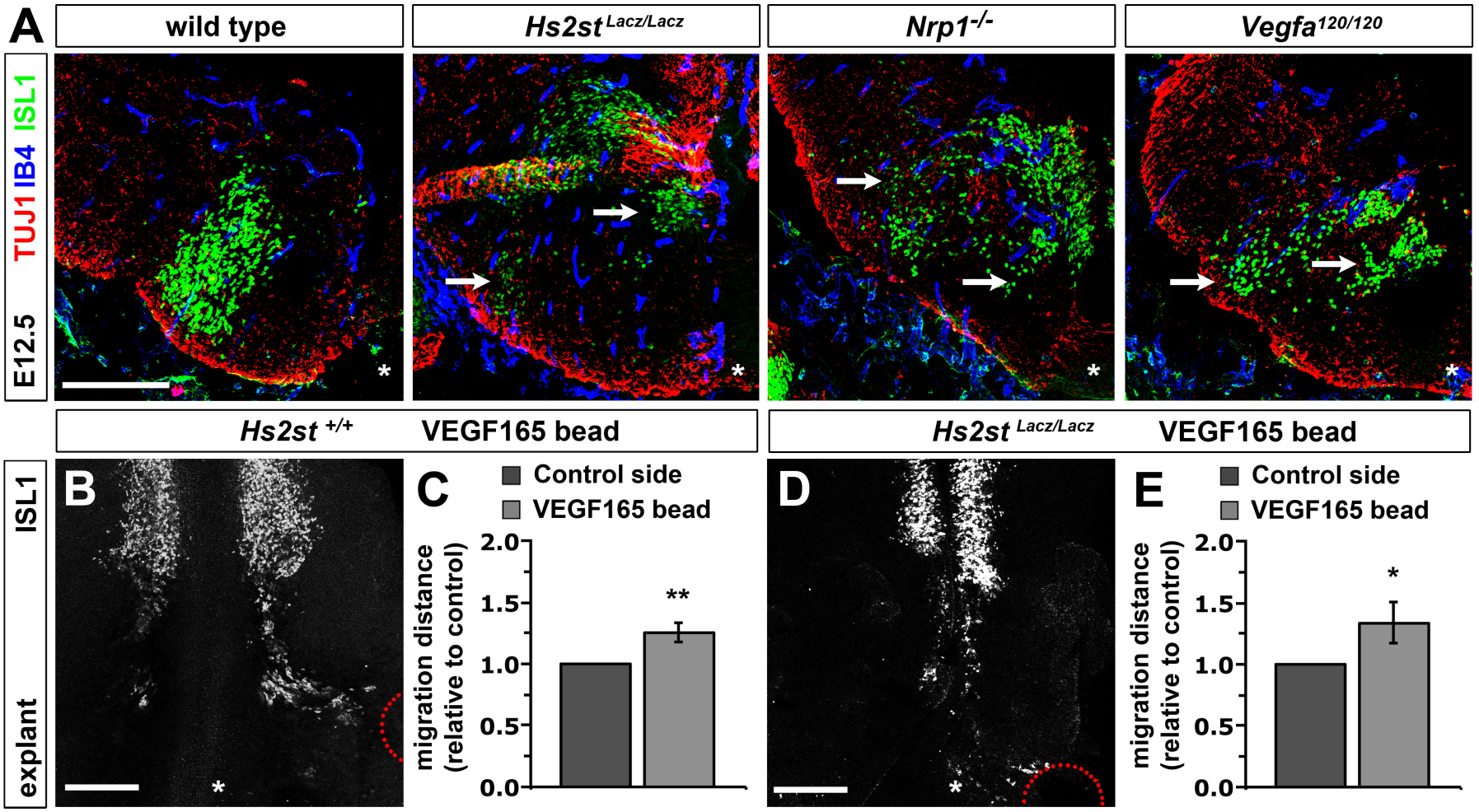
A
wild type
Hs2st Lacz/Lacz
Nrp1 -/-
Vegfa 120/120
E12.5 TUJ1 IB4 ISL1
Hs2st +/+ VEGF165 bead
Hs2st Lacz/Lacz VEGF165 bead
explant ISL1
B
C
D
E
Control side
VEGF165 bead
migration distance (relative to control)
2.0
1.5
1.0
0.5
0.0
**
*

Figure 4.5 *Hs2st* FBM neuron migration defect is similar to but not required for VEGF/NRP1 dependent FBM migration phenotype.

(A) *Hs2st* mutants show a FBM neuron migration phenotype similar to *Nrp1*$^{-/-}$ and *Vegfa*$^{120/120}$ mice. Transverse sections through E12.5 hindbrains at r6 level were immunolabelled for ISL1, TUJ1 and IB4. White arrows indicate split stream of migrating FBM neurons in *Hs2st*$^{Lacz/Lacz}$, *Nrp1*$^{-/-}$ and *Vegfa*$^{120/120}$ mice. Scale bar 200 μm.

(B, D) HS2ST is not essential for $VEGF_{165}$-mediated FBM migration**.** E12.5 *Hs2st*$^{Lacz/Lacz}$ and littermate control hindbrain were cultured *ex vivo* with heparin beads soaked in $VEGF_{165}$. Red dotted circles indicate the heparin bead position; asterisks indicate the midline. (**C, E**) The corresponding quantification of the distance migrated by FBM neurons are shown adjacent to each experiment. Scale bar 200 μm. The quantification of the distance migrated by FBM neurons (mean ± s.e.m.) are shown adjacent to each experiment: *Hs2st*$^{+/+}$ +$VEGF_{165}$ bead, n=15; *Hs2st*$^{Lacz/Lacz}$ +$VEGF_{165}$ bead, n=7. P-values: *=$p<0.05$, **=$p<0.01$ compared to control (t-test).

4.2.6 FGF receptors are expressed in the hindbrain during FBM neuron migration

HSPGs act as FGF co-receptors in FGF:FGFR:HS complexes and regulate the distribution and degradation of FGFs (Schlessinger et al., 2000; Hacker et al., 2005). I therefore examined if FGF signalling components are expressed during FBM neuron migration and whether loss of HS2ST affects FGF signalling during this process. RT-PCR showed that all four FGF receptors (*Fgfr1-4*) were expressed in the E11.5 hindbrain (Figure 4.6 **A**). ISH demonstrated that *Fgfr1-4* were expressed widely in the hindbrain at E10.5, the onset of FBM neuron migration, and that *Fgfr1-3* were expressed near the midline and *Fgfr4* in the same are as FBM neurons at E12.5 (Figure 4.6 **C**). The Allen Brain Atlas, a database of transcripts expressed in the mouse brain, showed expression of FGF1, FGF8, FGF9 and FGF15 in the hindbrain at E11.5. Work by others has also shown that FGFR1, FGFR2 and FGFR3 are differentially expressed in the hindbrain during chick development, whilst FGF3 and FGF8 signalling are required for normal zebrafish rhombomere patterning in the developing hindbrain (Walshe and Mason, 2000; Walshe et al., 2002). These findings are consistent with a role for FGF signalling in regulating FBM neuron migration.

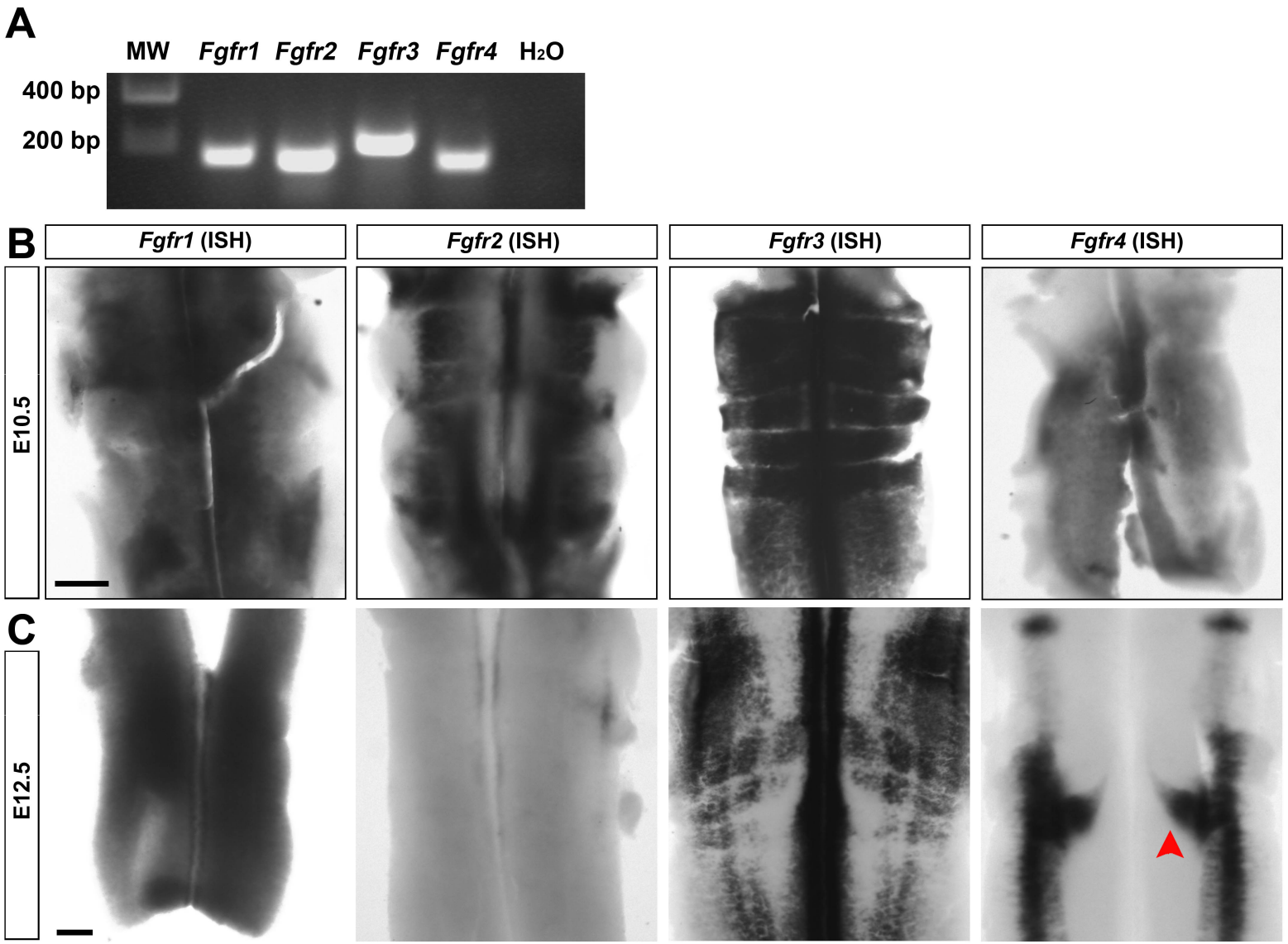
A
MW
Fgfr1
Fgfr2
Fgfr3
Fgfr4
H2O
400 bp
200 bp
B
Fgfr1 (ISH)
Fgfr2 (ISH)
Fgfr3 (ISH)
Fgfr4 (ISH)
E10.5
C
E12.5

Figure 4.6 FGF receptor expression in the hindbrain

(A) RT-PCR analysis shows expression of *Fgfr1* (148bp), *Fgfr2* (142bp), *Fgfr3* (197bp) and *Fgfr4* (141bp) in E11.5 hindbrain tissue, when FBM neurons migrate.

(B, C) ISH of E10.5 (B) and E12.5 (C) mouse hindbrains demonstrate the expression of *Fgf* receptors during FBM neuron development. Red arrowhead indicates *Fgfr4* expression in the same area asΩ migrating FBM neurons at E12.5. Scale bar 200 μm.

4.2.7 FGF promotes FBM neuron migration and is requires HS2ST for FBM neuron migration ex vivo

To examine whether FBM neurons can in principle respond to FGF ligands, I performed hindbrain explants with FGF-coated beads. Because I did not know which of the 22 FGF ligands were expressed in the hindbrain during FBM neuron migration, I tested FGF2, because it is known to require HSPGs for appropriate signalling (Matsuo and Kimura-Yoshida, 2013). I observed that FBM neurons in wild type brains were strongly attracted by FGF2-coated beads (Figure 4.7 **A**), whilst attraction was abolished in *Hs2st*-null hindbrains (Figure 4.7 **C**). Quantitation confirmed that loss of HS2ST significantly impaired FGF2-induced FBM neuron migration (Figure 4.7 **B**, **D**). These results raise the possibility that FGFs promote FBM neuron migration in a mechanism that requires 2-*O*-sulfated HSPGs. However, these experiments do not define which endogenous FGF ligand or receptor may regulate FBM neuron development.

Because *Hs2st* is prominently expressed in r4 at E10.5, I next considered the possibility that HSPGs modulate FGF-induced signalling events in this rhombomere to regulate the subsequent process of FBM neuron migration. I therefore examined the expression pattern of *Erm,* a member of the ETS transcription factor family that is positively regulated by FGF (Firnberg and Neubuser, 2002). *Erm* was expressed along the midline of E10.5 wild type hindbrains in the posterior hindbrain (Figure 4.7 **E**; r6-r8). ISH at E10.5 unexpectedly showed that *Erm* was ectopically expressed in the midline region of r2 and r4, the rhombomeres in which trigeminal and facial branchiomotor neurons arise, respectively (Figure 4.7 **E**). This finding agrees with prior observations that HSPGs can spatially restrict the diffusion or degradation of FGF ligands in the zebrafish embryo to modulate FGF signalling (Venero Galanternik et al., 2015). In contrast to *Erm*, the master regulator of r4 identify, *Hoxb1*, was expressed normally in *Hs2st*-null mice at E10.5 (Figure 4.7 **F**). This finding suggests that r4 had been specified normally in *Hs2st*-null mutants, and that the observed ectopic *Erm* expression is more likely caused by HS2ST-dependent alterations in FGF signalling.

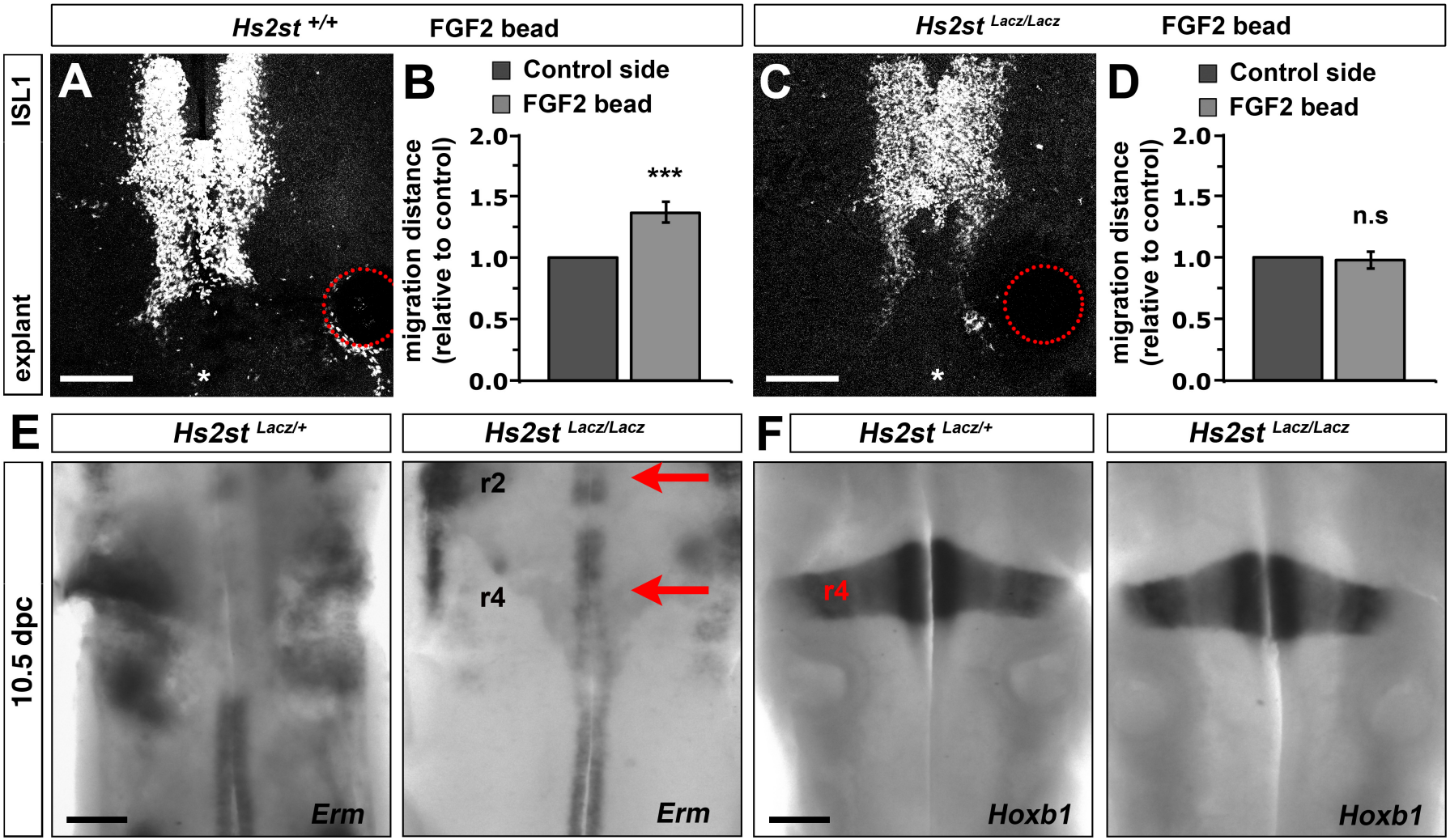
Hs2st +/+
FGF2 bead
Hs2st Lacz/Lacz
FGF2 bead
ISL1
explant
A
B
Control side
FGF2 bead
migration distance (relative to control)
2.0
1.5
1.0
0.5
0.0
***
C
D
Control side
FGF2 bead
migration distance (relative to control)
2.0
1.5
1.0
0.5
0.0
n.s
E
Hs2st Lacz/+
Hs2st Lacz/Lacz
10.5 dpc
r2
r4
Erm
Erm
F
Hs2st Lacz/+
Hs2st Lacz/Lacz
r4
Hoxb1
Hoxb1

Figure 4.7 FGF2 requires *Hs2st* to control FBM neuron migration.

(A, C) HS2ST promotes FGF2-stimulated FBM migration. E12.5 $Hs2st^{Lacz/Lacz}$ and littermate control hindbrain were cultured *ex vivo* with heparin beads soaked in FGF2. Red dotted circles indicate the position of the heparin bead in each hindbrain; asterisks indicate the midline. Scale bar 200 μm. (**B, D**) The quantification of the distance migrated by FBM neurons (mean ± s.e.m.) are shown adjacent to each experiment: $Hs2st^{+/+}$ +FGF2 bead, n=16; $Hs2st^{Lacz/Lacz}$ +FGF2 bead, n=5. P-value ***=p<0.001 compared to control (t-test); n.s., not significant.

(E) Ectopic *Erm* expression in *Hs2st* mutant hindbrains. Wholemount ISH of E10.5 *Hs2st* mutant and littermate control hindbrains for *Erm*, a target of FGF signalling. Scale bar 200 μm.

(F) Hindbrain architecture in *Hs2st* mutants (n=2). Wholemount ISH for the r4 marker *Hoxb1* at E10.5 shows normal rhombomere formation in the hindbrain at the level of FBM neurons. Scale bar 200 μm.

4.2.8 Syndecans 1, 2 and 4 are not essential for FBM neuron migration

Because *O*-sulfotransferases are modifiers of various HSPGs, I wanted to investigate which core HSPG was essential for the FBM migration phenotype observed. I focused on the syndecan (SDC) family because several members have been shown to interact with FGF (Tkachenko et al., 2005), and in *C. elegans Sdc* has a similar role to *Hs2st* during neuronal migration (Rhiner et al., 2005). To determine whether Syndecans are required for FBM neuron migration, I examined E12.5 and E13.5 hindbrains from various *Sdc*-null mice (in the laboratory of Professor Michael Simons, Yale University). I observed that *Sdc1*$^{-/-}$ and *Sdc2*$^{-/-}$ mice had normal FBM neuron migration (Figure 4.8 **A**, **B**). More over, *Sdc4*$^{-/-}$ mice also form normal facial nuclei (unpublished observation by Charlotte Maden). I also analysed *Sdc2*$^{-/-}$;*Sdc4*$^{-/-}$ double mutants and observed these also had normal FBM migration (Figure 4.8 **B**). This data indicates that syndecans 1, 2 and 4 do not mimic the phenotype observed in *Hs2st*-null mice and therefore are not essential for FBM migration.

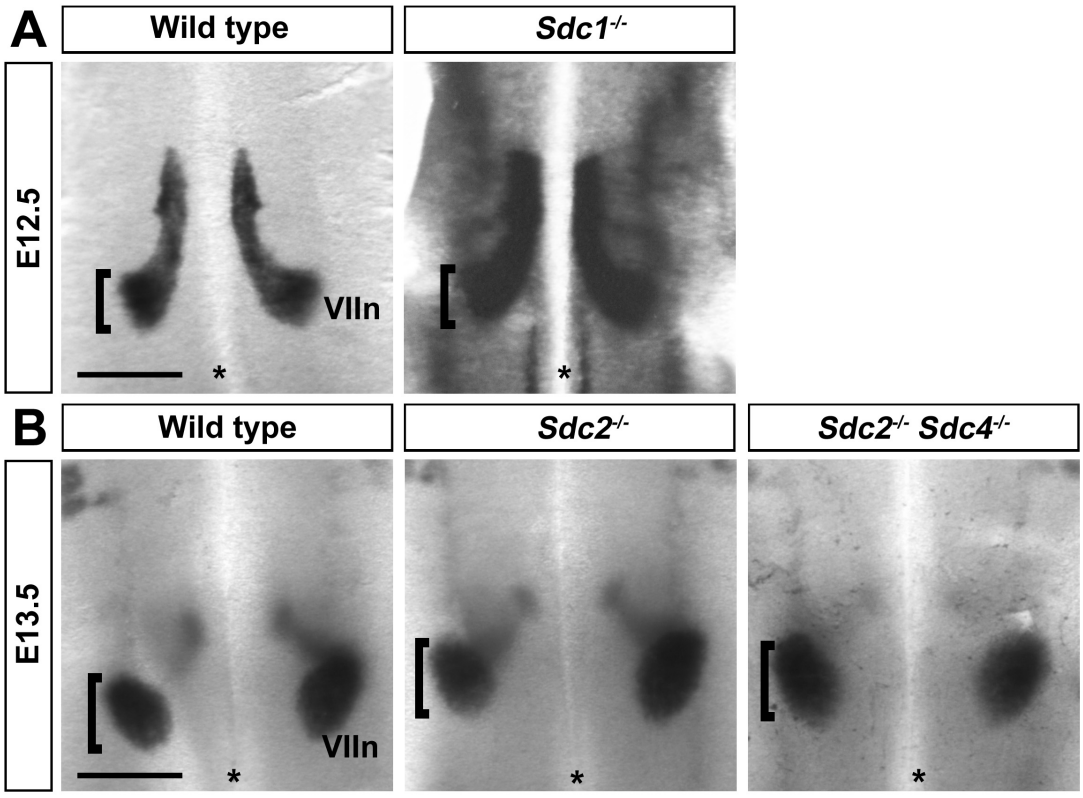

Figure 4.8 ***Syndecans*** **are non-essential HSPGs for FBM neuron migration**

(A, B) *Isl1* wholemount ISH at E12.5 (A) and E13.5 (B). VIIn, facial nucleus; brackets indicate the width of the neuronal stream; asterisks indicate the midline. Scale bar 200 μm. (**A**) Normal FBM neuron migration in *Sdc1*$^{-/-}$ mutants (n=2) hindbrains. (**B**) Normal facial nuclei in *Sdc2*$^{-/-}$ mutants (n=2) and *Sdc2*$^{-/-}$*;Sdc4*$^{-/-}$ double mutants (n=2).

4.3 DISCUSSION

Previous work described roles for *Hs6st1* in commissural axon guidance (Pratt et al., 2006; Conway et al., 2011; Clegg et al., 2014). My observations agree with an important role for this gene in axon guidance and additionally demonstrate that *Hs6st1* synergises with *Hs6st2* during cranial axon extension. Interestingly, *Hs6st1*$^{-/-}$;*Hs6st2*$^{-/-}$ double mutants have similar cranial nerve defects to *Slit/Robo* mutants (Hammond et al., 2005; Ma and Tessier-Lavigne, 2007), raising the possibility that 6-*O*-sulfotransferases regulate SLIT function during cranial nerve development. In agreement, *Hs6st1* interacts with *Slit2* during commissural axon guidance (Conway et al., 2011). However, this is only a hypothesis driven section of the chapter. In order to strengthen the results section and dissect the pathway downstream of *Hs6st1* and *Hs6st2* would require more experiments. To test the possible interaction between SLITs and HS6STs during cranial axon patterning, I might analyse mice with compound mutations in the *Slit* and *Hs6st* genes to look for an epistatic interaction, and also test explants of cranial ganglia from *Hs6st1* and *Hs6st2* mutants for their responsiveness to exogenous SLIT protein.

SEMA3A is another guidance cue important for cranial nerve patterning, with both *Sema3a*$^{-/-}$ and *Nrp1*$^{-/-}$ mice showing severe defasciculation of these axons (Fujisawa et al., 1997; Taniguchi et al., 1997; Schwarz et al., 2004). In contrast, *Hs6st1*$^{-/-}$;*Hs6st2*$^{-/-}$ double mutants did not fully extend their cranial axons. The opposing phenotypes seen in SLIT and HS6ST versus SEMA3A mutants suggest that the two pathways are independent, but that their correct balance is essential for normal cranial axon guidance. Interestingly, SEMA3A binds to CSPGs in mouse perineuronal nets, and in *Drosophila* SEMA5A binds to HSPGs or CSPGs in neurons to evoke attractive versus repulsive axon guidance responses, respectively (Kantor et al., 2004; Vo et al., 2013). This raises the question of whether CSPGs rather than HSPGs might be required for SEMA3A-mediated aspects of cranial axon guidance. To analyse if CSPGs are essential for cranial axon guidance, I might analyse different CSPG mouse mutants.

I have also uncovered a requirement of HS2ST in FBM neuron migration. Despite the fact that *Hs2st*-null mice had very similar FBM migration defects to *Nrp1*$^{-/-}$ and *Vegfa*$^{120/120}$ mice, a hindbrain explant assay showed that VEGF signalling

was not perturbed by loss of HS2ST. Even though *O*-sulfotransferase-modified HSPGs are dispensable for VEGF/NRP1-induced FBM neuron migration, VEGF and NRP1 may still interact with HSPGs modified by other enzymes, a possibility which I have not investigated. Interestingly, perlecan enhances VEGF binding to NRP1, has been implicated in VEGF-induced endothelial migration and influences *Vegfa* expression levels (Zoeller et al., 2009; Muthusamy et al., 2010; Ishijima et al., 2012). Furthermore, the gene encoding perlecan *(trol)* interacts with *Sema1a* in *Drosophila* to control axonal guidance. I might analyse perlecan (*Hspg2)*-deficient mice to investigate whether it is involved in FBM neuron migration or cranial axon guidance.

Prior work has suggested that a lack of 2-*O* sulfation increased 6-*O*- or N-sulfation within the chain location where 2-*O*-sulfation is lost, raising the possibility of compensation (Merry and Wilson, 2002). However, my results indicate that modifications induced by 6-*O*-sulfotransferases are unlikely to compensate for the loss of HS2ST-induced modifications during FBM neuron migration, as the 6-*O*-sulfotransferases do not seem to play an essential role in this process. Nevertheless, the possibility that N-sulfation may be required for FBM neuron migration remains to be studied. In order to confirm if any genetic compensation is taking place, it would be interesting to perform qPCR to compare the levels of the *Hs6st* and *Ndst* family members in *Hs2st*-null hindbrains relative to wild type hindbrains. Moreover, I could analyse mice lacking NDSTs for possible FBM neuron migration defects.

I have further shown that FGF can promote FBM neuron migration in an HS2ST-dependent manner. I have not examined which HS2ST-modifed HSPG may be involved in FGF-dependent FBM migration, but my results exclude the syndecans 1, 2 and 4. Syndecan 3 is an interesting candidate, because it is mainly expressed in the nervous system to promote radial migration of cortical neurons and can also interact with FGFs during chick limb development (Dealy et al., 1997; Hienola et al., 2006). Therefore, I should next analyse the expression pattern of syndecan 3 during FBM neuron migration and analyse *Sdc3*$^{-/-}$ mice for possible defects in FBM neuron migration.

My results show the expression of *Hs2st* in a domain adjacent to FBM neurons, thus suggesting that HS2ST acts in *trans* to regulate FBM neuron migration. To understand what cell type adjacent to the r4 FBM neuron domain expresses

Hs2st, I would have to perform co-expression studies with other r4 markers and then target a floxed *Hs2st* mouse with appropriate *Cre* drivers (Stanford et al., 2010). In the first instance, I could use *Hoxb1-Cre* (Arenkiel et al., 2003) to target the entire r4 territory to confirm that r4-derived *Hs2st* expression is indeed essential for FBM migration. Moreover, I could use a *Nestin-Cre* transgene, which would target all neuronal progenitors. Ideally, I would also seek to identify a *Cre* line that could specifically delete *Hs2st* in the as yet unidentified *Hs2st*-expressing cell type. In Chapter 5, I describe experiments that further investigated further the possibility of *trans* and/or *cis* role of HSPGs during FBM neuron migration.

Previous work using zebrafish shows that disrupting HSPGs by targeting exotosins in *extl3/ext2* double mutants increases FGF diffusion and impairs FGF signal transduction (Venero Galanternik et al., 2015). In these mutants, cells that require HSPGs and FGF for collective migration stop expressing the FGF target *pea3* and instead show increased expression of *pea3* in surrounding tissues, suggesting that HSPGs restrict FGF ligand localisation. Furthermore, loss of HSPGs in zebrafish also leads to ectopic WNT activation, which is normally repressed by FGF signalling, and thereby causes cell polarity defects, ultimately resulting in abnormal collective migration (Venero Galanternik et al., 2015). The authors suggest that HSPGs are required both for FGF signalling and to spatially restrict FGF ligand localisation (Venero Galanternik et al., 2015). Similar to these findings, I observed that the expression of the FGF target gene *Erm* is altered in *Hs2st*-null hindbrains. It would be important to test how other signalling pathways, besides FGF and VEGF, cooperate with the HS2ST-dependent FBM neuron migration. I should investigate whether other molecules that control FBM migration non-cell autonomously, such as cadherins and PCP pathway components, also rely on HS2ST (Vivancos et al., 2009; Qu et al., 2010; Stockinger et al., 2011; Zakaria et al., 2014).

Altogether, my findings suggest an important role for the HSPG-modifying enzyme HS2ST in FBM neuron migration through roles in FGF-mediated neuronal guidance and/or hindbrain patterning. In contrast, the HSPG-modifying enzyme HS6ST1 and HS6ST2 regulate cranial axon development. In conclusion, HS6ST1/2 and HS2ST have distinct, but complementary roles in cranial nerve development.

4.4 SUMMARY

The correct migration and axon extension of neurons in the developing brain is essential for the appropriate wiring and function of neural networks. Here, I showed that *O*-sulfotransferases, a class of enzymes that modify HSPGs, are essential to regulate neuronal migration and axon development. I found that the 6-*O*-sulfotransferases HS6ST1 and HS6ST2 are essential for cranial axon patterning, whilst the 2-*O*-sulfotransferase HS2ST is important for the normal migration of FBM neurons in the hindbrain. Furthermore, I showed that FGF signalling regulates FBM neuron migration in an HS2ST-dependent manner.

Chapter 5 CRE-LOXP-MEDIATED TARGETING OF FACIAL BRANCHIOMOTOR NEURONS

5.1 INTRODUCTION

The *Cre-LoxP* recombinase system is a valuable tool to bypass the embryonic lethality of certain constitutive knockout mouse strains and to target genes in a cell type specific fashion to explore cell autonomous versus non-cell autonomous roles in the processes under investigation (reviewed by (Nagy, 2000). Most published studies describing developmental defects in FBM neurons use full-knockout mice (Chandrasekhar, 2004; Wanner et al., 2013). However, this approach does not distinguish whether the observed phenotypes are caused by defects in these neurons themselves or are instead caused by defects in cell types they interact with or secondary to general deficiencies in hindbrain development. Identifying a *Cre* line suitable for FBM neuron targeting would therefore empower mechanistic studies of neuronal migration and axon guidance in the hindbrain.

I explored the efficiency of three different *Cre* lines in targeting migrating FBM neurons. The first one was *Phox2b-Cre* (D'Autreaux et al., 2011), a transgene in which *Cre* is expressed under the control of the promoter of the gene encoding PHOX2B, a well-described transcription factor in migrating FBM neurons and other subtypes of neurons in the developing hindbrain. The *Phox2b-Cre* line was generated using a BAC construct that introduced the *Cre* sequence together with the exon 2 coding sequence of *Phox2b*. This resulted in a fusion protein that contained the first 82 amino acids of PHOX2B. The transgene construct was then knocked into the endogenous *Phox2b* exon 2 locus, as previously described for generating the *Phox2b*-null mice (Pattyn et al., 1999; D'Autreaux et al., 2011).

I also studied the targeting efficiency of two different transgenes, in which *Cre* expression is controlled by the promoter for *Nestin*, which is expressed in neural and glial progenitors: the *Nestin-Cre* transgene (Tronche et al., 1999) and the *NesCre8* transgene (Petersen et al., 2002). The *Nestin-Cre* transgene was generated to express *Cre* under the control of the rat *Nestin* promoter and enhancer and is reported to recombine well in the neural tube from E10.5 onwards (Tronche et al., 1999). The

NesCre8 transgene also expresses *Cre* under the control of the *Nestin* promoter, but starts recombining neural progenitors from E8.5 onwards (Petersen et al., 2002).

To analyse the targeting efficiency of each *Cre* transgene, I used *Rosa26*^{Yfp} and *Rosa26*^{Dta} knockin mice (Srinivas et al., 2001; Ivanova et al., 2005), designed to express enhanced yellow fluorescent protein (eYFP) or diphtheria toxin a (DTA), respectively, whereby both the *eYfp* and *Dta* sequences contain a stop cassette flanked by LoxP sites. Therefore, when targeted by a CRE recombinase, the stop cassette will be excised and the green fluorescent protein or diphtheria toxin fragment, respectively, will be expressed. When combined with ISL1 immunostaining, YFP-labelled FBM neurons and the death of FBM neurons due to DTA expression can therefore be observed in the embryonic hindbrain targeted with the three *Cre* lines described above.

To analyse the efficiency of each *Cre* line, I also targeted the *Nrp1*^{fl} (Gu et al., 2003) and the *Ext1*^{fl} (Inatani et al., 2003) alleles. These target genes were chosen, because the Ruhrberg lab has previously shown that *Nrp1*-null mice have FBM neuron soma migration defects and altered cranial axon guidance (Schwarz et al., 2004). Further to that, in Chapter 4, I have shown that mice with defects in the enzymes acting downstream of EXT in the HSPG synthesis pathway also have hindbrain neuronal defects. Thus, *Hs2st*-null mice have defective FBM migration, whilst the *Hs6st1*$^{-/-}$*;Hs6st2*$^{-/-}$ have cranial axon guidance abnormalities. Moreover, conditionally knocking out *Ext1*^{fl} in the nervous system with *Nestin-Cre* was previously shown to cause midline commissure guidance defects (Inatani et al., 2003). Therefore, targeting either the floxed *Nrp1* or *Ext1* lines successfully in hindbrain neurons was expected to cause FBM defects similar to *Nrp1*-null and *Hs2st*-null mice, respectively, and thereby indicate successful CRE-mediated gene targeting in FBM neurons.

The aim of this chapter was therefore to characterise the *Phox2b-Cre* line as a tool for targeting FBM neurons, and also to investigate if the neural targeting lines *Nestin-Cre* and *NesCre8* can be used as alternative tools for FBM neuron studies. Ultimately, I wanted to identify a *Cre* line suitable for future studies of FBM neuron development, including NRP1 co-receptors and downstream targets. In addition,

such a *Cre* line would help to isolate FBM neurons for molecular biology and biochemistry assays using FACS methodology with the $Rosa26^{Yfp}$ reporter.

5.2 RESULTS

5.2.1 Phox2b-Cre targets migrating FBM neurons and other areas of the developing hindbrain

Previous work from D'Autreaux and colleagues showed that the *Phox2b-Cre* line targets FBM neurons by E13.5 and that the facial motor nuclei are lost in the *Phox2b*-null mouse (Pattyn et al., 1999; Pattyn et al., 2000; D'Autreaux et al., 2011). I analysed the CRE recombinase-mediated targeting of the $Rosa26^{Yfp}$ reporter with *Phox2b-Cre* at earlier stages, because genes regulating FBM neuron migration would have to be deleted before E12.5 to affect the migratory process.

I analysed a wholemount hindbrain at E12.0 using an antibody against GFP that recognised the YFP protein and an ISL1 antibody that labels motor neuron cell bodies. At this stage in development, FBM neurons are midway through their migration from r4 to r6, and neurons are distributed along the whole path of migration. In agreement with D'Auxtreaux and colleagues, I observed effective YFP expression in migrating FBM neurons (VIIm) as well as the facial motor nuclei (VIIn, Figure 3.1 **A**). I also observed that *Phox2b-Cre* targeted the most superficial layer of cells in r4 and r2 on the ventricular side of the hindbrain, in agreement with observation made by D'Auxtreaux and colleagues (Jean-Francois Brunet, personal communication). Furthermore, there were high levels of YFP in ISL1 negative cells along the midline as well as in the trigeminal motor neurons (Vm). I noted that ISL1 staining also unspecifically visualised blood vessels, probably due to the cross reaction of the secondary antibody (anti-mouse IgG) with IgG-containing blood cells.

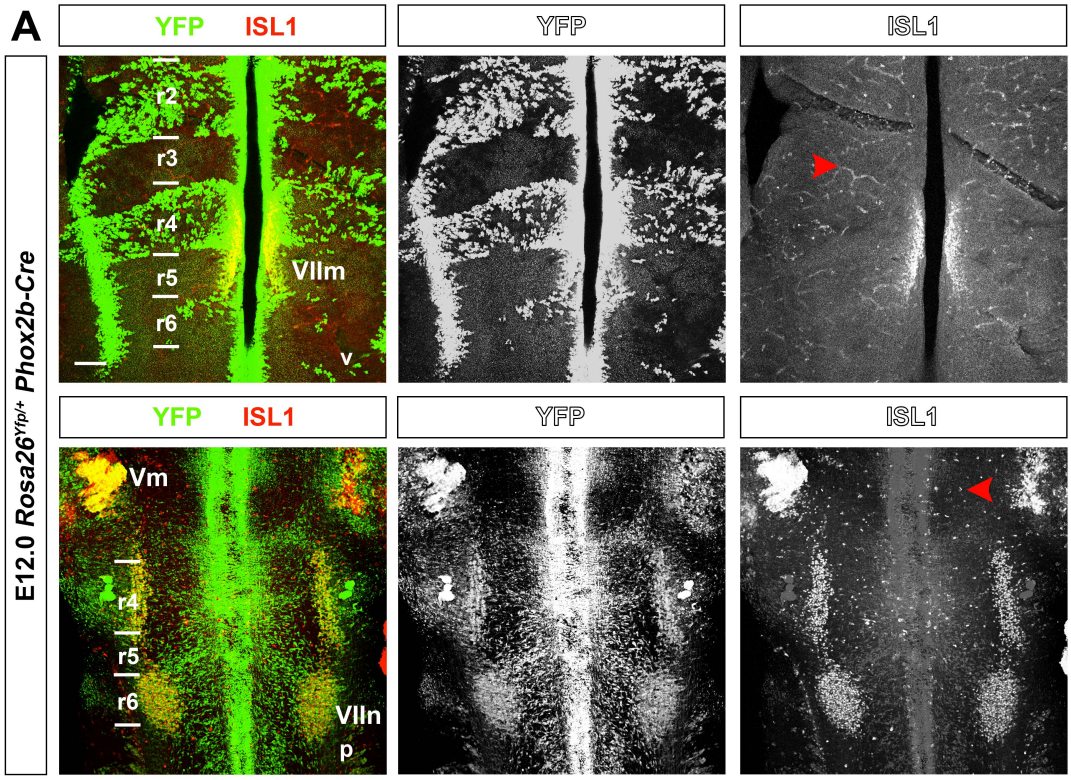

Figure 5.1 ***Rosa26*$^{Yfp/+}$ *Phox2b-Cre* is expressed in migration FBM neurons.**

(A) Wholemount E12.0 hindbrain showing *Phox2b-Cre* targeting. The top panels show ventricular (v) and the bottom panels pial (p) views of the hindbrain. YFP (green) indicates *Rosa26*^{Yfp} targeting and ISL1 (red) indicates migrating FBM neurons (VIIm) and the paired facial motor nuclei (VIIn). YFP and ISL1 are show as single channels in the adjacent panels. ISL1/anti-mouse IgG unspecifically binds to blood vessels, indicated by red arrowhead. Rhombomeres are indicated as r2-r6. Vm, trigeminal motor neurons. Scale bar: 100 µm.

5.2.2 Phox2b-Cre mediated targeting of floxed Nrp1 and Ext1 alleles does not cause FBM neuron defects

Previous work in the lab has shown that *Nrp1* is expressed by and essential for FBM neuron migration (Schwarz et al., 2004). I therefore used a floxed *Nrp1* allele to investigate the efficiency of *Phox2b-Cre* to target FBM neurons. I analysed E12.5 hindbrains from $Nrp1^{fl/fl}$ *Phox2b-Cre* mice using *Isl1* ISH and observed normal FBM migration (Figure 5.2 **A**). This was surprising, as I had confirmed with the $Rosa26^{Yfp}$ reporter that *Phox2b-Cre* targets migrating FBM neurons, and $Nrp1^{-/-}$ mice have split migrating streams of FBM neurons and dumbbell shaped nuclei on r6 with complete penetrance. I also immunolabelled E11.5 $Nrp1^{fl/fl}$ *Phox2b-Cre* embryos with TUJ1 to visualise cranial nerve extension and observed some nerve defasciculation in these mutants (Figure 5.2 **C**). There was mild defasciculation of every branch of the facial nerve, including the chorda tympani (VII_{ct}), facial branchiomotor nerve (VII_{bm}) and the greater superficial petrosal nerve (VII_{gspn}) (green arrowheads, Figure 5.2 **C**). The sensory nerves, at a more superficial level, were severely defasciculated and appeared to merge with the VII_{bm} (red arrowheads, Figure 5.2 **C**). The trigeminal nerve branches and the ophthalmic nerve extended normally. The defects observed are milder than those in *Nrp1*-null mice. Taken together, the absence of FBM defects and the mild axon defects compared to *Nrp1*-null mutants indicates that *Nrp1* was not efficiently deleted by *Phox2b-Cre*.

To analyse *Phox2b-Cre* targeting of FBM neurons using a different floxed gene target, I combined this transgene with a floxed allele of *Ext1*, an essential gene for HSPG synthesis upstream of *Hs2st*, which is important for FBM neuron migration (Chapter 4). I analysed E12.5 hindbrains from $Ext1^{fl/fl}$ *Phox2b-Cre* using an *Isl1* ISH and observed normal FBM neuron migration (Figure 5.2 **B**). This result may indicate inefficient targeting of the *Ext1* gene in FBM neurons by the CRE recombinase expressed under the control of the *Phox2b* promoter. Alternatively, the lack of an FBM neuron defect in $Ext1^{fl/fl}$ *Phox2b-Cre* mice is consistent with a non-cell autonomous function for EXT1 in FBM neurons, which would agree with *Hs2st* expression in a domain adjacent to FBM neurons (Chapter 4). I therefore needed to also target *Ext1* with a *Cre* line that targets hindbrain neural lineages more widely, i.e. a *Cre* controlled by the *Nestin* promoter.

A
E12.5 Nrp1fl/+ Phox2b-Cre
E12.5 Nrp1fl/+ Phox2b-Cre
E12.5 Nrp1fl/fl Phox2b-Cre
E12.5 Nrp1fl/fl Phox2b-Cre
Isl1
VIIm
VIIn
v
p
B
E12.5 Extfl/+ Phox2b-Cre
E12.5 Extfl/+ Phox2b-Cre
E12.5 Extfl/fl Phox2b-Cre
E12.5 Extfl/fl Phox2b-Cre
Isl1
VIIm
VIIn
v
p
C
E12.5 Nrp1fl/+ Phox2b-Cre
E12.5 Nrp1fl/fl Phox2b-Cre
TUJ1
Vop
Vg
VIIg
VIIgspn
VIIct
VIIbm
Vmx
Vmd
Sn

Figure 5.2 *Phox2b-Cre* targeted *Nrp1*$^{fl/fl}$ and *Ext1*$^{fl/fl}$ have normal FBM neuron migration and cranial axon guidance.

(A, B) Wholemount *Isl1* ISH of E12.5 hindbrains of the indicated genotypes detects migrating FBM neurons (VIIm) on the ventricular (v) and facial motor nuclei (VIIn) on the pial side (p). Note normal FBM migration in *Nrp1*$^{fl/fl}$ *Phox2b-Cre* (n=3) and *Ext1*$^{fl/fl}$ *Phox2b-Cre* (n=2) mutant hindbrains compared to heterozygous controls. Scale bar: 200 μm.

(C) Cranial axon patterning in *Nrp1*$^{fl/fl}$ *Phox2b-Cre* embryos. Lateral view of E11.5 wholemount heads immunolabelled with TUJ1. All *Nrp1*$^{fl/fl}$ *Phox2b-Cre* mutants (n=3) showed axon defasciculation of the sensory nerves (Sn) and the facial nerve branches, including the chorda tympani (VII_{ct}), facial branchiomotor nerve (VII_{bm}), and the greater superficial petrosal nerve (VII_{gspn}). Red arrowheads indicate severe and green arrowheads indicate mild defasciculation. The trigeminal nerve branches, including the mandibular nerve (V_{md}), the maxillary nerve (V_{mx}) and the ophthalmic nerve (V_{op}) extend normally. VII_g, facial ganglion; V_g, trigeminal ganglion. Scale bar: 200 μm.

5.2.3 *Phox2b-Cre efficiently targets some floxed genes, but not floxed Nrp1 in migrating FBM neurons*

To confirm that *Phox2b-Cre* can target FBM neurons effectively and to show that NRP1 was indeed expressed in FBM neurons, I used the $Rosa26^{Dta}$ mice, as they express DTA when targeted by a *Cre* line, which should result in death of the targeted cells (Ivanova et al., 2005). I performed an *Isl1* ISH on an E11.5 $Rosa26^{Dta/+}$ *Phox2b-Cre* hindbrain and observed that there were no FBM neurons remaining (Figure 5.3 **A**). These hindbrains still maintained their abducens motor neurons (VIm) in r5 (Sharma et al., 1998), but had disorganised hypoglossal motor neurons (VIIm) at the level of the midline compared to control $Rosa26^{+/+}$ *Phox2b-Cre* hindbrains (Figure 5.3 **A**). This suggests that *Phox2b-Cre* can target migrating FBM neurons effectively, as observed using the $Rosa26^{Yfp/+}$ reporter. Using an ISH probe for *Nrp1*, I observed that *Nrp1* mRNA was no longer present in an E12.5 wholemount $Rosa26^{Dta/+}$ *Phox2b-Cre* hindbrain in the location where all FBM neurons had died (compare Figure 5.3 **A** and **B**). This result implies that *Nrp1* is indeed expressed in FBM neurons that were targeted by the *Phox2b-Cre*.

I had observed that *Nrp1* targeting did not result in any FBM neuron migration phenotype, but this does not confirm that there was no targeting by *Phox2b-Cre.* I therefore explored the efficiency of *Phox2b-Cre*-mediated *Nrp1* targeting in the $Nrp1^{fl/fl}$ *Phox2b-Cre* hindbrain. Once more I used an *Nrp1* ISH probe to analyse the levels of *Nrp1* mRNA in control vs. mutant hindbrain. At E12.5, there was only a small decrease in the overall level of *Nrp1* mRNA in the hindbrain, and migrating FBM neurons were still expressing high levels of *Nrp1,* similar to control heterozygous $Nrp1^{fl/+}$ *Phox2b-Cre* hindbrains (Figure 5.3 **C**).

To investigate if the *Phox2b-Cre* can target genes other than *Nrp1* in FBM neurons, I next targeted *Nrp2*, a gene that is highly expressed in migrating FBM neurons, but is not required for their migration (Schwarz et al., 2004). I used a *Nrp2* ISH probe to compare the levels of *Nrp2* mRNA in $Nrp2^{fl/fl}$ *Phox2b-Cre* to heterozygous control in the same way as previously done for floxed *Nrp1*. Interestingly, the *Phox2b-Cre* targeting was very efficient in $Nrp2^{fl/fl}$ mice, as there was no *Nrp2* mRNA in FBM neurons and the general levels of *Nrp2* were dramatically reduced in most of the E12.5 hindbrain tissue (Figure 5.3 **D**).

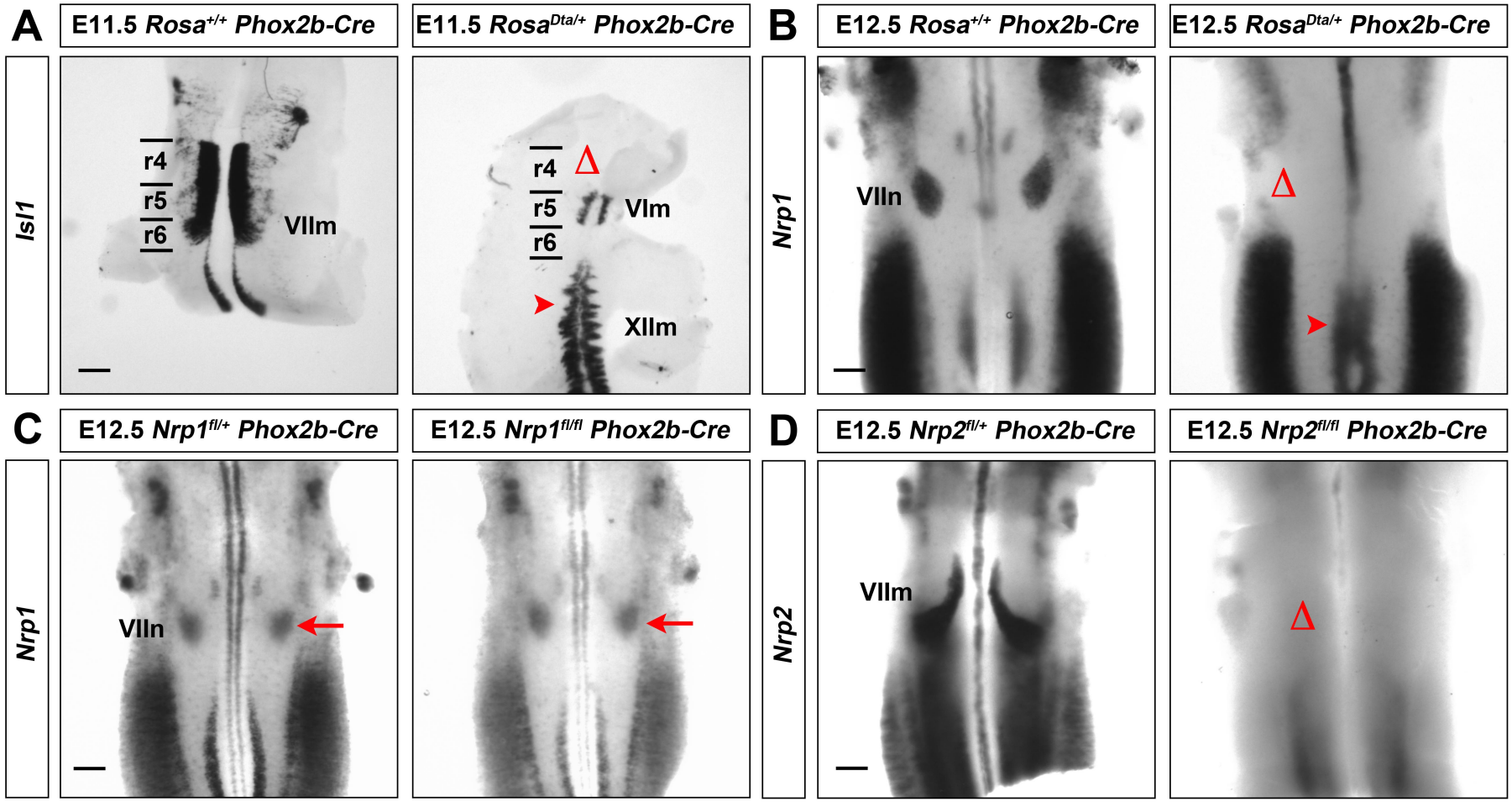
A
E11.5 Rosa+/+ Phox2b-Cre
E11.5 RosaDta/+ Phox2b-Cre
Isl1
r4
r5
r6
VIIm
Δ
VIm
XIIm
B
E12.5 Rosa+/+ Phox2b-Cre
E12.5 RosaDta/+ Phox2b-Cre
Nrp1
VIIn
Δ
C
E12.5 Nrp1fl/+ Phox2b-Cre
E12.5 Nrp1fl/fl Phox2b-Cre
Nrp1
VIIn
D
E12.5 Nrp2fl/+ Phox2b-Cre
E12.5 Nrp2fl/fl Phox2b-Cre
Nrp2
VIIm
Δ

Figure 5.3 *Phox2b-Cre* does not efficiently target floxed *Nrp1* in migrating FBM neurons.

(A) *Isl1* ISH of E11.5 wholemount hindbrains after *Phox2b-Cre* targeting of *Rosa26*$^{Dta/+}$. Most migrating FBM neurons (VIIm) are missing, indicated by open triangle. The abducens motor neurons (VIm) are still present in r5, and the hypoglossal motor neurons (XIIm) are disorganised. Rhombomeres are indicated as r4-r6. Scale bar: 200 μm.

(A) *Nrp1* ISH of E12.5 wholemount hindbrains after *Phox2b-Cre* targeting of *Rosa26*$^{Dta/+}$. Loss of *Nrp1* expression in the area where the facial motor nucleus (VIIn) is missing is indicated by an open triangle. The red arrowheads indicate misplaced *Nrp1*-expressing motor neurons at the midline. Scale bar: 200 μm.

(C) *Nrp1* ISH of E12.5 wholemount hindbrains shows that *Phox2b-Cre* does not delete *Nrp1*$^{fl/fl}$ in migrating FBM neurons or the facial motor nuclei (red arrow). (**D**) *Nrp2* ISH shows that *Phox2b-Cre* targets *Nrp2*$^{fl/fl}$ in migrating FBM neurons (open triangle). Scale bar: 200 μm.

5.2.4 Nestin-Cre targets most neuronal cells in the developing hindbrain

Previous work showed that the *Nestin-Cre* line effectively targets neural progenitors by E12.5 (Haigh et al., 2003). To analyse the CRE recombinase-mediated targeting with the *Nestin-Cre* line, I again used the *Rosa26*^{Yfp} reporter. I analysed a wholemount hindbrain at E12.0 using an antibody against GFP that recognised the YFP protein, and an ISL1 antibody that labels motor neuron cell bodies. I observed YFP expression in most neuronal hindbrain tissue, including the majority of migrating FBM neurons (VIIm) from r4 to r6 and the facial motor nuclei (VIIn, Figure 5.4 **A**). I also noticed that *Nestin-Cre* did not activate YFP expression in blood vessels, either in the ventricular or the pial side of the hindbrain, where the characteristic pattern of vessel networks was observed in between areas of YFP expression.

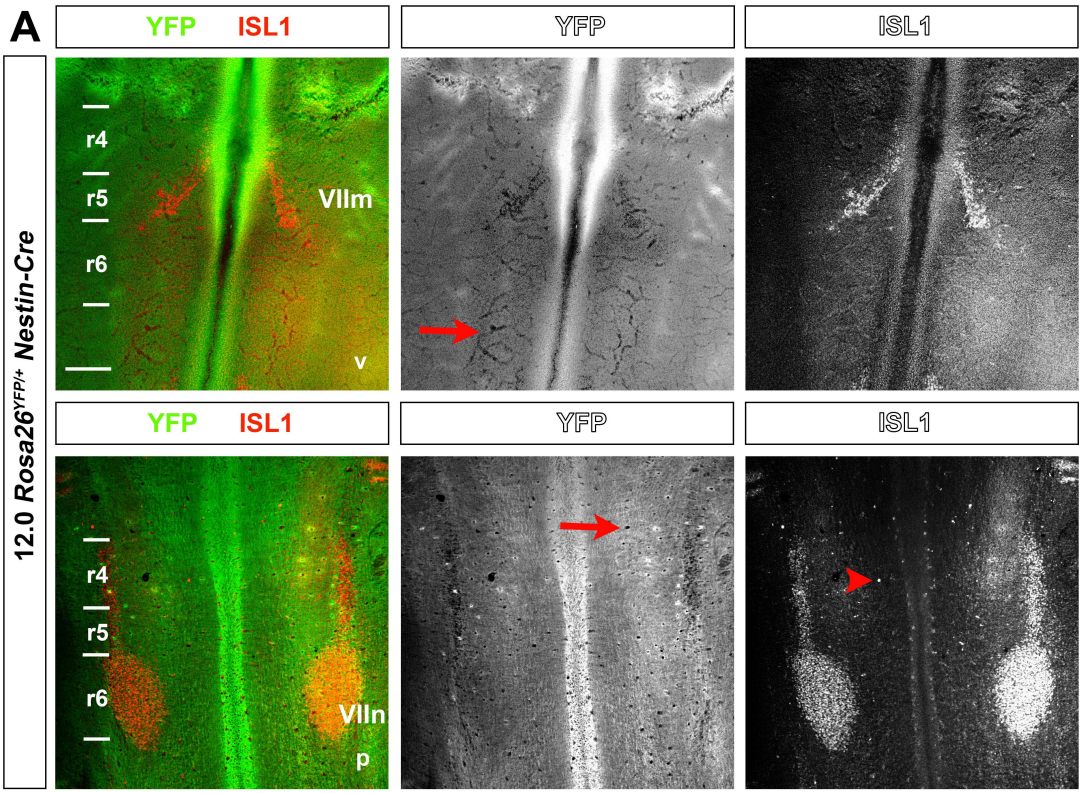

Figure 5.4 ***Rosa26*$^{Yfp/+}$ *Nestin-Cre* targeting of FBM neurons.**

(A) Wholemount E12.0 hindbrain showing *Nestin-Cre*-mediated targeting of *Rosa26*^{Yfp}. The top panels show ventricular (v) and the bottom panels pial (p) views of the hindbrain. YFP (green) indicates *Rosa26*^{Yfp} targeting and ISL1 (red) indicates migrating FBM neurons (VIIm) and the paired facial motor nuclei (VIIn). YFP and ISL1 are shown as single channels in the adjacent panels. ISL1/anti-mouse IgG unspecifically binds to blood vessels, indicated by red arrowheads. Rhombomeres are indicated as r2-r6. Scale bar: 200 µm.

5.2.5 *Nestin-Cre does not efficiently target floxed Nrp1 during migration of FBM neurons and cranial axon guidance*

I next investigated if *Nestin-Cre*, which seems to target most neural progenitors in the hindbrain, is a better tool than *Phox2b-Cre* to target *Nrp1* in FBM neurons. For this, I generated mice that contained one floxed allele and a null allele of *Nrp1* to make $Nrp1^{fl/-}$ *Nestin-Cre* mice. Given the disappointing experience I had with deleting *Nrp1* with the *Phox2b-Cre* transgene, this approach was used to maximise the targeting of *Nrp1*. I analysed E12.5 $Nrp1^{fl/-}$ *Nestin-Cre* wholemount hindbrains with an *Isl1* ISH probe and observed normal FBM neuron migration in mutant hindbrains (Figure 5.5 **A**). I also immunolabelled E11.5 $Nrp1^{fl/-}$ *Nestin-Cre* embryos with TUJ1 to visualise cranial nerve extension and observed no defects in these mutants (Figure 5.5 **B**). These results were unexpected, because my analysis using the $Rosa26^{Yfp}$ reporter had suggested that *Nestin-Cre* targets most neural progenitors in the embryonic hindbrain, and because loss of NRP1 in hindbrain neurons should result in cranial axon guidance defects.

To evaluate targeting efficiency, I compared *Nrp1* expression in $Nrp1^{fl/-}$ *Nestin-Cre* mutant and control hindbrain. I observed there was no reduction of *Nrp1* expression in mutant hindbrains compared to heterozygous control (Figure 5.5 **C**). Migrating FBM neurons and the facial nuclei express normal levels of *Nrp1* in $Nrp1^{fl/-}$ *Nestin-Cre* mutant hindbrains. This implies that floxed *Nrp1* is not efficiently targeted by *Nestin-Cre* in the hindbrain.

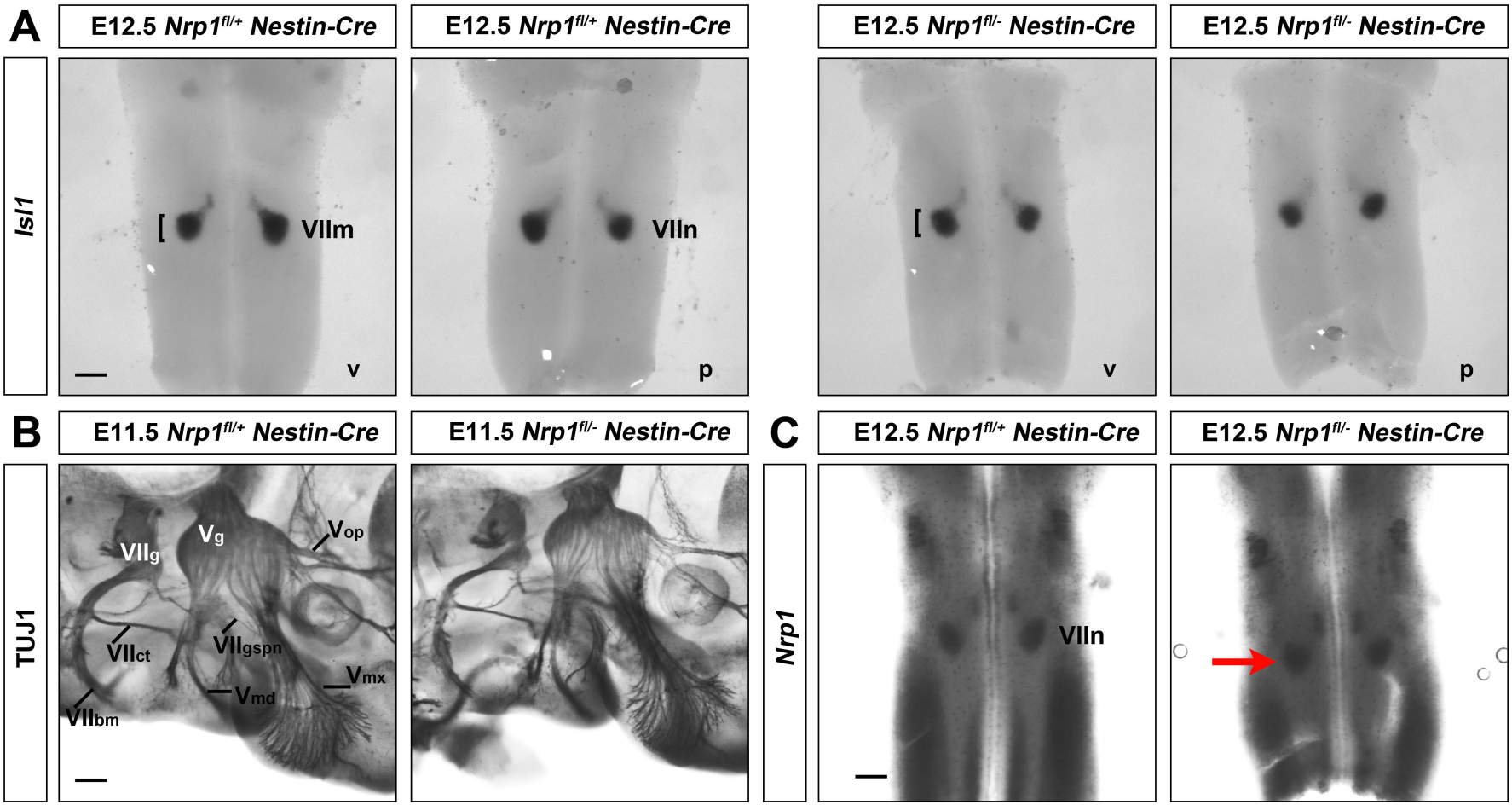
A
E12.5 Nrp1fl/+ Nestin-Cre
E12.5 Nrp1fl/+ Nestin-Cre
E12.5 Nrp1fl/- Nestin-Cre
E12.5 Nrp1fl/- Nestin-Cre
Isl1
[
VIIm
VIIn
[
v
p
v
p
B
E11.5 Nrp1fl/+ Nestin-Cre
E11.5 Nrp1fl/- Nestin-Cre
C
E12.5 Nrp1fl/+ Nestin-Cre
E12.5 Nrp1fl/- Nestin-Cre
TUJ1
VIIg
Vg
Vop
VIIct
VIIgspn
Vmx
Vmd
VIIbm
Nrp1
VIIn

Figure 5.5 *Nestin-Cre* does not efficiently target floxed *Nrp1* during FBM neuron migration or cranial axon guidance.

(A) Wholemount *Isl1* ISH of E12.5 hindbrains of the indicated genotypes detects migrating FBM neurons (VIIm) on the ventricular (v) and the paired facial motor nuclei (VIIn) on the pial side (p). Brackets indicate the width of the neuronal stream on the ventricular side. FBM neuron migration appeared normal in $Nrp1^{fl/-}$ *Nestin-Cre* hindbrains (n=4) compared to control. Scale bar: 200 μm.

(B) Cranial axon patterning in $Nrp1^{fl/-}$ *Nestin-Cre* embryos. Lateral views of E11.5 wholemount heads immunolabelled with TUJ1. $Nrp1^{fl/-}$ *Nestin-Cre* mutants (n=2) showed normal cranial nerve extension of the trigeminal nerve branches, including the mandibular nerve (V_{md}), the maxillary nerve (V_{mx}) and the ophthalmic nerve (V_{op}); and of the facial nerve branches, including the chorda tympani (VII_{ct}), facial branchiomotor nerve (VII_{bm}) and the greater superficial petrosal nerve (VII_{gspn}). VII_g, facial ganglion; V_g, trigeminal ganglion. Scale bar: 200 μm.

(**C**) E12.5 wholemount hindbrain showing *Nestin-Cre* does not target $Nrp1^{fl}$ in migrating FBM neurons. The red arrow indicates a facial motor nucleus (VIIn) expressing *Nrp1* by ISH in both control and $Nrp1^{fl/-}$ *Nestin-Cre* hindbrains. Scale bar: 200 μm.

5.2.6 *Nestin-Cre targets efficiently some neuronal tissue but not migration of FBM neurons.*

To establish whether *Nestin-Cre* can target other floxed alleles in the hindbrain, I generated mice that contained one floxed allele and a null allele of *Ext1* to make $Ext1^{fl/-}$ *Nestin-Cre* mice. My results showed that *Nestin-Cre* targets floxed *Ext1* inconsistently, resulting in variable phenotype penetrance. Thus, I observed that one in four $Ext1^{fl/-}$ *Nestin-Cre* mutant mice displayed anencephaly and brain abnormalities at E12.5 (Figure 5.6 **A**), in accordance with a role for HSPGs in spinal neurulation and general brain development (Yip et al., 2002; Inatani et al., 2003). Due to the severe defect, I was unable to dissect and analyse $Ext1^{fl/-}$ *Nestin-Cre* hindbrains with neural closure defects. I next analysed the other $Ext1^{fl/-}$ *Nestin-Cre* mutants, which had formed a hindbrain, using an *Isl1* ISH probe and observed normal FBM neuron migration (Figure 5.6 **B**). Thus, *Nestin-Cre* can target the $Ext1^{fl}$ allele with some efficiency, but does not result in FBM neuron migration defects.

To further analyse the efficiency of *Nestin-Cre* in hindbrain tissue, I also targeted floxed *Vegfa*, which is a haploinsufficient gene and deletion of just one allele results in a complete failure of blood vessel formation and consequently embryonic lethality (Carmeliet et al., 1996; Ferrara et al., 1996). Furthermore, combining the $Vegfa^{fl/fl}$ genotype (Gerber et al., 1999) with *Nestin-Cre* line causes early embryonic lethality. To bypass this problem, I bred mice with one *Vegfa* hypomorphic allele ($Vegfa^{Hypo/+}$) (Damert et al., 2002) to mice carrying *Nestin-Cre*, and then crossed the resulting double heterozygous mice with $Vegfa^{fl/fl}$ mice to generate $Vegfa^{Hypo/fl}$ *Nestin-Cre* mutants with severe neural VEGF deficiency, as previously described (Haigh et al., 2003). ISL1 wholemount ISH of $Vegfa^{Hypo/fl}$ *Nestin-Cre* E12.5 hindbrains showed a split in the migrating stream of FBM neurons (Figure 5.6 **C**). This phenotype resembled that seen in $Vegfa^{120/120}$ hindbrains, but was less severe than in $Nrp1^{-/-}$ mice. In addition to the migration phenotype, the $Vegfa^{Hypo/fl}$ *Nestin-Cre* hindbrains appear to have fewer motor neurons, indicating that there might be a role for VEGF in neuronal survival or proliferation, as previously observed for GnRH and cortical neural progenitors, respectively (Zhu et al., 2003; Cariboni et al., 2011).

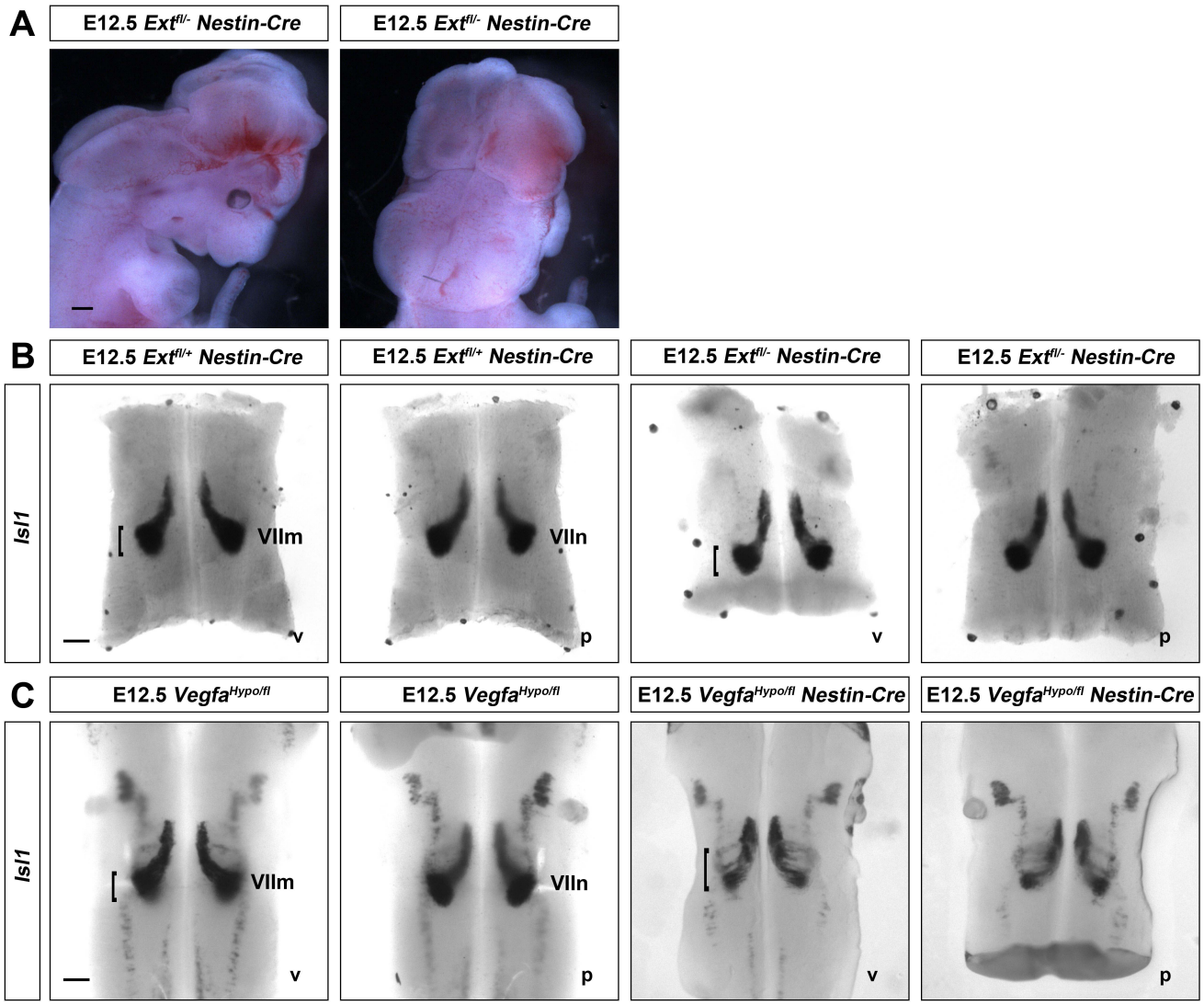
A
E12.5 Ext^fl/- Nestin-Cre
E12.5 Ext^fl/- Nestin-Cre
B
E12.5 Ext^fl/+ Nestin-Cre
E12.5 Ext^fl/+ Nestin-Cre
E12.5 Ext^fl/- Nestin-Cre
E12.5 Ext^fl/- Nestin-Cre
Isl1
VIIm
VIIn
v
p
C
E12.5 Vegfa^Hypo/fl
E12.5 Vegfa^Hypo/fl
E12.5 Vegfa^Hypo/fl Nestin-Cre
E12.5 Vegfa^Hypo/fl Nestin-Cre
Isl1
VIIm
VIIn
v
p

Figure 5.6 *Nestin-Cre* does not efficiently target floxed alleles of genes regulating FBM neuron migration.

(A) One in four E12.5 *Ext1*$^{fl/-}$ *Nestin-Cre* embryos showed brain malformations, including anencephaly.

(B) Wholemount *Isl1* ISH of E12.5 hindbrains shows similar migrating FBM neurons (VIIm) and the facial motor nuclei (VIIn) on the pial side (p) in *Ext1*$^{fl/-}$ *Nestin-Cre* embryos (n=3) and controls. Brackets indicate the width of the neuronal stream on the ventricular side (v).

(C) Abnormal migration of FBM motor neurons in mice with neural VEGF deficiency. Split track of migrating FBM neurons in *Vegfa*$^{Hypo/fl}$ *Nestin-Cre* mutant hindbrains (n=6) compared to control *Vegfa*$^{Hypo/fl}$ heterozygous hindbrains. The larger bracket on the ventricular hindbrain side indicates the wider span of migrating FBM neurons in mutants compared to control. Scale bar: 200 μm.

5.2.7 NesCre8 targets most neuronal cells in the developing hindbrain

To analyse CRE recombinase targeting with *NesCre8*, I used once more the *Rosa26*^{Yfp} reporter. Previous analyses of the *NesCre8* line using a similar approach had reported appropriate targeting of neural progenitors starting from E8.5 (Petersen et al., 2002). I analysed E11.5 *Rosa26*$^{Yfp/+}$ *NesCre8* cryosections and observed that most neuronal cells were YFP labelled at the r5 level. High magnification images showed that the majority of migrating FBM neuron nuclei labelled by ISL1 were also YFP positive, whilst the YFP reporter did not label blood vessels (Figure 5.7 **A**). I also analysed wholemount *Rosa26*$^{Yfp/+}$ *NesCre8* hindbrains at E12.0. I observed YFP expression in most neuronal hindbrain tissue, including the majority of migrating FBM neurons (VIIm) and the facial motor nuclei (VIIn, Figure 5.7 **B**). *NesCre8* did not recombine in blood vessels, neither on the ventricular nor the pial sides of the hindbrain (red arrowhead, Figure 5.7 **B)**.

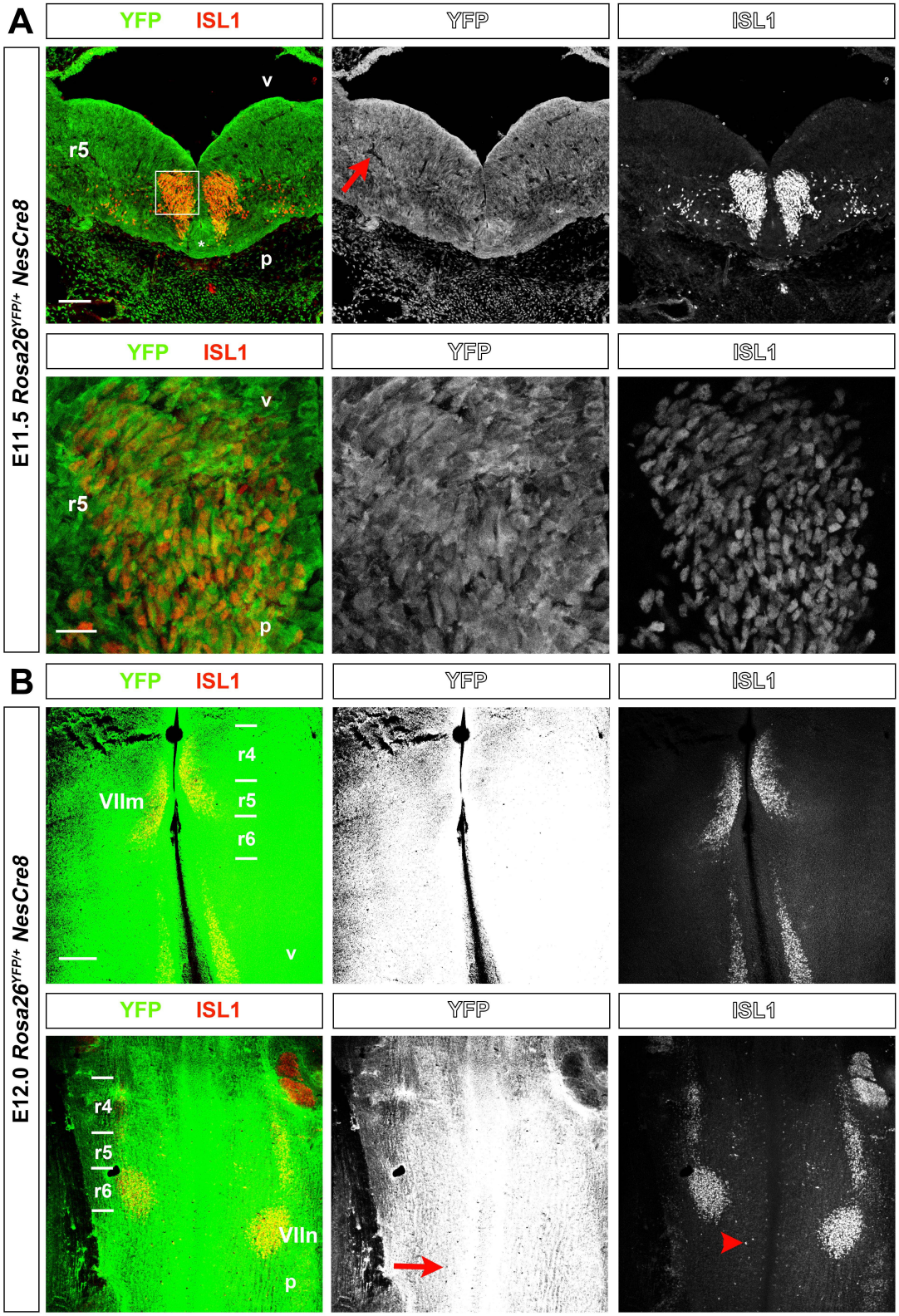

Figure 5.7 ***Rosa26*$^{Yfp/+}$** ***NesCre8*** **is expressed in migration FBM neurons.**

(A,B) *NesCre8*-mediated targeting of the *Rosa26*^{Yfp} reporter in the hindbrain at E11.5 (A) and E12.0 (B). YFP staining (green) indicates *Rosa26*^{Yfp} targeting by *NesCre8*

and ISL1 staining (red) indicates migrating FBM neurons. The YFP and ISL1 staining patterns are shown as single channels in the adjacent panels. YFP is observed in most neuronal cells in hindbrain tissue except for the characteristic blood vessel pattern, indicated by a red arrow. V, ventricular; p, pial. (**A**) Section through E11.5 hindbrain at r5 level. Scale bar: 100 μm. The higher magnification image of the squared region shows migrating FBM neurons positive for YFP. Scale bar: 20 μm.

(B) Wholemount E12.0 hindbrain. ISL1/anti-mouse IgG unspecifically binds to blood vessels, indicated by red arrowhead. Rhombomeres are indicated as r2-r6. Scale bar: 200 μm

5.2.8 NesCre8 does not efficiently target floxed Nrp1 and Ext1 alleles during the migration of FBM neurons or cranial axon guidance.

I investigated the efficiency of *NesCre8,* which is expressed from an earlier developmental stage (E8.5) than *Nestin-Cre*, in targeting the floxed *Nrp1* and *Ext1* alleles. I generated mice that contained a floxed allele and a null allele of *Nrp1* to make $Nrp1^{fl/-}$ *NesCre8* mice, and used the same approach to generate $Ext1^{fl/-}$ *NesCre8* mice. At E12.5, I observed that most $Nrp1^{fl/-}$ *NesCre8* mutants had normal FBM neuron migration (first $Nrp1^{fl/-}$ *NesCre8*, Figure 5.8 **A**), but 1 out of 4 mutants analysed had a small disruption in the formation of the facial motors nuclei (second $Nrp1^{fl/-}$ *NesCre8*, red arrowhead, Figure 5.8 **A**). However, this did not phenocopy the defect of $Nrp1^{-/-}$ mice. TUJ1 staining to visualise cranial axons at E11.5 showed defasciculation of several branches of the facial and the trigeminal nerve in $Nrp1^{fl/-}$ *NesCre8* mutants (Figure 5.8 **C**). These defects were similar to those observed in *Nrp1*-null mice (Kitsukawa et al., 1997; Schwarz et al., 2004). I analysed the knockdown level of *Nrp1* by ISH in $Nrp1^{fl/-}$ *NesCre8* mutants and observed normal *Nrp1* levels in FBM neurons in the hindbrain at E10.5 (Figure 5.8 **D**). However, I did not analyse the levels of *Nrp1* in extending cranial axons. This raises the possibility that *NesCre8* is more active in FBM neuron axons than in their somata, or that FBM neurons required different levels of *Nrp1* in somata compared to axons.

I analysed FBM neuron migration in $Ext1^{fl/-}$ *NesCre8* mutants and observed varying penetrance in phenotypes. In most mutants, FBM neurons migrated normally (first $Ext1^{fl/-}$ *NesCre8*, Figure 5.8 **B**), but one out of four $Ext1^{fl/-}$ *NesCre8* mutant hindbrains analysed had very small facial motor nuclei (second $Ext1^{fl/-}$ *NesCre8*, red arrowhead, Figure 5.8 **B**). Interestingly, this phenotype is not similar to that observed in Chapter 4. As a percentage of $Ext1^{fl/-}$ *NesCre8* mutants develop anencephaly (unpublished observation by Charlotte Maden, a previous PhD student in the Ruhrberg lab), similar to the $Ext1^{fl/-}$ *Nestin-Cre* analysed (Figure 5.6 **A**), it is likely that targeting of neuronal tissue surrounding the FBM neurons contributes o the phenotype.

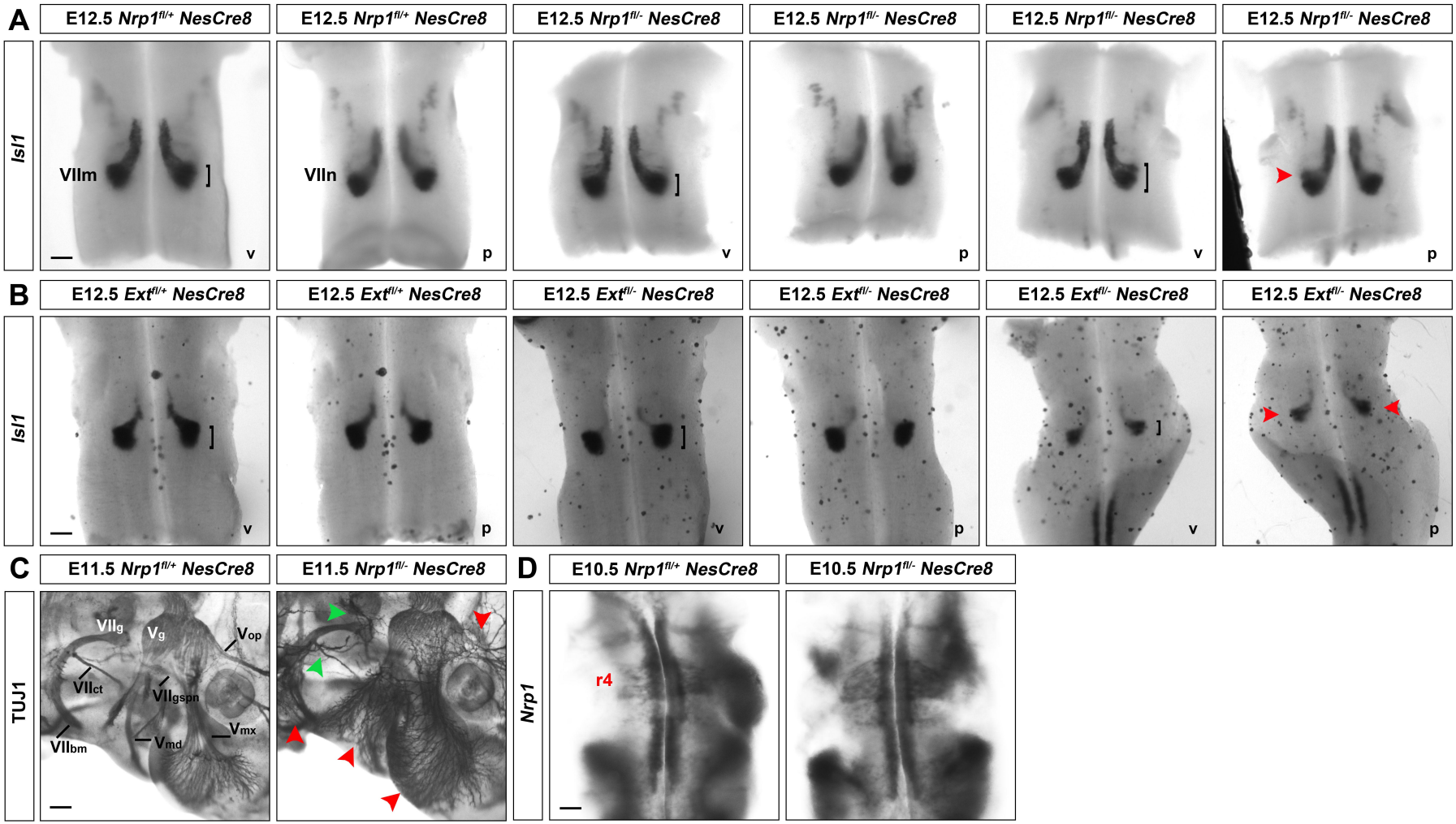
A
E12.5 Nrp1fl/+ NesCre8
E12.5 Nrp1fl/+ NesCre8
E12.5 Nrp1fl/- NesCre8
E12.5 Nrp1fl/- NesCre8
E12.5 Nrp1fl/- NesCre8
E12.5 Nrp1fl/- NesCre8
Isl1
VIIm
VIIn
v
p
B
E12.5 Extfl/+ NesCre8
E12.5 Extfl/+ NesCre8
E12.5 Extfl/- NesCre8
E12.5 Extfl/- NesCre8
E12.5 Extfl/- NesCre8
E12.5 Extfl/- NesCre8
Isl1
C
E11.5 Nrp1fl/+ NesCre8
E11.5 Nrp1fl/- NesCre8
TUJ1
VIIg
Vg
Vop
VIIct
VIIgspn
Vmx
VIIbm
Vmd
D
E10.5 Nrp1fl/+ NesCre8
E10.5 Nrp1fl/- NesCre8
Nrp1
r4

Figure 5.8 *NesCre8* partially targets *Nrp1*^{fl} and *Ext1*^{fl} during migration of FBM neurons and cranial axon guidance.

(A, B) Wholemount *Isl1* ISH of E12.5 hindbrains of the indicated genotypes detects migrating FBM neurons (VIIm) on the ventricular side (v) and facial motor nuclei (VIIn) on the pial side (p). **(A)** A small defect in FBM migration was observed in some *Nrp1*$^{fl/-}$ *NesCre8* mutants (n=2/4), as indicated by larger bracket on the ventricular side and red arrowhead pointing at split stream. **(B)** Small defect in FBM neuron migration and possibly survival was observed in the other two *Ext1*$^{fl/-}$ *NesCre8* mutants (n=2/4), as indicated by a smaller bracket on the ventricular side and red arrowheads. Scale bar: 200 μm.

(C) Cranial axon patterning in *Nrp1*$^{fl/-}$ *NesCre8* embryos (n=3). Lateral view of E11.5 wholemount heads, immunolabelled with TUJ1. All *Nrp1*$^{fl/-}$ *NesCre8* mutants showed severe axon defasciculation compared to control. All nerve branches appear to have formed correctly but branched excessively in mutants compared to controls. Red arrowheads indicate severe defasciculation and green arrowheads indicate mild defasciculation. The trigeminal nerve branches, including the mandibular nerve (V_{md}), the maxillary nerve (V_{mx}) and the ophthalmic nerve (V_{op}); and of the facial nerve, including the chorda tympani (VII_{ct}), facial branchiomotor nerve (VII_{bm}), and the greater superficial petrosal nerve (VII_{gspn}). VII_g, facial ganglion; V_g, trigeminal ganglion. Scale bar: 200 μm.

(D) E10.5 wholemount hindbrain showing that *NesCre8* does not delete *Nrp1* in migrating FBM neurons. Expressing of *Nrp1* by ISH can be seen in r4 in both control and *Nrp1*$^{fl/-}$ *NesCre8* hindbrains. Scale bar: 200 μm.

5.3 DISCUSSION

Using a Cre transgene controlled by the *Phox2b* promoter that was generated using the same approach as the *Phox2b*-null mouse, which is essential for FBM migration, seemed a suitable approach to target migrating FBM neurons (Pattyn et al., 1997; Pattyn et al., 2000; D'Autreaux et al., 2011). The fact that *Phox2b-Cre* was unable to target floxed *Nrp1* in FBM neurons, but could target other floxed lines such as *Nrp2, Rosa26*^{Dta} or *Rosa26*^{Yfp}, raises several questions. One possible explanation for the lack of floxed *Nrp1* targeting could be the delayed onset of *Phox2b-Cre* relative to *Nrp1* expression in FBM neurons. ISH showed that *Phox2b* is expressed by E9.0 in r4 neural progenitors (Pattyn et al., 1997), whilst *Nrp1* starts being expressed around E10.5 (Schwarz et al., 2004), but I only analysed the expression of *Phox2b-Cre* using a *Rosa26*^{Yfp} reporter at E12.0. If *Phox2b-Cre* were not expressed at E10.5, then floxed *Nrp1* would not be targeted early enough to impair NRP1-mediated FBM neuron migration. To address this issue, I could repeat the *Phox2b-Cre* analysis with the *Rosa26*^{Yfp} reporter at E10.5 or even earlier to confirm that *Cre* expression occurs at the same time as or before *Nrp1* starts being expressed in FBM neurons.

Unexpectedly, however, floxed *Nrp1* was also not fully targeted by either *Nestin-Cre* or *NesCre8*, as high levels of *Nrp1* mRNA remained in each conditional mutant, and accordingly, they displayed normal FBM neuron migration. Both these lines should target most neuronal cells in the hindbrain, especially as *NesCre8* is already expressed from E8.5 onwards, before motor neurons are specified. This raises the possibility that floxed *Nrp1* may not be targeted easily by any CRE recombinase in migrating FBM neurons. In contrast, previous work from the Ruhrberg lab has shown that *NesCre8* (Cariboni et al., 2011; Fantin et al., 2013) and two other *Cre* lines, *Wnt1*^{Cre} and *Tie2-Cre,* are efficient in targeting floxed *Nrp1* in other cell types (Schwarz et al., 2009; Fantin et al., 2013). This means that floxed *Nrp1* is readily targeted by CRE recombinase in principle, even though it was not effectively targeted in FBM neurons. Moreover, previous work showed that targeting *Tbx20*$^{fl/-}$ with *NesCre8* resulted in defective tangential migration of FBM neurons, which demonstrates that *NesCre8* can target genes in FBM neurons (Song et al., 2006).

Interestingly, *Nrp1*$^{fl/-}$ *NesCre8* mutants showed defective cranial axon guidance similar to *Nrp1*-null mice, and *Nrp1*$^{fl/fl}$ *Phox2b-Cre* mice also have mild facial nerve defasciculation, even though both mutants retained *Nrp1* expression in FBM neuron somata. This raises the possibility that very low levels of NRP1 are sufficient in the FBM soma to ensure their normal migration, whereas low levels of NRP1 may not be sufficient to ensure its function in the distal axon. In agreement with low NRP1 levels being sufficient for FBM neuron migration, I have never been able to identify NRP1 in the somas of FBM neurons using previously tested antibodies in the Ruhrberg lab, but I have seen NRP1 in some hindbrain axons and other neuron types (e.g. Figure 3.2). In addition, axon guidance has been shown to involve local translation at the axonal growth cone (Shigeoka et al., 2013), and if cranial axons require such a mechanism, then perhaps this would explain why axons are more sensitive to small changes in *Nrp1* levels. In future experiments, I should therefore compare NRP1 levels in the cranial axons of controls and mutants.

In Chapter 4, I identified a non-cell autonomous role for *Hs2st* in FBM neurons, because *Hs2st*$^{Lacz/+}$ was expressed in a neuronal cell-type adjacent to FBM neurons. I was unsuccessful at targeting floxed *Ext1* mice with *Phox2b-Cre*, which in some ways is not unexpected, because this line should target migrating FBM neurons and not adjacent cells. It was surprising that *Nestin-Cre*, which others have shown to cause neural defects in *Ext1*$^{fl/fl}$ mice (Inatani et al., 2003) and also targets *Vegfa in Vegfa*$^{Hypo/fl}$ mice to disrupt FBM neuron migration, was not able to cause defects in FBM neuron migration in *Ext1*$^{fl/fl}$ mice. It was even more surprising that *NesCre8* was also not able to disrupt FBM neuron migration in *Ext1*$^{fl/fl}$ mice, given that it recombines very efficiently throughout the hindbrain (Fantin et al., 2013). Nevertheless, I observed that *Ext1*$^{fl/-}$ *Nestin-Cre* mice developed a low penetrance anencephaly phenotype, whilst others have described full penetrance midline axon guidance defects in these mice (Inatani et al., 2003). Moreover, *Ext1*$^{fl/-}$ *NesCre8* also have anencephaly (observation by Charlotte Maden and Christiana Ruhrberg). It would therefore be interesting to further analyse these mutants using wholemount TUJ1 staining at E11.5 and determine if they phenocopy the defects observed in *Hs6st1*$^{-/-}$*;Hs6st2*$^{-/-}$ mice (Chapter 4). This could help determine if *Ext1*$^{fl/-}$ *Nestin-Cre* targeting causes axonal defects, in agreement with a previous report (Inatani et al., 2003); Alternatively, the low penetrance neuronal phenotypes observed in *Ext1*$^{fl/-}$

NesCre8 and *Ext1*$^{fl/-}$ *Nestin-Cre* might be explained by poor targeting of the *Ext1* floxed allele in general, since a recent paper using *MMTV-Cre* has reported variable targeting of floxed *Ext1* in mammary glands (Garner et al., 2011).

As an alternative to the *Cre* lines described this chapter, I could also target FBM neurons with CRE recombinase controlled under other promoters such as *Isl1*, which is expressed in all motor neurons. Two *Cre* lines under the control of the *Isl1* promoter have been published and described to target FBM neurons (Srinivas et al., 2001; Yang et al., 2006; Qu et al., 2010). Another alternative would be to use to use a *Hoxb1-Cre* line that targets only r4, where the FBM neuron population is specified by E10.5 (Arenkiel et al., 2003; Yang et al., 2008; Di Bonito et al., 2013). In order to inactivate genes from an even earlier stage, I could use a *Cre* line under the control of the *Nkx6.2* promoter, which is expressed in FBM neuron precursors (Vallstedt et al., 2001; Muller et al., 2003; Fogarty et al., 2007; Baudet et al., 2008). Using these lines to further target floxed *Nrp1* and *Ext1* may help establish whether the three *Cre* lines I have analysed so far are not appropriate to target FBM neurons, or whether instead the *Nrp1* and *Ext1* floxed alleles are not amenable to CRE recombination.

5.4 SUMMARY

In this chapter, I have explored the suitability of existing genetic tools to study FBM neuron migration and axonal guidance. Thus, I have characterised the recombination pattern of three *Cre* transgenes in the developing embryonic hindbrain, *Phox2b-Cre*; *Nestin-Cre*; and *NesCre8*. I also investigated the efficiency of these *Cre* lines in targeting floxed genes in migrating FBM neurons and axons. I found that all *Cre* lines were unable to efficiently delete floxed alleles of *Nrp1* in migrating FBM neurons. However, floxed *Nrp2* was efficiently deleted by *Phox2b-Cre* and *NesCre8*-mediated *Nrp1* targeting efficiently phenocopied axonal defects in *Nrp1*-null mice. Further work should explore the idea that different levels of NRP1 are required for FBM somata and axons to develop normal. Moreover, I found that all *Cre* lines did not efficiently target floxed *Ext1* allele in the hindbrain and there was no phenocopy of FBM neuron migration defects observed in *Hs2st*-null mice (Chapter 4). On the other hand, lowering levels of *Vegfa* in the hindbrain using $Vegfa^{Hypo/fl}$ *Nestin-Cre* mice phenocopied FBM neuron migration defects in $Vegfa^{120/120}$ mice. My results show that expression of reporter genes ($Rosa26^{Yfp}$) is not always a faithful predictor of *Cre* targeting of other floxed alleles in every cell type, and none of the *Cre* lines are sufficient to target genes in migrating FBM neurons.

Chapter 6 FINAL CONCLUSIONS AND FUTURE WORK

6.1 SUMMARY OF ACHIEVEMENTS AND FINAL REMARKS

During embryonic development a variety of organs and systems, composed of different cell types and with different functions, will develop alongside each other in a timed manner. A wide variety of signalling pathways are involved in these various processes of development, but often each pathway appears to be required during various developmental processes. For example, VEGF signalling was initially thought to be mostly required during vascular development, but recent work, including results in this thesis, has shown that VEGF is important for neuronal development or cancer biology. Therefore, during development there must be more levels of complexity that allow a limited number of genes and molecules to be reiteratively used in varying systems. In this thesis I have focused on the use of combinatorial signalling pathways and the reuse of single pathways in various developmental processes.

Alternative splicing is one way of creating a larger variety of possible signalling combinations using a limited pool of genes. *Vegfa* is alternatively spliced into different isoform that have varying diffusion properties and receptor binding affinities. My findings show that $VEGF_{189}$, similar to $VEGF_{165}$, can bind and signal through NRP1 during neuronal migration, axon guidance and neuronal survival. This shows that during some NRP1-dependend neuronal development events there can be compensation between VEGF isoforms. During vascular development this is not the case (Ruhrberg et al., 2002). The use of both $VEGF_{165}$ and $VEGF_{189}$ with similar functions in the same system could mean a more dynamic control of spatial and temporal expression of VEGF during development.

Axon guidance and neuronal migration share several signalling molecules and occur simultaneously in the same cell type. The two processes occur in parallel and cell autonomously. During neuronal migration, in addition to guidance of the cell in a similar fashion to axons there is also the requirement to move the cell body and its nucleus (nucleokinesis) (Tsai and Gleeson, 2005; Marin et al., 2010). Therefore, there must be specific control of each compartment of the neuron that would allow it

to migrate the cell body and extend its axon. For example NRP1 controls both neuronal migration and axon guidance in FBM neurons. Interestingly it uses separate ligands, SEMA3A and VEGF, to control each event separately (Schwarz et al., 2004). Furthermore, in addition to binding different ligands NRP1 can also signal through a variety of co-receptors and specifically uses PLXNA3/PLEXNA4 for cranial axon guidance (Schwarz et al., 2008). In this thesis I have explored how combinatorial signalling is important for axon guidance and neuronal migration and I have also focused on the importance of posttranslational modifications in these processes.

We know that different genes and molecules can affect different stages of FBM neuron migration. However, little is known about how various signalling pathways might integrate and converge during FBM migration to control the different stages of radial and tangential migration. Posttranslational modifications can greatly increase the diversity of signals available during nervous system development (Edwards et al., 2014). I have explored the role of HSPG posttranslational modifications, which results in immense protein heterogeneity, during neuronal migration and axon guidance. My results showed that 2-*O*-sulfation was important to control FBM neuron migration whilst 6-*O*-sulfation was required for correct cranial axon guidance. I also found that VEGF/NRP1-dependent migration does not require 2-*O*-sulfation whilst FGF-dependent chemoattraction was dependent on normal 2-*O*-sulfation. This demonstrates that different signals interact and are dependent on each other during FBM neuron migration. Interestingly, other signalling pathways required for FBM neuron migration, such as PCP pathway components and cadherins, have also been shown to associate with HPSGs and some of their specific posttranslational modifications (Ai et al., 2003; Vivancos et al., 2009; Qu et al., 2010; Stockinger et al., 2011; Zakaria et al., 2014). In the future, new studies should investigate neuronal migration as a process that integrates a combination of genes and molecules that depend on each other.

In brief summary, this project has identified novel combinatorial molecular mechanisms and examined which genetic tools might be useful for the study of hindbrain development. First, I found that the $VEGF_{189}$ isoform can bind to axonal NRP1 *in vivo* and is sufficient to control VEGF/NRP1-dependent axon guidance,

neuronal migration and survival, in a similar manner to $VEGF_{165}$. Secondly, I described a complementary function for 2- and 6-*O*-sulfotransferases during FBM neuron migration and cranial axon guidance. Moreover, I also found a novel role for HSPG/FGF signalling in regulating FBM neuron migration. Lastly, I have found that *Cre* lines under the control of the *Phox2b* or *Nestin* promoters can target some floxed genes during FBM neuron migration and cranial axon guidance, but are not ideal to target floxed *Nrp1* in FBM neurons.

My findings on the role of $VEGF_{189}$ signalling through NRP1 in nervous system development have been published in the journal Development (Tillo et al., 2015) and the explant method I used to study FBM neuron migration was published in the Journal of Visualized Experiments JoVE (Tillo et al., 2014). My work on the novel roles of *O*-sulfotransferases during cranial axon guidance and motor neuron migration has not yet been published, but has been submitted as a manuscript to undergo peer review. Altogether, the work presented in this thesis will advance our understanding of signalling pathways that regulate for neuronal migration in and axon extension from the developing hindbrain.

6.2 FUTURE WORK

6.2.1 The role of HSPGs in VEGF signalling

The ability of VEGF to bind NRP1 depends on exons 6 and 7, which are also responsible for VEGF binding to the extracellular matrix to create an isoform-dependent diffusion gradient *in vivo* (Ruhrberg et al., 2002). VEGF requires heparin to signal appropriately in cultured endothelial cells (Ashikari-Hada et al., 2005), and HSPGs derived from pericytes can potentiate $VEGF_{165}$ binding to VEGFR2 in *trans* during vessel sprouting in embryoid bodies (Jakobsson et al., 2006). However, it has not yet been demonstrated that HSPGs are required for VEGF signalling in either endothelial cells or neurons *in vivo*. Moreover, little is known about which native HSPGs might bind to VEGF for correct signalling and if different classes of HSPGs are required for VEGF binding in a tissue dependent manner, i.e. pericytes can interact with both endothelial cells and neurons.

In vitro, human endothelial cell derived glypican 1 can bind $VEGF_{165}$, but not $VEGF_{121}$ (Gengrinovitch et al., 1999), and $VEGF_{165}$ also binds shed syndecan 1 to promote endothelial invasion in a Boyden chamber-type assay (Purushothaman et al., 2010). To further investigate VEGF/HSPG interactions *in vivo*, I could perform *in situ* AP-binding assays using tissue from HSPG mutant mice, e.g. *Ext*$^{fl/fl}$ *Nestin-Cre*, syndecan or glypican mutants. Furthermore, I could use surface plasmon resonance assays to assess the affinity of VEGF to different HSPGs, and also compare the binding properties of $VEGF_{121}$, which does not contain a heparin-binding domain, and $VEGF_{165}$ or $VEGF_{189}$ to various HSPGs.

6.2.2 VEGF/NRP1 signalling during FBM neuron migration

I showed that NRP1 signalling through VEGF is required for FBM neuron migration in a pathway that does not require HS2ST. However, no co-receptor has been identified for VEGF/NRP1 signalling during FBM neuron migration, even though PLXNA3/PLXNA4 have already been identified as NRP1 co-receptors for SEMA3A signalling during cranial axon guidance (Schwarz et al., 2004; Schwarz et al., 2008). It would therefore be interesting to identify the co-receptor required for

VEGF/NRP1 to control FBM neuron migration attraction by ablating floxed candidate NRP1 co-receptors, e.g. plexins, FLK1, FLT1, taking advantage of the knowledge on the *Cre* tools I have characterised.

When analysing *Cre* recombination in migrating FBM neurons I observed that *Phox2b-Cre* could successfully target *Rosa26*$^{Yfp/+}$, *Rosa26*$^{Dta/+}$ and *Nrp2*$^{fl/fl}$ in these motor neurons. Furthermore, *Nestin-Cre* and *NesCre8* also successfully target *Rosa*$^{Yfp/+}$, which resulted in YFP expression in migrating FBM neurons. However, my results showed that none of these *Cre* lines could target floxed *Nrp1* in migrating FBM neurons. This suggests that floxed *Nrp1* mice are not an ideal target to use as a positive control for investigating *Cre*-targeting in FBM neurons; instead floxed *Nrp2* would be a more suitable control target gene. NRP2 is expressed but does not have a function in FBM neuron migration, therefore it could be important to use a floxed target gene known be required for FBM neuron development, e.g. *Celsr1*$^{fl/fl}$ (Qu et al., 2010). To investigate if floxed *Nrp1* can be deleted with another *Cre* transgenic in these neurons, I could target floxed *Nrp1* with *Isl1-Cre*, which has been shown by others to successfully delete genes in migrating FBM neurons (Qu et al., 2010). I also showed that targeting floxed *Nrp1* with *NesCre8* or *Phox2b-Cre* resulted in abnormal cranial axon guidance. My results show that it is most likely that floxed *Nrp1* cannot be targeted by CRE recombinase in FBM neurons. The fact that *Cre*-targeting floxed *Nrp1* results in facial axon defects but normal neuronal migration might be explained by differences between NRP1 levels in each compartment. Axons are likely to have lower levels of *Nrp1* than somata; therefore, even low-level CRE recombination might be enough to induce axonal defects. To examine levels of NRP1 in the somata versus axons of these mutants I could try to check local levels of NRP1 protein and mRNA in these compartments, although this would like be challenging.

Using a hindbrain explant assay, I observed that VEGF-soaked beads are only capable of attracting the front of the FBM neuron migration stream. Similar to zebrafish, there might therefore be a leading population of FBM neurons or other cell types controlling collective migration, which express NRP1 and lead to VEGF chemoattraction. It is not clear if the *Cre* transgenes I used would target such a hypothetical leading front, as they may be somewhat genetically different from the

following neurons. To address this question and further understand the role of NRP1 in FBM neuron migration and cranial axon guidance, I could use a new mouse line expressing a *Nrp1-Cre* transgene (personal communication from Dr. Quenten Schwarz) to target *Rosa26*$^{Yfp/+}$ and thereby characterise *Nrp1* expression across the FBM population in more detail. I could also combine *Nrp1-Cre* with *Rosa26*$^{Dta/+}$, to investigate if *Nrp1* targets most or only a subpopulation of migrating FBM neurons.

6.2.3 The role of HSPGs in migrating FBM neurons

To further understand the role of HSPGs in cranial axon guidance and FBM neuron migration, it would be interesting to use a ligand and carbohydrate engagement (LACE) assay to investigate *in situ* if FGF/FGFR complex formation depends on HSPGs in hindbrain tissue (Allen and Rapraeger, 2003; Pan et al., 2006). Briefly, tissue sections from wild type and *Hs2st*-null mice could be incubated with exogenous FGFs and AP-tagged FGFRs and AP signal would detect where FGF:FGFR complexes had formed. Thus, any changes in AP signal observed in wild type compared to *Hs2st*-null tissue would indicate a requirement for 2-*O*-sulfated HSPGs during FGF:FGFR complex formation.

As my results show that FGFR4 is expressed in migrating FBM neurons, it would be interesting to analyse the hindbrain of *Fgfr4*-null mice for FBM neuron migration defects. However, this analysis may not be straightforward, because mouse mutant analyses have previously shown that there is a high level of redundancy between FGFRs. Specifically, *Fgfr4*$^{-/-}$ mice develop normally and some studies have suggested this is due to *Fgfr3* compensation (Weinstein et al., 1998; Li et al., 2011). Thus, I might have to screen multiple combinations of *Fgfr*-null mice to identify which receptors are required for FBM neuron migration *in vivo*.

To identify the endogenous FGF involved in FBM neuron migration I could use ISH and RT-PCR to characterise the expression pattern of candidate FGFs in the hindbrain. Once relevant candidate FGFs are identified I could use the hindbrain explant assay to investigate if FBM neurons are chemoattracted to these, and could also analyse the hindbrains of relevant *Fgf*-null mice during FBM neurons migration.

Other studies might focus on WNTs as candidate regulators in HS2ST-dependent FBM neuron migration. Several components of the WNT/PCP pathway have been implicated in FBM neuron migration (Vivancos et al., 2009; Qu et al., 2010; Glasco et al., 2012), and WNTs are known to require HSPGs for correct signalling, including *O*-sulfated HS (Ai et al., 2003; Hacker et al., 2005; Cadwalader et al., 2012).For example, *Wnt5a* is highly expressed in the caudal hindbrain starting from r5/6, and *Wnt5a*$^{-/-}$ mice have a split stream of migrating FBM neurons (Vivancos et al., 2009). Therefore, I could use a hindbrain explant model to analyse if migrating FBM neurons are still attracted to WNT5A in *Hs2st*-null mice (Vivancos et al., 2009), as performed for VEGF and FGF. I could also examine if WNT and FGF signalling regulate each other during FBM neuron development. For example, in the chick isthmus *Wnt1* is required for maintenance of the *Fgf8*, which controls r1 identity and the midbrain-hindbrain boundary (Canning et al., 2007).

During collective cell migration in the zebrafish, FGF and WNT mutually repress each other by inducing the expression of *dkk1b*, a WNT inhibitor, and *sef*, an FGF inhibitor (Aman and Piotrowski, 2008). This mutual inhibition is required to maintain a boundary between FGF and WNT signalling domains. Interestingly, the distribution of FGFs in this system is controlled by HSPGs, thus, the inhibition of HS results in abnormal collective cell migration due to ectopic WNT and FGF activation (Venero Galanternik et al., 2015). My results show that there is also ectopic FGF activation in *Hs2st*-null hindbrains. I could therefore also examine whether the expression pattern of known WNT-pathway components required for FBM neuron migration, e.g. *Wnt5a* and *Fz3*, changes in *Hs2st*-null hindbrains. To study if the two pathways interact during hindbrain development, I could also analyse the role of WNT inhibitors on FGF signalling during FBM neuron migration and vice versa.

6.2.4 Identifying novel signalling mechanisms during FBM neuron migration and cranial axon guidance.

To identify additional signals required for FBM neuron migration and cranial axon guidance in the mouse, I could use two approaches, a candidate approach or an

unbiased search. In the case of a candidate approach, I suggest searching the literature for signals that are important during FBM neuron migration and cranial axon guidance in other model systems, such as zebrafish, and investigate if they also have a role in mice. Furthermore, one could also investigate signals known to interact with pathways that have already been shown to have a role in regulating neuron migration and axon guidance. Alternatively, I could use an unbiased approach to identify novel signals. For example, I could isolate RNA from E10.5 r4 cells isolated by FACS from a *Hoxb1-Cre Rosa26*$^{Yfp/+}$ hindbrain and use a DNA microarray to identify candidate genes that are highly expressed at the onset of FBM neuron migration and then validate them with expression studies. Combining both candidate and unbiased approaches in particular might identify an overlapping set of important target genes for future work on FBM neuron migration and cranial axon guidance.

I could use the previously described hindbrain explant model (Tillo et al., 2014) to screen for new molecules required during FBM neuron migration and functionally validate those identified in the approaches above. For example, I could treat hindbrain explants with chemical inhibitors or implant chemokine soaked beads to investigate new signalling pathways amenable to such manipulations. I could also attempt to live image FBM neuron migration using the hindbrain explant model on an *Isl1-Egpf* mouse, which has GFP-labelled cranial motor neurons (Shirasaki et al., 2006; Song et al., 2006). Recently, the use of *in utero* and *ex vivo* electroporation in mouse has become more common when studying early development. This technique would allow me to electroporate small interfering RNA to knockout genes in the embryonic hindbrain during FBM neuron migration. Therefore, I could easily screen a large number of genes thought to be involved in FBM neuron migration before using knockout mice. This would also allow me to test the interaction between multiple pathways by targeting more than one gene at the same time. However, the fact that FBM neuron migration occurs during early embryonic development makes it challenging to electroporate the hindbrain. Some studies have successfully used electroporation to target the mouse hindbrain at E11.5 and E12.5 (Holland et al., 2012; David et al., 2014), and this could be combined with the hindbrain culture assay used to study FBM neuron migration. Establishing a new protocol using *in utero* or *ex vivo* electroporation of hindbrains at early embryonic stages would help

advance the study of FBM neuron migration in the mouse. Any novel molecules essential for FBM neuron migration discovered using hindbrain explant assays or electroporation could then be confirmed by analysing mouse mutants *in vivo*.

REFERENCES

Ai, X., Do, A. T., Lozynska, O., Kusche-Gullberg, M., Lindahl, U. and Emerson, C. P., Jr. (2003). QSulf1 remodels the 6-O sulfation states of cell surface heparan sulfate proteoglycans to promote Wnt signaling. *The Journal of Cell Biology* **162**, 341-351.

Aikawa, J. and Esko, J. D. (1999). Molecular cloning and expression of a third member of the heparan sulfate/heparin GlcNAc N-deacetylase/ N-sulfotransferase family. *The Journal of Biological Chemistry* **274**, 2690-2695.

Aikawa, J., Grobe, K., Tsujimoto, M. and Esko, J. D. (2001). Multiple isozymes of heparan sulfate/heparin GlcNAc N-deacetylase/GlcN N-sulfotransferase. Structure and activity of the fourth member, NDST4. *The Journal of Biological Chemistry* **276**, 5876-5882.

Alexander, C. M., Reichsman, F., Hinkes, M. T., Lincecum, J., Becker, K. A., Cumberledge, S. and Bernfield, M. (2000). Syndecan-1 is required for Wnt-1-induced mammary tumorigenesis in mice. *Nature Genetics* **25**, 329-332.

Allen, B. L. and Rapraeger, A. C. (2003). Spatial and temporal expression of heparan sulfate in mouse development regulates FGF and FGF receptor assembly. *The Journal of Cell Biology* **163**, 637-648.

Allen, N. J., Bennett, M. L., Foo, L. C., Wang, G. X., Chakraborty, C., Smith, S. J. and Barres, B. A. (2012). Astrocyte glypicans 4 and 6 promote formation of excitatory synapses via GluA1 AMPA receptors. *Nature* **486**, 410-414.

Aman, A. and Piotrowski, T. (2008). Wnt/beta-catenin and Fgf signaling control collective cell migration by restricting chemokine receptor expression. *Developmental cell* **15**, 749-761.

Arenkiel, B. R., Gaufo, G. O. and Capecchi, M. R. (2003). Hoxb1 neural crest preferentially form glia of the PNS. *Developmental Dynamics* **227**, 379-386.

Arese, M., Serini, G. and Bussolino, F. (2011). Nervous vascular parallels: axon guidance and beyond. *Int J Dev Biol* **55**, 439-445.

Arikawa-Hirasawa, E., Rossi, S. G., Rotundo, R. L. and Yamada, Y. (2002). Absence of acetylcholinesterase at the neuromuscular junctions of perlecan-null mice. *Nature Neuroscience* **5**, 119-123.

Arikawa-Hirasawa, E., Watanabe, H., Takami, H., Hassell, J. R. and Yamada, Y. (1999). Perlecan is essential for cartilage and cephalic development. *Nature Genetics* **23**, 354-358.

Ashikari-Hada, S., Habuchi, H., Kariya, Y. and Kimata, K. (2005). Heparin regulates vascular endothelial growth factor165-dependent mitogenic activity, tube formation, and its receptor phosphorylation of human endothelial cells. Comparison of the effects of heparin and modified heparins. *The Journal of Biological Chemistry* **280**, 31508-31515.

Augsburger, A., Schuchardt, A., Hoskins, S., Dodd, J. and Butler, S. (1999). BMPs as mediators of roof plate repulsion of commissural neurons. *Neuron* **24**, 127-141.

Axelrod, J. D. and McNeill, H. (2002). Coupling planar cell polarity signaling to morphogenesis. *TheScientificWorldJournal* **2**, 434-454.

Bagri, A., Cheng, H. J., Yaron, A., Pleasure, S. J. and Tessier-Lavigne, M. (2003). Stereotyped pruning of long hippocampal axon branches triggered by retraction inducers of the semaphorin family. *Cell* **113**, 285-299.

Baudet, C., Pozas, E., Adameyko, I., Andersson, E., Ericson, J. and Ernfors, P. (2008). Retrograde signaling onto Ret during motor nerve terminal maturation. *The Journal of Neuroscience* **28**, 963-975.

Bellon, A., Luchino, J., Haigh, K., Rougon, G., Haigh, J., Chauvet, S. and Mann, F. (2010). VEGFR2 (KDR/Flk1) signaling mediates axon growth in response to semaphorin 3E in the developing brain. *Neuron* **66**, 205-219.

Bentivoglio, M. and Mazzarello, P. (1999). The history of radial glia. *Brain Res Bull* **49**, 305-315.

Bink, R. J., Habuchi, H., Lele, Z., Dolk, E., Joore, J., Rauch, G. J., Geisler, R., Wilson, S. W., den Hertog, J., Kimata, K. et al. (2003). Heparan sulfate 6-o-sulfotransferase is essential for muscle development in zebrafish. *Journal of Biological Chemistry* **278**, 31118-31127.

Bishop, J. R., Schuksz, M. and Esko, J. D. (2007). Heparan sulphate proteoglycans fine-tune mammalian physiology. *Nature* **446**, 1030-1037.

Briscoe, J., Pierani, A., Jessell, T. M. and Ericson, J. (2000). A homeodomain protein code specifies progenitor cell identity and neuronal fate in the ventral neural tube. *Cell* **101**, 435-445.

Briscoe, J., Sussel, L., Serup, P., Hartigan-O'Connor, D., Jessell, T. M., Rubenstein, J. L. and Ericson, J. (1999). Homeobox gene Nkx2.2 and specification of neuronal identity by graded Sonic hedgehog signalling. *Nature* **398**, 622-627.

Bullock, S. L., Fletcher, J. M., Beddington, R. S. and Wilson, V. A. (1998). Renal agenesis in mice homozygous for a gene trap mutation in the gene encoding heparan sulfate 2-sulfotransferase. *Genes & Development* **12**, 1894-1906.

Cadwalader, E. L., Condic, M. L. and Yost, H. J. (2012). 2-O-sulfotransferase regulates Wnt signaling, cell adhesion and cell cycle during zebrafish epiboly. *Development* **139**, 1296-1305.

Calvo, C. F., Fontaine, R. H., Soueid, J., Tammela, T., Makinen, T., Alfaro-Cervello, C., Bonnaud, F., Miguez, A., Benhaim, L., Xu, Y. et al. (2011). Vascular endothelial growth factor receptor 3 directly regulates murine neurogenesis. *Genes & Development* **25**, 831-844.

Canning, C. A., Lee, L., Irving, C., Mason, I. and Jones, C. M. (2007). Sustained interactive Wnt and FGF signaling is required to maintain isthmic identity. *Developmental Biology* **305**, 276-286.

Cano-Gauci, D. F., Song, H. H., Yang, H., McKerlie, C., Choo, B., Shi, W., Pullano, R., Piscione, T. D., Grisaru, S., Soon, S. et al. (1999). Glypican-3-deficient mice exhibit developmental overgrowth and some of the abnormalities

typical of Simpson-Golabi-Behmel syndrome. *The Journal of Cell Biology* **146**, 255-264.

Cariboni, A., Maggi, R. and Parnavelas, J. G. (2007). From nose to fertility: the long migratory journey of gonadotropin-releasing hormone neurons. *Trends in neurosciences* **30**, 638-644.

Cariboni, A., Davidson, K., Dozio, E., Memi, F., Schwarz, Q., Stossi, F., Parnavelas, J. G. and Ruhrberg, C. (2011). VEGF signalling controls GnRH neuron survival via NRP1 independently of KDR and blood vessels. *Development* **138**, 3723-3733.

Carmeliet, P. (1999). Basic Concepts of (Myocardial) Angiogenesis: Role of Vascular Endothelial Growth Factor and Angiopoietin. *Curr Interv Cardiol Rep* **1**, 322-335.

Carmeliet, P. (2005). Angiogenesis in life, disease and medicine. *Nature* **438**, 932-936.

Carmeliet, P., Ferreira, V., Breier, G., Pollefeyt, S., Kieckens, L., Gertsenstein, M., Fahrig, M., Vandenhoeck, A., Harpal, K., Eberhardt, C. et al. (1996). Abnormal blood vessel development and lethality in embryos lacking a single VEGF allele. *Nature* **380**, 435-439.

Carmeliet, P., Ng, Y. S., Nuyens, D., Theilmeier, G., Brusselmans, K., Cornelissen, I., Ehler, E., Kakkar, V. V., Stalmans, I., Mattot, V. et al. (1999). Impaired myocardial angiogenesis and ischemic cardiomyopathy in mice lacking the vascular endothelial growth factor isoforms VEGF164 and VEGF188. *Nature Medicine* **5**, 495-502.

Carrasco, A. E., McGinnis, W., Gehring, W. J. and De Robertis, E. M. (1984). Cloning of an X. laevis gene expressed during early embryogenesis coding for a peptide region homologous to Drosophila homeotic genes. *Cell* **37**, 409-414.

Caviness, V. S., Jr. and Sidman, R. L. (1973). Time of origin or corresponding cell classes in the cerebral cortex of normal and reeler mutant mice: an autoradiographic analysis. *J Comp Neurol* **148**, 141-151.

Chandrasekhar, A. (2004). Turning heads: development of vertebrate branchiomotor neurons. *Developmental Dynamics* **229**, 143-161.

Charron, F., Stein, E., Jeong, J., McMahon, A. P. and Tessier-Lavigne, M. (2003). The morphogen sonic hedgehog is an axonal chemoattractant that collaborates with netrin-1 in midline axon guidance. *Cell* **113**, 11-23.

Chauvet, S., Cohen, S., Yoshida, Y., Fekrane, L., Livet, J., Gayet, O., Segu, L., Buhot, M. C., Jessell, T. M., Henderson, C. E. et al. (2007). Gating of Sema3E/PlexinD1 signaling by neuropilin-1 switches axonal repulsion to attraction during brain development. *Neuron* **56**, 807-822.

Chen, E., Stringer, S. E., Rusch, M. A., Selleck, S. B. and Ekker, S. C. (2005). A unique role for 6-O sulfation modification in zebrafish vascular development. *Developmental Biology* **284**, 364-376.

Chen, G., Sima, J., Jin, M., Wang, K. Y., Xue, X. J., Zheng, W., Ding, Y. Q. and Yuan, X. B. (2008). Semaphorin-3A guides radial migration of cortical neurons during development. *Nature Neuroscience* **11**, 36-44.

Chen, H., Chedotal, A., He, Z., Goodman, C. S. and Tessier-Lavigne, M. (1997). Neuropilin-2, a novel member of the neuropilin family, is a high affinity receptor for the semaphorins Sema E and Sema IV but not Sema III. *Neuron* **19**, 547-559.

Chen, H., Bagri, A., Zupicich, J. A., Zou, Y., Stoeckli, E., Pleasure, S. J., Lowenstein, D. H., Skarnes, W. C., Chedotal, A. and Tessier-Lavigne, M. (2000). Neuropilin-2 regulates the development of selective cranial and sensory nerves and hippocampal mossy fiber projections. *Neuron* **25**, 43-56.

Cheng, H. J., Bagri, A., Yaron, A., Stein, E., Pleasure, S. J. and Tessier-Lavigne, M. (2001). Plexin-A3 mediates semaphorin signaling and regulates the development of hippocampal axonal projections. *Neuron* **32**, 249-263.

Clauss, M., Gerlach, M., Gerlach, H., Brett, J., Wang, F., Familletti, P. C., Pan, Y. C., Olander, J. V., Connolly, D. T. and Stern, D. (1990). Vascular permeability factor: a tumor-derived polypeptide that induces endothelial cell and monocyte

procoagulant activity, and promotes monocyte migration. *The Journal of Experimental Medicine* **172**, 1535-1545.

Clegg, J. M., Conway, C. D., Howe, K. M., Price, D. J., Mason, J. O., Turnbull, J. E., Basson, M. A. and Pratt, T. (2014). Heparan sulfotransferases Hs6st1 and Hs2st keep Erk in check for mouse corpus callosum development. *The Journal of Neuroscience* **34**, 2389-2401.

Conway, C. D., Howe, K. M., Nettleton, N. K., Price, D. J., Mason, J. O. and Pratt, T. (2011). Heparan sulfate sugar modifications mediate the functions of slits and other factors needed for mouse forebrain commissure development. *The Journal of Neuroscience* **31**, 1955-1970.

Cooper, J. A. (2013). Cell biology in neuroscience: mechanisms of cell migration in the nervous system. *The Journal of Cell Biology* **202**, 725-734.

Coppola, E., Pattyn, A., Guthrie, S. C., Goridis, C. and Studer, M. (2005). Reciprocal gene replacements reveal unique functions for Phox2 genes during neural differentiation. *The EMBO Journal* **24**, 4392-4403.

Cordes, S. P. (2001). Molecular genetics of cranial nerve development in mouse. *Nature Reviews. Neuroscience* **2**, 611-623.

Cordes, S. P. and Barsh, G. S. (1994). The mouse segmentation gene kr encodes a novel basic domain-leucine zipper transcription factor. *Cell* **79**, 1025-1034.

Costell, M., Carmona, R., Gustafsson, E., Gonzalez-Iriarte, M., Fassler, R. and Munoz-Chapuli, R. (2002). Hyperplastic conotruncal endocardial cushions and transposition of great arteries in perlecan-null mice. *Circ Res* **91**, 158-164.

Cubedo, N., Cerdan, E., Sapede, D. and Rossel, M. (2009). CXCR4 and CXCR7 cooperate during tangential migration of facial motoneurons. *Mol Cell Neurosci* **40**, 474-484.

D'Arcangelo, G., Miao, G. G., Chen, S. C., Soares, H. D., Morgan, J. I. and Curran, T. (1995). A protein related to extracellular matrix proteins deleted in the mouse mutant reeler. *Nature* **374**, 719-723.

D'Autreaux, F., Coppola, E., Hirsch, M. R., Birchmeier, C. and Brunet, J. F. (2011). Homeoprotein Phox2b commands a somatic-to-visceral switch in cranial sensory pathways. *Proceedings of the National Academy of Sciences of the United States of America* **108**, 20018-20023.

Damert, A., Miquerol, L., Gertsenstein, M., Risau, W. and Nagy, A. (2002). Insufficient VEGFA activity in yolk sac endoderm compromises haematopoietic and endothelial differentiation. *Development* **129**, 1881-1892.

David, L. S., Aitoubah, J., Lesperance, L. S. and Wang, L. Y. (2014). Gene delivery in mouse auditory brainstem and hindbrain using in utero electroporation. *Mol Brain* **7**, 51.

Dealy, C. N., Seghatoleslami, M. R., Ferrari, D. and Kosher, R. A. (1997). FGF-stimulated outgrowth and proliferation of limb mesoderm is dependent on syndecan-3. *Developmental Biology* **184**, 343-350.

Dejima, K., Kleinschmit, A., Takemura, M., Choi, P. Y., Kinoshita-Toyoda, A., Toyoda, H. and Nakato, H. (2013). The role of Drosophila heparan sulfate 6-O-endosulfatase in sulfation compensation. *The Journal of Biological Chemistry* **288**, 6574-6582.

Dhoot, G. K., Gustafsson, M. K., Ai, X., Sun, W., Standiford, D. M. and Emerson, C. P., Jr. (2001). Regulation of Wnt signaling and embryo patterning by an extracellular sulfatase. *Science* **293**, 1663-1666.

Di Bonito, M., Narita, Y., Avallone, B., Sequino, L., Mancuso, M., Andolfi, G., Franze, A. M., Puelles, L., Rijli, F. M. and Studer, M. (2013). Assembly of the auditory circuitry by a Hox genetic network in the mouse brainstem. *PLoS Genetics* **9**, e1003249.

Dickson, B. J. (2002). Molecular mechanisms of axon guidance. *Science* **298**, 1959-1964.

Ding, S., Luo, J. H. and Yuan, X. B. (2007). Semaphorin-3F attracts the growth cone of cerebellar granule cells through cGMP signaling pathway. *Biochem Biophys Res Commun* **356**, 857-863.

Echtermeyer, F., Streit, M., Wilcox-Adelman, S., Saoncella, S., Denhez, F., Detmar, M. and Goetinck, P. (2001). Delayed wound repair and impaired angiogenesis in mice lacking syndecan-4. *The Journal of Clinical Investigation* **107**, R9-R14.

Edwards, A. V., Edwards, G. J., Schwammle, V., Saxtorph, H. and Larsen, M. R. (2014). Spatial and temporal effects in protein post-translational modification distributions in the developing mouse brain. *J Proteome Res* **13**, 260-267.

Elsen, G. E., Choi, L. Y., Prince, V. E. and Ho, R. K. (2009). The autism susceptibility gene met regulates zebrafish cerebellar development and facial motor neuron migration. *Developmental Biology* **335**, 78-92.

Ericson, J., Thor, S., Edlund, T., Jessell, T. M. and Yamada, T. (1992). Early stages of motor neuron differentiation revealed by expression of homeobox gene Islet-1. *Science* **256**, 1555-1560.

Ericson, J., Morton, S., Kawakami, A., Roelink, H. and Jessell, T. M. (1996). Two critical periods of Sonic Hedgehog signaling required for the specification of motor neuron identity. *Cell* **87**, 661-673.

Ericson, J., Briscoe, J., Rashbass, P., van Heyningen, V. and Jessell, T. M. (1997a). Graded sonic hedgehog signaling and the specification of cell fate in the ventral neural tube. *Cold Spring Harb Symp Quant Biol* **62**, 451-466.

Ericson, J., Rashbass, P., Schedl, A., Brenner-Morton, S., Kawakami, A., van Heyningen, V., Jessell, T. M. and Briscoe, J. (1997b). Pax6 controls progenitor cell identity and neuronal fate in response to graded Shh signaling. *Cell* **90**, 169-180.

Erskine, L. and Herrera, E. (2007). The retinal ganglion cell axon's journey: insights into molecular mechanisms of axon guidance. *Developmental Biology* **308**, 1-14.

Erskine, L., Reijntjes, S., Pratt, T., Denti, L., Schwarz, Q., Vieira, J. M., Alakakone, B., Shewan, D. and Ruhrberg, C. (2011). VEGF signaling through neuropilin 1 guides commissural axon crossing at the optic chiasm. *Neuron* **70**, 951-965.

Esko, J. D. and Lindahl, U. (2001). Molecular diversity of heparan sulfate. *The Journal of Clinical Investigation* **108**, 169-173.

Esko, J. D. and Selleck, S. B. (2002). Order out of chaos: assembly of ligand binding sites in heparan sulfate. *Annual review of biochemistry* **71**, 435-471.

Fan, G., Xiao, L., Cheng, L., Wang, X., Sun, B. and Hu, G. (2000). Targeted disruption of NDST-1 gene leads to pulmonary hypoplasia and neonatal respiratory distress in mice. *FEBS letters* **467**, 7-11.

Fantin, A., Schwarz, Q., Davidson, K., Normando, E. M., Denti, L. and Ruhrberg, C. (2011). The cytoplasmic domain of neuropilin 1 is dispensable for angiogenesis, but promotes the spatial separation of retinal arteries and veins. *Development* **138**, 4185-4191.

Fantin, A., Vieira, J. M., Plein, A., Denti, L., Fruttiger, M., Pollard, J. W. and Ruhrberg, C. (2013). NRP1 acts cell autonomously in endothelium to promote tip cell function during sprouting angiogenesis. *Blood* **121**, 2352-2362.

Fantin, A., Herzog, B., Mahmoud, M., Yamaji, M., Plein, A., Denti, L., Ruhrberg, C. and Zachary, I. (2014). Neuropilin 1 (NRP1) hypomorphism combined with defective VEGF-A binding reveals novel roles for NRP1 in developmental and pathological angiogenesis. *Development* **141**, 556-562.

Fantin, A., Vieira, J. M., Gestri, G., Denti, L., Schwarz, Q., Prykhozhij, S., Peri, F., Wilson, S. W. and Ruhrberg, C. (2010). Tissue macrophages act as cellular chaperones for vascular anastomosis downstream of VEGF-mediated endothelial tip cell induction. *Blood* **116**, 829-840.

Ferrara, N., Gerber, H. P. and LeCouter, J. (2003). The biology of VEGF and its receptors. *Nature Medicine* **9**, 669-676.

Ferrara, N., Carver-Moore, K., Chen, H., Dowd, M., Lu, L., O'Shea, K. S., Powell-Braxton, L., Hillan, K. J. and Moore, M. W. (1996). Heterozygous embryonic lethality induced by targeted inactivation of the VEGF gene. *Nature* **380**, 439-442.

Ferreras, C., Rushton, G., Cole, C. L., Babur, M., Telfer, B. A., van Kuppevelt, T. H., Gardiner, J. M., Williams, K. J., Jayson, G. C. and Avizienyte, E. (2012). Endothelial heparan sulfate 6-O-sulfation levels regulate angiogenic responses of endothelial cells to fibroblast growth factor 2 and vascular endothelial growth factor. *The Journal of Biological Chemistry* **287**, 36132-36146.

Firnberg, N. and Neubuser, A. (2002). FGF signaling regulates expression of Tbx2, Erm, Pea3, and Pax3 in the early nasal region. *Developmental Biology* **247**, 237-250.

Fogarty, M., Grist, M., Gelman, D., Marin, O., Pachnis, V. and Kessaris, N. (2007). Spatial genetic patterning of the embryonic neuroepithelium generates GABAergic interneuron diversity in the adult cortex. *The Journal of Neuroscience* **27**, 10935-10946.

Fong, G. H., Rossant, J., Gertsenstein, M. and Breitman, M. L. (1995). Role of the Flt-1 receptor tyrosine kinase in regulating the assembly of vascular endothelium. *Nature* **376**, 66-70.

Forsberg, E., Pejler, G., Ringvall, M., Lunderius, C., Tomasini-Johansson, B., Kusche-Gullberg, M., Eriksson, I., Ledin, J., Hellman, L. and Kjellen, L. (1999). Abnormal mast cells in mice deficient in a heparin-synthesizing enzyme. *Nature* **400**, 773-776.

Fujisawa, H., Kitsukawa, T., Kawakami, A., Takagi, S., Shimizu, M. and Hirata, T. (1997). Roles of a neuronal cell-surface molecule, neuropilin, in nerve fiber fasciculation and guidance. *Cell Tissue Res* **290**, 465-470.

Garner, O. B., Bush, K. T., Nigam, K. B., Yamaguchi, Y., Xu, D., Esko, J. D. and Nigam, S. K. (2011). Stage-dependent regulation of mammary ductal branching by heparan sulfate and HGF-cMet signaling. *Developmental Biology* **355**, 394-403.

Gautam, M., Noakes, P. G., Moscoso, L., Rupp, F., Scheller, R. H., Merlie, J. P. and Sanes, J. R. (1996). Defective neuromuscular synaptogenesis in agrin-deficient mutant mice. *Cell* **85**, 525-535.

Gavalas, A., Ruhrberg, C., Livet, J., Henderson, C. E. and Krumlauf, R. (2003). Neuronal defects in the hindbrain of Hoxa1, Hoxb1 and Hoxb2 mutants reflect regulatory interactions among these Hox genes. *Development* **130**, 5663-5679.

Gavalas, A., Studer, M., Lumsden, A., Rijli, F. M., Krumlauf, R. and Chambon, P. (1998). Hoxa1 and Hoxb1 synergize in patterning the hindbrain, cranial nerves and second pharyngeal arch. *Development* **125**, 1123-1136.

Gelfand, M. V., Hagan, N., Tata, A., Oh, W. J., Lacoste, B., Kang, K. T., Kopycinska, J., Bischoff, J., Wang, J. H. and Gu, C. (2014). Neuropilin-1 functions as a VEGFR2 co-receptor to guide developmental angiogenesis independent of ligand binding. *eLife* **3**, e03720.

Gengrinovitch, S., Berman, B., David, G., Witte, L., Neufeld, G. and Ron, D. (1999). Glypican-1 is a VEGF165 binding proteoglycan that acts as an extracellular chaperone for VEGF165. *The Journal of Biological Chemistry* **274**, 10816-10822.

Gerber, H. P., Hillan, K. J., Ryan, A. M., Kowalski, J., Keller, G. A., Rangell, L., Wright, B. D., Radtke, F., Aguet, M. and Ferrara, N. (1999). VEGF is required for growth and survival in neonatal mice. *Development* **126**, 1149-1159.

Gerhardt, H., Golding, M., Fruttiger, M., Ruhrberg, C., Lundkvist, A., Abramsson, A., Jeltsch, M., Mitchell, C., Alitalo, K., Shima, D. et al. (2003). VEGF guides angiogenic sprouting utilizing endothelial tip cell filopodia. *The Journal of Cell Biology* **161**, 1163-1177.

Giger, R. J., Cloutier, J. F., Sahay, A., Prinjha, R. K., Levengood, D. V., Moore, S. E., Pickering, S., Simmons, D., Rastan, S., Walsh, F. S. et al. (2000). Neuropilin-2 is required in vivo for selective axon guidance responses to secreted semaphorins. *Neuron* **25**, 29-41.

Gilland, E. and Baker, R. (1993). Conservation of neuroepithelial and mesodermal segments in the embryonic vertebrate head. *Acta Anat (Basel)* **148**, 110-123.

Gingras, J., Rassadi, S., Cooper, E. and Ferns, M. (2007). Synaptic transmission is impaired at neuronal autonomic synapses in agrin-null mice. *Developmental Neurobiology* **67**, 521-534.

Gitay-Goren, H., Soker, S., Vlodavsky, I. and Neufeld, G. (1992). The binding of vascular endothelial growth factor to its receptors is dependent on cell surface-associated heparin-like molecules. *The Journal of Biological Chemistry* **267**, 6093-6098.

Gitay-Goren, H., Cohen, T., Tessler, S., Soker, S., Gengrinovitch, S., Rockwell, P., Klagsbrun, M., Levi, B. Z. and Neufeld, G. (1996). Selective binding of VEGF121 to one of the three vascular endothelial growth factor receptors of vascular endothelial cells. *The Journal of Biological Chemistry* **271**, 5519-5523.

Glasco, D. M., Sittaramane, V., Bryant, W., Fritzsch, B., Sawant, A., Paudyal, A., Stewart, M., Andre, P., Cadete Vilhais-Neto, G., Yang, Y. et al. (2012). The mouse Wnt/PCP protein Vangl2 is necessary for migration of facial branchiomotor neurons, and functions independently of Dishevelled. *Developmental Biology* **369**, 211-222.

Gluzman-Poltorak, Z., Cohen, T., Herzog, Y. and Neufeld, G. (2000). Neuropilin-2 is a receptor for the vascular endothelial growth factor (VEGF) forms VEGF-145 and VEGF-165. *The Journal of Biological Chemistry* **275**, 29922.

Goddard, J. M., Rossel, M., Manley, N. R. and Capecchi, M. R. (1996). Mice with targeted disruption of Hoxb-1 fail to form the motor nucleus of the VIIth nerve. *Development* **122**, 3217-3228.

Gotte, M., Joussen, A. M., Klein, C., Andre, P., Wagner, D. D., Hinkes, M. T., Kirchhof, B., Adamis, A. P. and Bernfield, M. (2002). Role of syndecan-1 in leukocyte-endothelial interactions in the ocular vasculature. *Investigative ophthalmology & visual science* **43**, 1135-1141.

Gotz, M. and Huttner, W. B. (2005). The cell biology of neurogenesis. *Nat Rev Mol Cell Bio* **6**, 777-788.

Grant, P. K. and Moens, C. B. (2010). The neuroepithelial basement membrane serves as a boundary and a substrate for neuron migration in the zebrafish hindbrain. *Neural Development* **5**, 9.

Grobe, K., Inatani, M., Pallerla, S. R., Castagnola, J., Yamaguchi, Y. and Esko, J. D. (2005). Cerebral hypoplasia and craniofacial defects in mice lacking heparan sulfate Ndst1 gene function. *Development* **132**, 3777-3786.

Gu, C., Rodriguez, E. R., Reimert, D. V., Shu, T., Fritzsch, B., Richards, L. J., Kolodkin, A. L. and Ginty, D. D. (2003). Neuropilin-1 conveys semaphorin and VEGF signaling during neural and cardiovascular development. *Developmental cell* **5**, 45-57.

Gu, C., Yoshida, Y., Livet, J., Reimert, D. V., Mann, F., Merte, J., Henderson, C. E., Jessell, T. M., Kolodkin, A. L. and Ginty, D. D. (2005). Semaphorin 3E and plexin-D1 control vascular pattern independently of neuropilins. *Science* **307**, 265-268.

Guerrin, M., Moukadiri, H., Chollet, P., Moro, F., Dutt, K., Malecaze, F. and Plouet, J. (1995). Vasculotropin/vascular endothelial growth factor is an autocrine growth factor for human retinal pigment epithelial cells cultured in vitro. *Journal of cellular physiology* **164**, 385-394.

Guimond, S., Maccarana, M., Olwin, B. B., Lindahl, U. and Rapraeger, A. C. (1993). Activating and inhibitory heparin sequences for FGF-2 (basic FGF). Distinct requirements for FGF-1, FGF-2, and FGF-4. *The Journal of Biological Chemistry* **268**, 23906-23914.

Guthrie, S. (2007). Patterning and axon guidance of cranial motor neurons. *Nature Reviews. Neuroscience* **8**, 859-871.

Habuchi, H., Nagai, N., Sugaya, N., Atsumi, F., Stevens, R. L. and Kimata, K. (2007). Mice deficient in heparan sulfate 6-O-sulfotransferase-1 exhibit defective heparan sulfate biosynthesis, abnormal placentation, and late embryonic lethality. *The Journal of Biological Chemistry* **282**, 15578-15588.

Habuchi, H., Tanaka, M., Habuchi, O., Yoshida, K., Suzuki, H., Ban, K. and Kimata, K. (2000). The occurrence of three isoforms of heparan sulfate 6-O-sulfotransferase having different specificities for hexuronic acid adjacent to the targeted N-sulfoglucosamine. *The Journal of Biological Chemistry* **275**, 2859-2868.

Hacker, U., Nybakken, K. and Perrimon, N. (2005). Heparan sulphate proteoglycans: the sweet side of development. *Nature Reviews. Molecular Cell Biology* **6**, 530-541.

Hagner-McWhirter, A., Hannesson, H. H., Campbell, P., Westley, J., Roden, L., Lindahl, U. and Li, J. P. (2000). Biosynthesis of heparin/heparan sulfate: kinetic studies of the glucuronyl C5-epimerase with N-sulfated derivatives of the Escherichia coli K5 capsular polysaccharide as substrates. *Glycobiology* **10**, 159-171.

Haigh, J. J., Morelli, P. I., Gerhardt, H., Haigh, K., Tsien, J., Damert, A., Miquerol, L., Muhlner, U., Klein, R., Ferrara, N. et al. (2003). Cortical and retinal defects caused by dosage-dependent reductions in VEGF-A paracrine signaling. *Developmental Biology* **262**, 225-241.

Hammond, R., Vivancos, V., Naeem, A., Chilton, J., Mambetisaeva, E., Andrews, W., Sundaresan, V. and Guthrie, S. (2005). Slit-mediated repulsion is a key regulator of motor axon pathfinding in the hindbrain. *Development* **132**, 4483-4495.

Han, C., Belenkaya, T. Y., Khodoun, M., Tauchi, M., Lin, X. and Lin, X. (2004). Distinct and collaborative roles of Drosophila EXT family proteins in morphogen signalling and gradient formation. *Development* **131**, 1563-1575.

Hatten, M. E. (1999). Central nervous system neuronal migration. *Annu Rev Neurosci* **22**, 511-539.

He, Z. and Tessier-Lavigne, M. (1997). Neuropilin is a receptor for the axonal chemorepellent Semaphorin III. *Cell* **90**, 739-751.

Herve, M. A., Buteau-Lozano, H., Vassy, R., Bieche, I., Velasco, G., Pla, M., Perret, G., Mourah, S. and Perrot-Applanat, M. (2008). Overexpression of vascular endothelial growth factor 189 in breast cancer cells leads to delayed tumor uptake with dilated intratumoral vessels. *The American journal of pathology* **172**, 167-178.

Hienola, A., Tumova, S., Kulesskiy, E. and Rauvala, H. (2006). N-syndecan deficiency impairs neural migration in brain. *The Journal of Cell Biology* **174**, 569-580.

Holland, P. J., George, A. M., Worrell, L. T. and Landsberg, R. L. (2012). In vitro electroporation of the lower rhombic lip of midgestation mouse embryos. *Journal of Visualized Experiments : JoVE*, e3983.

Holmborn, K., Habicher, J., Kasza, Z., Eriksson, A. S., Filipek-Gorniok, B., Gopal, S., Couchman, J. R., Ahlberg, P. E., Wiweger, M., Spillmann, D. et al. (2012). On the roles and regulation of chondroitin sulfate and heparan sulfate in zebrafish pharyngeal cartilage morphogenesis. *The Journal of Biological Chemistry* **287**, 33905-33916.

Holtfreter, J. (1943). A study of the mechanics of gastrulation Part I. *J Exp Zool* **94**, 261-318.

Holtfreter, J. (1944). A study of the mechanics of gastrulation Part II. *J Exp Zool* **95**, 171-212.

Hook, M., Kjellen, L. and Johansson, S. (1984). Cell-surface glycosaminoglycans. *Annual review of biochemistry* **53**, 847-869.

Hook, M., Lindahl, U., Hallen, A. and Backstrom, G. (1975). Biosynthesis of heparin. Studies on the microsomal sulfation process. *The Journal of Biological Chemistry* **250**, 6065-6071.

Houck, K. A., Ferrara, N., Winer, J., Cachianes, G., Li, B. and Leung, D. W. (1991). The vascular endothelial growth factor family: identification of a fourth molecular species and characterization of alternative splicing of RNA. *Molecular endocrinology* **5**, 1806-1814.

Huber, A. B., Kania, A., Tran, T. S., Gu, C., De Marco Garcia, N., Lieberam, I., Johnson, D., Jessell, T. M., Ginty, D. D. and Kolodkin, A. L. (2005). Distinct roles for secreted semaphorin signaling in spinal motor axon guidance. *Neuron* **48**, 949-964.

Humphries, D. E., Wong, G. W., Friend, D. S., Gurish, M. F., Qiu, W. T., Huang, C., Sharpe, A. H. and Stevens, R. L. (1999). Heparin is essential for the storage of specific granule proteases in mast cells. *Nature* **400**, 769-772.

Inatani, M., Irie, F., Plump, A. S., Tessier-Lavigne, M. and Yamaguchi, Y. (2003). Mammalian brain morphogenesis and midline axon guidance require heparan sulfate. *Science* **302**, 1044-1046.

Iozzo, R. V. (1998). Matrix proteoglycans: from molecular design to cellular function. *Annual review of biochemistry* **67**, 609-652.

Irie, A., Yates, E. A., Turnbull, J. E. and Holt, C. E. (2002). Specific heparan sulfate structures involved in retinal axon targeting. *Development* **129**, 61-70.

Irving, C. and Mason, I. (1999). Regeneration of isthmic tissue is the result of a specific and direct interaction between rhombomere 1 and midbrain. *Development* **126**, 3981-3989.

Ishijima, M., Suzuki, N., Hozumi, K., Matsunobu, T., Kosaki, K., Kaneko, H., Hassell, J. R., Arikawa-Hirasawa, E. and Yamada, Y. (2012). Perlecan modulates VEGF signaling and is essential for vascularization in endochondral bone formation. *Matrix Biol* **31**, 234-245.

Ito, K., Kawasaki, T., Takashima, S., Matsuda, I., Aiba, A. and Hirata, T. (2008). Semaphorin 3F confines ventral tangential migration of lateral olfactory tract neurons onto the telencephalon surface. *The Journal of Neuroscience* **28**, 4414-4422.

Ivanova, A., Signore, M., Caro, N., Greene, N. D., Copp, A. J. and Martinez-Barbera, J. P. (2005). In vivo genetic ablation by Cre-mediated expression of diphtheria toxin fragment A. *Genesis* **43**, 129-135.

Jacob, J. and Guthrie, S. (2000). Facial visceral motor neurons display specific rhombomere origin and axon pathfinding behavior in the chick. *The Journal of Neuroscience* **20**, 7664-7671.

Jacobsson, I. and Lindahl, U. (1980). Biosynthesis of heparin. Concerted action of late polymer-modification reactions. *The Journal of Biological Chemistry* **255**, 5094-5100.

Jakobsson, L., Kreuger, J., Holmborn, K., Lundin, L., Eriksson, I., Kjellen, L. and Claesson-Welsh, L. (2006). Heparan sulfate in trans potentiates VEGFR-mediated angiogenesis. *Developmental cell* **10**, 625-634.

Jemth, P., Smeds, E., Do, A. T., Habuchi, H., Kimata, K., Lindahl, U. and Kusche-Gullberg, M. (2003). Oligosaccharide library-based assessment of heparan sulfate 6-O-sulfotransferase substrate specificity. *The Journal of Biological Chemistry* **278**, 24371-24376.

Jen, Y. H., Musacchio, M. and Lander, A. D. (2009). Glypican-1 controls brain size through regulation of fibroblast growth factor signaling in early neurogenesis. *Neural Development* **4**, 33.

Jessell, T. M. (2000). Neuronal specification in the spinal cord: inductive signals and transcriptional codes. *Nature reviews. Genetics* **1**, 20-29.

Jessen, J. R., Topczewski, J., Bingham, S., Sepich, D. S., Marlow, F., Chandrasekhar, A. and Solnica-Krezel, L. (2002). Zebrafish trilobite identifies new roles for Strabismus in gastrulation and neuronal movements. *Nature cell biology* **4**, 610-615.

Jia, H., Bagherzadeh, A., Hartzoulakis, B., Jarvis, A., Lohr, M., Shaikh, S., Aqil, R., Cheng, L., Tickner, M., Esposito, D. et al. (2006). Characterization of a bicyclic peptide neuropilin-1 (NP-1) antagonist (EG3287) reveals importance of vascular endothelial growth factor exon 8 for NP-1 binding and role of NP-1 in KDR signaling. *The Journal of Biological Chemistry* **281**, 13493-13502.

Jimenez-Guri, E. and Pujades, C. (2011). An ancient mechanism of hindbrain patterning has been conserved in vertebrate evolution. *Evol Dev* **13**, 38-46.

Jin, K., Zhu, Y., Sun, Y., Mao, X. O., Xie, L. and Greenberg, D. A. (2002). Vascular endothelial growth factor (VEGF) stimulates neurogenesis in vitro and in

vivo. *Proceedings of the National Academy of Sciences of the United States of America* **99**, 11946-11950.

Kaksonen, M., Pavlov, I., Voikar, V., Lauri, S. E., Hienola, A., Riekki, R., Lakso, M., Taira, T. and Rauvala, H. (2002). Syndecan-3-deficient mice exhibit enhanced LTP and impaired hippocampus-dependent memory. *Mol Cell Neurosci* **21**, 158-172.

Kamimura, K., Koyama, T., Habuchi, H., Ueda, R., Masu, M., Kimata, K. and Nakato, H. (2006). Specific and flexible roles of heparan sulfate modifications in Drosophila FGF signaling. *The Journal of Cell Biology* **174**, 773-778.

Kantor, D. B., Chivatakarn, O., Peer, K. L., Oster, S. F., Inatani, M., Hansen, M. J., Flanagan, J. G., Yamaguchi, Y., Sretavan, D. W., Giger, R. J. et al. (2004). Semaphorin 5A is a bifunctional axon guidance cue regulated by heparan and chondroitin sulfate proteoglycans. *Neuron* **44**, 961-975.

Kawasaki, T., Kitsukawa, T., Bekku, Y., Matsuda, Y., Sanbo, M., Yagi, T. and Fujisawa, H. (1999). A requirement for neuropilin-1 in embryonic vessel formation. *Development* **126**, 4895-4902.

Keller, R., Shih, J. and Sater, A. (1992). The Cellular Basis of the Convergence and Extension of the Xenopus Neural Plate. *Dev Dynam* **193**, 199-217.

Kennedy, T. E., Serafini, T., de la Torre, J. R. and Tessier-Lavigne, M. (1994). Netrins are diffusible chemotropic factors for commissural axons in the embryonic spinal cord. *Cell* **78**, 425-435.

Kim, B. T., Kitagawa, H., Tamura, J., Saito, T., Kusche-Gullberg, M., Lindahl, U. and Sugahara, K. (2001). Human tumor suppressor EXT gene family members EXTL1 and EXTL3 encode alpha 1,4- N-acetylglucosaminyltransferases that likely are involved in heparan sulfate/ heparin biosynthesis. *Proceedings of the National Academy of Sciences of the United States of America* **98**, 7176-7181.

Kinnunen, T., Huang, Z., Townsend, J., Gatdula, M. M., Brown, J. R., Esko, J. D. and Turnbull, J. E. (2005). Heparan 2-O-sulfotransferase, hst-2, is essential for

normal cell migration in Caenorhabditis elegans. *Proceedings of the National Academy of Sciences of the United States of America* **102**, 1507-1512.

Kitsukawa, T., Shimono, A., Kawakami, A., Kondoh, H. and Fujisawa, H. (1995). Overexpression of a membrane protein, neuropilin, in chimeric mice causes anomalies in the cardiovascular system, nervous system and limbs. *Development* **121**, 4309-4318.

Kitsukawa, T., Shimizu, M., Sanbo, M., Hirata, T., Taniguchi, M., Bekku, Y., Yagi, T. and Fujisawa, H. (1997). Neuropilin-semaphorin III/D-mediated chemorepulsive signals play a crucial role in peripheral nerve projection in mice. *Neuron* **19**, 995-1005.

Koch, S., Tugues, S., Li, X., Gualandi, L. and Claesson-Welsh, L. (2011). Signal transduction by vascular endothelial growth factor receptors. *Biochem J* **437**, 169-183.

Kolodkin, A. L., Levengood, D. V., Rowe, E. G., Tai, Y. T., Giger, R. J. and Ginty, D. D. (1997). Neuropilin is a semaphorin III receptor. *Cell* **90**, 753-762.

Kraus, F., Haenig, B. and Kispert, A. (2001). Cloning and expression analysis of the mouse T-box gene tbx20. *Mech Dev* **100**, 87-91.

Kreuger, J. and Kjellen, L. (2012). Heparan sulfate biosynthesis: regulation and variability. *Journal of Histochemisty and Cytochemistry* **60**, 898-907.

Ksiazek, I., Burkhardt, C., Lin, S., Seddik, R., Maj, M., Bezakova, G., Jucker, M., Arber, S., Caroni, P., Sanes, J. R. et al. (2007). Synapse loss in cortex of agrin-deficient mice after genetic rescue of perinatal death. *The Journal of Neuroscience* **27**, 7183-7195.

Kusche-Gullberg, M., Eriksson, I., Pikas, D. S. and Kjellen, L. (1998). Identification and expression in mouse of two heparan sulfate glucosaminyl N-deacetylase/N-sulfotransferase genes. *The Journal of Biological Chemistry* **273**, 11902-11907.

Kwon, H. B., Fukuhara, S., Asakawa, K., Ando, K., Kashiwada, T., Kawakami, K., Hibi, M., Kwon, Y. G., Kim, K. W., Alitalo, K. et al. (2013). The parallel growth of motoneuron axons with the dorsal aorta depends on Vegfc/Vegfr3 signaling in zebrafish. *Development* **140**, 4081-4090.

Lanahan, A., Zhang, X., Fantin, A., Zhuang, Z., Rivera-Molina, F., Speichinger, K., Prahst, C., Zhang, J., Wang, Y., Davis, G. et al. (2013). The Neuropilin 1 Cytoplasmic Domain Is Required for VEGF-A-Dependent Arteriogenesis. *Developmental cell* **25**, 156-168.

Lanahan, A. A., Hermans, K., Claes, F., Kerley-Hamilton, J. S., Zhuang, Z. W., Giordano, F. J., Carmeliet, P. and Simons, M. (2010). VEGF receptor 2 endocytic trafficking regulates arterial morphogenesis. *Developmental cell* **18**, 713-724.

Lee, P., Goishi, K., Davidson, A. J., Mannix, R., Zon, L. and Klagsbrun, M. (2002). Neuropilin-1 is required for vascular development and is a mediator of VEGF-dependent angiogenesis in zebrafish. *Proceedings of the National Academy of Sciences of the United States of America* **99**, 10470-10475.

Leighton, P. A., Mitchell, K. J., Goodrich, L. V., Lu, X., Pinson, K., Scherz, P., Skarnes, W. C. and Tessier-Lavigne, M. (2001). Defining brain wiring patterns and mechanisms through gene trapping in mice. *Nature* **410**, 174-179.

Li, H., Martin, A., David, V. and Quarles, L. D. (2011). Compound deletion of Fgfr3 and Fgfr4 partially rescues the Hyp mouse phenotype. *Am J Physiol Endocrinol Metab* **300**, E508-517.

Li, J., Hagner-McWhirter, A., Kjellen, L., Palgi, J., Jalkanen, M. and Lindahl, U. (1997). Biosynthesis of heparin/heparan sulfate. cDNA cloning and expression of D-glucuronyl C5-epimerase from bovine lung. *The Journal of Biological Chemistry* **272**, 28158-28163.

Li, J., Partovian, C., Li, J., Hampton, T. G., Metais, C., Tkachenko, E., Sellke, F. W. and Simons, M. (2002). Modulation of microvascular signaling by heparan sulfate matrix: studies in syndecan-4 transgenic mice. *Microvascular research* **64**, 38-46.

Lidholt, K. and Lindahl, U. (1992). Biosynthesis of heparin. The D-glucuronosyl- and N-acetyl-D-glucosaminyltransferase reactions and their relation to polymer modification. *Biochem J* **287 (Pt 1)**, 21-29.

Lin, X., Wei, G., Shi, Z., Dryer, L., Esko, J. D., Wells, D. E. and Matzuk, M. M. (2000). Disruption of gastrulation and heparan sulfate biosynthesis in EXT1-deficient mice. *Developmental Biology* **224**, 299-311.

Lindahl, U. and Hook, M. (1978). Glycosaminoglycans and their binding to biological macromolecules. *Annual review of biochemistry* **47**, 385-417.

Lindahl, U., Kusche-Gullberg, M. and Kjellen, L. (1998). Regulated diversity of heparan sulfate. *The Journal of Biological Chemistry* **273**, 24979-24982.

Linhardt, R. J., Turnbull, J. E., Wang, H. M., Loganathan, D. and Gallagher, J. T. (1990). Examination of the substrate specificity of heparin and heparan sulfate lyases. *Biochemistry* **29**, 2611-2617.

Long, H., Sabatier, C., Ma, L., Plump, A., Yuan, W., Ornitz, D. M., Tamada, A., Murakami, F., Goodman, C. S. and Tessier-Lavigne, M. (2004). Conserved roles for Slit and Robo proteins in midline commissural axon guidance. *Neuron* **42**, 213-223.

Lumsden, A. and Keynes, R. (1989). Segmental patterns of neuronal development in the chick hindbrain. *Nature* **337**, 424-428.

Lundin, L., Larsson, H., Kreuger, J., Kanda, S., Lindahl, U., Salmivirta, M. and Claesson-Welsh, L. (2000). Selectively desulfated heparin inhibits fibroblast growth factor-induced mitogenicity and angiogenesis. *The Journal of Biological Chemistry* **275**, 24653-24660.

Ma, L. and Tessier-Lavigne, M. (2007). Dual branch-promoting and branch-repelling actions of Slit/Robo signaling on peripheral and central branches of developing sensory axons. *The Journal of Neuroscience* **27**, 6843-6851.

Ma, X., Kawamoto, S., Hara, Y. and Adelstein, R. S. (2004). A point mutation in the motor domain of nonmuscle myosin II-B impairs migration of distinct groups of neurons. *Molecular biology of the cell* **15**, 2568-2579.

Maccarana, M., Casu, B. and Lindahl, U. (1993). Minimal sequence in heparin/heparan sulfate required for binding of basic fibroblast growth factor. *The Journal of Biological Chemistry* **268**, 23898-23905.

Mackenzie, F. and Ruhrberg, C. (2012). Diverse roles for VEGF-A in the nervous system. *Development* **139**, 1371-1380.

Mamluk, R., Gechtman, Z., Kutcher, M. E., Gasiunas, N., Gallagher, J. and Klagsbrun, M. (2002). Neuropilin-1 binds vascular endothelial growth factor 165, placenta growth factor-2, and heparin via its b1b2 domain. *The Journal of Biological Chemistry* **277**, 24818-24825.

Mapp, O. M., Wanner, S. J., Rohrschneider, M. R. and Prince, V. E. (2010). Prickle1b mediates interpretation of migratory cues during zebrafish facial branchiomotor neuron migration. *Developmental Dynamics* **239**, 1596-1608.

Marin, O., Valiente, M., Ge, X. and Tsai, L. H. (2010). Guiding neuronal cell migrations. *Cold Spring Harbor Perspectives in Biology* **2**, a001834.

MarÌn, O. and Rubenstein, J. (2003). Cell migration in the forebrain. *Annu Rev Neurosci* **26**, 441-483.

Marti, E., Bumcrot, D. A., Takada, R. and McMahon, A. P. (1995). Requirement of 19K form of Sonic hedgehog for induction of distinct ventral cell types in CNS explants. *Nature* **375**, 322-325.

Martyn, U. and Schulte-Merker, S. (2004). Zebrafish neuropilins are differentially expressed and interact with vascular endothelial growth factor during embryonic vascular development. *Developmental Dynamics* **231**, 33-42.

Matsuo, I. and Kimura-Yoshida, C. (2013). Extracellular modulation of Fibroblast Growth Factor signaling through heparan sulfate proteoglycans in mammalian development. *Current Opinion in Genetic Development* **23**, 399-407.

McCormick, C., Duncan, G., Goutsos, K. T. and Tufaro, F. (2000). The putative tumor suppressors EXT1 and EXT2 form a stable complex that accumulates in the Golgi apparatus and catalyzes the synthesis of heparan sulfate. *Proceedings of the National Academy of Sciences of the United States of America* **97**, 668-673.

McGinnis, W., Garber, R. L., Wirz, J., Kuroiwa, A. and Gehring, W. J. (1984). A homologous protein-coding sequence in Drosophila homeotic genes and its conservation in other metazoans. *Cell* **37**, 403-408.

McKay, I. J., Lewis, J. and Lumsden, A. (1997). Organization and development of facial motor neurons in the kreisler mutant mouse. *Eur J Neurosci* **9**, 1499-1506.

McKay, I. J., Muchamore, I., Krumlauf, R., Maden, M., Lumsden, A. and Lewis, J. (1994). The kreisler mouse: a hindbrain segmentation mutant that lacks two rhombomeres. *Development* **120**, 2199-2211.

McLaughlin, D., Karlsson, F., Tian, N., Pratt, T., Bullock, S. L., Wilson, V. A., Price, D. J. and Mason, J. O. (2003). Specific modification of heparan sulphate is required for normal cerebral cortical development. *Mech Dev* **120**, 1481-1488.

Merry, C. L. and Wilson, V. A. (2002). Role of heparan sulfate-2-O-sulfotransferase in the mouse. *Biochim Biophys Acta* **1573**, 319-327.

Merry, C. L., Bullock, S. L., Swan, D. C., Backen, A. C., Lyon, M., Beddington, R. S., Wilson, V. A. and Gallagher, J. T. (2001). The molecular phenotype of heparan sulfate in the Hs2st-/- mutant mouse. *The Journal of Biological Chemistry* **276**, 35429-35434.

Mitchell, K. J., Pinson, K. I., Kelly, O. G., Brennan, J., Zupicich, J., Scherz, P., Leighton, P. A., Goodrich, L. V., Lu, X., Avery, B. J. et al. (2001). Functional analysis of secreted and transmembrane proteins critical to mouse development. *Nature Genetics* **28**, 241-249.

Mitsi, M., Hong, Z., Costello, C. E. and Nugent, M. A. (2006). Heparin-mediated conformational changes in fibronectin expose vascular endothelial growth factor binding sites. *Biochemistry* **45**, 10319-10328.

Mohammadi, M., Olsen, S. K. and Ibrahimi, O. A. (2005). Structural basis for fibroblast growth factor receptor activation. *Cytokine Growth Factor Rev* **16**, 107-137.

Morimoto-Tomita, M., Uchimura, K., Werb, Z., Hemmerich, S. and Rosen, S. D. (2002). Cloning and characterization of two extracellular heparin-degrading endosulfatases in mice and humans. *The Journal of Biological Chemistry* **277**, 49175-49185.

Muller, M., Jabs, N., Lorke, D. E., Fritzsch, B. and Sander, M. (2003). Nkx6.1 controls migration and axon pathfinding of cranial branchio-motoneurons. *Development* **130**, 5815-5826.

Muthusamy, A., Cooper, C. R. and Gomes, R. R., Jr. (2010). Soluble perlecan domain I enhances vascular endothelial growth factor-165 activity and receptor phosphorylation in human bone marrow endothelial cells. *BMC Biochem* **11**, 43.

Nagamine, S., Tamba, M., Ishimine, H., Araki, K., Shiomi, K., Okada, T., Ohto, T., Kunita, S., Takahashi, S., Wismans, R. G. et al. (2012). Organ-specific sulfation patterns of heparan sulfate generated by extracellular sulfatases Sulf1 and Sulf2 in mice. *The Journal of Biological Chemistry* **287**, 9579-9590.

Nagy, A. (2000). Cre recombinase: the universal reagent for genome tailoring. *Genesis* **26**, 99-109.

Nakagawa, S., Brennan, C., Johnson, K. G., Shewan, D., Harris, W. A. and Holt, C. E. (2000). Ephrin-B regulates the Ipsilateral routing of retinal axons at the optic chiasm. *Neuron* **25**, 599-610.

Ng, A., Wong, M., Viviano, B., Erlich, J. M., Alba, G., Pflederer, C., Jay, P. Y. and Saunders, S. (2009). Loss of glypican-3 function causes growth factor-dependent defects in cardiac and coronary vascular development. *Developmental Biology* **335**, 208-215.

Ng, Y. S., Rohan, R., Sunday, M. E., Demello, D. E. and D'Amore, P. A. (2001). Differential expression of VEGF isoforms in mouse during development and in the

adult. *Developmental dynamics : an official publication of the American Association of Anatomists* **220**, 112-121.

Noguer, O., Villena, J., Lorita, J., Vilaro, S. and Reina, M. (2009). Syndecan-2 downregulation impairs angiogenesis in human microvascular endothelial cells. *Exp Cell Res* **315**, 795-808.

Orellana, A., Hirschberg, C. B., Wei, Z., Swiedler, S. J. and Ishihara, M. (1994). Molecular cloning and expression of a glycosaminoglycan N-acetylglucosaminyl N-deacetylase/N-sulfotransferase from a heparin-producing cell line. *The Journal of Biological Chemistry* **269**, 2270-2276.

Pallerla, S. R., Lawrence, R., Lewejohann, L., Pan, Y., Fischer, T., Schlomann, U., Zhang, X., Esko, J. D. and Grobe, K. (2008). Altered heparan sulfate structure in mice with deleted NDST3 gene function. *The Journal of Biological Chemistry* **283**, 16885-16894.

Pan, Q., Chathery, Y., Wu, Y., Rathore, N., Tong, R. K., Peale, F., Bagri, A., Tessier-Lavigne, M., Koch, A. W. and Watts, R. J. (2007). Neuropilin-1 binds to VEGF121 and regulates endothelial cell migration and sprouting. *The Journal of Biological Chemistry* **282**, 24049-24056.

Pan, Y., Woodbury, A., Esko, J. D., Grobe, K. and Zhang, X. (2006). Heparan sulfate biosynthetic gene Ndst1 is required for FGF signaling in early lens development. *Development* **133**, 4933-4944.

Pan, Y., Carbe, C., Powers, A., Zhang, E. E., Esko, J. D., Grobe, K., Feng, G. S. and Zhang, X. (2008). Bud specific N-sulfation of heparan sulfate regulates Shp2-dependent FGF signaling during lacrimal gland induction. *Development* **135**, 301-310.

Paridaen, J. T. M. L. and Huttner, W. B. (2014). Neurogenesis during development of the vertebrate central nervous system. *EMBO Rep* **15**, 351-364.

Park, J. E., Keller, G. A. and Ferrara, N. (1993). The vascular endothelial growth factor (VEGF) isoforms: differential deposition into the subepithelial extracellular

matrix and bioactivity of extracellular matrix-bound VEGF. *Molecular biology of the cell* **4**, 1317-1326.

Parker, M. W., Xu, P., Li, X. and Vander Kooi, C. W. (2012). Structural basis for selective vascular endothelial growth factor-A (VEGF-A) binding to neuropilin-1. *The Journal of Biological Chemistry* **287**, 11082-11089.

Patterson, A. M., Gardner, L., Shaw, J., David, G., Loreau, E., Aguilar, L., Ashton, B. A. and Middleton, J. (2005). Induction of a CXCL8 binding site on endothelial syndecan-3 in rheumatoid synovium. *Arthritis and rheumatism* **52**, 2331-2342.

Pattyn, A., Hirsch, M., Goridis, C. and Brunet, J. F. (2000). Control of hindbrain motor neuron differentiation by the homeobox gene Phox2b. *Development* **127**, 1349-1358.

Pattyn, A., Morin, X., Cremer, H., Goridis, C. and Brunet, J. F. (1997). Expression and interactions of the two closely related homeobox genes Phox2a and Phox2b during neurogenesis. *Development* **124**, 4065-4075.

Pattyn, A., Morin, X., Cremer, H., Goridis, C. and Brunet, J. F. (1999). The homeobox gene Phox2b is essential for the development of autonomic neural crest derivatives. *Nature* **399**, 366-370.

Pattyn, A., Vallstedt, A., Dias, J. M., Sander, M. and Ericson, J. (2003a). Complementary roles for Nkx6 and Nkx2 class proteins in the establishment of motoneuron identity in the hindbrain. *Development* **130**, 4149-4159.

Pattyn, A., Vallstedt, A., Dias, J. M., Samad, O. A., Krumlauf, R., Rijli, F. M., Brunet, J. F. and Ericson, J. (2003b). Coordinated temporal and spatial control of motor neuron and serotonergic neuron generation from a common pool of CNS progenitors. *Genes & Development* **17**, 729-737.

Paulus, J. D. and Halloran, M. C. (2006). Zebrafish bashful/laminin-alpha 1 mutants exhibit multiple axon guidance defects. *Developmental Dynamics* **235**, 213-224.

Petersen, P. H., Zou, K., Hwang, J. K., Jan, Y. N. and Zhong, W. (2002). Progenitor cell maintenance requires numb and numblike during mouse neurogenesis. *Nature* **419**, 929-934.

Petitou, M., Casu, B. and Lindahl, U. (2003). 1976-1983, a critical period in the history of heparin: the discovery of the antithrombin binding site. *Biochimie* **85**, 83-89.

Pikas, D. S., Eriksson, I. and Kjellen, L. (2000). Overexpression of different isoforms of glucosaminyl N-deacetylase/N-sulfotransferase results in distinct heparan sulfate N-sulfation patterns. *Biochemistry* **39**, 4552-4558.

Piltonen, M., Planken, A., Leskela, O., Myohanen, T. T., Hanninen, A. L., Auvinen, P., Alitalo, K., Andressoo, J. O., Saarma, M. and Mannisto, P. T. (2011). Vascular endothelial growth factor C acts as a neurotrophic factor for dopamine neurons in vitro and in vivo. *Neuroscience* **192**, 550-563.

Plump, A. S., Erskine, L., Sabatier, C., Brose, K., Epstein, C. J., Goodman, C. S., Mason, C. A. and Tessier-Lavigne, M. (2002). Slit1 and Slit2 cooperate to prevent premature midline crossing of retinal axons in the mouse visual system. *Neuron* **33**, 219-232.

Polleux, F., Morrow, T. and Ghosh, A. (2000). Semaphorin 3A is a chemoattractant for cortical apical dendrites. *Nature* **404**, 567-573.

Praloran, V., Mirshahi, S., Favard, C., Moukadiri, H. and Plouet, J. (1991). [Mitogenic activity of vasculotropin for peripheral human lymphocytes]. *C R Acad Sci III* **313**, 21-26.

Pratt, T., Conway, C. D., Tian, N. M., Price, D. J. and Mason, J. O. (2006). Heparan sulphation patterns generated by specific heparan sulfotransferase enzymes direct distinct aspects of retinal axon guidance at the optic chiasm. *The Journal of Neuroscience* **26**, 6911-6923.

Price, S. R. and Briscoe, J. (2004). The generation and diversification of spinal motor neurons: signals and responses. *Mech Dev* **121**, 1103-1115.

Pringle, N. P., Yu, W. P., Howell, M., Colvin, J. S., Ornitz, D. M. and Richardson, W. D. (2003). Fgfr3 expression by astrocytes and their precursors: evidence that astrocytes and oligodendrocytes originate in distinct neuroepithelial domains. *Development* **130**, 93-102.

Prydz, K. and Dalen, K. T. (2000). Synthesis and sorting of proteoglycans. *J Cell Sci* **113 Pt 2**, 193-205.

Purushothaman, A., Uyama, T., Kobayashi, F., Yamada, S., Sugahara, K., Rapraeger, A. C. and Sanderson, R. D. (2010). Heparanase-enhanced shedding of syndecan-1 by myeloma cells promotes endothelial invasion and angiogenesis. *Blood* **115**, 2449-2457.

Qu, X., Pan, Y., Carbe, C., Powers, A., Grobe, K. and Zhang, X. (2012). Glycosaminoglycan-dependent restriction of FGF diffusion is necessary for lacrimal gland development. *Development* **139**, 2730-2739.

Qu, X., Carbe, C., Tao, C., Powers, A., Lawrence, R., van Kuppevelt, T. H., Cardoso, W. V., Grobe, K., Esko, J. D. and Zhang, X. (2011a). Lacrimal gland development and Fgf10-Fgfr2b signaling are controlled by 2-O- and 6-O-sulfated heparan sulfate. *The Journal of biological chemistry* **286**, 14435-14444.

Qu, X., Carbe, C., Tao, C., Powers, A., Lawrence, R., van Kuppevelt, T. H., Cardoso, W. V., Grobe, K., Esko, J. D. and Zhang, X. (2011b). Lacrimal gland development and Fgf10-Fgfr2b signaling are controlled by 2-O- and 6-O-sulfated heparan sulfate. *The Journal of Biological Chemistry* **286**, 14435-14444.

Qu, Y., Glasco, D. M., Zhou, L., Sawant, A., Ravni, A., Fritzsch, B., Damrau, C., Murdoch, J. N., Evans, S., Pfaff, S. L. et al. (2010). Atypical cadherins Celsr1-3 differentially regulate migration of facial branchiomotor neurons in mice. *The Journal of Neuroscience* **30**, 9392-9401.

Raimondi, C. and Ruhrberg, C. (2013). Neuropilin signalling in vessels, neurons and tumours. *Semin Cell Dev Biol* **24**, 172-178.

Raimondi, C., Fantin, A., Lampropoulou, A., Denti, L., Chikh, A. and Ruhrberg, C. (2014). Imatinib inhibits VEGF-independent angiogenesis by

targeting neuropilin 1-dependent ABL1 activation in endothelial cells. *The Journal of Experimental Medicine* **211**, 1167-1183.

Rapraeger, A. C., Krufka, A. and Olwin, B. B. (1991). Requirement of heparan sulfate for bFGF-mediated fibroblast growth and myoblast differentiation. *Science* **252**, 1705-1708.

Reifers, F., Bohli, H., Walsh, E. C., Crossley, P. H., Stainier, D. Y. and Brand, M. (1998). Fgf8 is mutated in zebrafish acerebellar (ace) mutants and is required for maintenance of midbrain-hindbrain boundary development and somitogenesis. *Development* **125**, 2381-2395.

Reizes, O., Lincecum, J., Wang, Z., Goldberger, O., Huang, L., Kaksonen, M., Ahima, R., Hinkes, M. T., Barsh, G. S., Rauvala, H. et al. (2001). Transgenic expression of syndecan-1 uncovers a physiological control of feeding behavior by syndecan-3. *Cell* **106**, 105-116.

Rhiner, C., Gysi, S., Frohli, E., Hengartner, M. O. and Hajnal, A. (2005). Syndecan regulates cell migration and axon guidance in C. elegans. *Development* **132**, 4621-4633.

Riesenfeld, J., Hook, M. and Lindahl, U. (1982a). Biosynthesis of heparin. Concerted action of early polymer-modification reactions. *The Journal of Biological Chemistry* **257**, 421-425.

Riesenfeld, J., Hozok, M. and Lindahl, U. (1982b). Biosynthesis of heparan sulfate in rat liver. Characterization of polysaccharides obtained with intact cells and with a cell-free system. *The Journal of Biological Chemistry* **257**, 7050-7055.

Ringvall, M., Ledin, J., Holmborn, K., van Kuppevelt, T., Ellin, F., Eriksson, I., Olofsson, A. M., Kjellen, L. and Forsberg, E. (2000). Defective heparan sulfate biosynthesis and neonatal lethality in mice lacking N-deacetylase/N-sulfotransferase-1. *The Journal of Biological Chemistry* **275**, 25926-25930.

Risau, W. and Flamme, I. (1995). Vasculogenesis. *Annu Rev Cell Dev Biol* **11**, 73-91.

Robinson, C. J., Mulloy, B., Gallagher, J. T. and Stringer, S. E. (2006). VEGF165-binding sites within heparan sulfate encompass two highly sulfated domains and can be liberated by K5 lyase. *The Journal of Biological Chemistry* **281**, 1731-1740.

Roelink, H., Porter, J. A., Chiang, C., Tanabe, Y., Chang, D. T., Beachy, P. A. and Jessell, T. M. (1995). Floor plate and motor neuron induction by different concentrations of the amino-terminal cleavage product of sonic hedgehog autoproteolysis. *Cell* **81**, 445-455.

Rossel, M., Loulier, K., Feuillet, C., Alonso, S. and Carroll, P. (2005). Reelin signaling is necessary for a specific step in the migration of hindbrain efferent neurons. *Development* **132**, 1175-1185.

Ruhrberg, C. (2003). Growing and shaping the vascular tree: multiple roles for VEGF. *BioEssays : news and reviews in molecular, cellular and developmental biology* **25**, 1052-1060.

Ruhrberg, C., Gerhardt, H., Golding, M., Watson, R., Ioannidou, S., Fujisawa, H., Betsholtz, C. and Shima, D. T. (2002). Spatially restricted patterning cues provided by heparin-binding VEGF-A control blood vessel branching morphogenesis. *Genes & Development* **16**, 2684-2698.

Ruiz de Almodovar, C., Fabre, P. J., Knevels, E., Coulon, C., Segura, I., Haddick, P. C., Aerts, L., Delattin, N., Strasser, G., Oh, W. J. et al. (2011). VEGF mediates commissural axon chemoattraction through its receptor Flk1. *Neuron* **70**, 966-978.

Ruiz de Almodovar, C., Coulon, C., Salin, P. A., Knevels, E., Chounlamountri, N., Poesen, K., Hermans, K., Lambrechts, D., Van Geyte, K., Dhondt, J. et al. (2010). Matrix-binding vascular endothelial growth factor (VEGF) isoforms guide granule cell migration in the cerebellum via VEGF receptor Flk1. *The Journal of Neuroscience* **30**, 15052-15066.

Safaiyan, F., Lindahl, U. and Salmivirta, M. (2000). Structural diversity of N-sulfated heparan sulfate domains: distinct modes of glucuronyl C5 epimerization,

iduronic acid 2-O-sulfation, and glucosamine 6-O-sulfation. *Biochemistry* **39**, 10823-10830.

Sahay, A., Molliver, M. E., Ginty, D. D. and Kolodkin, A. L. (2003). Semaphorin 3F is critical for development of limbic system circuitry and is required in neurons for selective CNS axon guidance events. *The Journal of Neuroscience* **23**, 6671-6680.

Salikhova, A., Wang, L., Lanahan, A. A., Liu, M., Simons, M., Leenders, W. P., Mukhopadhyay, D. and Horowitz, A. (2008). Vascular endothelial growth factor and semaphorin induce neuropilin-1 endocytosis via separate pathways. *Circ Res* **103**, e71-79.

Sapede, D., Rossel, M., Dambly-Chaudiere, C. and Ghysen, A. (2005). Role of SDF1 chemokine in the development of lateral line efferent and facial motor neurons. *Proceedings of the National Academy of Sciences of the United States of America* **102**, 1714-1718.

Sarrazin, S., Lamanna, W. C. and Esko, J. D. (2011). Heparan sulfate proteoglycans. *Cold Spring Harbor Perspectives in Biology* **3**.

Schlessinger, J., Plotnikov, A. N., Ibrahimi, O. A., Eliseenkova, A. V., Yeh, B. K., Yayon, A., Linhardt, R. J. and Mohammadi, M. (2000). Crystal structure of a ternary FGF-FGFR-heparin complex reveals a dual role for heparin in FGFR binding and dimerization. *Mol Cell* **6**, 743-750.

Schneider-Maunoury, S., Topilko, P., Seitandou, T., Levi, G., Cohen-Tannoudji, M., Pournin, S., Babinet, C. and Charnay, P. (1993). Disruption of Krox-20 results in alteration of rhombomeres 3 and 5 in the developing hindbrain. *Cell* **75**, 1199-1214.

Schwarz, Q. and Ruhrberg, C. (2010). Neuropilin, you gotta let me know: should I stay or should I go? *Cell Adhesion & Migration* **4**, 61-66.

Schwarz, Q., Maden, C. H., Vieira, J. M. and Ruhrberg, C. (2009). Neuropilin 1 signaling guides neural crest cells to coordinate pathway choice with cell

specification. *Proceedings of the National Academy of Sciences of the United States of America* **106**, 6164-6169.

Schwarz, Q., Waimey, K. E., Golding, M., Takamatsu, H., Kumanogoh, A., Fujisawa, H., Cheng, H. J. and Ruhrberg, C. (2008). Plexin A3 and plexin A4 convey semaphorin signals during facial nerve development. *Developmental Biology* **324**, 1-9.

Schwarz, Q., Gu, C., Fujisawa, H., Sabelko, K., Gertsenstein, M., Nagy, A., Taniguchi, M., Kolodkin, A. L., Ginty, D. D., Shima, D. T. et al. (2004). Vascular endothelial growth factor controls neuronal migration and cooperates with Sema3A to pattern distinct compartments of the facial nerve. *Genes & Development* **18**, 2822-2834.

Sedita, J., Izvolsky, K. and Cardoso, W. V. (2004). Differential expression of heparan sulfate 6-O-sulfotransferase isoforms in the mouse embryo suggests distinctive roles during organogenesis. *Developmental Dynamics* **231**, 782-794.

Senay, C., Lind, T., Muguruma, K., Tone, Y., Kitagawa, H., Sugahara, K., Lidholt, K., Lindahl, U. and Kusche-Gullberg, M. (2000). The EXT1/EXT2 tumor suppressors: catalytic activities and role in heparan sulfate biosynthesis. *EMBO Rep* **1**, 282-286.

Serpinskaya, A. S., Feng, G., Sanes, J. R. and Craig, A. M. (1999). Synapse formation by hippocampal neurons from agrin-deficient mice. *Developmental Biology* **205**, 65-78.

Shalaby, F., Rossant, J., Yamaguchi, T. P., Gertsenstein, M., Wu, X. F., Breitman, M. L. and Schuh, A. C. (1995). Failure of blood-island formation and vasculogenesis in Flk-1-deficient mice. *Nature* **376**, 62-66.

Sharma, K., Sheng, H. Z., Lettieri, K., Li, H., Karavanov, A., Potter, S., Westphal, H. and Pfaff, S. L. (1998). LIM homeodomain factors Lhx3 and Lhx4 assign subtype identities for motor neurons. *Cell* **95**, 817-828.

Shigeoka, T., Lu, B. and Holt, C. E. (2013). Cell biology in neuroscience: RNA-based mechanisms underlying axon guidance. *The Journal of Cell Biology* **202**, 991-999.

Shimizu, M., Murakami, Y., Suto, F. and Fujisawa, H. (2000). Determination of cell adhesion sites of neuropilin-1. *The Journal of Cell Biology* **148**, 1283-1293.

Shirasaki, R., Lewcock, J. W., Lettieri, K. and Pfaff, S. L. (2006). FGF as a target-derived chemoattractant for developing motor axons genetically programmed by the LIM code. *Neuron* **50**, 841-853.

Sidman, R. L. and Rakic, P. (1973). Neuronal migration, with special reference to developing human brain: a review. *Brain Res* **62**, 1-35.

Skarnes, W. C., Rosen, B., West, A. P., Koutsourakis, M., Bushell, W., Iyer, V., Mujica, A. O., Thomas, M., Harrow, J., Cox, T. et al. (2011). A conditional knockout resource for the genome-wide study of mouse gene function. *Nature* **474**, 337-342.

Smeds, E., Habuchi, H., Do, A. T., Hjertson, E., Grundberg, H., Kimata, K., Lindahl, U. and Kusche-Gullberg, M. (2003). Substrate specificities of mouse heparan sulphate glucosaminyl 6-O-sulphotransferases. *Biochem J* **372**, 371-380.

Soker, S., Gollamudi-Payne, S., Fidder, H., Charmahelli, H. and Klagsbrun, M. (1997). Inhibition of vascular endothelial growth factor (VEGF)-induced endothelial cell proliferation by a peptide corresponding to the exon 7-encoded domain of VEGF165. *The Journal of Biological Chemistry* **272**, 31582-31588.

Soker, S., Takashima, S., Miao, H. Q., Neufeld, G. and Klagsbrun, M. (1998). Neuropilin-1 is expressed by endothelial and tumor cells as an isoform-specific receptor for vascular endothelial growth factor. *Cell* **92**, 735-745.

Soker, S., Miao, H. Q., Nomi, M., Takashima, S. and Klagsbrun, M. (2002). VEGF165 mediates formation of complexes containing VEGFR-2 and neuropilin-1 that enhance VEGF165-receptor binding. *J Cell Biochem* **85**, 357-368.

Song, M. R., Shirasaki, R., Cai, C. L., Ruiz, E. C., Evans, S. M., Lee, S. K. and Pfaff, S. L. (2006). T-Box transcription factor Tbx20 regulates a genetic program for cranial motor neuron cell body migration. *Development* **133**, 4945-4955.

Srinivas, S., Watanabe, T., Lin, C. S., William, C. M., Tanabe, Y., Jessell, T. M. and Costantini, F. (2001). Cre reporter strains produced by targeted insertion of EYFP and ECFP into the ROSA26 locus. *BMC developmental biology* **1**, 4.

Stalmans, I., Ng, Y. S., Rohan, R., Fruttiger, M., Bouche, A., Yuce, A., Fujisawa, H., Hermans, B., Shani, M., Jansen, S. et al. (2002). Arteriolar and venular patterning in retinas of mice selectively expressing VEGF isoforms. *The Journal of Clinical Investigation* **109**, 327-336.

Stanford, K. I., Wang, L., Castagnola, J., Song, D., Bishop, J. R., Brown, J. R., Lawrence, R., Bai, X., Habuchi, H., Tanaka, M. et al. (2010). Heparan sulfate 2-O-sulfotransferase is required for triglyceride-rich lipoprotein clearance. *The Journal of Biological Chemistry* **285**, 286-294.

Stickens, D., Zak, B. M., Rougier, N., Esko, J. D. and Werb, Z. (2005). Mice deficient in Ext2 lack heparan sulfate and develop exostoses. *Development* **132**, 5055-5068.

Stockinger, P., Maitre, J. L. and Heisenberg, C. P. (2011). Defective neuroepithelial cell cohesion affects tangential branchiomotor neuron migration in the zebrafish neural tube. *Development* **138**, 4673-4683.

Storkebaum, E., Quaegebeur, A., Vikkula, M. and Carmeliet, P. (2011). Cerebrovascular disorders: molecular insights and therapeutic opportunities. *Nature Neuroscience* **14**, 1390-1397.

Studer, M. (2001). Initiation of facial motoneurone migration is dependent on rhombomeres 5 and 6. *Development* **128**, 3707-3716.

Studer, M., Lumsden, A., Ariza-McNaughton, L., Bradley, A. and Krumlauf, R. (1996). Altered segmental identity and abnormal migration of motor neurons in mice lacking Hoxb-1. *Nature* **384**, 630-634.

Sugaya, N., Habuchi, H., Nagai, N., Ashikari-Hada, S. and Kimata, K. (2008). 6-O-sulfation of heparan sulfate differentially regulates various fibroblast growth factor-dependent signalings in culture. *The Journal of Biological Chemistry* **283**, 10366-10376.

Suto, F., Ito, K., Uemura, M., Shimizu, M., Shinkawa, Y., Sanbo, M., Shinoda, T., Tsuboi, M., Takashima, S., Yagi, T. et al. (2005). Plexin-a4 mediates axon-repulsive activities of both secreted and transmembrane semaphorins and plays roles in nerve fiber guidance. *The Journal of Neuroscience* **25**, 3628-3637.

Swiatek, P. J. and Gridley, T. (1993). Perinatal lethality and defects in hindbrain development in mice homozygous for a targeted mutation of the zinc finger gene Krox20. *Genes & Development* **7**, 2071-2084.

Takagi, S., Tsuji, T., Amagai, T., Takamatsu, T. and Fujisawa, H. (1987). Specific cell surface labels in the visual centers of Xenopus laevis tadpole identified using monoclonal antibodies. *Developmental Biology* **122**, 90-100.

Takahashi, T., Nakamura, F., Jin, Z., Kalb, R. G. and Strittmatter, S. M. (1998). Semaphorins A and E act as antagonists of neuropilin-1 and agonists of neuropilin-2 receptors. *Nature Neuroscience* **1**, 487-493.

Tamamaki, N., Fujimori, K., Nojyo, Y., Kaneko, T. and Takauji, R. (2003). Evidence that Sema3A and Sema3F regulate the migration of GABAergic neurons in the developing neocortex. *J Comp Neurol* **455**, 238-248.

Tang, T., Li, L., Tang, J., Li, Y., Lin, W. Y., Martin, F., Grant, D., Solloway, M., Parker, L., Ye, W. et al. (2010). A mouse knockout library for secreted and transmembrane proteins. *Nat Biotechnol* **28**, 749-755.

Taniguchi, M., Yuasa, S., Fujisawa, H., Naruse, I., Saga, S., Mishina, M. and Yagi, T. (1997). Disruption of semaphorin III/D gene causes severe abnormality in peripheral nerve projection. *Neuron* **19**, 519-530.

Tessler, S., Rockwell, P., Hicklin, D., Cohen, T., Levi, B. Z., Witte, L., Lemischka, I. R. and Neufeld, G. (1994). Heparin modulates the interaction of

VEGF165 with soluble and cell associated flk-1 receptors. *The Journal of Biological Chemistry* **269**, 12456-12461.

Tillo, M., Ruhrberg, C. and Mackenzie, F. (2012). Emerging roles for semaphorins and VEGFs in synaptogenesis and synaptic plasticity. *Cell Adhesion & Migration* **6**, 541-546.

Tillo, M., Schwarz, Q. and Ruhrberg, C. (2014). Mouse hindbrain ex vivo culture to study facial branchiomotor neuron migration. *Journal of visualized experiments : JoVE*.

Tillo, M., Erskine, L., Cariboni, A., Fantin, A., Joyce, A., Denti, L. and Ruhrberg, C. (2015). VEGF189 binds NRP1 and is sufficient for VEGF/NRP1-dependent neuronal patterning in the developing brain. *Development* **142**, 314-319.

Tischer, E., Mitchell, R., Hartman, T., Silva, M., Gospodarowicz, D., Fiddes, J. C. and Abraham, J. A. (1991). The human gene for vascular endothelial growth factor. Multiple protein forms are encoded through alternative exon splicing. *The Journal of Biological Chemistry* **266**, 11947-11954.

Tkachenko, E., Rhodes, J. M. and Simons, M. (2005). Syndecans: new kids on the signaling block. *Circ Res* **96**, 488-500.

Toma, L., Berninsone, P. and Hirschberg, C. B. (1998). The putative heparin-specific N-acetylglucosaminyl N-Deacetylase/N-sulfotransferase also occurs in non-heparin-producing cells. *The Journal of Biological Chemistry* **273**, 22458-22465.

Tran, T. S., Rubio, M. E., Clem, R. L., Johnson, D., Case, L., Tessier-Lavigne, M., Huganir, R. L., Ginty, D. D. and Kolodkin, A. L. (2009). Secreted semaphorins control spine distribution and morphogenesis in the postnatal CNS. *Nature* **462**, 1065-1069.

Trokovic, R., Trokovic, N., Hernesniemi, S., Pirvola, U., Vogt Weisenhorn, D. M., Rossant, J., McMahon, A. P., Wurst, W. and Partanen, J. (2003). FGFR1 is independently required in both developing mid- and hindbrain for sustained response to isthmic signals. *The EMBO Journal* **22**, 1811-1823.

Trokovic, R., Jukkola, T., Saarimaki, J., Peltopuro, P., Naserke, T., Weisenhorn, D. M., Trokovic, N., Wurst, W. and Partanen, J. (2005). Fgfr1-dependent boundary cells between developing mid- and hindbrain. *Developmental Biology* **278**, 428-439.

Tronche, F., Kellendonk, C., Kretz, O., Gass, P., Anlag, K., Orban, P. C., Bock, R., Klein, R. and Schutz, G. (1999). Disruption of the glucocorticoid receptor gene in the nervous system results in reduced anxiety. *Nature Genetics* **23**, 99-103.

Tsai, L. H. and Gleeson, J. G. (2005). Nucleokinesis in neuronal migration. *Neuron* **46**, 383-388.

Turing, A. M. (1952). The Chemical Basis of Morphogenesis. *Philos T Roy Soc B* **237**, 37-72.

Turnbull, J. E., Fernig, D. G., Ke, Y., Wilkinson, M. C. and Gallagher, J. T. (1992). Identification of the basic fibroblast growth factor binding sequence in fibroblast heparan sulfate. *The Journal of Biological Chemistry* **267**, 10337-10341.

Vallstedt, A., Muhr, J., Pattyn, A., Pierani, A., Mendelsohn, M., Sander, M., Jessell, T. M. and Ericson, J. (2001). Different levels of repressor activity assign redundant and specific roles to Nkx6 genes in motor neuron and interneuron specification. *Neuron* **31**, 743-755.

Vanpouille, C., Deligny, A., Delehedde, M., Denys, A., Melchior, A., Lienard, X., Lyon, M., Mazurier, J., Fernig, D. G. and Allain, F. (2007). The heparin/heparan sulfate sequence that interacts with cyclophilin B contains a 3-O-sulfated N-unsubstituted glucosamine residue. *The Journal of Biological Chemistry* **282**, 24416-24429.

Venero Galanternik, M., Kramer, K. L. and Piotrowski, T. (2015). Heparan Sulfate Proteoglycans Regulate Fgf Signaling and Cell Polarity during Collective Cell Migration. *Cell Reports* **10**, 414-428.

Vintonenko, N., Pelaez-Garavito, I., Buteau-Lozano, H., Toullec, A., Lidereau, R., Perret, G. Y., Bieche, I. and Perrot-Applanat, M. (2011). Overexpression of

VEGF189 in breast cancer cells induces apoptosis via NRP1 under stress conditions. *Cell Adhesion & Migration* **5**, 332-343.

Vivancos, V., Chen, P., Spassky, N., Qian, D., Dabdoub, A., Kelley, M., Studer, M. and Guthrie, S. (2009). Wnt activity guides facial branchiomotor neuron migration, and involves the PCP pathway and JNK and ROCK kinases. *Neural Development* **4**, 7.

Vo, T., Carulli, D., Ehlert, E. M., Kwok, J. C., Dick, G., Mecollari, V., Moloney, E. B., Neufeld, G., de Winter, F., Fawcett, J. W. et al. (2013). The chemorepulsive axon guidance protein semaphorin3A is a constituent of perineuronal nets in the adult rodent brain. *Mol Cell Neurosci* **56**, 186-200.

Wada, H., Tanaka, H., Nakayama, S., Iwasaki, M. and Okamoto, H. (2006). Frizzled3a and Celsr2 function in the neuroepithelium to regulate migration of facial motor neurons in the developing zebrafish hindbrain. *Development* **133**, 4749-4759.

Wada, H., Iwasaki, M., Sato, T., Masai, I., Nishiwaki, Y., Tanaka, H., Sato, A., Nojima, Y. and Okamoto, H. (2005). Dual roles of zygotic and maternal Scribble1 in neural migration and convergent extension movements in zebrafish embryos. *Development* **132**, 2273-2285.

Wallingford, J. B., Fraser, S. E. and Harland, R. M. (2002). Convergent extension: The molecular control of polarized cell movement during embryonic development. *Developmental cell* **2**, 695-706.

Walsh, G. S., Grant, P. K., Morgan, J. A. and Moens, C. B. (2011). Planar polarity pathway and Nance-Horan syndrome-like 1b have essential cell-autonomous functions in neuronal migration. *Development* **138**, 3033-3042.

Walshe, J. and Mason, I. (2000). Expression of FGFR1, FGFR2 and FGFR3 during early neural development in the chick embryo. *Mech Dev* **90**, 103-110.

Walshe, J., Maroon, H., McGonnell, I. M., Dickson, C. and Mason, I. (2002). Establishment of hindbrain segmental identity requires signaling by FGF3 and FGF8. *Current Biology* **12**, 1117-1123.

Walz, A., Rodriguez, I. and Mombaerts, P. (2002). Aberrant sensory innervation of the olfactory bulb in neuropilin-2 mutant mice. *The Journal of Neuroscience* **22**, 4025-4035.

Wanner, S. J. and Prince, V. E. (2013). Axon tracts guide zebrafish facial branchiomotor neuron migration through the hindbrain. *Development* **140**, 906-915.

Wanner, S. J., Saeger, I., Guthrie, S. and Prince, V. E. (2013). Facial motor neuron migration advances. *Current Opinion in Neurobiology* **23**, 943-950.

Watterson, R. L., Fowler, I. and Fowler, B. J. (1954). The role of the neural tube and notochord in development of the axial skeleton of the chick. *Am J Anat* **95**, 337-399.

Weinstein, M., Xu, X., Ohyama, K. and Deng, C. X. (1998). FGFR-3 and FGFR-4 function cooperatively to direct alveogenesis in the murine lung. *Development* **125**, 3615-3623.

Whitaker, G. B., Limberg, B. J. and Rosenbaum, J. S. (2001). Vascular endothelial growth factor receptor-2 and neuropilin-1 form a receptor complex that is responsible for the differential signaling potency of VEGF(165) and VEGF(121). *The Journal of Biological Chemistry* **276**, 25520-25531.

Wilkinson, D. G., Bhatt, S., Chavrier, P., Bravo, R. and Charnay, P. (1989). Segment-specific expression of a zinc-finger gene in the developing nervous system of the mouse. *Nature* **337**, 461-464.

Williams, S. E., Mann, F., Erskine, L., Sakurai, T., Wei, S., Rossi, D. J., Gale, N. W., Holt, C. E., Mason, C. A. and Henkemeyer, M. (2003). Ephrin-B2 and EphB1 mediate retinal axon divergence at the optic chiasm. *Neuron* **39**, 919-935.

Wilson, V. A., Gallagher, J. T. and Merry, C. L. (2002). Heparan sulfate 2-O-sulfotransferase (Hs2st) and mouse development. *Glycoconjugate journal* **19**, 347-354.

Wolpert, L. (1969). Positional information and the spatial pattern of cellular differentiation. *J Theor Biol* **25**, 1-47.

Xu, D. and Esko, J. D. (2014). Demystifying heparan sulfate-protein interactions. *Annual review of biochemistry* **83**, 129-157.

Xu, D., Fuster, M. M., Lawrence, R. and Esko, J. D. (2011). Heparan sulfate regulates VEGF165- and VEGF121-mediated vascular hyperpermeability. *The Journal of Biological Chemistry* **286**, 737-745.

Yang, L., Cai, C. L., Lin, L., Qyang, Y., Chung, C., Monteiro, R. M., Mummery, C. L., Fishman, G. I., Cogen, A. and Evans, S. (2006). Isl1Cre reveals a common Bmp pathway in heart and limb development. *Development* **133**, 1575-1585.

Yang, X., Zhou, Y., Barcarse, E. A. and O'Gorman, S. (2008). Altered neuronal lineages in the facial ganglia of Hoxa2 mutant mice. *Developmental Biology* **314**, 171-188.

Yaron, A., Huang, P. H., Cheng, H. J. and Tessier-Lavigne, M. (2005). Differential requirement for Plexin-A3 and -A4 in mediating responses of sensory and sympathetic neurons to distinct class 3 Semaphorins. *Neuron* **45**, 513-523.

Yayon, A., Klagsbrun, M., Esko, J. D., Leder, P. and Ornitz, D. M. (1991). Cell surface, heparin-like molecules are required for binding of basic fibroblast growth factor to its high affinity receptor. *Cell* **64**, 841-848.

Yip, G. W., Ferretti, P. and Copp, A. J. (2002). Heparan sulphate proteoglycans and spinal neurulation in the mouse embryo. *Development* **129**, 2109-2119.

Zakaria, S., Mao, Y., Kuta, A., Ferreira de Sousa, C., Gaufo, G. O., McNeill, H., Hindges, R., Guthrie, S., Irvine, K. D. and Francis-West, P. H. (2014). Regulation of neuronal migration by Dchs1-Fat4 planar cell polarity. *Current Biology* **24**, 1620-1627.

Zhao, S. and Frotscher, M. (2010). Go or stop? Divergent roles of Reelin in radial neuronal migration. *Neuroscientist* **16**, 421-434.

Zhou, Y., Gunput, R. A. and Pasterkamp, R. J. (2008). Semaphorin signaling: progress made and promises ahead. *Trends Biochem Sci* **33**, 161-170.

Zhu, Y., Jin, K., Mao, X. O. and Greenberg, D. A. (2003). Vascular endothelial growth factor promotes proliferation of cortical neuron precursors by regulating E2F expression. *FASEB Journal* **17**, 186-193.

Zoeller, J. J., Whitelock, J. M. and Iozzo, R. V. (2009). Perlecan regulates developmental angiogenesis by modulating the VEGF-VEGFR2 axis. *Matrix Biol* **28**, 284-291.

LIST OF SUPPORTING PUBLICATIONS

Tillo, M., Ruhrberg, C., and Mackenzie, F. (2012). Emerging roles for semaphorins and VEGFs in synaptogenesis and synaptic plasticity. *Cell Adhesion & Migration* **6**, 541–546.

Tillo, M., Schwarz, Q., and Ruhrberg, C. (2014). Mouse Hindbrain Ex Vivo Culture to Study Facial Branchiomotor Neuron Migration. *Journal of Visualized Experiments: JoVE* **1** (85).

Tillo, M., Erskine, L., Cariboni, A., Fantin, A., Joyce, A., Denti, L., and Ruhrberg, C. (2015). VEGF189 binds NRP1 and is sufficient for VEGF/NRP1-dependent neuronal patterning in the developing brain. *Development **142***, 314–319.

© 2015. Published by The Company of Biologists Ltd | Development (2015) 142, 314-319 doi:10.1242/dev.115998

RESEARCH REPORT

$VEGF_{189}$ binds NRP1 and is sufficient for VEGF/NRP1-dependent neuronal patterning in the developing brain

Miguel Tillo[1], Lynda Erskine[2], Anna Cariboni[1,3], Alessandro Fantin[1], Andy Joyce[1], Laura Denti[1] and Christiana Ruhrberg[1,*]

ABSTRACT

The vascular endothelial growth factor (VEGFA, VEGF) regulates neurovascular patterning. Alternative splicing of the *Vegfa* gene gives rise to three major isoforms termed $VEGF_{121}$, $VEGF_{165}$ and $VEGF_{189}$. $VEGF_{165}$ binds the transmembrane protein neuropilin 1 (NRP1) and promotes the migration, survival and axon guidance of subsets of neurons, whereas $VEGF_{121}$ cannot activate NRP1-dependent neuronal responses. By contrast, the role of $VEGF_{189}$ in NRP1-mediated signalling pathways has not yet been examined. Here, we have combined expression studies and *in situ* ligand-binding assays with the analysis of genetically altered mice and *in vitro* models to demonstrate that $VEGF_{189}$ can bind NRP1 and promote NRP1-dependent neuronal responses.

KEY WORDS: Vascular endothelial growth factor (VEGF), VEGF189, Neuron, Neuropilin, Mouse

INTRODUCTION

Vascular endothelial growth factor A (VEGFA, VEGF) is a potent inducer of blood vessel growth, but also has essential roles in neurodevelopment (Mackenzie and Ruhrberg, 2012). In humans, VEGF is encoded by a single gene (*VEGFA*) of eight exons that is alternatively spliced into isoforms, the major ones containing 121, 165 and 189 amino acid residues and therefore termed $VEGF_{121}$, $VEGF_{165}$ and $VEGF_{189}$, respectively (Fig. 1A; Koch et al., 2011). The alternatively spliced exons 6 and 7 encode domains that enable extracellular matrix (ECM) binding and additionally mediate differential binding to VEGF receptors. All VEGF isoforms bind the receptor tyrosine kinases VEGFR1 (FLT1) and VEGFR2 (KDR, FLK1), whereas the non-catalytic receptors neuropilin (NRP) 1 and NRP2 are VEGF isoform-specific receptors that preferentially bind $VEGF_{165}$ over $VEGF_{121}$ (Fig. 1A; Gluzman-Poltorak et al., 2000; Soker et al., 1998). Unexpectedly, recent studies showed that VEGF binding to NRP1 is largely dispensable for embryonic angiogenesis (Fantin et al., 2014). By contrast, VEGF signalling through NRP1 has multiple roles in neurodevelopment, including guiding migrating facial branchiomotor (FBM) neurons in the hindbrain (Schwarz et al., 2004), promoting the survival of migrating gonadotropin-releasing hormone (GnRH) neurons (Cariboni et al., 2011) and enhancing the contralateral projection of retinal ganglion cell (RGC) axons across the optic chiasm (Erskine et al., 2011).

To demonstrate roles for VEGF binding to NRP1 in neurons, prior studies used $Vegfa^{120/120}$ mice, which express $VEGF_{120}$, the murine equivalent of $VEGF_{121}$, but lack $VEGF_{164}$ and $VEGF_{188}$, corresponding to human $VEGF_{165}$ and $VEGF_{189}$, respectively (Carmeliet et al., 1999). $Vegfa^{120/120}$ mice phenocopy the defects of NRP1 knockouts in FBM neuron migration, GnRH neuron survival and RGC axon guidance (Cariboni et al., 2011; Erskine et al., 2011; Schwarz et al., 2004). In all three systems, VEGF signalling was attributed to the activity of $VEGF_{165}$ because it evokes appropriate neuronal responses in tissue culture models (Cariboni et al., 2011; Erskine et al., 2011; Schwarz et al., 2004), and because the ability of NRP1 to bind $VEGF_{165}$ is well established (Fantin et al., 2014; Soker et al., 1998). However, $Vegfa^{120/120}$ mutants lack $VEGF_{188}$ in addition to $VEGF_{164}$. Yet, it has never previously been examined whether $VEGF_{189}$ can also function as a NRP1 ligand *in vivo*. Moreover, it is not known whether $VEGF_{121}$ can bind NRP1 in a physiologically relevant context, even though it has been suggested that the exon 8 domain, which is present in all major VEGF isoforms, including $VEGF_{121}$, can mediate NRP1 binding *in vitro* (Jia et al., 2006; Pan et al., 2007; Parker et al., 2012).

Here, we have generated alkaline phosphatase (AP)-conjugated VEGF isoforms for *in situ* ligand-binding assays (Fantin et al., 2014) to examine whether $VEGF_{121}$ or $VEGF_{189}$ can bind NRP1 *in vivo*, as previously reported for $VEGF_{165}$. Our studies demonstrate that $VEGF_{189}$ binds NRP1-expressing axon tracts in intact hindbrain tissue, but that $VEGF_{121}$ is unable to do so. We further show that $VEGF_{188}$ is co-expressed with the other isoforms during VEGF/NRP1-dependent FBM migration, GnRH neuron survival and RGC axon guidance, and that $VEGF_{188}$ is sufficient to control all three processes, whereas $VEGF_{120}$ is not. We conclude that $VEGF_{188}$ effectively binds NRP1 and has the capacity to evoke NRP1-dependent signalling events, similar to $VEGF_{164}$. Considering that $VEGF_{189}$ has the highest affinity for ECM and therefore tissue retention amongst the VEGF isoforms, future research may therefore wish to consider the mechanistic contribution and therapeutic potential of this understudied VEGF isoform.

RESULTS AND DISCUSSION

$VEGF_{188}$ is co-expressed with $VEGF_{120}$ and $VEGF_{164}$ in developing hindbrain, nose and diencephalon, and binds axons in a NRP1-dependent fashion

Because prior studies implicated VEGF signalling through NRP1 in FBM neuron migration in the hindbrain, GnRH neuron survival in the nose and RGC axon guidance in the diencephalon (Cariboni et al., 2011; Erskine et al., 2011; Schwarz et al., 2004), we asked which *Vegfa* isoforms were expressed in these developmental contexts. For this experiment, we designed isoform-specific primers that can distinguish the *Vegfa120*, *Vegfa164* and *Vegfa188* mRNA

[1]UCL Institute of Ophthalmology, University College London, 11-43 Bath Street, London EC1V 9EL, UK. [2]School of Medical Sciences, Institute of Medical Sciences, University of Aberdeen, Aberdeen AB25 2ZD, UK. [3]University of Milan, Department of Pharmacological and Biomolecular Sciences, Via Balzaretti 9, Milan 20133, Italy.

*Author for correspondence (c.ruhrberg@ucl.ac.uk)

Received 1 August 2014; Accepted 26 November 2014

Development (2015) 142, 314-319 doi:10.1242/dev.115998

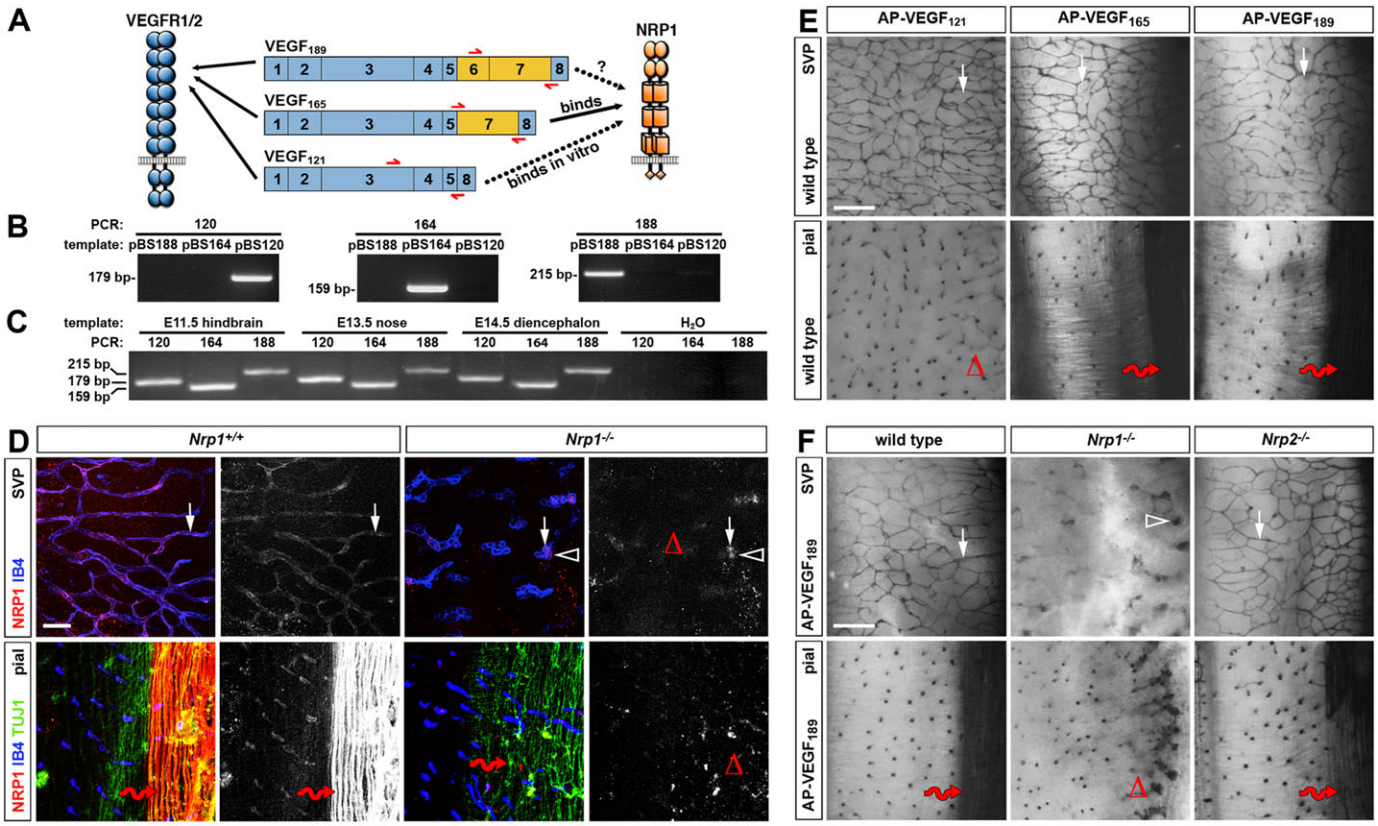

Fig. 1. $VEGF_{189}$ is expressed in developing mouse tissues and binds NRP1 in the developing hindbrain. (A) Current knowledge of VEGF isoform binding to their receptors. All isoforms bind VEGFR1/2, whereas only $VEGF_{165}$ is known to bind NRP1. $VEGF_{121}$ can bind NRP1 with low affinity *in vitro*, but whether this association occurs *in vivo* has not been shown. Moreover, it has not been shown whether $VEGF_{189}$ binds NRP1 *in vivo*. Red arrows below each isoform indicate the position of oligonucleotide primers used for RT-PCR in B. (B) *Vegfa* isoform-specific oligonucleotide primers for RT-PCR were validated with pBlueScript vectors (pBS) containing mouse *Vegfa120*, *Vegfa164* or *Vegfa188* cDNA, respectively. (C) RT-PCR analysis of the indicated tissues shows that *Vegfa120* (179 bp), *Vegfa164* (159 bp) and *Vegfa188* (215 bp) are co-expressed. (D) Whole-mount staining of E12.5 wild-type hindbrains for NRP1 and TUJ1 together with IB4; single NRP1 channels are shown in grey scale adjacent to each panel. The white arrows indicate IB4-positive vessels; the arrowhead indicates nonspecific NRP1 staining of blood cells inside mutant vessels; the red wavy arrows indicate TUJ1-positive axons; open triangles indicate absent NRP1 staining in subventricular plexus (SVP) vessels and pial axons. Scale bar: 200 µm. (E,F) AP-$VEGF_{121}$, AP-$VEGF_{165}$ and AP-$VEGF_{189}$ binding to E12.5 wild-type hindbrains (E) and AP-$VEGF_{189}$ binding to E12.5 *Nrp1*$^{-/-}$ and *Nrp2*$^{-/-}$ hindbrains (F). The white arrows indicate VEGF binding to vessels; the red wavy arrows indicate binding to axons; the open triangles indicate absence of $VEGF_{121}$ binding to wild-type axons in E and absence of $VEGF_{189}$ binding to axons in *Nrp1*$^{-/-}$ hindbrains in F. The arrowhead indicates vascular tufts. Scale bars: 25 µm.

species by reverse transcription (RT)-PCR (Fig. 1A,B; supplementary material Fig. S1A). This analysis demonstrated that all three isoforms were co-expressed during relevant periods of VEGF/NRP1-dependent neurodevelopment in mice (Fig. 1C).

Because prior studies of VEGF binding to NRP1 have not examined whether $VEGF_{189}$ or $VEGF_{121}$ can bind NRP1 *in vivo*, we used the mouse hindbrain as a physiologically relevant model to compare the ability of the three major VEGF isoforms to bind NRP1 in a tissue context. We first performed immunostaining with a validated antibody for NRP1 (Fantin et al., 2010) to confirm that NRP1 localises to blood vessels in wild-type, but not NRP1 knockout, hindbrains (Fig. 1D; note unspecific staining of blood in the dilated vessels of mutants). Immunolabelling also confirmed NRP1 expression in TUJ1-positive dorsolateral axons on the pial side of wild-type, but not mutant, hindbrains (Fig. 1D; supplementary material Fig. S1B). *Nrp1*$^{-/-}$ hindbrains showed some defasciculation of these dorsolateral axons, but they were still clearly present in the mutant, suggesting that this are a suitable model to examine VEGFA isoform binding to NRP1.

To compare the binding properties of $VEGF_{121}$, $VEGF_{165}$ and $VEGF_{189}$, we fused each isoform to AP and performed *in situ* ligand binding assays on E12.5 hindbrains. As expected, all three isoforms bound vessels (Fig. 1E), because they express the pan-VEGF isoform receptor VEGFR2 (Lanahan et al., 2013). We next examined binding to dorsolateral axons, because they express NRP1, but lack VEGFR2 (Lanahan et al., 2013). Both $VEGF_{165}$ and $VEGF_{189}$ bound these axons, whereas $VEGF_{121}$ did not (Fig. 1E). These observations indicate that all VEGF isoforms are capable of binding VEGFR2/NRP1-positive vessels. By contrast, only $VEGF_{165}$ and $VEGF_{189}$, but not $VEGF_{121}$, bound NRP1-expressing axons lacking VEGFR2, consistent with the previously reported 10-fold lower affinity of $VEGF_{121}$ for NRP1 *in vitro* (Parker et al., 2012). The finding that $VEGF_{121}$ does not bind endogenous neuronal NRP1 at detectable levels also agrees with prior genetic studies, which showed that $VEGF_{120}$ is unable to compensate for $VEGF_{164}$ in FBM, RGC and GnRH neurons (Cariboni et al., 2011; Erskine et al., 2011; Schwarz et al., 2004). Thus, low-affinity binding of $VEGF_{121}$ to NRP1, even though previously observed *in vitro*, is unlikely to be relevant *in vivo*, at least in a neuronal context.

We next confirmed that axonal $VEGF_{189}$ binding is NRP1 dependent. The AP ligand-binding assay showed that $VEGF_{189}$ bound vessels (Fig. 1F) in *Nrp1*-null mutant hindbrains with their characteristic vascular tufts (Fantin et al., 2013a). Strikingly, AP-$VEGF_{189}$ failed to bind axons in *Nrp1*-null hindbrains, similar to AP-$VEGF_{165}$ (Fig. 1F). $VEGF_{189}$ can therefore bind axons in a

Development (2015) 142, 314-319 doi:10.1242/dev.115998

NRP1-dependent fashion. By contrast, loss of NRP2 (Giger et al., 2000) did not abolish $VEGF_{189}$ binding (Fig. 1F). Taken together, the ligand binding assays of intact hindbrain tissue show that NRP1 serves as a neuronal receptor for $VEGF_{165}$ and $VEGF_{189}$, but not for $VEGF_{121}$.

$VEGF_{188}$ is sufficient for the NRP1-dependent migration of FBM neurons

Vegfa is a haploinsufficient gene for which deletion of just one allele results in early embryonic lethality due to a complete failure of blood vessel formation (Carmeliet et al., 1996; Ferrara et al., 1996). However, retention of any one of the major VEGF isoforms rescues this severe phenotype and instead gives rise to more subtle neuronal and vascular phenotypes (Ruhrberg et al., 2002; Stalmans et al., 2002). Understanding the receptor-binding properties of the VEGF isoforms has therefore become a priority in the field. We first examined if $VEGF_{188}$ can substitute for $VEGF_{164}$ in FBM neuron guidance with an established hindbrain explant assay in which implanted beads provide exogenous VEGF, and FBM neuron migration is visualised by immunolabelling with the motor neuron marker ISL1 (Schwarz et al., 2004; Tillo et al., 2014). Agreeing with previous observations, FBM neurons were attracted to $VEGF_{164}$, but not to control beads lacking growth factors (Fig. 2B). $VEGF_{188}$ beads also attracted FBM neurons (Fig. 2B). Quantification confirmed that FBM neuron migration was significantly enhanced on the hindbrain side containing a $VEGF_{164}$- or $VEGF_{188}$-soaked bead relative to the control side of the same hindbrain (Fig. 2C). $VEGF_{188}$ can therefore promote NRP1-dependent neuronal migration similar to $VEGF_{164}$.

We next examined FBM neuron migration *in vivo* by *Isl1 in situ* hybridisation. As previously shown (Schwarz et al., 2004), $Vegfa^{120/120}$ hindbrains demonstrated abnormal streaming of FBM neurons on the ventricular side and dumbbell-shaped nuclei on the pial side (Fig. 2D). By contrast, $Vegfa^{188/188}$ mice, which express only $VEGF_{188}$, showed normal FBM neuron migration (Fig. 2D). Moreover, replacing one $Vegfa^{120}$ allele in $Vegfa^{120/120}$ mutants with the $Vegfa^{188}$ allele was sufficient to prevent FBM neuron defects (Fig. 2D). Unlike $VEGF_{120}$, $VEGF_{188}$ is therefore sufficient to direct NRP1-dependent neuronal migration.

$VEGF_{188}$ is sufficient to guide NRP1-dependent axon crossing at the optic chiasm

We next investigated whether $VEGF_{188}$ can evoke neuronal responses similar to $VEGF_{164}$ in the developing visual system. To establish binocular vision, RGC axons project through the optic chiasm to both the ipsilateral and contralateral brain hemispheres (Erskine and Herrera, 2007). $VEGF_{164}$, but not $VEGF_{120}$, promotes RGC axon guidance in a NRP1-dependent fashion *in vitro*, and $Vegfa^{120/120}$ mice therefore develop an abnormal chiasm (Erskine et al., 2011). To examine whether $VEGF_{188}$ can also promote RGC axon guidance, we performed DiI labelling in VEGF isoform mutants. Anterograde labelling of RGC axons from one eye at E14.5 demonstrated that $VEGF_{188}$ was sufficient for NRP1-mediated chiasm patterning (Fig. 3A). Thus, $Vegfa^{120/120}$ mice had a significantly increased ipsilateral projection index as well as defasciculation of the ipsilateral and contralateral optic tracts (Erskine et al., 2011), but the ipsilateral index and shape of the optic chiasm appeared unaffected in $Vegfa^{188/188}$ mice (Fig. 3B,C). Moreover, replacing one $Vegfa^{120}$ with the $Vegfa^{188}$ allele was sufficient to prevent chiasm defects in $Vegfa^{120/120}$ mutants (Fig. 3B,C).

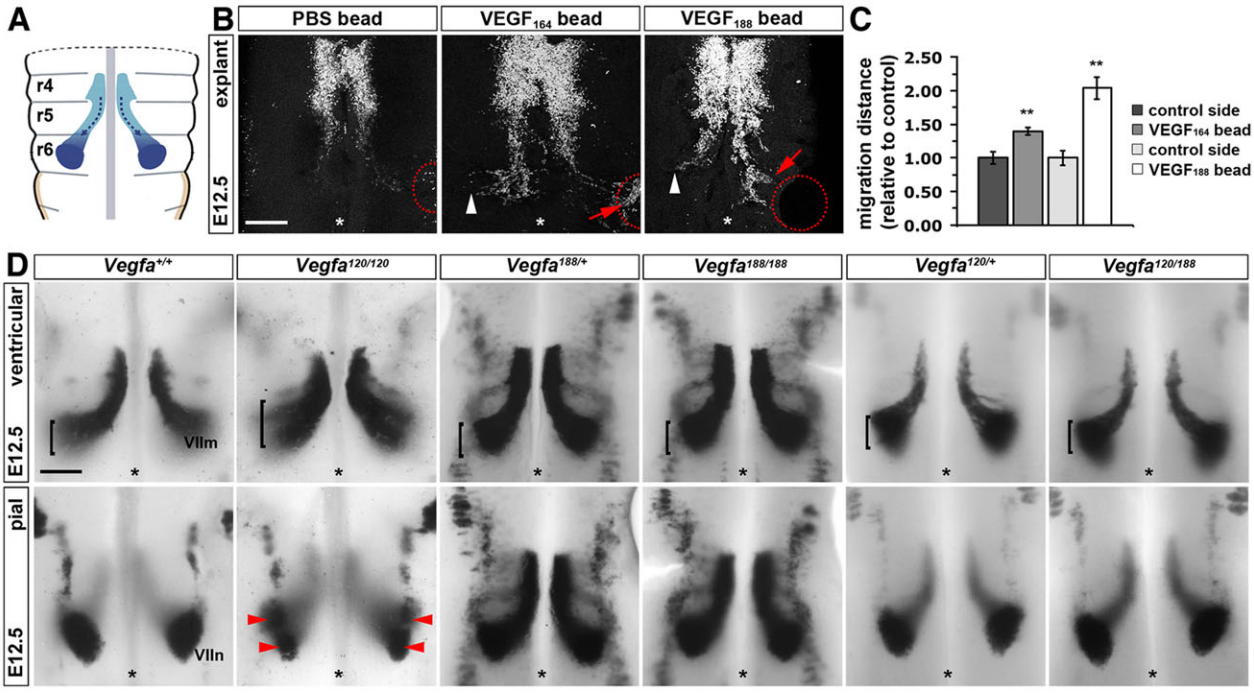

Fig. 2. $VEGF_{188}$ is sufficient for FBM neuron migration. (A) Schematic representation of FBM neuron migration in the mouse. (B) ISL1 staining of E12.5 hindbrain explants containing implanted heparin beads soaked in PBS (n=10) or PBS containing $VEGF_{164}$ (n=10) or $VEGF_{188}$ (n=6). Red dotted circles indicate the position of heparin beads; white arrowheads indicate normal migration; red arrows indicate migration towards heparin beads; asterisks indicate the midline. Scale bar: 200 µm. (C) Distance migrated by FBM neurons. Migration distance was quantified as migration away from r5 territory on the hindbrain side with a bead relative to the control half of the same hindbrain; mean±s.e.m. control 1±0.09 versus $VEGF_{164}$ bead 1.39±0.05; control 1±0.11 versus $VEGF_{188}$ bead 2.04±0.17; $^{**}P$<0.01, VEGF compared with control (t-test). (D) Whole-mount *Isl1 in situ* hybridisation of E12.5 hindbrains of the indicated genotypes detects migrating FBM neurons (VIIm) (control, n=10; $Vegfa^{120/120}$, n=6; $Vegfa^{188/188}$, n=4; $Vegfa^{120/188}$, n=5). Brackets indicate the width of the neuronal stream on the ventricular side; red arrowheads indicate dumbbell-shaped nuclei on the pial side; asterisks indicate the midline. Scale bar: 25 µm.

Development (2015) 142, 314-319 doi:10.1242/dev.115998

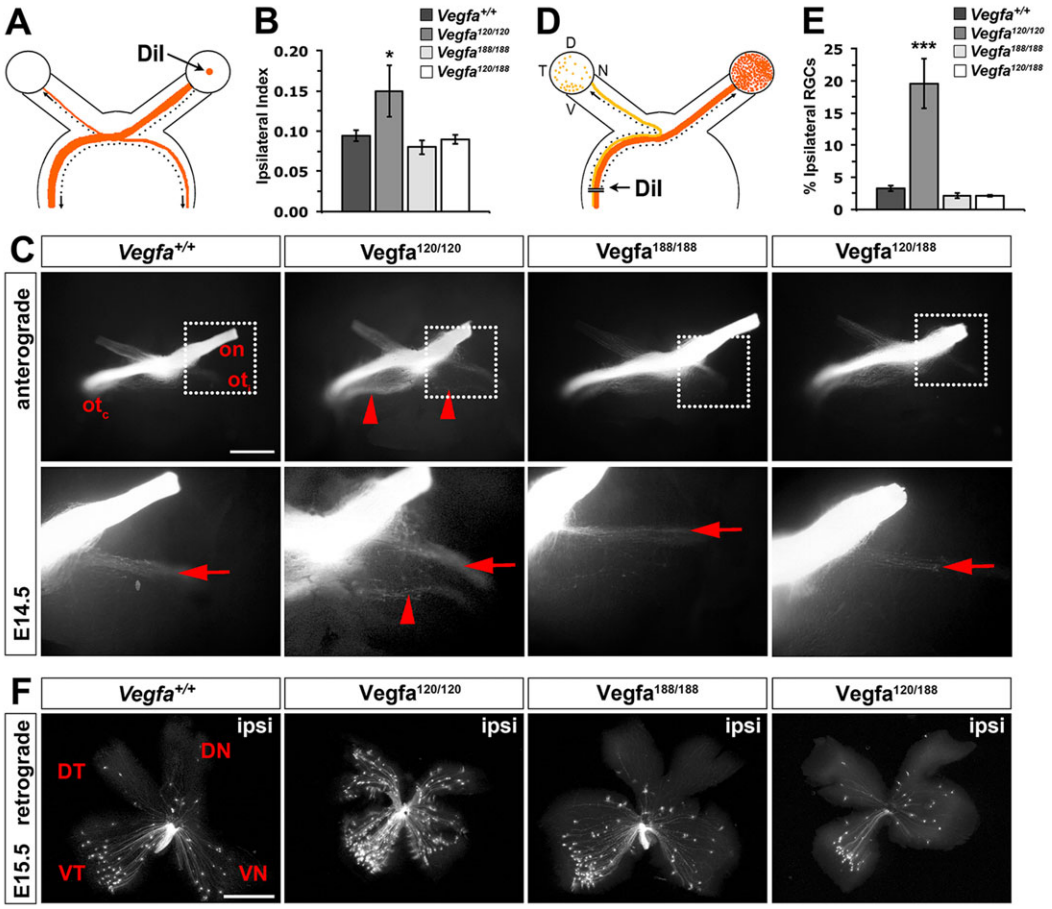

Fig. 3. VEGF$_{188}$ is sufficient to guide commissural axons across the optic chiasm. (A) Schematic illustration of the method used to anterogradely label RGC projections. DiI crystals were placed onto the retina in one eye to label axons extending through the optic chiasm into the ipsilateral and contralateral optic tracts. (B) Ipsilateral index in the indicated genotypes (mean±s.e.m.): control, 0.095±0.01, *n*=11; *Vegfa*$^{120/120}$, 0.15±0.03, *n*=5; *Vegfa*$^{188/188}$, 0.083±0.01, *n*=3; *Vegfa*$^{120/188}$, 0.09±0.01, *n*=3; *t*-test, **P*<0.05 compared with control. (C) Whole-mount views of RGC axons at the optic chiasm from embryos of the indicated genotypes, labelled anterogradely with DiI at E14.5; ventral view, anterior upwards; optic nerve (on), contralateral optic tract (ot$_c$) and ipsilateral optic tract (ot$_i$). Red arrows indicate the normal position of the ipsilateral projection; red arrowheads indicate the secondary tract and axon defasciculation in *Vegfa*$^{120/120}$ mutants. Scale bar: 500 µm. Higher magnifications of each boxed areas are shown beneath the respective panels. (D) Schematic illustration of the method used to retrogradely label RGC projections. DiI crystals were placed unilaterally into the optic tract in the dorsal thalamus. (E) Proportion of ipsilaterally projecting RGCs relative to total number of RGCs in both eyes of the indicated genotypes at E15.5 (mean±s.e.m.): control, 3.28±0.44%, *n*=8; *Vegfa*$^{120/120}$, 19.64±3.89%, *n*=4; *Vegfa*$^{188/188}$, 2.16±0.42%, *n*=4; *Vegfa*$^{120/188}$, 2.12±0.14%, *n*=2; *t*-test, ****P*<0.001 compared with control. (F) Flatmounted ipsilateral retinas from E15.5 embryos of the indicated genotypes after retrograde labelling from the optic tract in the right thalamus. DT, dorsotemporal; VN, ventronasal; DN, dorsonasal; VT, ventrotemporal. Scale bar: 500 µm.

We next performed retrograde DiI labelling of RGC axons from the dorsal thalamus in VEGF isoform mice and compared the number of labelled RGCs in flatmounted ipsilateral and contralateral retina (Fig. 3D). Quantitation showed that the proportion of DiI-labelled ipsilateral RGCs was significantly increased in *Vegfa*$^{120/120}$ compared with control mice, but was normal in *Vegfa*$^{188/188}$ and *Vegfa*$^{120/188}$ mice (Fig. 3E). Flat-mount images also revealed the preferential origin of ipsilaterally projecting neurons from the ventrotemporal retina in wild types (Fig. 3F). Their distribution is affected in *Vegfa*$^{120/120}$ mice, which contain ipsilaterally projecting RGCs throughout the nasal retina (Erskine et al., 2011), but this defect was rescued by the introduction of a single *Vegfa*^{188} allele (Fig. 3F). VEGF$_{188}$ is therefore sufficient to promote NRP1-dependent aspects of optic chiasm development.

VEGF$_{188}$ is sufficient to ensure normal GnRH neuron survival

As a third model to study VEGF$_{188}$ in neurodevelopment, we investigated GnRH neuron survival. GnRH neurons are born in the nasal placode and travel along nasal axons to reach the forebrain (Fig. 4A; Cariboni et al., 2007). We have previously shown that *Vegfa*$^{120/120}$ mice have significantly fewer migrating GnRH neurons and demonstrated that VEGF$_{164}$ signals through NRP1 to promote the survival of GN11 cells, which recapitulate many features of migratory GnRH neurons (Cariboni et al., 2011). We therefore examined whether VEGF$_{188}$ promotes GN11 survival, similar to VEGF$_{164}$. Whereas 72 h of serum withdrawal caused the death of over half of the GN11 cells, the inclusion of serum, VEGF$_{164}$ or VEGF$_{188}$ for the last 12 h of culture significantly reduced cell death, and VEGF$_{188}$ was as effective as VEGF$_{164}$ in preventing cell death; by contrast, and as expected, VEGF$_{120}$ did not promote survival (Fig. 4B; percentage of propidium iodide-positive cells, mean±s.e.m.: control, 44±3%; serum, 2±1%; VEGF$_{120}$, 37±3; VEGF$_{164}$, 11±2%; VEGF$_{188}$, 11±2%). These observations suggest that VEGF$_{188}$, similar to VEGF$_{164}$, can promote GnRH neuron survival. The ineffectiveness of VEGF$_{120}$ agreed with the previously observed NRP1-dependent neuroprotection of GN11 cells and the

Development (2015) 142, 314-319 doi:10.1242/dev.115998

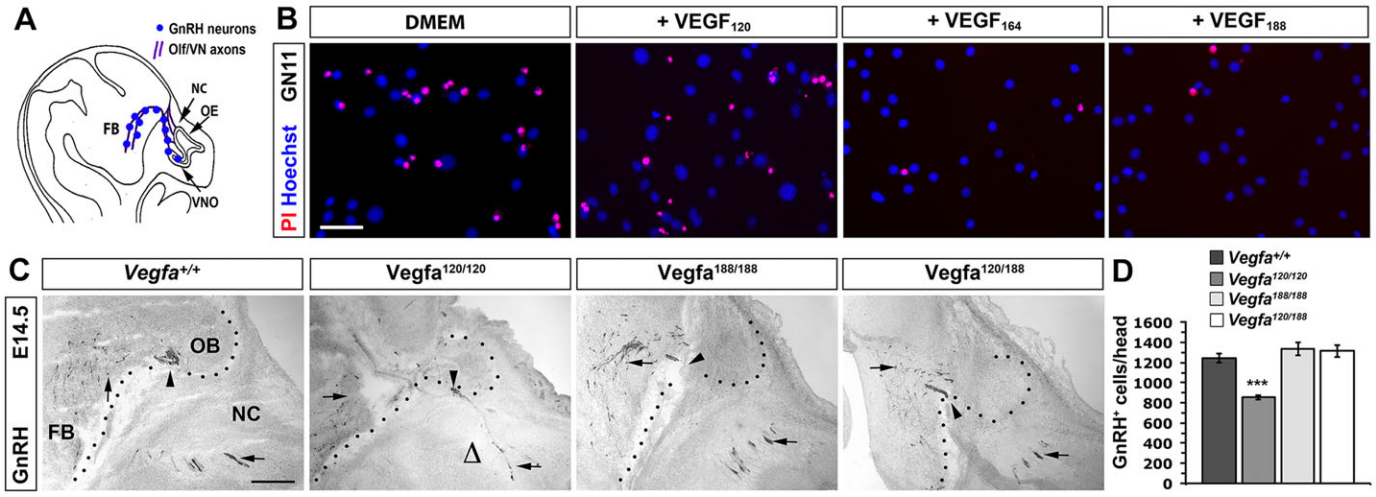

Fig. 4. $VEGF_{188}$ is sufficient to promote GnRH neuron survival. (A) GnRH neuron migration (blue dots). The neurons are born in the nasal placodes that give rise to the olfactory and vomeronasal epithelia (OE, VNO) and migrate along olfactory and vomeronasal axons (purple, Olf/VN) through the nasal compartment (NC) to reach the forebrain (FB). (B) Serum-starved GN11 cells were treated with DMEM or DMEM-containing serum, $VEGF_{120}$, $VEGF_{164}$ or $VEGF_{188}$; cell death was visualised by propidium iodide staining (red); Hoechst staining (blue) identified the total number of cells. Scale bar: 25 µm. (C) Sagittal sections of E14.5 mouse heads of the indicated genotypes, immunolabelled for GnRH. Arrows indicate migrating neurons; arrowheads indicate blood vessels; open triangles indicate the absence of migrating neurons; dotted lines indicate the FB boundary. OB, olfactory bulb. Scale bar: 100 µm. (D) GnRH neuron number in E14.5 heads of the indicated genotypes (mean±s.e.m.): control, 1246±46, *n*=6; *Vegfa*$^{120/120}$, 854±21, *n*=5; *Vegfa*$^{188/188}$, 1335±63, *n*=3; *Vegfa*$^{120/188}$, 1314±58, *n*=3; *t*-test; ***P<0.001 compared with control.

fact that *Vegfa*$^{120/120}$ mice have fewer GnRH neurons (Cariboni et al., 2011). Also in agreement with the *in vitro* findings, the GnRH neuron number was normal in *Vegfa*$^{188/188}$ mice that express $VEGF_{188}$ but lack $VEGF_{164}$ (Fig. 4C,D). Moreover, replacing one *Vegfa*^{120} allele in *Vegfa*$^{120/120}$ mutants with the *Vegfa*^{188} allele was sufficient to prevent their GnRH neuron survival defect (Fig. 4C,D). Together, these data show that $VEGF_{188}$ is sufficient to promote NRP1-dependent neuronal survival.

Conclusions

Our study has demonstrated that human $VEGF_{189}$, but not $VEGF_{121}$, binds NRP1 in a tissue context, that mouse $VEGF_{188}$ is co-expressed with $VEGF_{164}$ in a neuronal context, and that mouse $VEGF_{188}$ expressed from the endogenous *Vegfa* locus can evoke NRP1-dependent neuronal responses *in vitro* and *in vivo*, similar to $VEGF_{164}$ and unlike $VEGF_{121}$. Future work on the role of VEGF signalling through NRP1, especially studies using *Vegfa*$^{120/120}$ or tissue-specific *Vegfa*-null alleles, should therefore consider the possibility that $VEGF_{188}$, similar to $VEGF_{164}$, can regulate the process under investigation. This consideration would be relevant for both neural and vascular studies, or indeed any context in which VEGF signalling through NRP1 is implicated. The finding that the relatively understudied $VEGF_{189}$ is capable of evoking VEGF isoform-specific signalling events may have broad implications for the therapeutic use of VEGF. Thus, VEGF application has been considered in many studies for pro-angiogenic, pro-neurogenic and neuroprotective therapies, e.g. the treatment of amyotrophic lateral sclerosis (reviewed by Storkebaum et al., 2011). Most prior studies have used $VEGF_{165}$ to ensure comprehensive receptor targeting; however, the retention of $VEGF_{165}$ in tissues is inferior to that of $VEGF_{189}$ due to the presence of only one instead of two heparin/matrix-binding domains. Our work demonstrating that $VEGF_{189}$ is fully capable of engaging NRP1, in addition to its known ability to bind VEGFR1 and VEGFR2, therefore suggests that $VEGF_{189}$ may be better suited than $VEGF_{165}$ to induce localised tissue effects in therapeutic applications.

MATERIALS AND METHODS

Animals

Animal procedures were preformed in accordance with institutional and UK Home Office guidelines. The *Vegfa*^{120} and *Vegfa*^{188} alleles (Carmeliet et al., 1999; Stalmans et al., 2002), and *Nrp1*$^{-/-}$ and *Nrp2*$^{-/-}$ mice have been described previously (Giger et al., 2000; Kitsukawa et al., 1997).

RT-PCR and sequencing

Total RNA was reverse transcribed using Superscript III (Life Technologies) and *Vegfa* isoforms amplified by PCR using MegaMix (Microzone) and the following oligonucleotide pairs: 120-F 5′-GTAACGATGAAGCCCTG-GAG-3′ and 120-R 5′-CCTTGGCTTGTCACATTTTTC-3′; 164-F 5′-AG-CCAGAAAATCACTGTGAGC-3′ and 164-R 5′-GCCTTGGCTTGTCA-CATCT-3′; 188-F 5′-AGTTCGAGGAAAGGGAAAGG-3′ and 188-R 5′-GCCTTGGCTTGTCACATCT-3′.

AP-fusion protein binding assays

Open reading frames for the VEGF isoforms were amplified by PCR with the oligonucleotides 5′-AATAATGGATCCGCACCCATGGCAGAAGG-AG-3′ and 5′-TATATGCTCGAGCTCACCGCCTCGGCTTGTC-3′. The PCR products were cloned into pAG3-AP containing an upstream in-frame AP cassette. Binding assay were performed as described previously (Fantin et al., 2013b).

Immunolabelling and *in situ* hybridisation

Primary antibodies used were: rabbit anti-mouse GnRH (Immunostar, 20075, 1:1000), goat anti-rat NRP1 (R&D Systems, AF566, 1:100), rabbit anti-mouse TUJ1 (Covance, MRB-435p, 1:250) and mouse anti-rat ISL1 (DSHB, 39.4D5, 1:100). Secondary antibodies used were: Alexa594-conjugated rabbit anti-goat Fab (Jackson ImmunoResearch, 305-587-003, 1:200), Alexa488-conjugated donkey anti-rabbit Fab (Jackson ImmunoResearch, 711-547-003, 1:200), Alexa488-conjugated goat anti-mouse (Life Technologies, A-110011, 1:200) and biotinylated goat anti-rabbit (Vector Laboratories, BA-1000, 1:200). To detect blood vessels, we used biotinylated IB4 (Sigma) followed by Alexa633-conjugated streptavidin (Life Technologies). For *in situ* hybridisation, we used a digoxigenin-labelled *Isl1* probe (Schwarz et al., 2004).

Development (2015) 142, 314-319 doi:10.1242/dev.115998

Hindbrain explant culture

Hindbrain explants were cultured as previously described (Schwarz et al., 2004; Tillo et al., 2014). Affi-Gel heparin beads (Bio-Rad) were soaked overnight in 100 ng/ml of $VEGF_{164}$ in PBS (Preprotech) or $VEGF_{188}$ (Reliatech). FBM neuron migration was measured with ImageJ (NIH) as the distance travelled from r5 to the leading group of cells in r6 in each hindbrain and normalised to the control side of each hindbrain.

DiI labelling

DiI labelling was performed with fixed tissues as described previously (Erskine et al., 2011). Briefly, a DiI crystal (Life Technologies) was placed over the optic disc of one eye for anterograde labelling. After 3 days at 37°C, dissected brains were imaged ventral side upwards. ImageJ was used to determine the pixel intensity in defined areas of the ipsilateral and contralateral optic tracts, and the ipsilateral index calculated as the ratio of fluorescent intensity in the ipsilateral relative to the ipsilateral plus contralateral tracts. For retrograde labelling, the cortex was removed unilaterally and DiI crystals placed in a row over the dorsal thalamus for 15 weeks at room temperature; we imaged flatmounted retinas as above and determined the percentage of labelled ipsilateral RGCs relative to the ipsilateral plus contralateral RGCs.

GnRH neuron analysis and survival assays

Immunolabelled GnRH-positive cells were quantitated and GN11 survival assays performed as described previously (Cariboni et al., 2011). For survival assays, cells were serum starved for 72 h and treated for 12 h with media containing 10% FBS, 10 ng/ml $VEGF_{120}$, $VEGF_{164}$ or $VEGF_{188}$.

Acknowledgements

We thank Dr Jonathan Raper for the pAG3-AP plasmid and the staff of the Biological Resources Unit at the UCL Institute of Ophthalmology for help with mouse husbandry.

Competing interests

The authors declare no competing financial interests.

Author contributions

C.R. and M.T. planned the experiments and wrote the manuscript. M.T., L.E., A.C., A.F., A.J., L.D. and C.R. performed the experiments. All authors have read, commented on and approved the manuscript.

Funding

This research was funded by a Wellcome Trust PhD fellowship to M.T. [092839/Z/10/Z] and a BBSRC project grant to C.R. and L.E. [BB/J00930X/1]. Deposited in PMC for immediate release.

Supplementary material

Supplementary material available online at
http://dev.biologists.org/lookup/suppl/doi:10.1242/dev.115998/-/DC1

References

Cariboni, A., Maggi, R. and Parnavelas, J. G. (2007). From nose to fertility: the long migratory journey of gonadotropin-releasing hormone neurons. *Trends Neurosci.* **30**, 638-644.

Cariboni, A., Davidson, K., Dozio, E., Memi, F., Schwarz, Q., Stossi, F., Parnavelas, J. G. and Ruhrberg, C. (2011). VEGF signalling controls GnRH neuron survival via NRP1 independently of KDR and blood vessels. *Development* **138**, 3723-3733.

Carmeliet, P., Ferreira, V., Breier, G., Pollefeyt, S., Kieckens, L., Gertsenstein, M., Fahrig, M., Vandenhoeck, A., Harpal, K., Eberhardt, C. et al. (1996). Abnormal blood vessel development and lethality in embryos lacking a single VEGF allele. *Nature* **380**, 435-439.

Carmeliet, P., Ng, Y.-S., Nuyens, D., Theilmeier, G., Brusselmans, K., Cornelissen, I., Ehler, E., Kakkar, V. V., Stalmans, I., Mattot, V. et al. (1999). Impaired myocardial angiogenesis and ischemic cardiomyopathy in mice lacking the vascular endothelial growth factor isoforms VEGF164 and VEGF188. *Nat. Med.* **5**, 495-502.

Erskine, L. and Herrera, E. (2007). The retinal ganglion cell axon's journey: insights into molecular mechanisms of axon guidance. *Dev. Biol.* **308**, 1-14.

Erskine, L., Reijntjes, S., Pratt, T., Denti, L., Schwarz, Q., Vieira, J. M., Alakakone, B., Shewan, D. and Ruhrberg, C. (2011). VEGF signaling through neuropilin 1 guides commissural axon crossing at the optic chiasm. *Neuron* **70**, 951-965.

Fantin, A., Vieira, J. M., Gestri, G., Denti, L., Schwarz, Q., Prykhozhij, S., Peri, F., Wilson, S. W. and Ruhrberg, C. (2010). Tissue macrophages act as cellular chaperones for vascular anastomosis downstream of VEGF-mediated endothelial tip cell induction. *Blood* **116**, 829-840.

Fantin, A., Vieira, J. M., Plein, A., Denti, L., Fruttiger, M., Pollard, J. W. and Ruhrberg, C. (2013a). NRP1 acts cell autonomously in endothelium to promote tip cell function during sprouting angiogenesis. *Blood* **121**, 2352-2362.

Fantin, A., Vieira, J. M., Plein, A., Maden, C. H. and Ruhrberg, C. (2013b). The embryonic mouse hindbrain as a qualitative and quantitative model for studying the molecular and cellular mechanisms of angiogenesis. *Nat. Protoc.* **8**, 418-429.

Fantin, A., Herzog, B., Mahmoud, M., Yamaji, M., Plein, A., Denti, L., Ruhrberg, C. and Zachary, I. (2014). Neuropilin 1 (NRP1) hypomorphism combined with defective VEGF-A binding reveals novel roles for NRP1 in developmental and pathological angiogenesis. *Development* **141**, 556-562.

Ferrara, N., Carver-Moore, K., Chen, H., Dowd, M., Lu, L., O'Shea, K. S., Powell-Braxton, L., Hillan, K. J. and Moore, M. W. (1996). Heterozygous embryonic lethality induced by targeted inactivation of the VEGF gene. *Nature* **380**, 439-442.

Giger, R. J., Cloutier, J.-F., Sahay, A., Prinjha, R. K., Levengood, D. V., Moore, S. E., Pickering, S., Simmons, D., Rastan, S., Walsh, F. S. et al. (2000). Neuropilin-2 is required in vivo for selective axon guidance responses to secreted semaphorins. *Neuron* **25**, 29-41.

Gluzman-Poltorak, Z., Cohen, T., Herzog, Y. and Neufeld, G. (2000). Neuropilin-2 is a receptor for the vascular endothelial growth factor (VEGF) forms VEGF-145 and VEGF-165. *J. Biol. Chem.* **275**, 18040-18045.

Jia, H., Bagherzadeh, A., Hartzoulakis, B., Jarvis, A., Lohr, M., Shaikh, S., Aqil, R., Cheng, L., Tickner, M., Esposito, D. et al. (2006). Characterization of a bicyclic peptide neuropilin-1 (NP-1) antagonist (EG3287) reveals importance of vascular endothelial growth factor exon 8 for NP-1 binding and role of NP-1 in KDR signaling. *J. Biol. Chem.* **281**, 13493-13502.

Kitsukawa, T., Shimizu, M., Sanbo, M., Hirata, T., Taniguchi, M., Bekku, Y., Yagi, T. and Fujisawa, H. (1997). Neuropilin-semaphorin III/D-mediated chemorepulsive signals play a crucial role in peripheral nerve projection in mice. *Neuron* **19**, 995-1005.

Koch, S., Tugues, S., Li, X., Gualandi, L. and Claesson-Welsh, L. (2011). Signal transduction by vascular endothelial growth factor receptors. *Biochem. J.* **437**, 169-183.

Lanahan, A., Zhang, X., Fantin, A., Zhuang, Z., Rivera-Molina, F., Speichinger, K., Prahst, C., Zhang, J., Wang, Y., Davis, G. et al. (2013). The neuropilin 1 cytoplasmic domain is required for VEGF-A-dependent arteriogenesis. *Dev. Cell* **25**, 156-168.

Mackenzie, F. and Ruhrberg, C. (2012). Diverse roles for VEGF-A in the nervous system. *Development* **139**, 1371-1380.

Pan, Q., Chathery, Y., Wu, Y., Rathore, N., Tong, R. K., Peale, F., Bagri, A., Tessier-Lavigne, M., Koch, A. W. and Watts, R. J. (2007). Neuropilin-1 binds to VEGF121 and regulates endothelial cell migration and sprouting. *J. Biol. Chem.* **282**, 24049-24056.

Parker, M. W., Xu, P., Li, X. and Vander Kooi, C. W. (2012). Structural basis for selective vascular endothelial growth factor-A (VEGF-A) binding to neuropilin-1. *J. Biol. Chem.* **287**, 11082-11089.

Ruhrberg, C., Gerhardt, H., Golding, M., Watson, R., Ioannidou, S., Fujisawa, H., Betsholtz, C. and Shima, D. T. (2002). Spatially restricted patterning cues provided by heparin-binding VEGF-A control blood vessel branching morphogenesis. *Genes Dev.* **16**, 2684-2698.

Schwarz, Q., Gu, C., Fujisawa, H., Sabelko, K., Gertsenstein, M., Nagy, A., Taniguchi, M., Kolodkin, A. L., Ginty, D. D., Shima, D. T. et al. (2004). Vascular endothelial growth factor controls neuronal migration and cooperates with Sema3A to pattern distinct compartments of the facial nerve. *Genes Dev.* **18**, 2822-2834.

Soker, S., Takashima, S., Miao, H. Q., Neufeld, G. and Klagsbrun, M. (1998). Neuropilin-1 is expressed by endothelial and tumor cells as an isoform-specific receptor for vascular endothelial growth factor. *Cell* **92**, 735-745.

Stalmans, I., Ng, Y.-S., Rohan, R., Fruttiger, M., Bouché, A., Yuce, A., Fujisawa, H., Hermans, B., Shani, M., Jansen, S. et al. (2002). Arteriolar and venular patterning in retinas of mice selectively expressing VEGF isoforms. *J. Clin. Invest.* **109**, 327-336.

Storkebaum, E., Quaegebeur, A., Vikkula, M. and Carmeliet, P. (2011). Cerebrovascular disorders: molecular insights and therapeutic opportunities. *Nat. Neurosci.* **14**, 1390-1397.

Tillo, M., Schwarz, Q. and Ruhrberg, C. (2014). Mouse hindbrain ex vivo culture to study facial branchiomotor neuron migration. *J. Vis. Exp.* **85**, e51397.

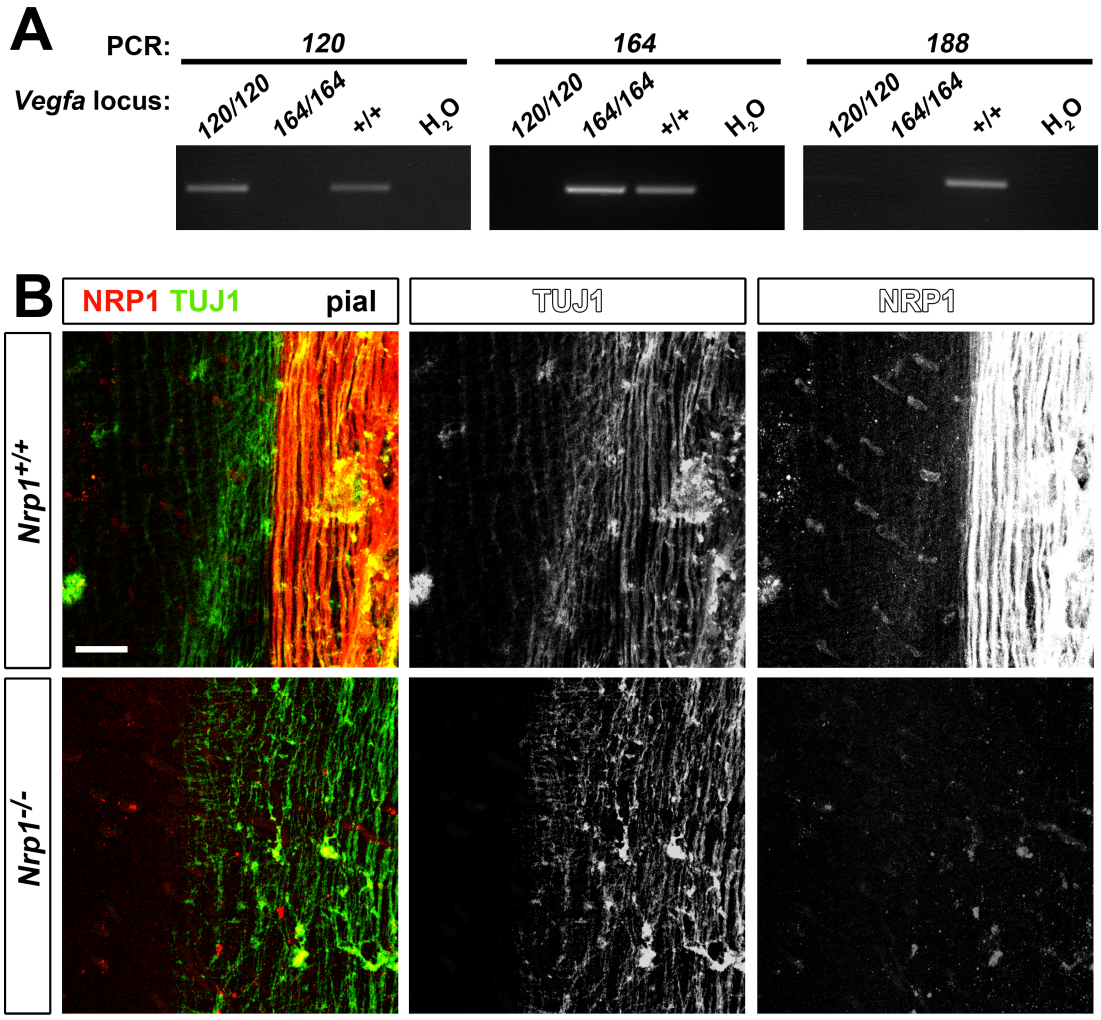

Fig. S1. ***Specificity of Vegfa isoform PCR reagents and perseverance of the dorsolateral fascicles in Nrp1-null mutants.***

(A) The specificity of oligonucleotide primers for *Vegfa* isoform expression analysis was validated by RT-PCR using cDNA derived from *Vegfa*$^{120/120}$, *Vegfa*$^{164/164}$ or wildtype E12.5 mouse embryo trunks, respectively. Note that a molecular weight standard confirmed the predicted sizes of each isoform as 179, 159 and 215 bp, respectively.

(**B**) Wholemount staining of E12.5 wildtype hindbrains for NRP1 and TUJ1; the single NRP1 and TUJ1 channels are shown in grey scale adjacent to each panel. Scale bar: 200 μm.